UNIVERSITY OF SOUTHAMPTON

FACULTY OF ENGINEERING, SCIENCE AND MATHEMATICS

School of Chemistry

TOWARDS NOVEL METAL-ORGANIC FRAMEWORKS: SYNTHESIS, CHARACTERISATION AND SELF-ASSEMBLY

by

Samuel Matthew Keltie

Thesis for the degree of Doctor of Philosophy

October 2013

UNIVERSITY OF SOUTHAMPTON

ABSTRACT

FACULTY OF ENGINEERING, SCIENCE AND MATHEMATICS

SCHOOL OF CHEMISTRY

Doctor of Philosophy

TOWARDS NOVEL METAL-ORGANIC FRAMEWORKS: SYNTHESIS, CHARACTERISATION AND SELF-ASSEMBLY

By Samuel Matthew Keltie

The synthesis, characterisation and self-assembly of novel metal-organic frameworks was investigated and reported in this thesis with a view for these materials to be used in heterogeneous catalysis after further modification. Three new materials have been synthesised and their properties discussed with all three structures being solved by single crystal X-ray diffraction methods. Three known and five new elaborate, chiral MOF ligands were synthesised in this investigation. The new ligands were a dicarboxylic acid, two tetracarboxylic acids and two dipyridinyl compounds. All the ligands are based on a bi-2-naphthol core unit. The carbon-carbon cross-coupling reactions used in the synthesis of the new ligands were optimised.

All of the ligands produced that contained unprotected, free diols were found not to form novel MOFs in an extensive investigation. A wide range of synthetic conditions were employed in attempt to produce novel MOFs. The ligand with protected diols in conjugation with an achiral co-ligand forms a highly interpenetrated novel MOF, with Zn^{2+} secondary building units. Two other MOF-like coordination polymers were also successfully synthesised and characterised. One completes a void in the well-known series of MOFs containing the Zn_4O secondary building unit and simple dicarboxylic acids.

The self-assembly of a series of prototypical MOFs was investigated by a novel solution ^1H NMR technique. The solution behaviour of the MOF ligands during the MOF synthesis in these systems is discussed. MOFs containing the Zn_4O secondary building unit appear to show fluctuations in ligand concentration, indicating the formation of crystallite species during the first few hours of the synthesis. Some insights are gained about the crystallisation mechanism of the pillared MOFs that were investigated. A dual decrease in the concentrations of both the dicarboxylate and pillaring ligands during the reaction is observed.

Table of Contents

DECLARATION OF AUTHORSHIP

I, **Samuel Matthew Keltie**, declare that the thesis entitled

Towards novel metal-organic frameworks: synthesis, characterisation and self-assembly

And the work presented in the thesis are both my own, and have been generated by me as the result of my own original research. I confirm that:

- this work was done wholly or mainly while in candidature for a research degree at this University;
- where any part of this thesis has previously been submitted for a degree or any other qualification at this University or any other institution, this has been clearly stated;
- where I have consulted the published work of others, this is always clearly attributed;
- where I have quoted from the work of others, the source is always given. With the exception of such quotations, this thesis is entirely my own work;
- I have acknowledged all main sources of help;
- where the thesis is based on work done by myself jointly with others, I have made clear exactly what was done by others and what I have contributed myself;
- parts of this work have been published as:

"A linear rod-packing coordination polymer constructed from a non-linear dicarboxylate and the $[Zn_4O]^{6+}$ cluster" S M Keltie, P A Gale, M E Light and M Tromp, *J. Coord. Chem.*, 2013, **66**, 3058.

Signed:…….

Date:…….

Acknowledgements

I would firstly like to thank my supervisors Professors Moniek Tromp and Phil Gale for their supervision and guidance throughout my PhD. I would especially like to thank Phil for allowing me to carry out my research in his lab over the last three years. I would to thank Moniek for her visits to the synchrotron with me and for a week's hospitality in Munich! I would also like to thank my advisor Dr Robert Raja and Professor John Evans for many thoughtful and enlightening discussions.

The Gale lab has been a constant source of amusement and fun over the last few years and for this I would like to thank all the members of the Gale group past and present, especially Christine, Matt, Pete, Steve, Cally, Issy, Nathalie, and Marco and also all the members of the Tromp/Evans group, past and present, especially Sarah, Rowena, Peter and Stuart for all their help and good times in and outside the lab. Special thanks goes to Cally and Steve for being part of the tripod and our many helpful discussions that often stretched to wider zoological themes. A special mention also has to be made to some of the computation chemists: Mike, Dan and Andrew for there contributions to this work and my bank balance.

This project has been made possible with the help of several members of staff and technicians at the University of Southampton and also the synchrotrons facilities the SLS and ANKA at KIT. I would like to thank Neil Wells for help with NMR, John Langley and Julie Heriman for mass spectrometry. In particular, I would like to thank the members of the X-ray crystallography service, espically Dr Mark Light for all his time and effort with my samples.

I would like to thank the EPSRC for funding this PhD.

A big thank you to my family and friends for their support and encouragement during my studies. Finally, a special thank you to Ciara for her never ending support and love.

Abbreviations

A pull-out page at the end of thesis shows the chemical structures of some of the ligands listed here as well as the chiral ligands discussed in **Chapters 3** and **4**.

Ac	Acetyl
ADC	Acetylenedicarboxylate
as	as-synthesised
a.u.	arbitrary units
ALPO	Aluminophosphate
Ar	Aryl
Aq.	Aqueous
BDC	1,4-Benzenedicarboxylate
1,2-BDC	1,2-Benzenedicarboxylate
BET	Brunauer-Emmett-Teller
BINOL	1,1’-bi(2-naphthol)
Bn	Benzyl
BPY	4,4’-Bipyridine
BTB	4,4’,4’’-Benezene-1,3,5-triyl-tris(benzoate)

BTC	1,3,5-Benzenetricarboxylate
conc.	Concentrated
DABCO	1,4-Diazabicyclo[2.2.2]octane
DBF	*N*,*N*-Dibutylformamide
DEF	*N*,*N*-Diethylformamide
DMA	*N*,*N*-Dimethylacetamide
DME	1,2-Dimethoxyethane
DMF	*N*,*N*-Dimethylformamide
DMSO	Dimethyl sulfoxide
DPE	1,2-Di(4-pyridyl)ethylene
dppf	1,1'-Bis(diphenylphosphino)ferrocene
EDXRD	Energy-dispersive x-ray diffraction
eq.	Equivalents
h	hours
HKUST	Hong Kong University of Science and Technology
ht	High temperature
IR	Infrared
IRMOF	Isoreticular Metal-Organic Framework

J	Coupling constant
M	Molar
MIL	Material from Institut Lavoisier
mmol	Millimoles
MOF	Metal-Organic Framework
Mp	Melting point (°C)
NMP	*N*-methyl-2-pyrrolidone
NMR	Nuclear Magnetic Resonance
Piv	Pivaloyl
PSD	Post Synthetic Deprotection
PSM	Post Synthetic Modification
SBU	Secondary Building Unit
TCPB	1,2,4,5-Tetrakis(4-carboxyphenyl)benzene
TGA	Thermogravimetric Analysis
TPDC	Terphenyl- 4,4’’-dicarboxylate
UiO	Universitetet i Oslo [University of Oslo] (MOF series)
XRD	X-ray Diffraction

1 Metal-Organic Frameworks

1.1 Porous Materials

Our industrial society relies heavily on catalytic processes from the platinum group from metal catalysts for catalytic converters in automobiles to the production of fine chemicals in drug synthesis. Over nine-out-of-ten chemical processes utilise heterogeneous catalysts.[1] Heterogeneous catalysis occurs when the reagents and catalyst in a chemical reaction are in different phases (the opposite being homogeneous). Homogeneous catalysts have many advantages over heterogeneous catalysts. The catalytic sites are all available, because the catalyst is an organometallic species dissolved in the same solvent as the reactants. Typically, they show higher selectivities because the chemio-, regio- and enantio-selectivity can be specifically tuned for a certain process. However, their major disadvantage that limits their applications is their recyclability (catalyst/product separation).[2] This occurs, because often homogeneous catalysts are not thermally stable and therefore distillation, which is the main method of separation, cannot be used.

Porous materials are of immense interest in research laboratories all over the world due to their many beneficial properties and applications.[3] The International Union of Pure and Applied Chemistry (IUPAC) definition for a porous material distinguishes between three types based on pore size: microporous (<2 nm); mesoporous (2 – 50 nm); macroporous (> 50 nm).[4, 5] Porous materials have been of significant interest since the first zeolite was discovered in 1756.[6] Zeolites are a prime example of microporous materials. Zeolites are crystalline aluminosilicates, which occur naturally as minerals and can be synthesised hydrothermally producing materials with a wide variety of applications.[7] These include use as ion exchange resins, molecular sieves, in gas absorption and in catalysis.[7-11] Many other

zeolite-type materials with similar properties have been discovered such as aluminophosphates (ALPOs), arsenates and zinc phosphates.[7, 12]

Zeolites can be described as inorganic open-framework materials with regular pore architectures.[13] Zeolites are crystalline materials that contain large uniform channels or pores typically ranging from 4 – 13 Å.[14] They have been shown to have many applications that take advantage of their intrinsic porosity. One such application is the incorporation of catalytic organometallic species (**Figure 1.1**).

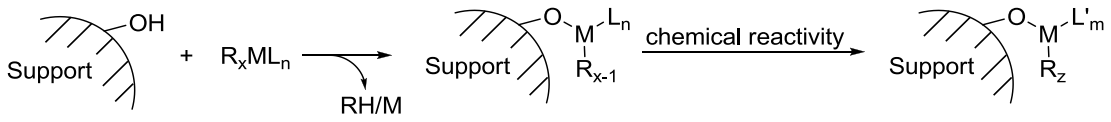

Figure 1.1: General scheme of catalyst (M) binding to support structure.[15]

Heterogeneous catalysts are an important and wide-used class of catalysts. Many heterogeneous catalysts are organometallic species bound to a support. Zeolite porosity gives large internal surface areas, which facilitates the diffusion of these species. The catalyst binds to the zeolite and because it has a regular structure, the resulting heterogeneous catalyst-zeolite is well-defined.

In the last 20 years, a new class of inorganic-organic hybrid porous materials known as metal-organic frameworks (MOFs) have been synthesised. They are, like zeolites, highly crystalline and possess permanent mircoporosity, which is the root of many of their applications.[10, 11, 16-21] MOFs[22] have many similar features to inorganic zeolites such as high surface area and porosity. However, because they are assembled from organic building blocks the chemical variety to which they can be synthesised is extensive. There are a handful of examples where MOFs show reasonable thermal stability (*ca.* 500 °C),[23, 24] but none show the same stability as zeolites. As for catalytic potential Lee *et al.* conclude that MOFs will not likely be competitive with zeolites as catalysts for reactions requiring forcing conditions, but instead will find a niche in high-value-added reactions where the reaction conditions are relatively mild.[25]

MOFs are a form of coordination network[26] where the bonding, between the inorganic and organic moieties is based on coordinative bonding and not covalent or Van der Waals

interactions. In 1989, Hoskins and Robson reported the first example of a coordination network or MOF when describing the X-ray crystal structure of $[Cu[C(C_6H_4{\cdot}CN)_4]BF_4{\cdot}xC_6H_5NO_2]$ ($x \geq 7.7$).[27] In 1990 they discussed the potential of these types of materials and predicted some of their associated properties and pitfalls that are discussed later in this **Chapter**. They reported the X-ray single crystal structures of $Zn(CN)_2$ and $Cd(CN)_2$ as diamond based frameworks with M-CN-M rods connecting the tetrahedral metal centres.[28] The term "MOF" was not coined until 1995 when Yaghi described the structure of $[CoC_6H_3(CO_2H_{1/3})_3{\cdot}(NC_5H_5)_2]$. [29]

MOFs are constructed from metal ions or clusters and organic bridging ligands in a node and spacer motif. The array that is formed is highly dependent on the connectivity of the node and the chemical structure of the ligand. The connectivity of the node arises from the coordination number of the metal ion/cluster and the directionality of the ligand. The ligand is also the predominant factor in the porosity of the MOF. Generally speaking larger/longer ligands result in larger pores and therefore higher porosity although interpenetration can attenuate this. There are a variety of arrays that can be formed from simple linear, 2-connected to 3 dimensional, 6-connected systems (**Figure 1.2**).

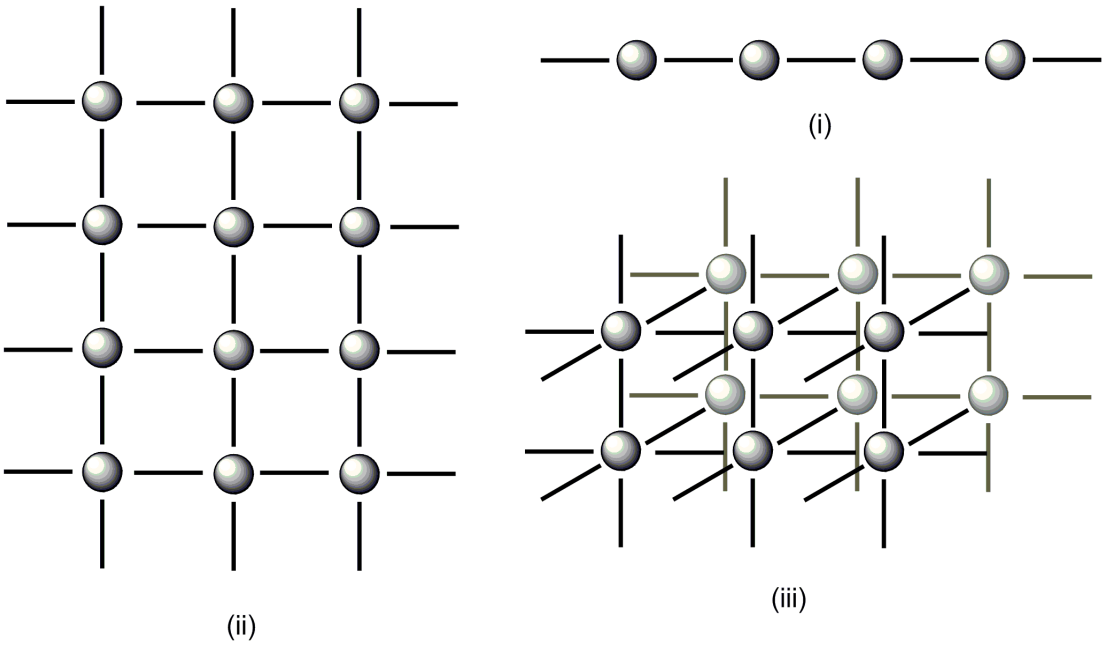

Figure 1.2: Examples of node and spacer modular arrays found in MOFs: (i) 2-connected; (ii) 4-connected square-planar; (iii) 6-connected.[30]

A large range of network topologies are designed by the connection of molecular building blocks to generate a specific structure and function. These can form infinite 1D, 2D and 3D

networks (**Figure 1.3**). The higher order dimensional structure can exhibit cavities, pores or open channels. This leads to record high surface areas for porous materials and structural rigidity. As will be outlined in this **Chapter**, the potentially enormous range of organic ligands for novel MOFs, enables fine-tuning of these properties for many applications.

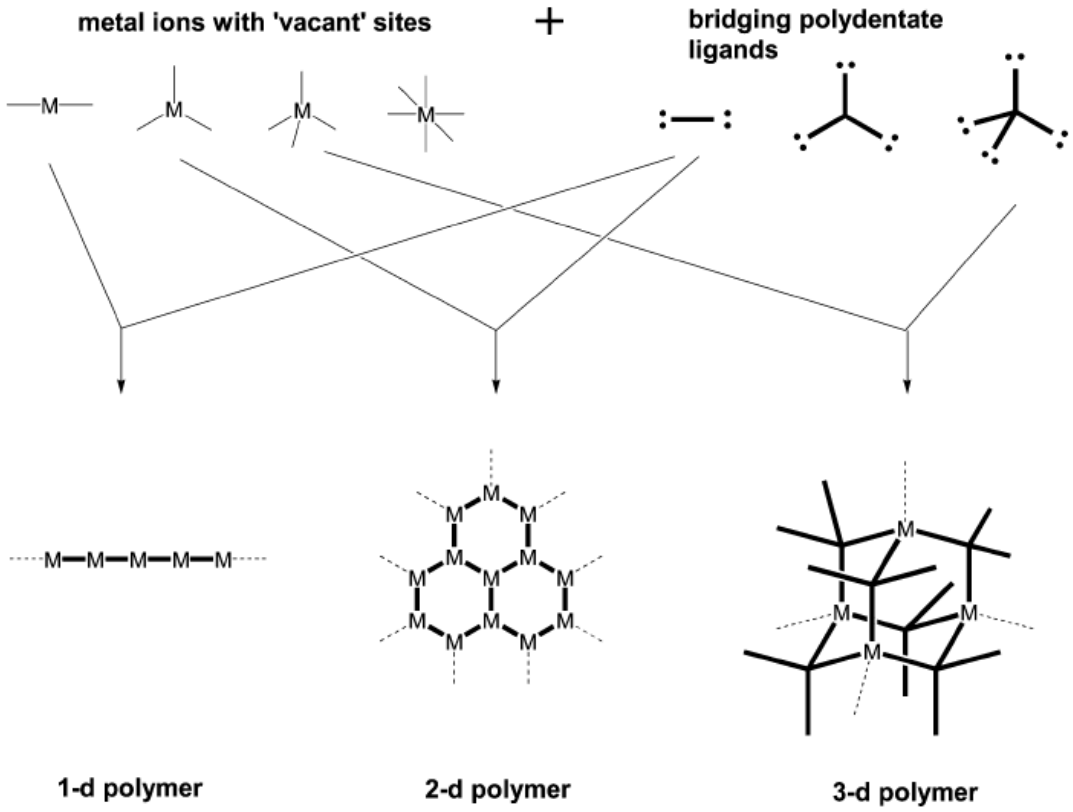

Figure 1.3: The building block, or modular, principle behind forming coordination polymers.[31]

1.2 Synthesis Concepts

1.2.1 Hydrothermal and solvothermal methods

The self-assembly of MOFs uses supramolecular concepts in which metal ions or clusters link to polytopic (mulitdentate) organic ligands in solution generating infinite frameworks that precipitate from solution as crystalline materials (**Figure 1.4**). This is typically achieved using hydrothermal or solvothermal conditions in sealed autoclaves or scintillation vials.

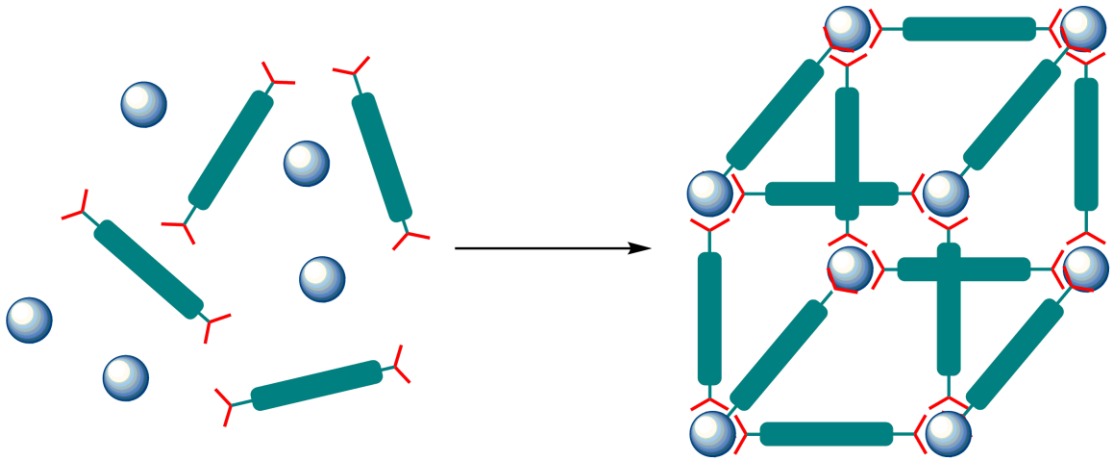

Figure 1.4: Self-assembly of MOFs.

Crystallisation occurs from high temperature and high vapour pressure solutions either aqueous in nature, in the case of hydrothermal synthesis, or solvents except water for solvothermal synthesis. Often mixtures of solvents are used that include water, which are also referred to as solvothermal synthesis. In many examples of solvothermal synthesis, alkyl amides such as dimethylformamide (DMF) are used as solvents. Small changes in one or more of the reaction variables, such as temperature, time, pH or the solvent type can have a profound influence on the product. In some cases organic amines or alkylammonium cations are used as templates in the crystallisation process.[32]

In MOF synthesis involving carboxylic acid ligands, under solvothermal conditions, the metal can catalyse the decomposition of the alkyl amide to the corresponding alkyl amine (**Figure 1.5)**. This then acts as a Brønsted base, deprotonating the acid forming the corresponding carboxylate ion that can subsequently coordinate to the cationic metals/clusters in solution and begin the self-assembly process.

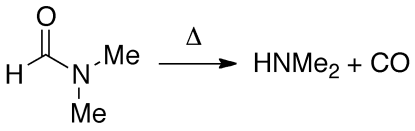

Figure 1.5: Decomposition of DMF at high temperatures.

Slower decomposition of amide to amine, results in slower coordination of the ligand to the metal. Thus the MOF crystallisation process is slower. As an example, switching from DMF to diethylformamide (DEF), which decomposes more slowly, often results in higher quality, MOF single crystals.

1.2.2 Post synthetic modification

The one pot preparation of MOFs limits the opportunity to adjust the properties during the formation. It is not always possible to pre-install complexity or functionality into the molecular components (ligands) before or during MOF synthesis. These limitations arise because the desired functionality may disturb the formation of the MOF. The precursor(s) may not withstand the MOF synthesis process, for example due to thermal instability or steric bulk. Another approach that avoids these limitations is to chemically modify an as-synthesised MOF in a single-crystal-to-single-crystal fashion. This Post-Synthetic Modification[33] (PSM) approach can be used so long as the MOF has the porosity and robustness to allow the PSM reagents to diffuse and react whilst not compromising framework stability.

PSM can take the form of coordinative interactions or covalent bonding. In the MOF $[Cd_3(L)_3Cl_6]$ (L = 6,6'-dichloro-4,4'-di(pyridin-4-yl)-[1,1'-binaphthalene]-2,2'-diol), the dihydroxyl groups are accessible for functionalisation and coordinate to Ti upon treatment with $Ti(O^iPr)_4$. In another example, the benzene rings present in MOF-5 have been shown to coordinate $M(CO)_3$ (M = Cr, Mo, W) fragment in an η^6 fashion to from a metal arene.[34]

Cohen *et al*. have shown that there are various covalent transformations that MOFs can undergo.[35-38] They have chosen IRMOF-3, $[Zn_4O(NH_2\text{-BDC})_3]$, as a suitable candidate to carry out their investigations because of its high porosity, crystalline structure and the presence of a non-coordinating pendant amino-group on the NH_2-BDC linker. Acetylation of IRMOF-3 with acetic acid was the first attempt of PSM.[35] The reaction starts to occur within hours (formation of AcOH was monitored by ^1H NMR) and after approximately 3 days there is >90% conversion. Next Cohen and co-workers modified stepwise,[36] by first modifying with a group that has latent functionality (crotonic anhydride). The incorporated alkene was then subjected to halogenation with bromine to yield IRMOF-3-AM3Br_2 (**Figure 1.6**). IRMOF-3 has been reacted with a series of isocyanates to generate ureas (**Figure 1.6**).[37]

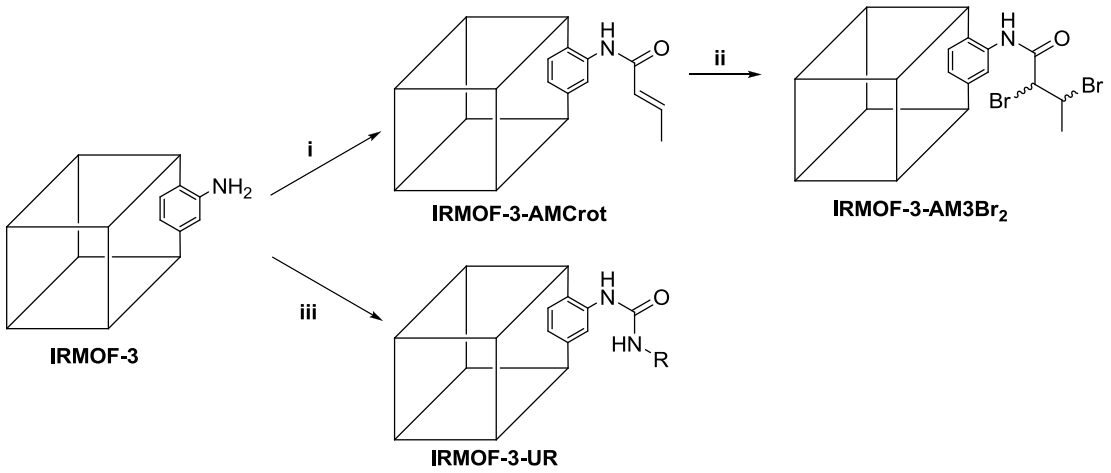

Figure 1.6: Post synthetic modification of IRMOF-3 (i = crotonic anhydride, $CHCl_3$, RT; ii = Br_2, $CHCl_3$, RT; iii = OCN-R, $CHCl_3$, RT, where R = ethyl, propyl, pentyl, allyl, cyclohexyl, phenyl, tert-butyl, TMS).

BTB is a linker that when present in a MOF framework gives structures that are particularly highly porous and have large surface areas. It was first employed in the synthesis of MOF-177,[39] a MOF consisting of BTB linked *via* Zn_4O units which has a surface area of 4500 m^2/g. Matzger *et al*. then used BTB in conjugation with BDC and $Zn(NO_3)_2$ to synthesise UMCM-1 which has a higher surface area of 4730 m^2/g.[40] Cohen *et al*. have taken advantage of the exceptionally porosity of this MOF by synthesising a derivative using NH_2-BDC in the place of BDC so termed UMCM-1-NH_2.[38] These MOFs form the beginning of a new isoreticular series. In a similar fashion to IRMOF-3, the new MOF was subjected to PSM using some simple alkyl anhydrides with high conversion yields (**Figure 1.7**).

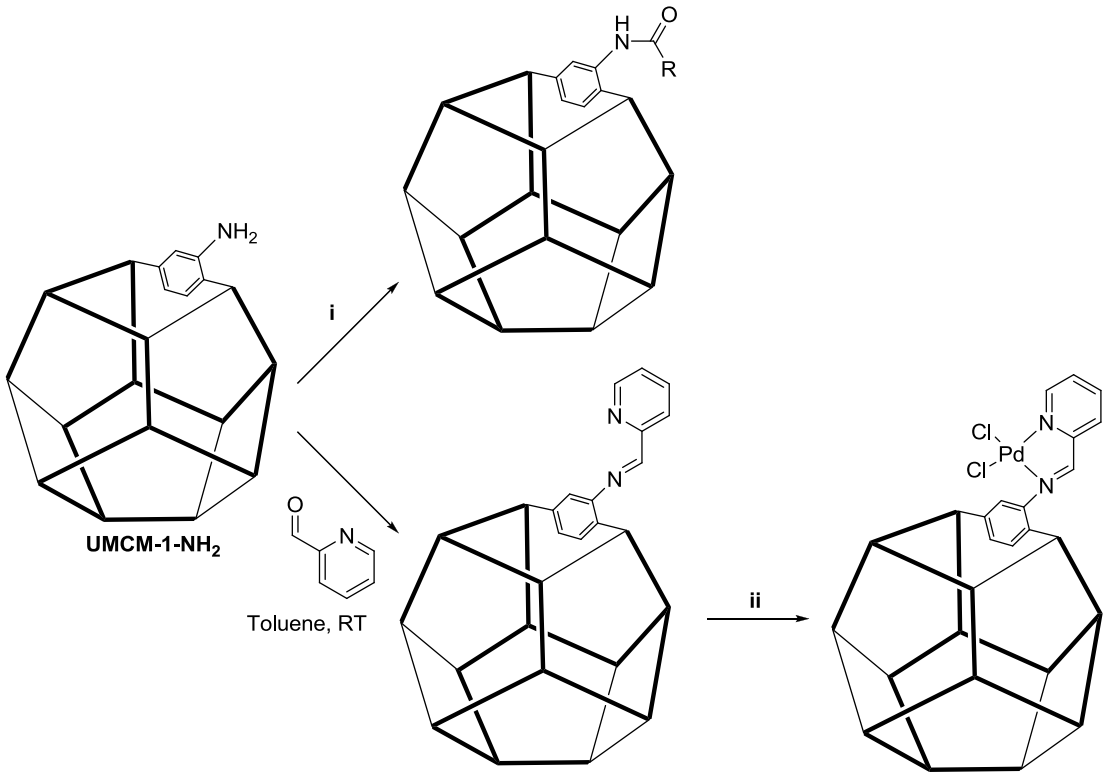

Figure 1.7: Post synthetic modification of UMCM-1-NH_2: i = ($[CH_3(CH_2)_nCO]O$ where n = 0, 2, 4, 8, 12, 18); ii = $Pd(CH_3CN)_2Cl_2$, DCM, RT. BTB represented as bold line.

More interesting is the isoreticular metalation of modified UMCM-1-NH_2 by Yaghi and co-workers (**Figure 1.7**).[41] PSM of UMCM-1-NH_2 with 2-pyridinecarboxaldehyde leads to a bidentate chelating species within the MOF, which when treated with $Pd(CH_3CN)_2Cl_2$ produces the metal-complexed MOF $[(Zn_4O)_3(BDC\text{-}C_6H_5N_2PdCl_2)_3(BTB)_4]$ (**Figure 1.6**). Pd was confirmed to be bound to the iminopyridine unit using EXAFS. Data analysis of the Pd K-edge indicated the presence of two Pd-Cl and two Pd-N ligands at 2.276(2) and 1.993(2) Å respectively.

1.3 Network Geometry

The network geometry of a MOF results from the coordination between the metal ions or clusters and the ligands. A particular coordination mode of a metal ion or the formation of a discrete metal cluster can be predicted when using a certain set of reaction conditions. Metal clusters that become the nodes of the framework are termed secondary building units (SBUs). The metal ions are typically transition metals that can adopt all the standard metal ion geometries such as linear, T-shaped, tetrahedral, square-planar, square-pyramidal,

trigonal-bipyramidal and octahedral; and their pseudo/distorted forms. SBUs consisting of several metals bound together, often by metal-oxygen bonds, can also adopt some of these geometries.

MOF ligands are normally multidentate bridging linker molecules, being at least ditopic and having some rigidity.[31] This means that rigid ligands and their functional group directionality will be in control of the structural topologies during the synthesis.[42] Most ligands are built from an aromatic core providing intrinsic rigidity and they also help prevent structural collapse of the framework upon guest removal. The metal binding sites of the ligand are commonly nitrogen- or oxygen-donor groups (**Figure 1.8**). Ligands can contain purely one type of donating group or a mixture of groups. MOFs can also be formed from two or more different ligands. The length of the ligand, its flexibility and number of binding sites are considered important when selecting a ligand for the synthesis of a certain network.[42]

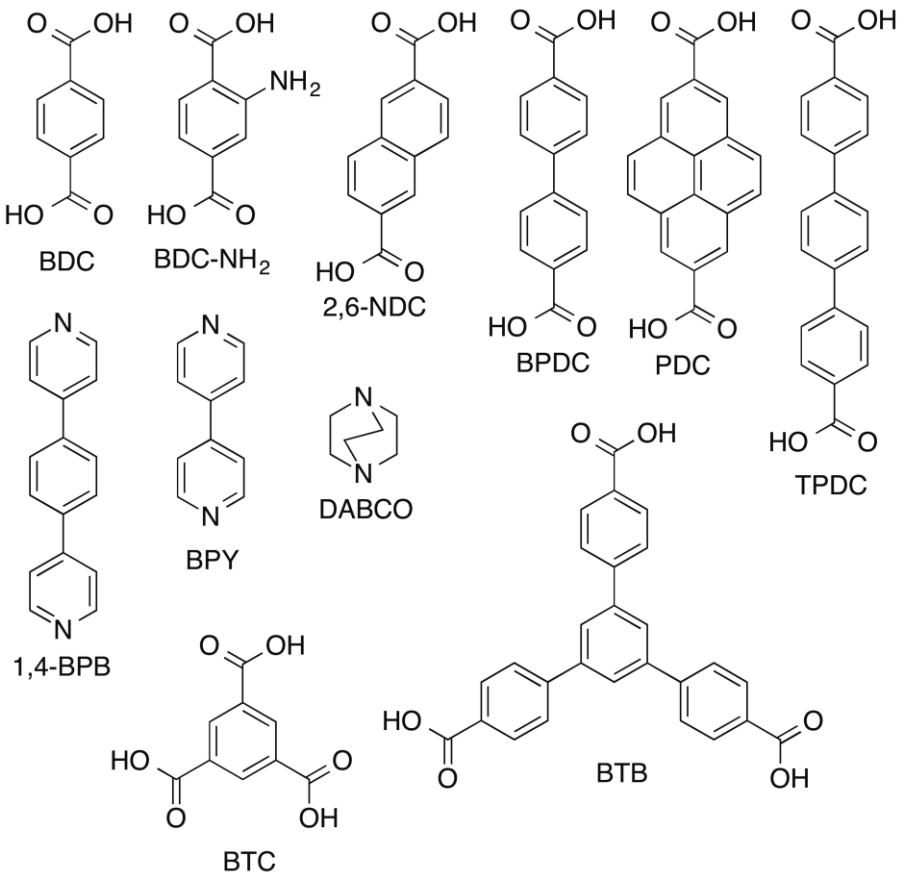

Figure 1.8: Some common ligands used in the synthesis of MOFs.

1.4 Interpenetration

The synthesis of MOFs often leads to porous structures, where the pores or voids are filled by solvent molecules that can be evacuated. However, if there is sufficient space, often another identical framework will grow juxtaposed to the original framework. This phenomenon is known as interpenetration or catenation.[43] The two (or more) frameworks that form are not chemically linked, but the rings of each framework pass through the ring of the other. This can lead to unfavourable results such as dramatically decreased porosity.

High dilution reaction mixtures can be one way of avoiding interpenetration, however even with some small ligand systems such as in the MOFs $[Zn_4(O)(BDC)_3]$ (IRMOF-1 / MOF-5)[44] or even $[Zn_4(O)(ADC)_3]$ (IRMOF-0, ADC = acetylenedicarboxylate)[45] only the doubled interpenetrated versions are formed.

Recently Farha, Hupp and co-workers have reported a method to attenuate interpenetration by ligand design by the judicious choice of ligand (**Figure 1.9**).[46] In a series of zinc paddle wheel SBU based frameworks containing **1** and linear dipyridinyl ligands, interpenetration is observed. When the dipyridinyl ligands have hydrogen-bonding groups or are bulky porphyrins there is no interpenetration observed. From this, sterics were reasoned to be an important factor during the crystal growth as to whether interpenetration occurs. Farha and Hupp then synthesised **2**, which with two bulky bromine atoms replacing the two protons in **1**, adds steric bulk to the ligand. Using the same solvothermal reaction conditions to produce the interpenetrated frameworks with **1**, a series of non-interpenetrated frameworks with **2** were synthesised. A change from aryl-H to aryl-Br is enough to close the opening in which the second framework would grow.

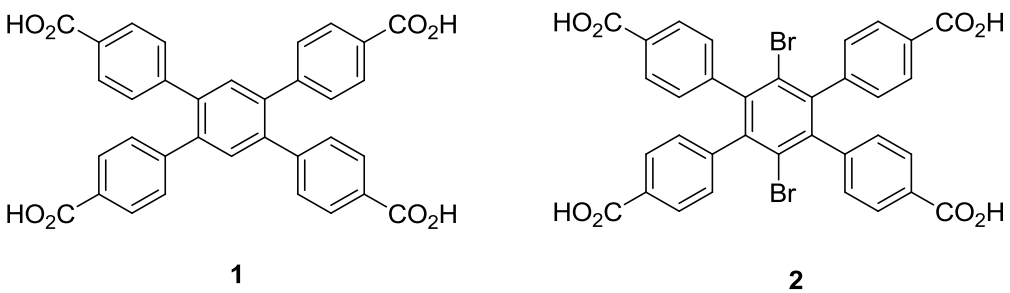

Figure 1.9: Ligands used in a series of interpenetrated and non-interpenetrated MOFs.[46]

1.5 Secondary building units

Secondary building units (SBUs) are molecular complexes and cluster moieties that are linked together by organic ligands to form extended porous networks. The concept of SBUs comes from zeolites structural analysis.[47] The synthesis of MOFs not only relies on the selection of appropriate ligands, but the selection of appropriate ligands with a metal source that is known to form a well-defined SBU under certain reaction conditions. This approach has allowed the synthesis and use of a large number of inorganic SBUs with varying geometries (**Figure 1.10**).

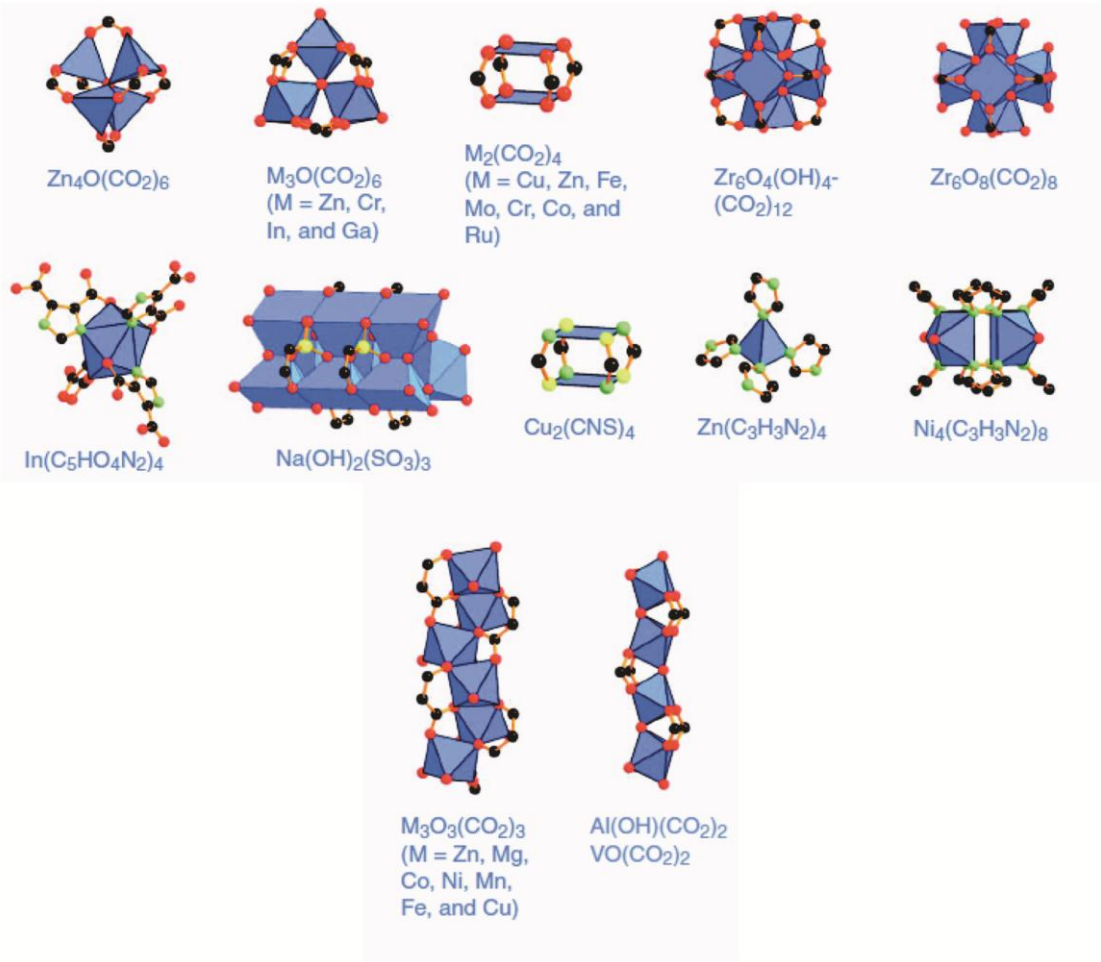

Figure 1.10: Examples of SBUs (carbon [black]; oxygen [red]; nitrogen [green]; sulphur [yellow]; phosphorous [purple]; chlorine [light green]; metal ions [blue polyhedra].[8]

The use of SBUs is attractive because of their steric requirements and rigidity, which reduces the number of possible network topologies arising from a given different node-liner combintion.[48] This is analogous to the aluminosilate zeolite chemistry, where nine SBUs based on tetrahedral AlO_4 and SiO_4 primary building units have been classified.[48]

Although many of the SBUs can be observed in molecular form, they are not generally introduced directly, but these specific SBUs can be generated *in situ* under the specific conditions as mentioned previously.

The most prolific SBUs are Yaghi's $[Zn_4(O)(CO_2)_4]$ pseudo-octahedral basic zinc acetate cluster[49] and the $[M_2(CO_2)_4]$ square-planar paddlewheel (where M = Cu, Zn) (**Figure 1.11**). The paddle wheel can also be octahedral if the apical sites on the metal are bound by solvent molecules or bridging ligands with 2 mono-donor atoms (e.g. 4,4'-bipyridine).

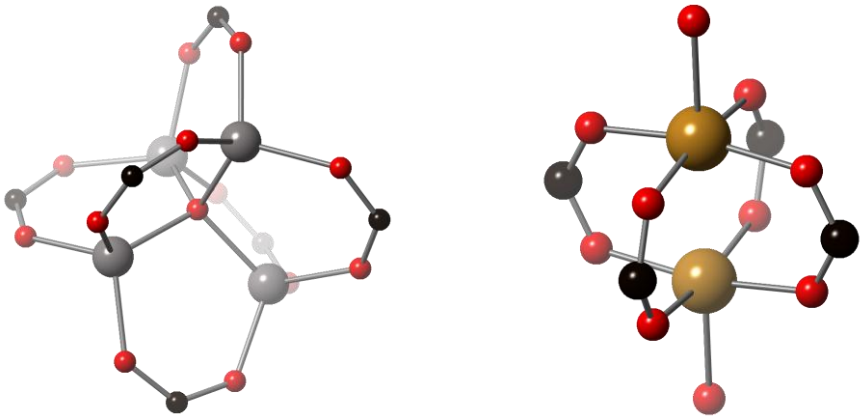

Figure 1.11: Examples of SBUs: zinc acetate cluster (left) and copper paddle wheel (right) (carbon [black]; oxygen [red]; copper [brown]; zinc [grey]).

The zinc-acetate SBU is formed from simple Zn^{II} salts during the synthesis of MOFs containing polytopic carboxylate ligands. At the core of the SBU is a μ_4O bound by four Zn^{II} ions creating a $[Zn_4O]^{6+}$ tetrahedron. The edges of the tetrahedron formed between the zinc ions are then capped by six CO_2 groups from the carboxylate ligands to give $Zn_4(O)(O_2CR)_6$ units. The first example of a MOF with this SBU is the infamous MOF-5 synthesised by Yaghi *et al*.[49] Each $Zn_4(O)$ SBU is linked by a BDC ligand to form a well-defined repeat unit (**Figure 1.12**).

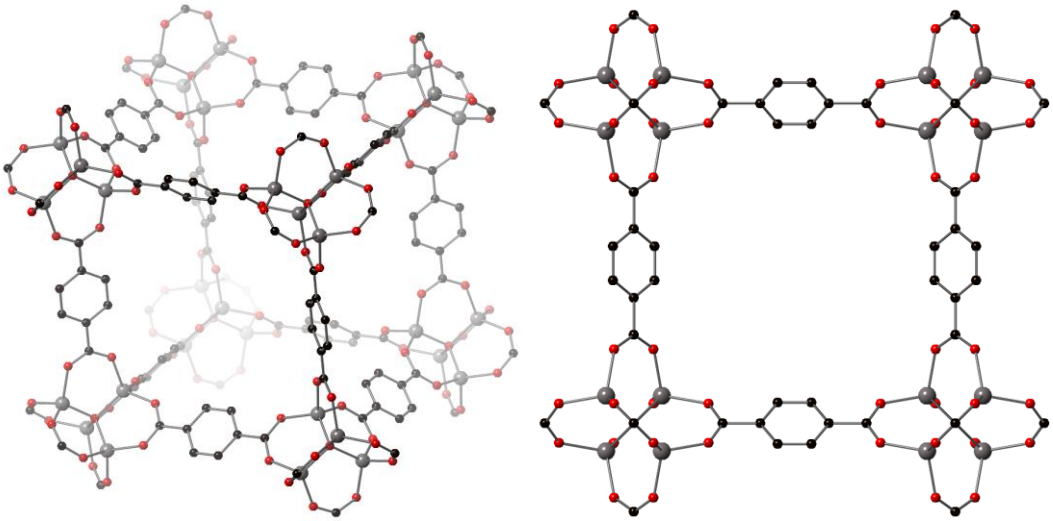

Figure 1.12: The MOF-5 framework: 3D view (left) and view down the a axis (right) (carbon [black]; oxygen [red]; zinc [grey]).

The paddle wheel SBU is formed *in situ* from the combination of M^{II} ions and four carboxylate groups (**Figure 1.13**). The apical site can be bound by a different ligand or by a solvent molecule. For example, Williams and co-workers synthesised the first copper paddle wheel based MOF, $[Cu_3(TMA)_2 \cdot (H_2O)_3]$ (HKUST-1, TMA = benzene-1,3,5-tricarboxylate), in 1999. Each dinuclear copper paddle wheel is bound to a TMA

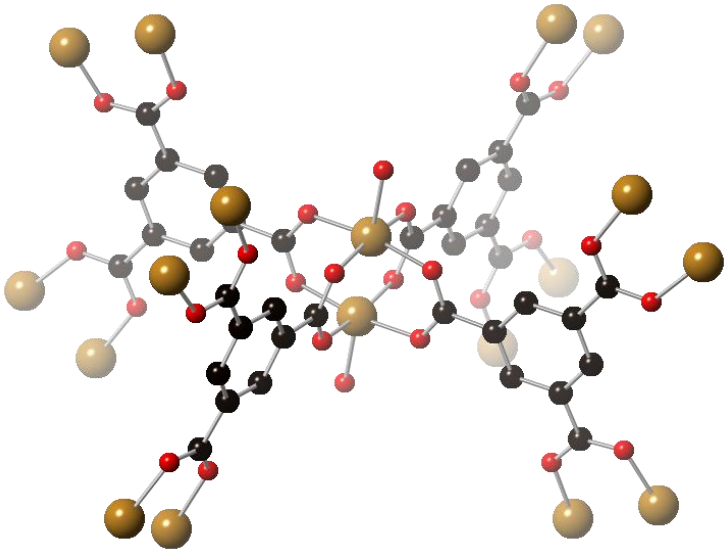

Figure 1.13: Building block unit of HKUST-1 (carbon [black]; copper [brown]; oxygen [red]).

1.6 Reticular synthesis

There has been intense interest in the last two decades in the field of MOFs because rather than just placing a random assortment of metal salt and organic ligand starting materials together and synthesising a material, a level of design and forethought can be applied to MOF synthesis. An appropriate selection of starting materials and conditions can be chosen to result in the desired material. This originates from the concept of well-known SBUs and their *in situ* synthesis from a raw material such as a metal salt as previously discussed.

Reticular synthesis is designing syntheses to produce materials of predetermined ordered structures.[50] This technique was developed as a way of identifying the principles governing the way target frameworks assemble and these principles are then used to develop new frameworks with similar topologies, but with varying functional groups and properties. The prime example of reticular synthesis is the series of 16 isoreticular MOFs (IRMOFs) reported by Yaghi *et al*. (**Figure 1.14**).[51, 52] The IRMOFs have the same underlying topology, similar synthesis conditions, but have different polarity, reactivity and ligand bulk. The series shows how the design of porous structures can be systemically varied to produce materials with different pore sizes and functionalities.[51, 52] The series also introduced the famous yellow ball to represent the pore volume within these materials.

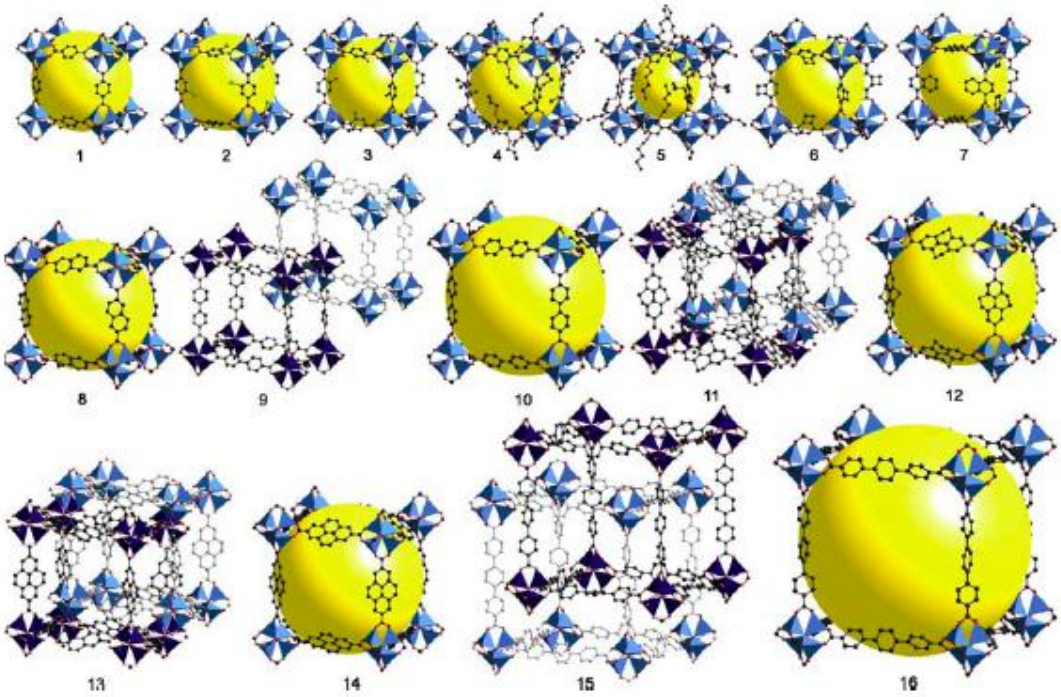

Figure 1.14: A large series of IRMOFS in which each MOF shares the same cubic topology.[51, 52]

1.7 Rigidity, flexibility and stability of MOFs

One of the most interesting features of MOFs, is how they react to loss of guest molecules. The use of multidentate ligands in MOFs leads to stable frameworks, which can be reactive to guest molecules. MOFs can undergo structural transformations after guest molecule accommodation.[48, 53] The characteristic of being able to react to external stimuli, is unique to MOFs when compared to rigid zeolites or activated carbon.

MOFs that exhibit flexibility can undergo reversible structural transformations upon applying external stimuli such as guest molecule removal or inclusion, heat, magnetic and electric fields. Well known examples of flexible MOFs are MIL-53 and MIL-89.[49, 54-57] The flexibility of the framework is advantageous in gas separation applications.[53]

1.8 Examples of MOF chemistry

The following section will present how these concepts come about in the development of coordination polymers and MOFs over the last 10 – 15 years. Where reported in the literature, associated with the MOFs presented, their properties and structural features will

be mentioned. This section is designed to give a broad overview of examples of MOFs and their structures.

MOF chemistry began with metal-organic materials (MOMs). These are coordination complexes that have an open-framework type structure generally with low dimensionality.[58] The concepts introduced by Robson and Hoskins along with simple N-donor chemistry allowed the field to start. For example, 4,4'-bipyridine is a longer analogue of cyanide used by Robson and Hoskins. 4,4'-bipyridine (and its derivatives) have been extensively used to construct MOMs and MOFs. In 1990, Fujita and co-workers synthesised the MOM $[Pd(en)(BPY)]_4 \cdot (NO_3)_8$ (en = ethyldiamine; BPY = 4,4'-bypridine), now known as the famous molecular square.[59] The structure consists of isolated squares of square-planar Pd^{2+} ions and BPY ligands *cis*-capped by en molecules (**Figure 1.15**). More recent work by Fujita has shown that by the use of polytopic N-donor ligands, a number of other low dimensional structures based on *cis*-capped Pd^{2+} ions are possible.[60]

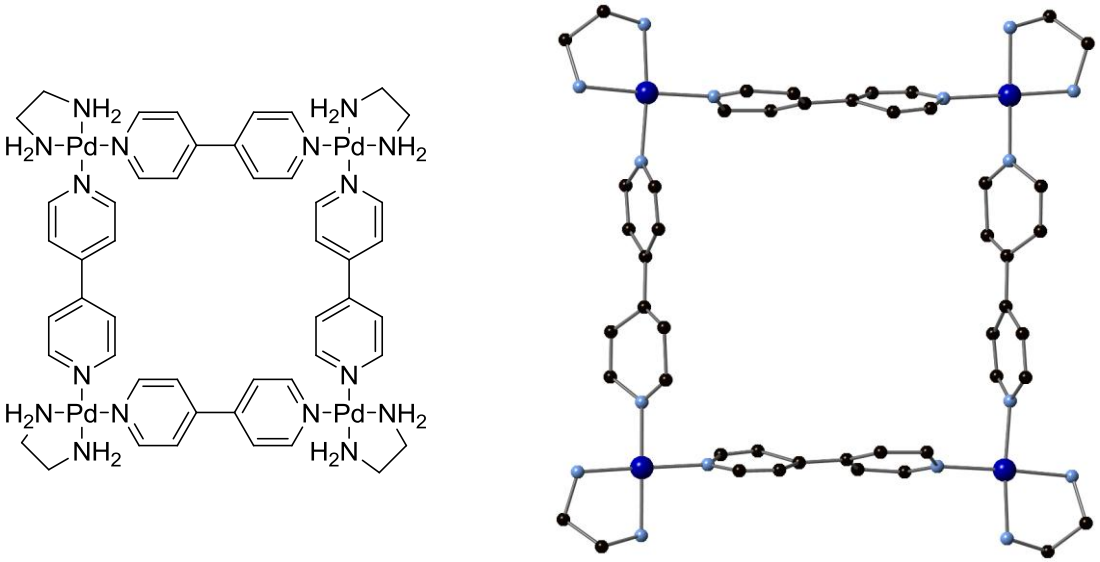

Figure 1.15: Structure of $[Pd(en)(BPY)]_4 \cdot (NO_3)_8$ (carbon [black]; nitrogen [blue]; palladium [dark blue]). Nitrate ions omitted for clarity.

The first use of BPY in a MOF was reported by Yaghi *et al*. in the synthesis of $[Cu(BPY)_{1.5} \cdot NO_3(H_2O)_{1.5}]$ from hydrothermal reaction of a mixture of copper nitrate, BPY and 1,3,5-triazine in water at 140 °C (**Figure 1.16**).[61]

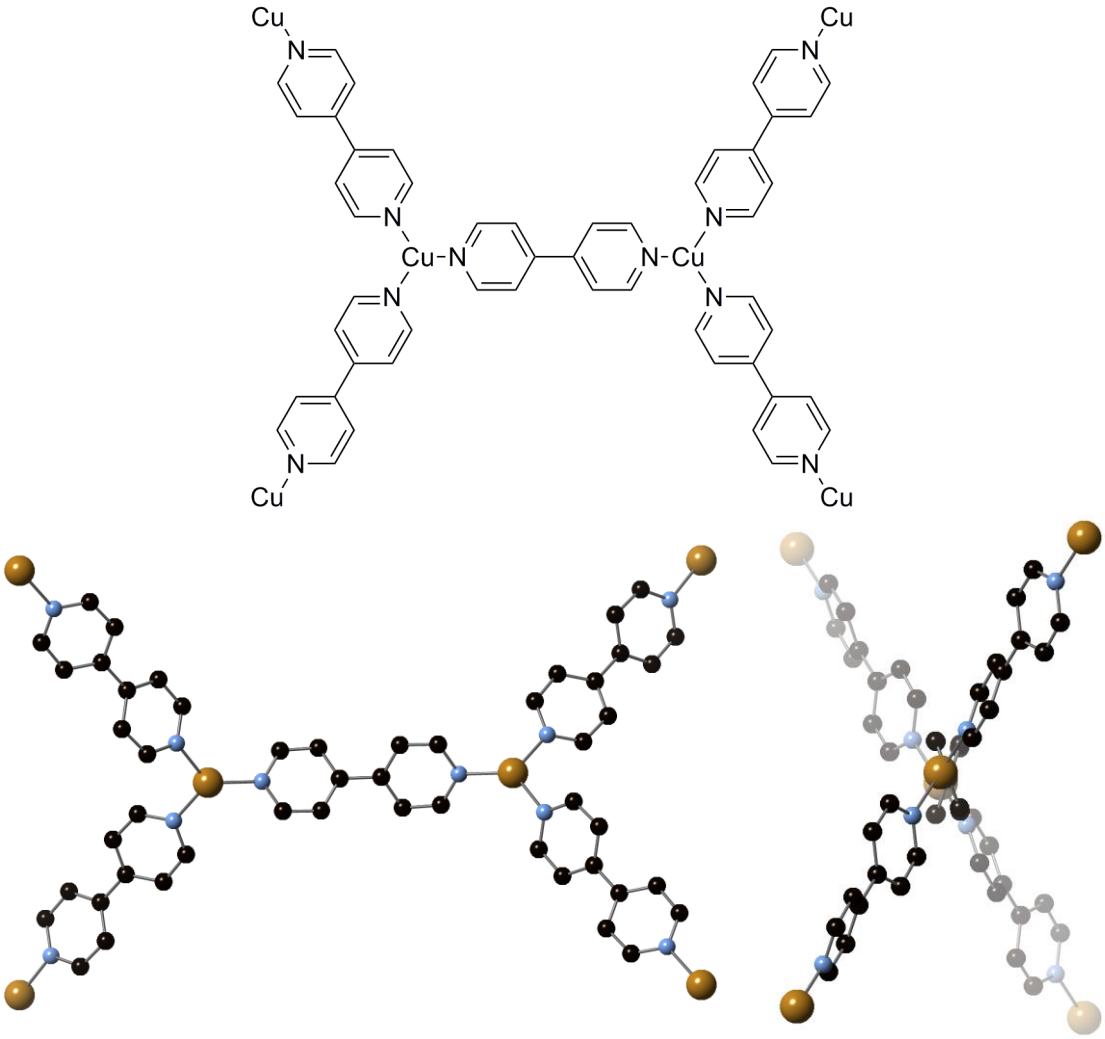

Figure 1.16: Building block unit of $[Cu(BPY)_{1.5}{\cdot}NO_3(H_2O)_{1.5}]$ (left) and view down the *b* axis (right) (carbon [black]; copper [brown]; nitrogen [blue]). Nitrate ions and water molecules omitted for clarity.

Each trigonal-planar copper ion is linked by the coordination of BPY ligands to form a 3D framework. The 3D nature of the framework occurs from the rotation of the BPY ligands around the central C-C bonds and rotation of the two central copper centres (highlighted by bold bonds in **Figure 1.16**). The coordination of neutral BPY ligands results in a framework that is cationic and has six-fold interpenetration. However, the MOF is still porous and contains two different channels of dimensions 8 x 6 Å and 4 x 5 Å, which are filled by nitrate anions and water molecules.

Ligands that contain a mixture of donating groups often consist of pyridinyl rings with carboxylic acid groups.[62-64] These ligands can coordinate to metal ions through both groups to produce MOFs that are often very robust because all of the metal coordination sites are

occupied by the ligand donating groups (and not solvent molecules). Champness, Schröder and co-workers have synthesised the MOF [Zn_2(4,4'-bipyridine-2,6,2',6'-tetracarboxylate)·$4H_2O$ from the hydrothermal reaction of a mixture of zinc chloride, 4,4'-bipyridine-2,6,2',6'-tetracarboxylic acid and 2,6-lutidine in water at 130 °C (**Figure 1.17**).[65]

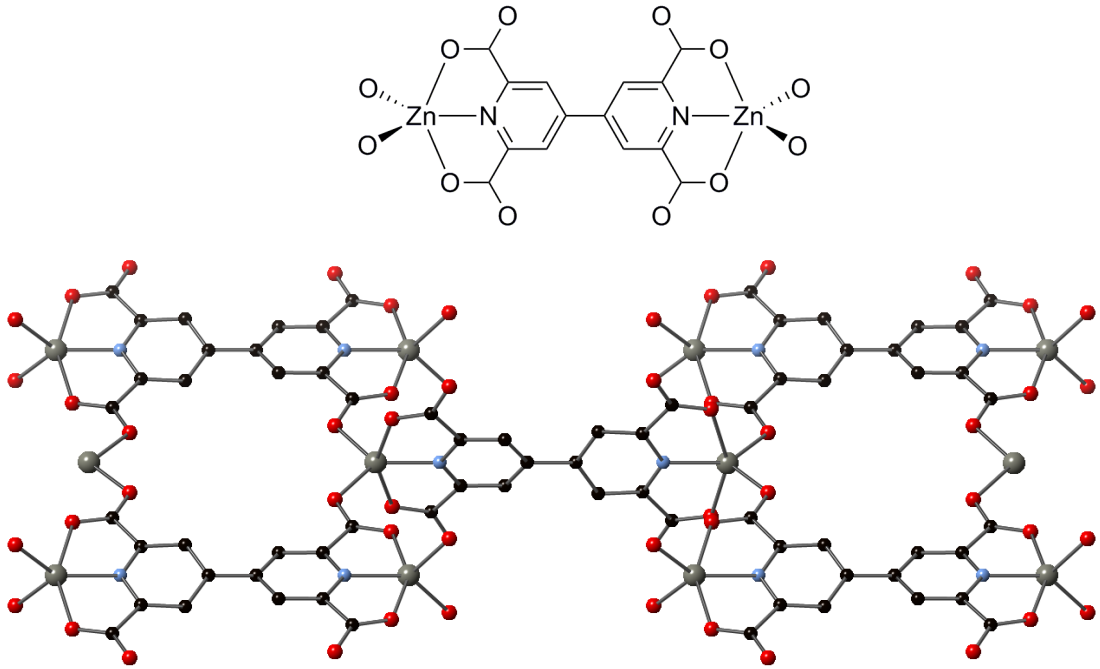

Figure 1.17: Building block unit of [Zn_2(4,4'-bipyridine-2,6,2',6'-tetracarboxylate)]·$4H_2O$ (carbon [black]; nitrogen [blue]; oxygen [red]; zinc [grey]). Water molecules omitted for clarity.

The distorted trigonal-bipyramidal zinc ions are coordinated in a tridentate fashion by two O-donors from the carboxylate groups and the N-donor of the pyridinyl of one ligand. The 3D framework arises from coordination of two O-donors from carboxylate groups of neighbouring ligands. The MOF is porous, but contains water molecules within channels along the *ab* face diagonals. The MOF can be dehydrated by heating in vacuum to give [Zn_2(4,4'-bipyridine-2,6,2',6'-tetracarboxylate)]$_\infty$. This anhydrous material is porous (BET surface area of 312.7 m^2/g), highly thermally stable (decomposes at 450 °C under nitrogen) and chemically inert.

MOFs formed from two different ligands can be made by a pillaring strategy. In this method, 2D grids of carboxylate ligands and metal can be connected together covalently by coordination of ditopic nitrogen heterocycles *via* the metal apical binding sites. The group of Kim have synthesised a series of these pillared MOFs,[66] The first example being the

MOF $[Zn_2(BDC)_2(DABCO)]\cdot 4DMF(H_2O)_{1.5}$.[67] which is synthesised from solvothermal reaction of a mixture of zinc nitrate, terephthalic acid (BDC) and 1,4-diazabicyclo[2.2.2]octane (DABCO) in DMF at 110 °C (**Figure 1.18**).

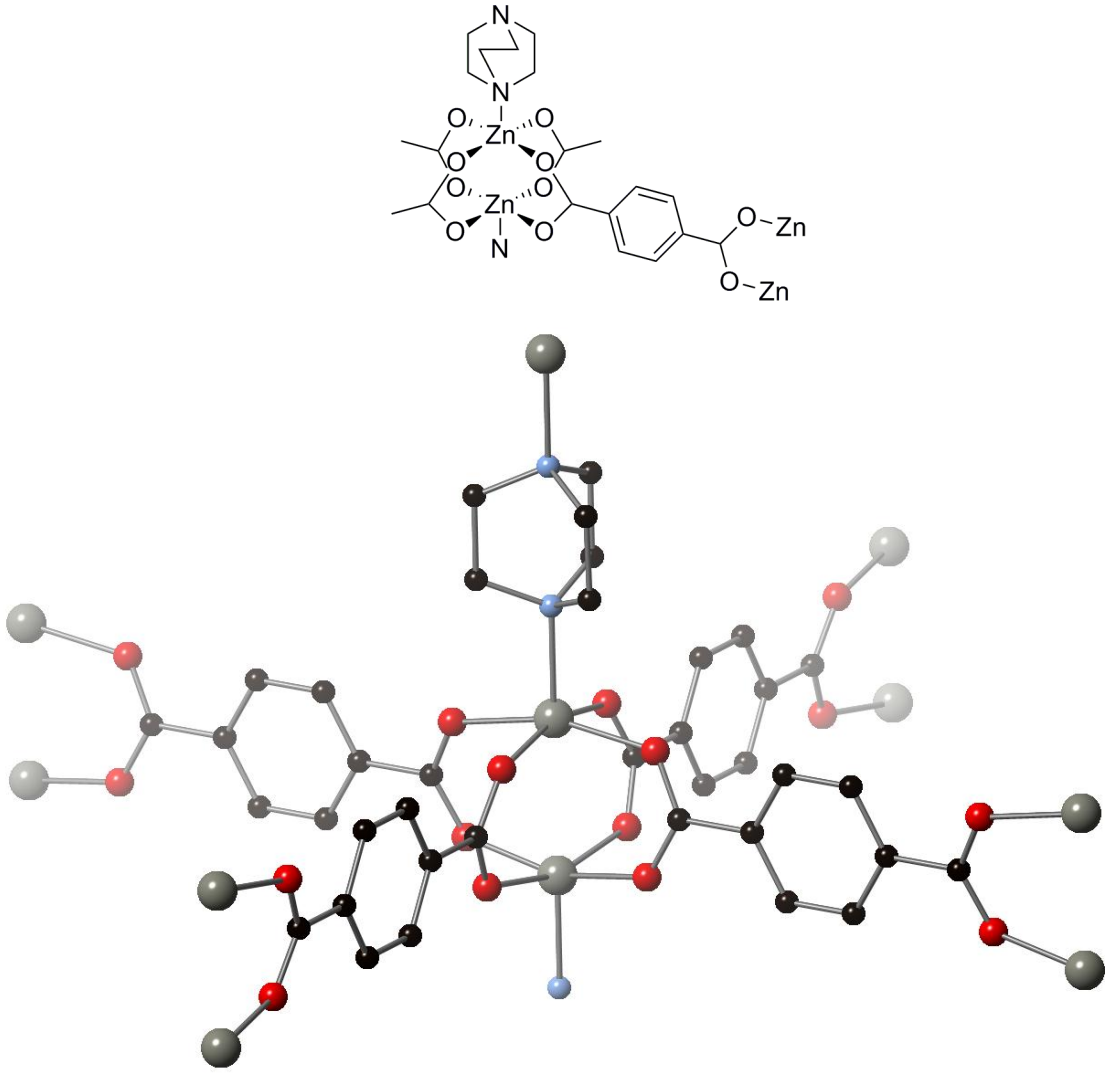

Figure 1.18: Building block unit of $[Zn_2(BDC)_2(dabco)].4DMF(H_2O)_{1.5}$ (carbon [black]; nitrogen [blue]; oxygen [red]; zinc [grey]). Solvent molecules omitted for clarity.

The dinuclear zinc ions are coordinated by the four oxygen atoms from four different terephthalate ligands. The DABCO ligand then forms a coordinative bond with the apical binding site of the zinc, thereby linking the 2D grids of zinc-carboxylate together. The resulting 3D framework has a cubic topology, is porous (BET surface area of 1450 m^2/g) and stable to 300 °C in air.

Other MOFs formed from two different ligands are the University of Michigan Crystalline Materials (UMCM) which are all based on the first MOF in the series, UMCM-1

($[Zn_4(O)(BDC)(BTB)_{4/3}]$) (**Figure 1.19**).[40] All are synthesised in a one-pot synthesis from solvothermal reaction of a mixture of the corresponding terephthalic analogue and BTB analogue in DMF. These MOFs have some of the highest porosities reported (BET surface areas up to 6500 m^2/g).[38, 68, 69]

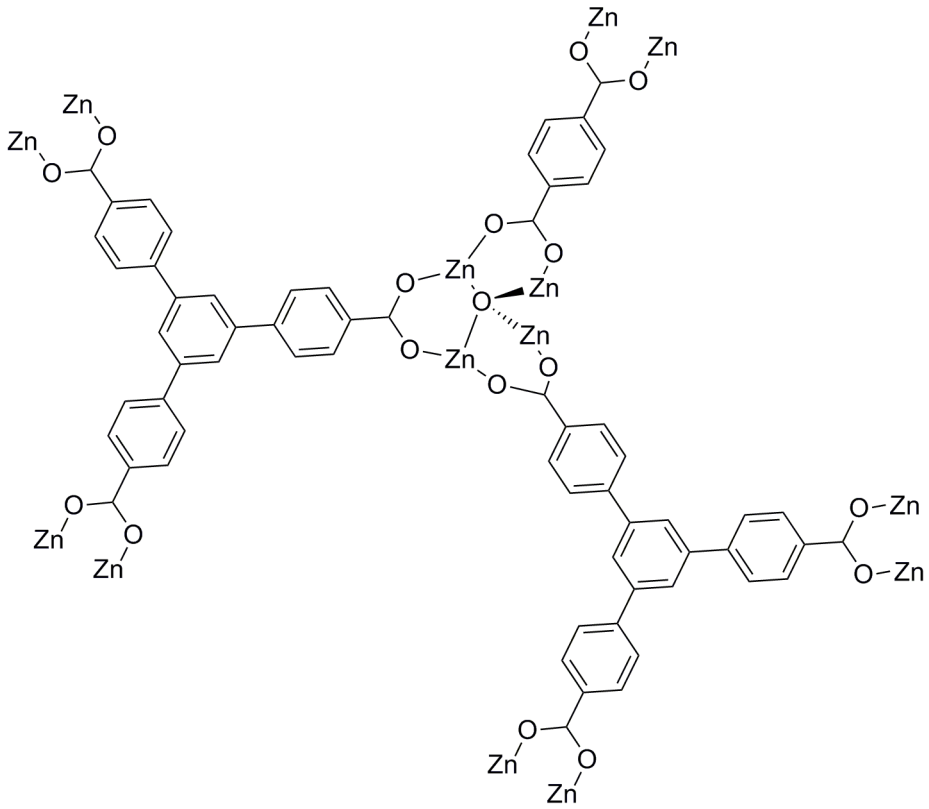
Zn
O
Zn
O
Zn
O
Zn
O
Zn
O
Zn
O
Zn
O
Zn
O
Zn
O
Zn
O
Zn
O
Zn
O
Zn
O
Zn
O
Zn
O
Zn
O
Zn
O
Zn
O
Zn

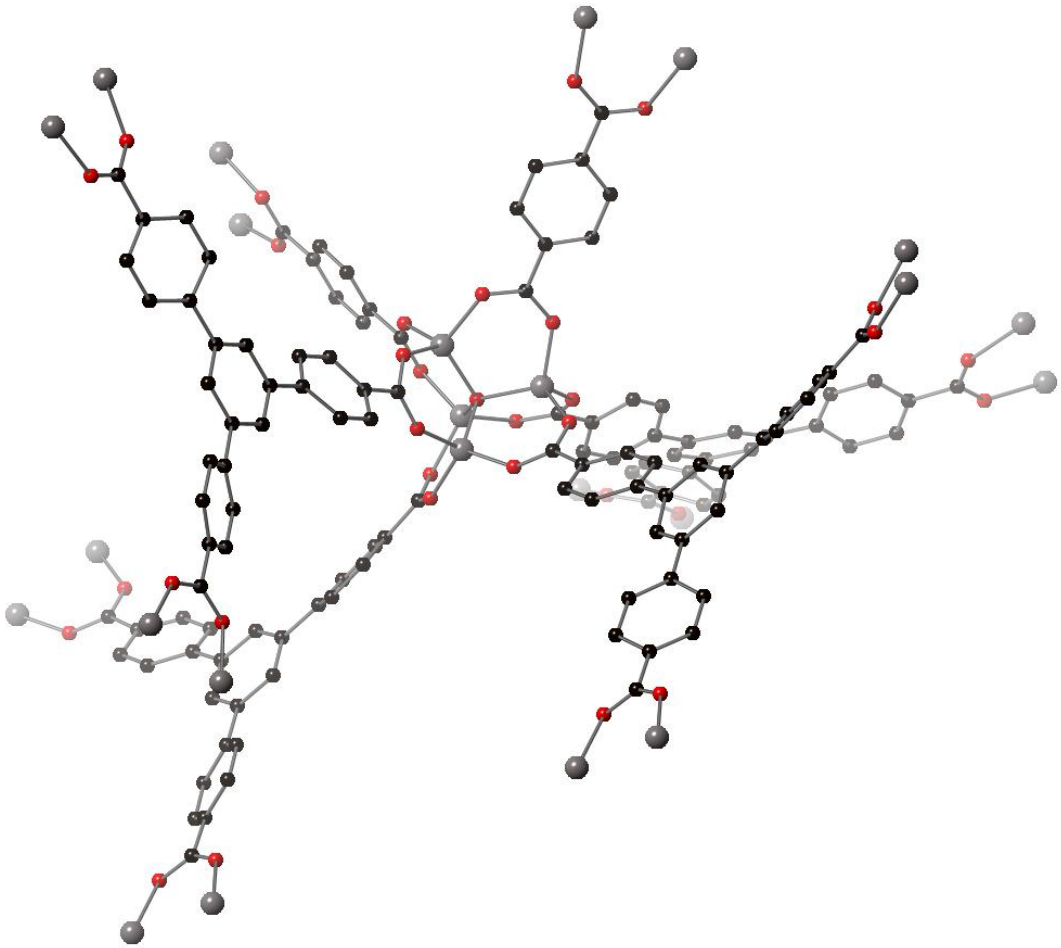

Figure 1.19: Simplified view of $[Zn_4(O)(BDC)(BTB)_{4/3}]$ building block unit (carbon [black]; nitrogen [blue]; oxygen [red]; zinc [grey

In 2008, Lillerud and co-workers reported the synthesis of some ultra-stable MOFs containing dicarboxylates and a novel Zr^{IV} oxide SBU.[70] This was the first report of the $Zr_6O_4(OH)_4(O_2CR)_{12}$ SBU in a MOF. The SBU is 12-coordinated (the highest reported for a MOF) and is key to the stability of the material. It consists of an inner $Zr_6O_4(OH)_4$ core in which the triangular faces of the Zr_6 octahedron are alternatively capped by μ_3-O and μ_3-OH groups.[70] The polyhedra are all bridged by the carboxylate groups of the BDC ligands (**Figure 1.20**).

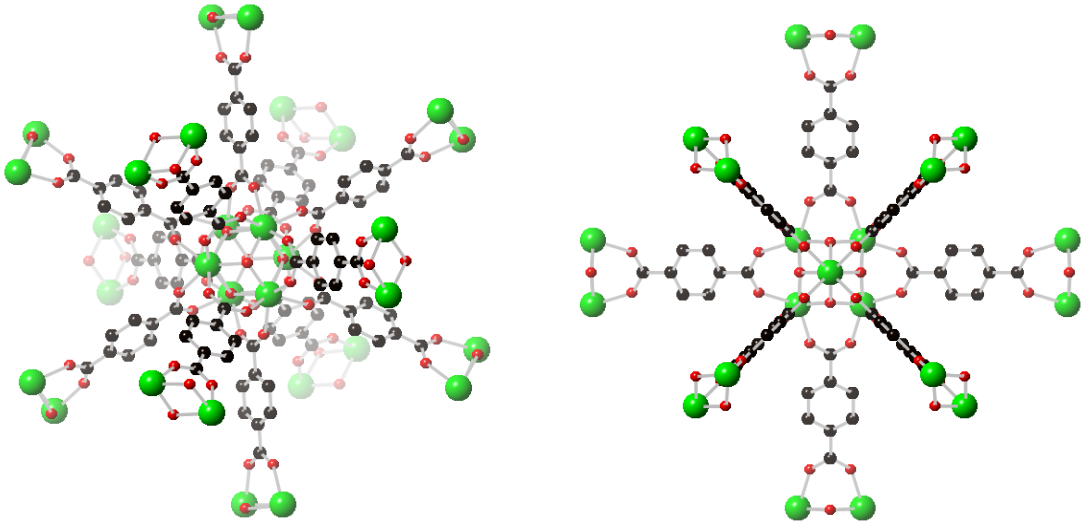

Figure 1.20: Building block unit of UiO-66 (carbon [black]; oxygen [red]; zirconium [green]).[70]

Recently, Champness and Schröder have reported a series of isostructural MOFs formulated as $[Cu_2(L)(H_2O)_2]$ (L = tetracarboxylate ligand).[71] The MOFs are constructed from the Cu_2 paddle wheel SBU linked by tetracarboxylate ligands resulting in a NbO type network of $6^4.8^2$ topology. By changing the ligand in these frameworks, the authors show that the size and shape of the cages within the structure can be influenced. Changing the ligands in the MOFs from the linear bi-phenyl tetracarboxylate to the linear tetra-phenyl tetra carboxylate increases the pore sizes from 8.0 Å and 10 Å to 10 Å and 32 Å in the $Cu_{12}(L)_{12}$ and $Cu_{24}(L)_{12}$ cavities, respectively.[71]

1.9 Properties and Applications

MOFs have a vast array of applications including gas storage, gas separation, magnetic, non-linear optics, biomedical applications and catalysis. [10, 11, 16-21] The synthesis of MOFs is performed in a way that the product exhibits the relevant attributes of the starting materials. Therefore when synthesising MOFs the starting materials should be carefully chosen in order to get the desired properties. Some of the catalytic examples of MOFs will be discussed later in this **Chapter**.

1.9.1 MOFs as heterogeneous catalysts

The immobilisation of homogeneous catalysts to form heterogeneous catalysts has been widely explored as a method of diversifying their practical applications (recovery and reusability).[2] There are three main types of heterogeneous catalytic MOF systems.[17] The first is simply that the MOF is used as a classical catalytic support much like platinum on carbon. Gold, palladium and copper have all been deposited onto MOF-5 to produce a catalytically active species (Au@MOF-5, Pd@MOF-5 and Cu@MOF-5 respectively).[72] In this method the metal precursors were introduced by CVD. Ag@MOF-5 catalyses the epoxidation of propylene with molecular O_2, Pd@MOF-5 was used for the reduction of cyclooctene with H_2 and Cu@MOF-5 was active in the synthesis of methanol from synthesis gas.[17]

Second, a catalytically active centre can be immobilised in the framework. Either the linker in the framework is the active catalyst or an active metal can be tethered to a secondary functionality on a linker. For example, Hupp *et al.*[73] have synthesised the MOF $[Zn_2(BPDC)_2(\mathbf{3})]$ which contains a 2D array of Zn_2 paddle-wheel units linked by the ditopic acid BPDC which are then further linked by the catalytic strut **3** (**Figure 1.21**) to form a 3D network.

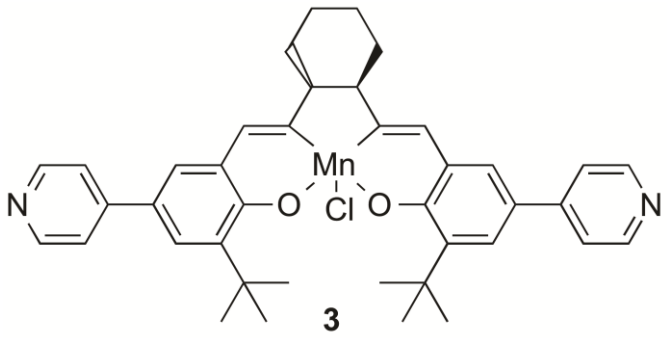

Figure 1.21: Chemical structure of compound **3**.

The MOF shows catalytic activity towards asymmetric epoxidation of 2,2-dimethyl-2*H*-chromene under ambient conditions with 2-(*tert*-butylsulfonyl)iodosylbenzene as oxidant. The catalytic behaviour of free **3** was examined and initially showed high activity, however after a few hours almost all activity was lost. The immobilised **3** showed almost constant reactivity, yielding nearly four times the number of turnovers. It was suggested that loss of catalytic activity arises from oxidation of salen(Mn) by encounters with other catalysts, which cannot occur in the immobilised version, thereby extending the catalyst lifetime. The enantioselectivity of the immobilised **3** was only slightly lower than that of free **3** (82% ee *vs*. 88% ee).

Lin *et al*. have synthesised many MOFs, which contain chiral BINOL-derivatives as bridging linkers.[74-77] The MOF $[Cd_3(\mathbf{4})_3Cl_6]$[74, 75] contains the SBU $[Cd(\mu\text{-}Cl)_2]$ which form a 1D zigzag chain. The SBUs are then bridged with **4**[78] (**Figure 1.22**) *via* coordination to pyridinyl groups to form a 3D network with the largest channel opening of 16 x 18 Å. No interpenetration is observed, even though a relatively long linker is employed.

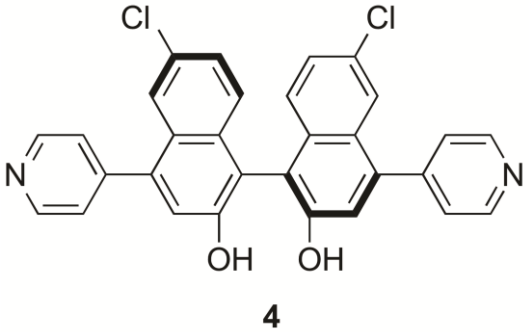

Figure 1.22: Chemical structure of compound **4**.

One third of the orthogonal hydroxyl groups in **4** point into the channels within the MOF. Treatment of $[Cd_3(\mathbf{4})_3Cl_6]$ with $Ti(O^iPr)_4$ allows the readily accessible hydroxyl groups to

coordinate to the Ti and form an analogue of the Lewis acidic (BINOLate)Ti(O^iPr)$_2$ compounds which catalyse $ZnEt_2$ additions to aromatic aldehydes.[79] The activated MOF does indeed catalyse the $ZnEt_2$ addition reactions of four simple aromatic aldehydes (Ar = 1-Naph, Ph, 4-Cl-Ph, 3-Br-Ph) and four large dendritic derivatives at room temperature. The enantioselectivity approximately matches that of the free catalyst and the conversion yields match the free catalyst systems (>99%) for the simple aldehydes. There is however a marked difference in conversion of the dendritic aldehydes. As the size of the aldehyde increases, the conversion yield decreases. This size selectivity suggests that this is a true heterogeneous catalytic process.

In the third type, the SBU is the active catalyst. The coordinated metal(s) in the SBU are effectively immobilised within the assembly of the framework. This allows for coordination species that are unstable or even unknown in the homogenous complex chemistry of the metal allowed because of framework stabilisation. For example, Corma *et al*.[80] have used the porous MOF $[Pd(HPMO)_2]_n$[81] containing the linker 2-hydroxy-pyrimidinolate[82] (HPMO) as the active catalyst for alcohol oxidation, Suzuki C-C coupling and olefin hydrogenation. The synthesis involves the condensation of $[Pd(HPMO)_2Cl_2]$ by refluxing in aqueous solution at pH 6.0 for 5 days. The Pd(II) ions in the MOF all have square-planar geometry and the overall 3D structure is made up from Pd(II) centres connected by HPMO bridges to form 3 different structural motives (**Figure 1.23**).

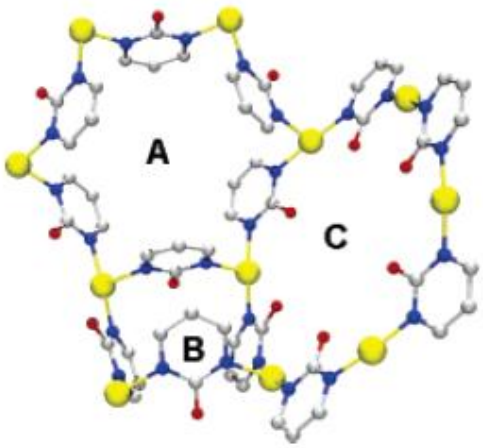

Figure 1.23: Structural motifs found in the crystal structure of $[Pd(HPMO)_2]_n$: metallacalix[6]arene (A), metallacalix[4]arene (B) and planar molecular hexagon (C) (palladium [yellow]; oxygen [red]; nitrogen[blue]; carbon [grey]).

$[Pd(HPMO)_2]_n$ was chosen because the diameters of the two hexagonal cages are 4.8 Å and 8.8 Å (C and A respectively in **Figure 1.22**). The framework has 42% of the crystal volume available for guest inclusion. The structure is thermally stable in air up to 330 °C and is not moisture sensitive. The MOF catalysed the Suzuki-Miyaura C-C cross coupling between phenylboronic and 4-bromoanisole at 150 °C with a good conversion yield (85%) and high selectivity towards the biphenyl product (99%) after 5 hours. Cinnamylalcohol was oxidised to cinnamylaldehyde at room temperature in 20 hours with 74% selectivity – a value close to that reported in the literature for Pd-catalysed oxidations of allylic alcohols.[83] The hydrogenation of 1-octene and cyclododecane was also tested. It was found that 1-octene was completely converted to octane after 40 minutes, but cyclododecane was not hydrogenated at all. This indicates that the smaller alkene was able to diffuse to the active centres inside the MOF, but that the bulkier cyclododecane was not. This is therefore is an example of shape-selective heterogeneous catalysis.

1.10 Aims of this thesis

MOFs exhibit a wide variety of structural types and chemical composition leading to a vast array of properties and potential applications (far more so than traditional porous solids such as zeolites and activated carbon).[7, 31, 49, 84-87] The overall aim of this project is to design and synthesise novel MOFs, where there is the potential to immobilise a catalytically active centre within the framework. It is expected that once a framework has been constructed, metals coukld be tethered to the orthogonal groups of an appropriate ligands. A careful choice of metal is expected is lead to a catalytic MOF system. An analogous scheme to that shown in **Figure 1.11** can then be drawn (**Figure 1.24**).

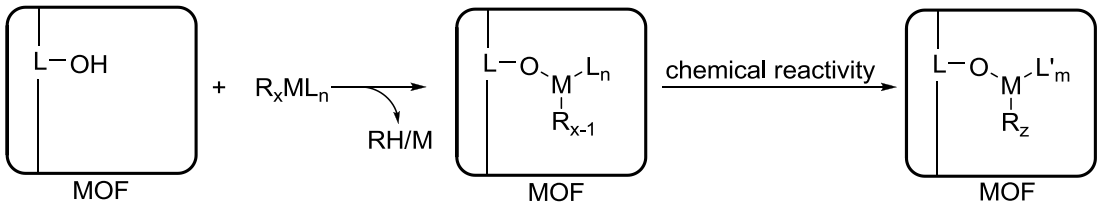

Figure 1.24: General scheme of catalyst (M) binding to a MOF.

Following the successful synthesis of these new MOFs, various characterisation techniques will be employed to investigate their properties.

Reviewing the methodologies in which to do this, the synthesis of homochiral MOFs from chiral ligands is identified as a synthetically reliable approach. This will give MOFs with built in chiral auxiliaries for potential in heterogeneous catalysis.[20]

This will require the synthesis of new MOF ligands, as well as the reuse of appropriate known ligands, for the synthesis of novel MOFs. A systematic investigation into the synthesis of new MOFs using each ligand will be carried out. The properties of newly synthesised MOFs based on their synthesis conditions will also be examined.

Chapter 3 examines the progress in ligand design from structurally simple 1,1'-binaphthalene dicarboxylates to more elaborate binaphthalene polycarboxylates and polypyridinyls. **Chapter 4** reports the use of these ligands in the synthesis of new MOFs. **Chapter 5** reports insights into the self-assembly of some prototypical MOFs.

1.11 References

1. National Research Council (U.S.). Panel on New Directions in Catalytic Science and Technology., *Catalysis looks to the future*, National Academy Press, Washington, D.C., 1992.
2. Z. Wang, G. Chen and K. L. Ding, *Chem. Rev.*, 2009, **109**, 322.
3. R. Xu, *Chemistry of zeolites and related porous materials : synthesis and structure*, John Wiley & Sons (Asia), Singapore ; Hoboken, N.J., 2007.
4. K. S. W. Sing, D. H. Everett, R. A. W. Haul, L. Moscou, R. A. Pierotti, J. Rouquerol and T. Siemieniewska, *Pure Appl. Chem.*, 1985, **57**, 603.
5. J. Rouquerol, D. Avnir, C. W. Fairbridge, D. H. Everett, J. H. Haynes, N. Pernicone, J. D. F. Ramsay, K. S. W. Sing and K. K. Unger, *Pure Appl. Chem.*, 1994, **66**, 1739.
6. A. F. Cronstedt, *Akad. Handl. Stockholm*, 1756, **18**, 120.
7. C. S. Cundy and P. A. Cox, *Chem. Rev.*, 2003, **103**, 663.
8. H. Furukawa, K. E. Cordova, M. O'Keeffe and O. M. Yaghi, *Science*, 2013, **341**, 974.
9. L. Schlapbach and A. Zuttel, *Nature*, 2001, **414**, 353.

10. L. J. Murray, M. Dinca and J. R. Long, *Chem. Soc. Rev.*, 2009, **38**, 1294.
11. R. J. Kuppler, D. J. Timmons, Q. R. Fang, J. R. Li, T. A. Makal, M. D. Young, D. Q. Yuan, D. Zhao, W. J. Zhuang and H. C. Zhou, *Coord. Chem. Rev.*, 2009, **253**, 3042.
12. S. T. Wilson, B. M. Lok, C. A. Messina, T. R. Cannan and E. M. Flanigen, *J. Am. Chem. Soc.*, 1982, **104**, 1146.
13. J. H. Yu and R. R. Xu, *Acc. Chem. Res.*, 2003, **36**, 481.
14. M. E. Davis, *Acc. Chem. Res.*, 1993, **26**, 111.
15. C. Coperet, M. Chabanas, R. P. Saint-Arroman and J. M. Basset, *Angew. Chem. Int. Ed.*, 2003, **42**, 156.
16. J. R. Li, R. J. Kuppler and H. C. Zhou, *Chem. Soc. Rev.*, 2009, **38**, 1477.
17. A. U. Czaja, N. Trukhan and U. Muller, *Chem. Soc. Rev.*, 2009, **38**, 1284.
18. M. Kurmoo, *Chem. Soc. Rev.*, 2009, **38**, 1353.
19. M. D. Allendorf, C. A. Bauer, R. K. Bhakta and R. J. T. Houk, *Chem. Soc. Rev.*, 2009, **38**, 1330.
20. L. Q. Ma, C. Abney and W. B. Lin, *Chem. Soc. Rev.*, 2009, **38**, 1248.
21. A. C. McKinlay, R. E. Morris, P. Horcajada, G. Ferey, R. Gref, P. Couvreur and C. Serre, *Angew. Chem. Int*, 2010, **49**, 6260.
22. J. R. Long and O. M. Yaghi, *Chem. Soc. Rev.*, 2009, **38**, 1213.
23. O. K. Farha, A. M. Spokoyny, K. L. Mulfort, M. F. Hawthorne, C. A. Mirkin and J. T. Hupp, *J. Am. Chem. Soc.*, 2007, **129**, 12680.
24. J. H. Cavka, S. Jakobsen, U. Olsbye, N. Guillou, C. Lamberti, S. Bordiga and K. P. Lillerud, *J. Am. Chem. Soc.*, 2008, **130**, 13850.
25. J. Lee, O. K. Farha, J. Roberts, K. A. Scheidt, S. T. Nguyen and J. T. Hupp, *Chem. Soc. Rev.*, 2009, **38**, 1450.
26. S. R. Batten, N. R. Champness, X. M. Chen, J. Garcia-Martinez, S. Kitagawa, L. Ohrstrom, M. O'Keeffe, M. P. Suh and J. Reedijk, *Pure Appl. Chem.*, 2013, **85**, 1715.
27. B. F. Hoskins and R. Robson, *J. Am . Chem. Soc.*, 1989, **111**, 5962.
28. B. F. Hoskins and R. Robson, *J. Am . Chem. Soc.*, 1990, **112**, 1546.
29. O. M. Yaghi, G. Li and H. Li, *Nature*, 1995, **378**, 703.
30. P. Hubberstey, X. Lin, N. R. Champness and M. Schröder, John Wiley & Sons, Inc., 2010, p. 131.
31. S. L. James, *Chem. Soc. Rev.*, 2003, **32**, 276.

32. A. K. Cheetham, G. Ferey and T. Loiseau, *Angew. Chem. Int*, 1999, **38**, 3268.
33. Z. Q. Wang and S. M. Cohen, *Chem. Soc. Rev.*, 2009, **38**, 1315.
34. S. S. Kaye and J. R. Long, *J. Am. Chem. Soc.*, 2008, **130**, 806.
35. Z. Q. Wang and S. M. Cohen, *J. Am . Chem. Soc.*, 2007, **129**, 12368.
36. Z. Q. Wang and S. M. Cohen, *Angew. Chem. Int. Ed.*, 2008, **47**, 4699.
37. E. Dugan, Z. Q. Wang, M. Okamura, A. Medina and S. M. Cohen, *Chem. Commun.*, 2008, 3366.
38. Z. Q. Wang, K. K. Tanabe and S. M. Cohen, *Inorg. Chem.*, 2009, **48**, 296.
39. H. K. Chae, D. Y. Siberio-Perez, J. Kim, Y. Go, M. Eddaoudi, A. J. Matzger, M. O'Keeffe and O. M. Yaghi, *Nature*, 2004, **427**, 523.
40. K. Koh, A. G. Wong-Foy and A. J. Matzger, *Angew. Chem. Int. Ed.*, 2008, **47**, 677.
41. C. J. Doonan, W. Morris, H. Furukawa and O. M. Yaghi, *J. Am. Chem. Soc.*, 2009, **131**, 9492.
42. C. Janiak, *Dalton Trans.*, 2003, 2781.
43. S. R. Batten, in *Metal-Organic Frameworks*, John Wiley & Sons, Inc., 2010, p. 91.
44. J. Hafizovic, M. Bjorgen, U. Olsbye, P. D. C. Dietzel, S. Bordiga, C. Prestipino, C. Lamberti and K. P. Lillerud, *J. Am. Chem. Soc.*, 2007, **129**, 3612.
45. D. J. Tranchemontagne, J. R. Hunt and O. M. Yaghi, *Tetrahedron*, 2008, **64**, 8553.
46. O. K. Farha, C. D. Malliakas, M. G. Kanatzidis and J. T. Hupp, *J. Am . Chem. Soc.*, 2010, **132**, 950.
47. C. Baerlocher, W. M. Meier and D. Olson, *Atlas of zeolite framework types*, 5th rev. edn., Elsevier, Amsterdam ; New York, 2001.
48. M. Eddaoudi, D. B. Moler, H. L. Li, B. L. Chen, T. M. Reineke, M. O'Keeffe and O. M. Yaghi, *Acc. Chem. Res.*, 2001, **34**, 319.
49. H. Li, M. Eddaoudi, M. O'Keeffe and O. M. Yaghi, *Nature*, 1999, **402**, 276.
50. O. M. Yaghi, M. O'Keeffe, N. W. Ockwig, H. K. Chae, M. Eddaoudi and J. Kim, *Nature*, 2003, **423**, 705.
51. M. Eddaoudi, J. Kim, N. Rosi, D. Vodak, J. Wachter, M. O'Keeffe and O. M. Yaghi, *Science*, 2002, **295**, 469.
52. J. L. C. Rowsell and O. M. Yaghi, *Microporous and Mesoporous Mater.*, 2004, **73**, 3
53. S. Bureekaew, S. Shimomura and S. Kitagawa, *Sci. Techno.l Adv. Mat.*, 2008, **9**.
54. S. S. Y. Chui, S. M. F. Lo, J. P. H. Charmant, A. G. Orpen and I. D. Williams, *Science*, 1999, **283**, 1148.

55. C. Serre, F. Millange, C. Thouvenot, M. Nogues, G. Marsolier, D. Louer and G. Ferey, *J. Am. Chem. Soc.*, 2002, **124**, 13519.
56. T. Chalati, P. Horcajada, R. Gref, P. Couvreur and C. Serre, *J. Mater. Chem.*, 2011, **21**, 2220.
57. F. Millange, C. Serre and G. Ferey, *Chem. Commun.*, 2002, 822.
58. M. Eddaoudi and J. F. Eubank, in *Metal-Organic Frameworks*, John Wiley & Sons, Inc., 2010, p. 37.
59. M. Fujita, J. Yazaki and K. Ogura, *J. Am . Chem. Soc.*, 1990, **112**, 5645.
60. M. Fujita, M. Tominaga, A. Hori and B. Therrien, *Acc. Chem. Res.*, 2005, **38**, 369.
61. O. M. Yaghi and H. L. Li, *J. Am . Chem. Soc.*, 1995, **117**, 10401.
62. P. E. Kruger, E. Tynan, P. Jensen and A. C. Lees, *Chem. Commun.*, 2004, 776.
63. M. H. Zeng, Z. T. Liu, H. H. Zou and H. Liang, *J. Mol. Struct.*, 2007, **828**, 75.
64. D. T. Tran, D. Chu, A. G. Oliver and S. R. J. Oliver, *Inorg. Chem. Commun.*, 2010, **13**, 649.
65. X. Lin, A. J. Blake, C. Wilson, X. Z. Sun, N. R. Champness, M. W. George, P. Hubberstey, R. Mokaya and M. Schroder, *J. Am . Chem. Soc.*, 2006, **128**, 10745.
66. H. Chun, D. N. Dybtsev, H. Kim and K. Kim, *Chem. Eur. J.*, 2005, **11**, 3521.
67. D. N. Dybtsev, H. Chun and K. Kim, *Angew. Chem. Int. Ed.*, 2004, **43**, 5033.
68. H. Furukawa, N. Ko, Y. B. Go, N. Aratani, S. B. Choi, E. Choi, A. O. Yazaydin, R. Q. Snurr, M. O'Keeffe, J. Kim and O. M. Yaghi, *Science*, 2010, **329**, 424.
69. A. J. Matzger, K. Koh and A. G. Wong-Foy, *J. Am . Chem. Soc.*, 2010, **132**, 15005.
70. J. H. Cavka, S. Jakobsen, U. Olsbye, N. Guillou, C. Lamberti, S. Bordiga and K. P. Lillerud, *J. Am . Chem. Soc.*, 2008, **130**, 13850.
71. X. Lin, I. Telepeni, A. J. Blake, A. Dailly, C. M. Brown, J. M. Simmons, M. Zoppi, G. S. Walker, K. M. Thomas, T. J. Mays, P. Hubberstey, N. R. Champness and M. Schroder, *J. Am . Chem. Soc.*, 2009, **131**, 2159.
72. S. Hermes, M. K. Schroter, R. Schmid, L. Khodeir, M. Muhler, A. Tissler, R. W. Fischer and R. A. Fischer, *Angew. Chem. Int. Ed.*, 2005, **44**, 6237.
73. S. H. Cho, B. Q. Ma, S. T. Nguyen, J. T. Hupp and T. E. Albrecht-Schmitt, *Chem. Commun.*, 2006, 2563.
74. C. D. Wu, A. Hu, L. Zhang and W. B. Lin, *J. Am. Chem. Soc.*, 2005, **127**, 8940.
75. C. D. Wu and W. B. Lin, *Angew. Chem. Int. Ed.*, 2007, **46**, 1075.
76. L. Q. Ma and W. B. Lin, *J. Am. Chem. Soc.*, 2008, **130**, 13834.
77. L. Q. Ma, D. J. Mihalcik and W. B. Lin, *J. Am. Chem. Soc.*, 2009, **131**, 4610.

78. S. J. Lee and W. B. Lin, *J. Am. Chem. Soc.*, 2002, **124**, 4554.
79. L. Pu and H. B. Yu, *Chem. Rev.*, 2001, **101**, 757.
80. F. X. L. I. Xamena, A. Abad, A. Corma and H. Garcia, *J. Catal.*, 2007, **250**, 294.
81. J. A. R. Navarro, E. Barea, J. M. Salas, N. Masciocchi, S. Galli, A. Sironi, C. O. Ania and J. B. Parra, *Inorg. Chem.*, 2006, **45**, 2397.
82. L. C. Tabares, J. A. R. Navarro and J. M. Salas, *J. Am . Chem. Soc.*, 2001, **123**, 383.
83. A. Abad, C. Almela, A. Corma and H. Garcia, *Chem. Commun.*, 2006, 3178.
84. M. E. Davis, *Nature*, 2002, **417**, 813.
85. S. Inagaki, Y. Fukushima and K. Kuroda, *Chem. Commun.* 1993, 680.
86. A. Imhof and D. J. Pine, *Nature*, 1997, **389**, 948.
87. T. F. Degnan, G. K. Chitnis and P. H. Schipper, *Microporous and Mesoporous Mater.*, 2000, **35-6**, 245.

2 Materials Techniques

2.1 Introduction

A variety of experimental techniques were used in the synthesis and characterisation of the MOFs reported in this work. The MOFs and coordination polymers presented were synthesised using solvothermal synthesis and characterised using one or combination of the following techniques: single crystal X-ray diffraction, powder X-ray diffraction, infrared spectroscopy and MOF digestion NMR spectroscopy. The main scope of this **Chapter** is to discuss the background of these experimental techniques used in this work. Two techniques (thermogravmetric analysis and surface area and porosity methods) commonly used in MOF chemistry that were not employed in this work, but are relevant to some of the discussion points will be discussed.

2.2 MOF and coordination polymer synthesis

The vast majority of MOFs reported in the literature are synthesised using one of three methods: diffusion techniques, hydrothermal or solvothermal synthesis. Diffusion techniques predominantly take place at room temperature and can involve either diffusion of a counter solvent into a mixture of ligand(s) and metal salt in solvent thereby desolubising metal-ligand complexes in solution as crystalline material (left diagram, **Figure 2.1**). Alternatively, two solvent layers, one containing dissolved ligand and one containing dissolved metal salt, can be carefully layered in a thin tube or vial (right diagram, **Figure 2.1**). This leads to slow diffusion of one layer into the other either resulting in crystal growth at or near the solvent interface.

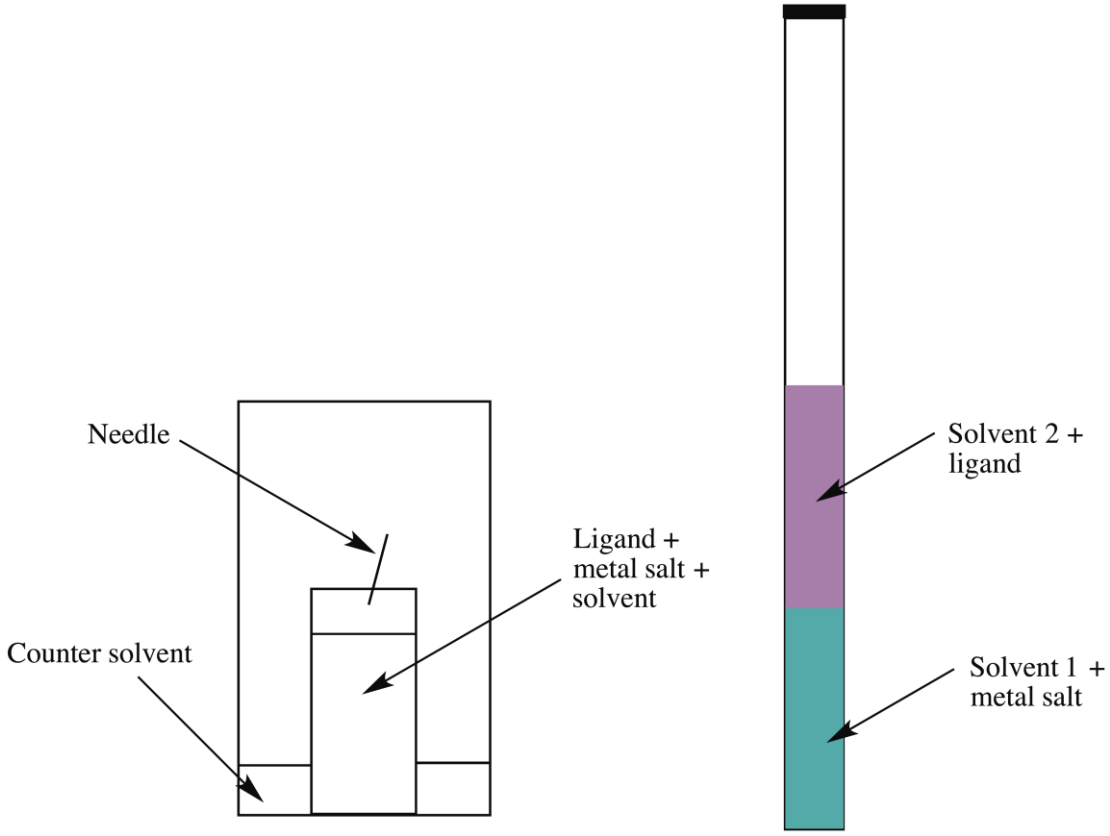

Figure 2.1: Diffusion techniques for MOF and coordination polymer synthesis (left: counter solvent diffusion using a vial in a vial; right: layered diffusion in a tube).

Hydrothermal and solvothermal synthesis both involve high temperatures and pressures in a closed system. Hydrothermal methods use aqueous medium, whereas solvothermal use non-aqueous solvent (or a mix of predominantly non-aqueous solvent with a smaller amount of aqueous solvent). These reactions are typically carried out in autoclave, however due to the smaller synthesis reported in this thesis and their systematic nature, 12 ml scintillation vials were used (**Figure 2.2**).

Figure 2.2: A 12 ml scintillation vial (reproduced with permission from Fisher Scientific©)

2.3 Crystallography[1-6]

A crystal structure can be defined as a particular repeating arrangement of atoms (molecules or ions) and as a lattice exhibiting a long-range order and symmetry. The unit cell is the smallest repeat unit, which shows the full symmetry of the crystal structure. The unit cell can be classified into 4 categories depending on the positions of the lattice points within the unit cell. When the lattice points occupy the corners of the unit cell, the cell is known as a primitive (P) cell. If there is a lattice point in the centre of a primitive cell it is called body centered (I), if there are lattice points in the centre of each face of a primitive cell, it is called face centered (F) and if one additional lattice point at the centre of each of one pair of the cell faces of a primitive cell it is known as base centered (A, B or C).

The size and the shape of the unit cell is described in terms of its unit cell parameters. These are the edge lengths (a, b and c) and the angles of the unit cell (α, β and γ). There are 7 possible combinations of lengths and angles, which give rise to seven crystal systems (**Figure 2.3** and **Table 2.1**).

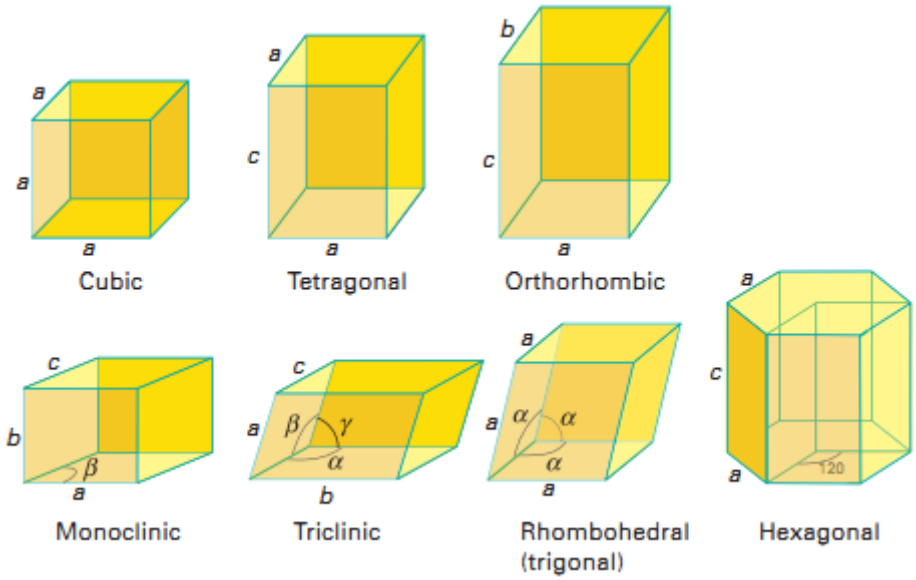

Figure 2.3: The seven crystal systems (reproduced with permission from http://chemistrytextbookcrawl.blogspot.co.uk).

Table 2.1: The seven crystal systems.

Name	Hermann-Mauguin group names	Axis orientation	Unit cell parameter restrictions
Triclinic	1, $\bar{1}$		$a \neq b \neq c$, $\alpha \neq \beta \neq \gamma \neq 90°$
Monoclinic	2, m, 2/m	b || to C_2	$a \neq b \neq c$, $\alpha = \gamma = 90° \neq \beta$
Orthorhombic	222, mm2, mmm	a, b, c || to $3C_2$	$a \neq b \neq c$, $\alpha = \beta = \gamma = 90°$
Rhombohedral	$\bar{3}$	S_3 || to body diagonal	$a = b = c$, $\alpha = \beta = \gamma \neq 90°$
Tetragonal	4, $\bar{4}$, 4/m, 422, 4mm, $\bar{4}$2m, 4/mmm	c || to C_4	$a = b \neq c$, $\alpha = \beta = \gamma = 90°$
Hexagonal	6, $\bar{6}$, 6/m, 6222, 6mm, $\bar{6}$m2, 6/mmm	c ||to C_6	$a = b \neq c$, $\alpha = \beta = 90°$, $\gamma = 120°$
Cubic	23, m$\bar{3}$, 432, $\bar{4}$3m, m$\bar{3}$m	a, b, c || to $3C_4$	$a = b = c$, $\alpha = \beta = \gamma = 90°$

The number of lattices that can fill 2D or 3D space with periodically repeating units without leaving gaps or overlaps is limited. These so called Bravais lattices are distinct lattice types which when repeated fill the whole space. There are 14 Bravais lattices (**Table**

2.2) formed by a combination of the crystal systems and the lattice types. All crystal structures have translational symmetry. In addition, it is possible to have point symmetry or symmetry which has both point and translational symmetry. The elements of point symmetry which can be observed in crystal systems are rotation axes, inversion axes and mirror planes. The elements of point and translational symmetry are screw axes (rotation + translation) and glide planes (reflection + translation). These symmetry elements may occur either alone or in combination to give a total of 32 possible crystallographic point groups. The combination of possible symmetry operators within the 14 Bravais lattices results in 230 space groups. Space groups are mathematical descriptions of the symmetry, to which all crystalline materials belong.

Table 2.2: Bravais lattices

Crystal system	Lattice centering possible
Triclinic	P
Monoclinic	P, C
Orthorhombic	P, C, I, F
Rhombohedral	P, I
Tetragonal	P
Hexagonal	P
Cubic	P, I, F

There is a specific notation for describing space groups: the first descriptor defines the lattice type (P, B, F, I); the following descriptors describe the point group symmetry of which the principal axis (if present) is noted first. For the remaining characters, different rules apply for different crystal systems. Each space group is fully described in the International Tables for Crystallography.[7, 8]

The asymmetric unit is the smallest part of the crystal structure, which cannot be projected on to it by applying symmetry operations. On applying symmetry operators to the asymmetric unit gives all the atomic positions within one unit cell. On repeating the unit cell this gives all atomic positions in the crystal.

2.3.1 X-ray diffraction

As crystals have a regular repeating structure they can diffract radiation that has a wavelength similar to the interatomic distances. X-rays have a wavelength in the order of a few Angstroms, which is comparable to typical interatomic distance in crystalline solids. When X-rays are scattered from a crystal lattice, the scattered/diffracted beams can interfere either constructively or destructively. Only the reflected beams that satisfy the following conditions are in phase and interfere constructively are observed (**Figure 2.4**) the angle of incidence = angle of scattering and 2) the path length difference is equal to an integer number of wavelength.

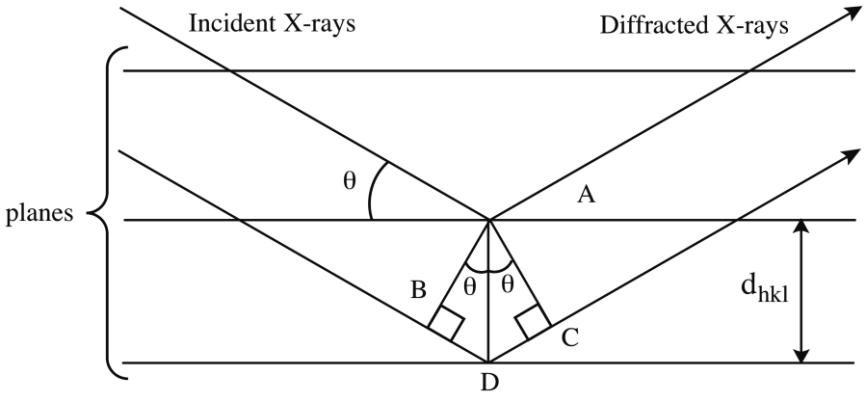

Figure 2.4: Derivation of Braggs law through X-rays reflecting off adjacent planes

The scattering of the incident X-rays from points A and D in the neighboring planes will produce in phase diffracted X-ray beams (constructive interference) if the additional distance travelled by the X-ray photon scattered from D is a n integer number of wavelengths. This path difference BD + DC will depend on the lattice spacing d_{hkl}, where *hkl* are the Miller indices for the planes under consideration, and will also be related to the angel of incidence of the X-ray beam, θ. for an integral wavelength pathlength difference the following relationship between θ and d_{hkl} can be obtained:

$$\text{Path difference} = = \text{BD} + \text{DC} = 2d_{hkl}\sin q = nl \qquad (2.1)$$

Where,

d = inter-plane distance

θ = scattering angle

n = integer representing the order of the diffraction peak

λ = wavelength of the X-ray beam

This is known as Bragg's law and shows that the diffraction angle ($sin\theta$) is inversely related to the lattice spacing (d) in a crystalline sample.

2.3.2 Single crystal method[3, 6]

Single crystal X-ray diffraction is a non-destructive analytical technique, which provides detailed information to facilitate the determination of the structure of a material. The information collected includes; crystal symmetry, unit cell dimensions, details of site-ordering, atomic positions and space group. These unit cell parameters can be used to verify if a structure is new or known in the literature by comparing this data with online databases.[9]

A Bruker Nonius KappaCCD was used to collect the data presented in this thesis. For single crystal XRD work, a suitable crystal had to be selected; one with straight edges, which extinguishes light uniformly under polarised light, was chosen. The crystal was picked up on a pip using silicon oil and rapidly transferred to the instrument and placed immediately under a flowing stream of liquid nitrogen. The crystal is mounted in the instrument such that all orientations of the lattice planes can be accessed by changing the geometry of the incident X-rays as well as the orientation of the crystal in relation to the detector. Once a data set is collected, the data is integrated to correct intensities for each hkl value. *hkl* values are assigned to each spot in the diffraction pattern. The data is also corrected for adsorption and polarization. The experimental intensity data is related to the structure factor by the following equation:

$$I \propto |F(hkl)|^2 \qquad (\mathbf{2.2})$$

The structure factor is a function that describes the amplitude and phase of a wave diffracted from crystal lattice planes characterized by Millar indices *h, k, l.* The structure factor can be expressed in the following equation:

$$F_{hkl} = \sum_j f_j^{'}.\exp[2\pi i(hx_j + ky_j + lz_j)] \qquad (\mathbf{2.3})$$

The intensity of a diffracted beam is directly related to the amplitude of the structure factor, but the phase must normally be deduced by indirect means. In structure determination, phases are estimated and an initial description of the positions and anisotropic displacements of the scattering atoms is deduced. From this initial model, structure factors are calculated and compared with those experimentally observed. Iterative refinement procedures attempt to minimise the difference between calculation and experiment, until a satisfactory fit has been obtained. This is known as the phase problem. On solving the phase problem a unique set of phases is obtained which, when combined with the structure factors, allows the diffraction data to be converted into a 3D map of electron density. There are two methods for solving the crystal structures using the electron density map, the Patterson method and direct methods.

2.3.3 Patterson Methods[1-3]

This method is usually used when the unit cell contains heavy atoms. The peaks in the Patterson map are the interatomic distances; their weights are proportional to the product of the electron densities at the tips of the vectors in the real cell. In this method, the amplitude of the square of the structure factor, which is taken from the diffraction data, is used to overcome the phase problem as shown in the following expression:

$$Puvw = \frac{\sum_{hkl} \left|F_{hkl}\right|^2 \cos 2\pi\left(hu + kv + lw\right)}{v} \qquad (\mathbf{2.4})$$

2.3.4 Direct methods[1-3]

This method is the most commonly used to determine the crystal structures. It deals with the structure factor phases directly from the observed F_{hkl} using mathematical models. This method is derived based on two main properties of electron density function. They are:

- Electron density is always positive
- It is composed of discrete atoms

The principle of positivity of electron density may be extended to three dimensions and given below:

$$s(h_1 s(h_1 k_1 l_1) s(h_2 k_2 l_2) \approx s(h_1 + h_2, k_1 + k_2 + k_2, l_1 + l_2) \qquad (\mathbf{2.5})$$

where,

s = sign of the phase in question

(h_1,k_1,l_1), (h_2,k_2,l_2), (h_1 + h_2, k_1 + k_2, l_1 + l_2) = strong reflections

It is often possible to derive phases for almost all strong reflections and to determine the structure from the resulting electron density map, although there are limitations to the possible phase angles for individual reflections.

2.3.5 Structure refinement[1]

Once a suitable model has been constructed the model is refined to a best fit of the experimental data using a least squares refinement program. The structure solution program SHELXL-97[10] has been used to carry out the least squares refinement. This program compares the calculated intensities from the structural model with the experimentally measured intensities in order to obtain the best model to minimize M:

$$M = \sum w(F_o^2 - F_c^2)^2 \qquad (\mathbf{2.6})$$

Where,

M = minimisation function

w = weighing factor

F_o = observed structure factor

F_c = calculated structure factor

The quality of the model is determined by using various residual factors, which are known as *R*-factors. The *R*-factor should attain a minimum during the refinement. The weighted *R*-factor is given by the following equation:

$$wR = \left[\frac{\sum w(F_o^2 - F_c^2)^2}{\sum w(F_o^2)^2} \right] \quad (\mathbf{2.7})$$

The un-weighted residual factor *R* can be obtained from the *F* values as follows:

$$R = \frac{\sum \| F_o | - | F_c \|}{\sum | F_o |} \quad (\mathbf{2.8})$$

Based on F^2 the goodness of fit, GoF or *S* can be obtained as follows:

$$S = \left[\frac{\sum w(F_o^2 - F_c^2)^2}{(N_R - N_P)} \right]^{-0.5} \quad (\mathbf{2.9})$$

Where,

N_R = number of independent reflections

N_P = number of refined parameters

Once the refinement is complete the goodness of fit should be close to 1.0. A goodness of fit of $S < 1$ suggests that the model is better than the data. The R index for *F* should be below 5%. However it is possible to get a low *R*-value although the structure is not correct therefore it is always important to make sure that the structure makes chemical sense with sensible bond lengths, bond angles and site occupancy.

2.3.6 Powder X-ray diffraction method[6]

Powder X-ray diffraction is a rapid analytical technique, which is used for characterisation of crystalline materials. The sample is typically a powdered (polycrystalline) material, which is composed of many small crystallites, thus it is possible that more than one crystal can satisfy Bragg's law. Hence from a powder, the diffracted beams are cones of diffraction from the Miller planes (*hkl*), which resemble rings on the screen. These rings can be indexed and integrated to obtain a powder pattern. This technique is primarily used for phase identification as the powder pattern can be seen as a fingerprint of a specific structure. The resultant experimental patterns recorded were compared with simulated

patterns from solved single crystal data to check for sample purity. The experimental data was compared with known powder diffraction patterns in the literature to find out whether novel structures had been prepared. Analysis of PXRD powder patterns was carried out using WinXPow software.

Powder X-ray diffraction patterns were collected on a Siemens D5000 powder diffractometer using a copper anode, which produced monochromated, X-rays at 1.5406 Å.

2.4 Infrared spectroscopy[11]

Fourier transform infrared (IR) spectroscopy is one of the most common spectroscopic techniques used by organic and inorganic chemists. Infrared radiation is passed through the sample and a detector measures the energy of the transmitted radiation. Examination of this transmitted light shows how much energy has been absorbed at each wavelength. The spectrum produced shows at which particular wavelength the sample absorbed which in turn reveals details regarding the molecular structure of the material since different functional groups absorb at known characteristic frequencies. IR is used here to determine the types of functional groups present in the MOFs and also can be used as an indicator of moisture content in a MOF sample.

The concept is based on the notion that most adsorptions occurring at different energies, which in turn correspond, to the energies involved in bond vibrations. In covalent bonds, atoms are not joined by rigid links. The two atoms are held together because both nuclei are attracted to the same pair of electrons. Such nuclei can have movements, which are known as molecular vibrations. For example in a diatomic molecule the two atoms are joined by a covalent bond, which can undergo a stretching vibration where the atoms move back and forth. These stretching vibrations can be either symmetric or asymmetric (**Figure 2.5**). In addition to stretching vibrations, polyatomic molecules can have bending type vibrational modes (**Figure 2.5**).

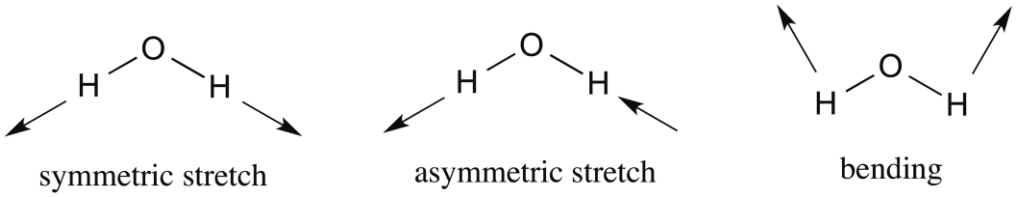

Figure 2.5: Stretching and bending modes of a H_2O molecule.

The stretching frequency of a bond is related to the masses of the two atoms involved in the bond and to the bond strength. The strength of a bond is related to its force constant. The stretching frequency of a bond in a diatomic molecule can be given in the following equation:

$$\bar{\nu} = \frac{1}{2\pi c}\left[\frac{f(m_1+m_2)}{m_1 m_2}\right]^{0.5} \qquad \textbf{(2.10)}$$

where,

$\bar{\nu}$ = frequency (cm^{-1})

c = velocity of light

f = force constant (Nm^{-1})

m_1,m_2 = masses of two atoms

In this work, IR spectra were collected on an Infrared spectra were recorded on a Matterson Satellite (ATR). The IR spectra gave an insight into the nature of the functional groups of the organic linker molecules forming the framework structure of the MOFs.

2.5 MOF Digestion and NMR

Nuclear Magnetic Resonance (NMR) spectroscopy is another form of absorption spectroscopy, whereby the energy of radio waves are absorbed by nuclei in the molecule, when placed in a strong magnetic field. The theory behind NMR will not be discussed here, only its application in this technique. The post-synthetic modification of MOFs[12-15] has been discussed in **Chapter 1**. The extent of the post synthetic modification can be monitored and confirmed by digesting a sample of MOF crystals in deuterated DCl/D_2O

and measuring a ^{1}H NMR spectrum. To do this, the MOF crystals/sample are processed in the following way:

1. The reaction vessel is removed from the reaction heat source and cooled to room temperature
2. The mother liquor is decanted and the crystals are immersed in flesh solvent
3. This process is replaced several times (typically 3) to remove unwanted reactants
4. The solvent is decanted for a final time and the sample dried under vacuum
5. The dry crystals are sonicated in a dilute DCl/D_2O solution or dilute HCl/H_2O/DMSO-d_6 solution to digestion them
6. A ^{1}H NMR spectrum is measured

As the MOF ligands react within the MOF crystals during post-synthetic modification, ^{1}H NMR can identify the resulting compounds that will be formed upon digestion. As a reaction proceeds both the original MOF ligand and chemically altered ligand will have reformed and thus be present in the ^{1}H NMR spectrum. When the post synthetic modification reaction has gone to completion, no starting MOF ligand should be present in the ^{1}H NMR spectrum, only 100% of the newly formed ligand.

2.6 Thermogravmetric analysis

Thermogravmetric analysis (TGA) measures the mass change in a sample as a function of temperature, under a controlled atmosphere. It provides a quantitative measurement of the mass changes in a material associated with both material transitions and thermal degradation and thus can be used in the determination of the thermal stability and decomposition products of a material. The instrument used was a Stanton-Redcroft simultaneous DTA/TGA STA 1500 systems. Samples were heated at a rate of 1 °C min-1 to a maximum temperature of 600 °C in a flowing atmosphere of argon.

2.7 Determination of surface area and porosity

2.7.1 Langmuir theory

Whenever a gas is in contact with a solid, equilibrium will be established between the gaseous phase and the adsorbed gases bound on the surface of the solid. The Langmuir theory describes the relationship between the number of active sites for adsorption on the surface as a function of pressure. The surface coverage can be calculated by the Langmuir equation, which states:

$$\theta = \frac{KP}{1+KP} \qquad \textbf{(2.12)}$$

The same equation can be expressed in terms of pressure:

$$\frac{P}{V} = \frac{P}{V_{mono}} + \frac{1}{KV_{mono}} \qquad \textbf{(2.13)}$$

However, the Langmuir equation is more applicable to chemisorption than physisorption as it assumes that the gas will only form a monolayer on the solid. Moreover for the Langmuir equation to give an accurate measurement, the adsorbed gas has to behave ideally in the vapour phase, which can be fulfilled only at low pressures.

2.7.2 BET theory

BET theory, proposed by Brunauer, Emmett and Teller is an extension of the Langmuir theory as it incorporates the concept of multimolecular layer adsorption. The BET equation is given below:

$$\frac{x}{v(1-x)} = \frac{1}{v_{mon}c} + \frac{x(c-1)}{v_{mon}c} \qquad \textbf{(2.14)}$$

where,

$x = P/P_0$

v is the STP volume of adsorbate

v_{mon} is STP volume of the amount of adsorbate required to form a monolayer

c is the equilibrium constant.

A key assumption used in deriving the BET equation is that the successive heats of adsorption for all layers except the first are equal to the heats of condensation of the adsorbate. It also assumes that there are no lateral interactions between adsorbed species. Hence, BET theory models the process of physisorption better than the Langmuir theory although it is generally still not a good model for adsorption on microporous materials.

2.8 References

1. P. Müller, *Crystal structure refinement : a crystallographers guide to SHELXL*, Oxford University Press, Oxford, 2006.
2. A. R. West, *Basic solid state chemistry*, 2nd ed. edn., John Wiley & Sons, Chichester, 1999.
3. D. W. Bennett, *Understanding single-crystal x-ray crystallography*, Wiley-VCH ; Chichester : John Wiley, Weinheim, 2010.
4. W. Clegg, *Crystal structure determination*, Oxford University Press, Oxford, 1998.
5. J. P. Glusker and K. N. Trueblood, *Crystal structure analysis : a primer*, 2nd ed. edn., Oxford University Press, New York ; Oxford, 1985.
6. M. T. Weller, *Inorganic materials chemistry*, Oxford University Press, Oxford, 1994.
7. T. Hahn, U. Shmueli, A. J. C. Wilson and International Union of Crystallography., *International tables for crystallography*, D. Reidel Pub. Co.
   Sold and distributed in the U.S.A. and Canada by Kluwer Academic Publishers Group, Dordrecht, Holland ; Boston, U.S.A.
   Hingham, MA, 1984.
8. T. Hahn and International Union of Crystallography., *International tables for crystallography. Brief teaching edition of volume A, Space-group symmetry*, 2nd, rev. edn., Published for the International Union of Crystallography by D. Reidel ;
   Sold and distributed in the U.S.A. and Canada by Kluwer Academic, Dordrecht ; Boston, Norwell, MA, U.S.A., 1988.
9. D. A. Fletcher, R. F. McMeeking and D. Parkin, *J. Chem. In.f Comp. Sci.*, 1996, **36**, 746.
10. G. M. Sheldrick, *Acta. Cryst*., 2008, A64, 112.

11. A. K. Brisdon, *Inorganic spectroscopic methods*, Oxford University Press, Oxford, 1998.
12. E. Dugan, Z. Q. Wang, M. Okamura, A. Medina and S. M. Cohen, *Chem. Commun.*, 2008, 3366.
13. Z. Q. Wang and S. M. Cohen, *Angew. Chem. Int. Ed.*, 2008, **47**, 4699.
14. Z. Q. Wang, K. K. Tanabe and S. M. Cohen, *Inorg. Chem.*, 2009, **48**, 296.
15. K. K. Tanabe and S. M. Cohen, *Chem. Soc. Rev.*, 2011, **40**, 498.

3 Synthesis of known and novel polycarboxylic acid and polypyridinyl ligands for the construction of homochiral MOFs

The following sections will describe the isostructural relationships between MOF ligands and MOF synthesis that allows for the design of new ligands and hence new MOFs. Compounds structurally similar to the ligands discussed in **Chapter 1** will form the basis of the synthetic targets in this **Chapter**. The synthetic work towards these new ligands will be discussed as well as other methodologies to incorporate BINOL based compounds into MOFs. This work then forms the basis for **Chapter 4**.

3.1 Designing ligands for isoreticular MOF synthesis

It is well established in homogeneous asymmetric catalysis that chiral auxiliaries when chelated to metal centers, are able to form single site catalysts that give excellent enantiomeric control and conversions.[1, 2] The advantages of immobilising catalytic centers in solid materials such as MOFs are also apparent. The review of MOF catalysts from **Chapter 1** shows that there are several ways to immobilise catalytic centers in MOFs and one of these methods is to use the MOF ligand as an effective chiral auxiliary to catalytic metal centre. There are many different compounds and their derivatives that can be used as chiral auxiliaries. The most common are termed 'privileged' ligands and include BINAP (2,2'-bis(diphenylphosphino)-1,1'-binaphthalene), BINOL (1,1'-bi(2-naphthol)), DuPhos (phospholanes produced by DuPont), BOX (bisoxazoline) and salen compounds and many more (**Figure 3.1**).[3]

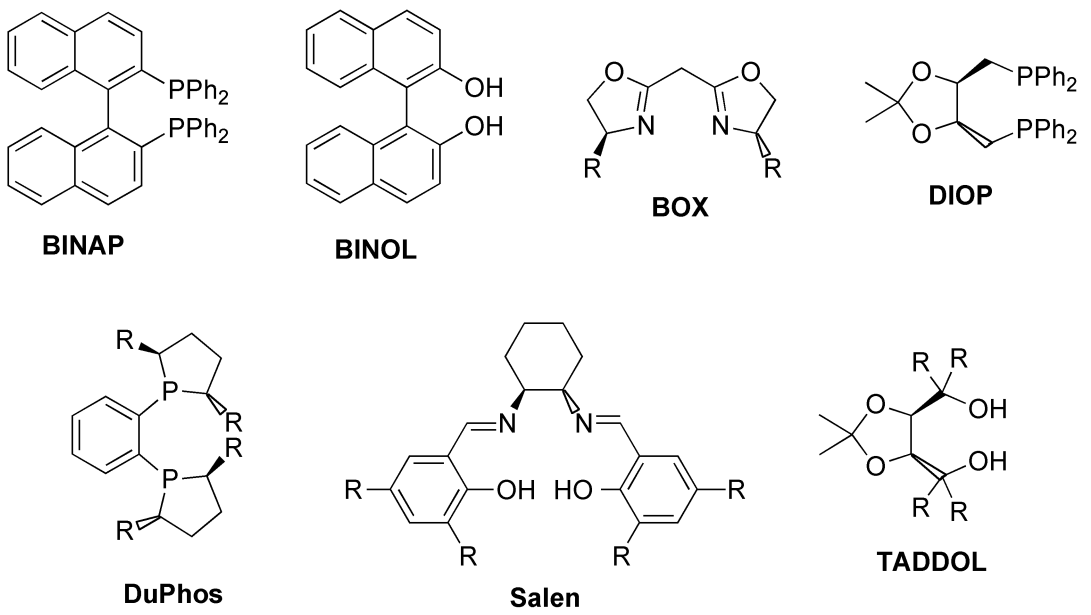

Figure 3.1: Selected privileged chiral ligands.[3]

Surveying the chiral ligands as potential MOF ligands for the synthesis of novel MOFs, only the BINAP, BINOL and Salen ligands have the required rigid core and thus are relativity inflexible. In **Chapter 1**, a Salen ligand chelated to Mn^{III} was used to create a mixed-ligand MOF with dinuclear Zn_2 paddle-wheels.[4] There are many examples of BINOL based ligands within MOFs by the groups of Tanaka *et al*.[5, 6] and Lin *et al*.[7] For example, recently Lin has reported the synthesis of a series of isoreticular chiral MOFs as asymmetric catalysts.[7] The MOFs are synthesised from solvothermal heating of DEF-H_2O solutions of a tetracarboxylic acid ligand (**5-8**) and copper nitrate to give porous, non-interpenetrating single crystals (**Figure 3.2**). The diols from the ligand point into the open channels and can react with $Ti(O^iPr)_4$ to from active catalysts for the diethylzinc addition to aromatic aldehydes as has been reported many times by Lin *et al*.[8, 9]

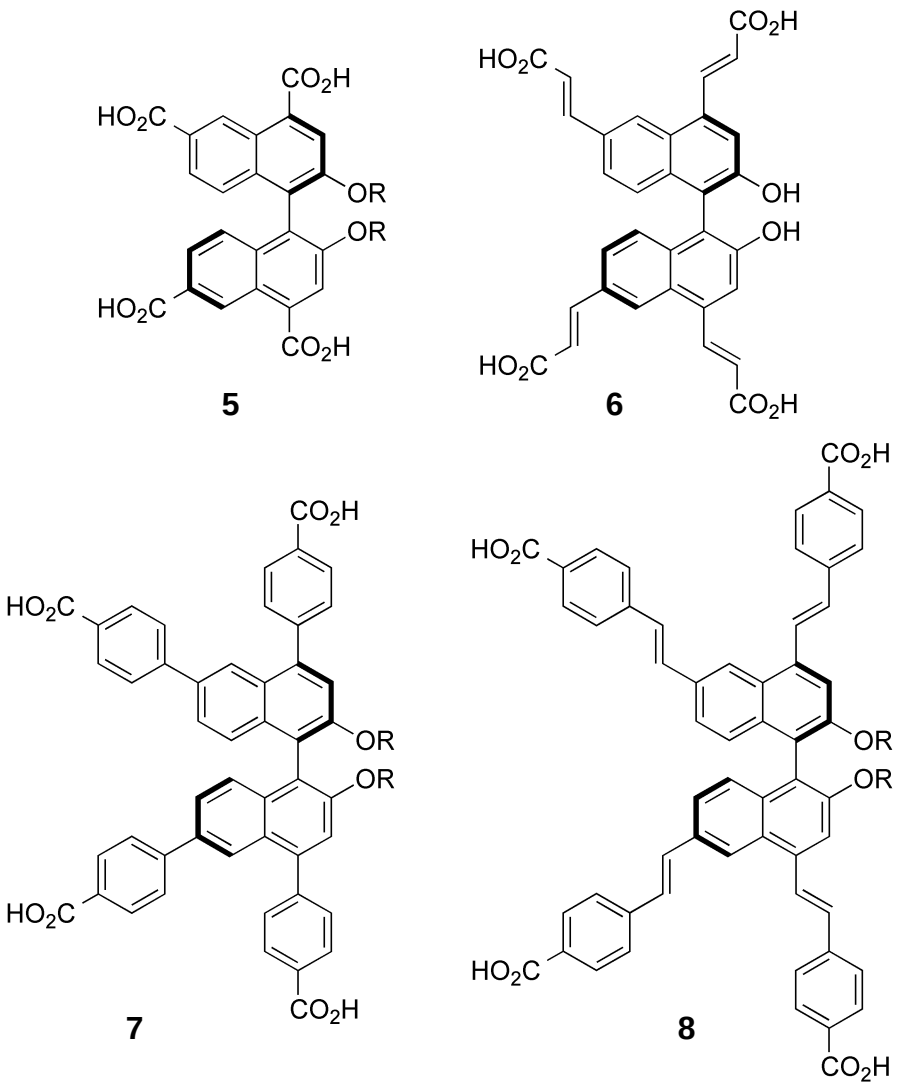

Figure 3.2: Chemical structures of the (*R*)-tetracarboxylic acid ligands used by Lin *et al.* to produce a series of isoreticular chiral MOFs (R = Et and H).[7]

What is evident from the literature is that of the many privileged chiral auxiliaries used in homogeneous catalysis, BINOL based ligands are the most commonly employed in MOF synthesis. The judicious choice of functionalisation possible at the different positions (3,3'-, 4,4'-, 5,5'-, 6,6'- and combinations) and the intrinsic rigidity provided by the core binaphthalene rings makes BINOL based ligands ideal synthetic targets. Another important factor, especially when synthesising MOFs with a secondary functional group on the ligand to chelate to a metal for catalysis, is that the diols on the BINOL unit will inevitably be pointing into a void, channel or open pore. This is because their directionality is perpendicular to the

binaphthalene axis, upon which the primary functional groups required to synthesise the MOF will lie.

The selectivity in the positional functionalisation around the binaphthalene rings has further advantages because a functional group can be installed directly to the ring system or a spacer unit can be placed between the BINOL core and the functional group. For example, carboxyl becomes phenylcarboxyl or acrylcarboxyl (such as in **Figure 3.3**). This enables tuning of the dimensions of the MOF: longer ligands should produce MOFs with larger channels and voids, which leads to higher porosity. The bulkiness of the BINOL ligands tends to inhibit interpenetration, which is also advantageous. The theoretical beauty of MOF synthesis is the idea of isoreticulation; that an structurally similar ligand can be used with the same metal precursor and solvent in the same molar ratios to product an structurally similar MOF. It is clear that BINOL based ligands are isostructural to biphenyls. If we consider the simple ditopic dicarboxylate BINOL compound where the carboxylate groups are along the chiral binaphthalene axis, the isostructural biphenyl compound is 1,1'-biphenyl-4,4-dicarboxylic acid. This is in turn isostructural to one of the most prolifically employed MOF ligands, 1,4-benzenedicarboxylic acid (**Figure 3.3**).

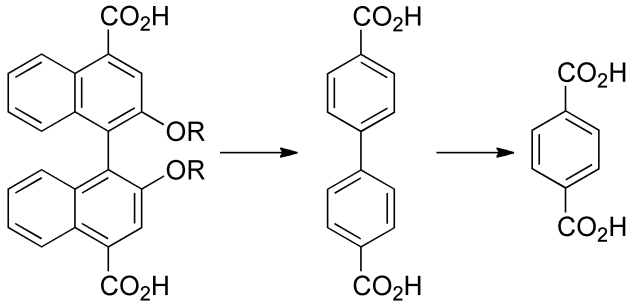

Figure 3.3: Structurally similar dicarboxylate compounds.

Likewise, inserting a linking unit between the BINOL core and the terminal carboxylate groups gives isostructural compounds. This method is extended from many MOF ligands such as the diisophthalic acid ligand based series of MOFs reported by Schroder *et al*.[10] (**Figure 3.4**).

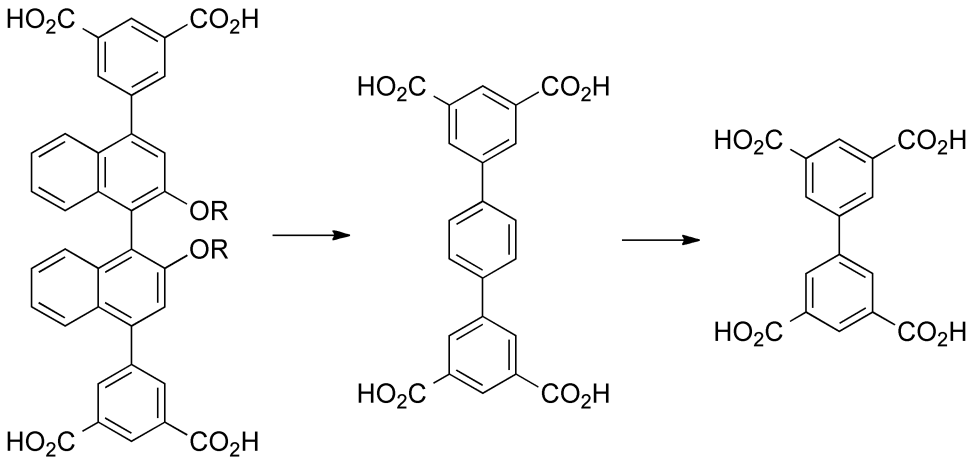

Figure 3.4: Structurally similar diisophthalic compounds.

Examining the bipyridine compounds known to produce MOFs, 4,4'-bipyridine (BPY) is widely used. Among its analogues are the longer versions of itself with multiple benzene rings connecting the terminal pyridine rings or other connectors such as *trans*-alkenes. A BINOL based compound with pyridine units connected along the chiral axis would be isostructural to these (**Figure 3.5**).

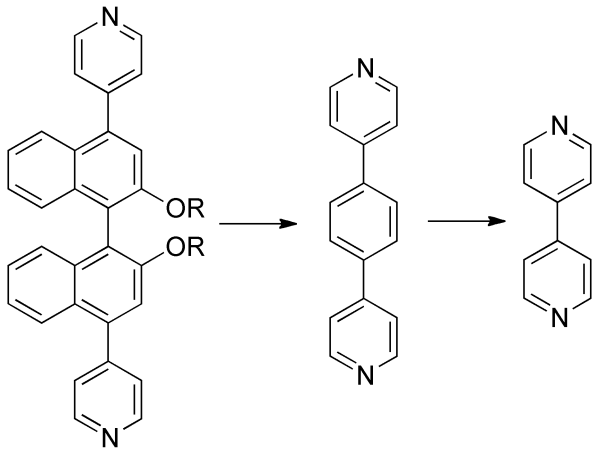

Figure 3.5: Structurally similar dipyridine compounds.

Another method in which the internal dimensions of a MOF can be tuned is to use a co-ligand in conjunction with the primary ligand of interest. The length or size of the co-ligand can then be altered, thus changing the dimensions of the MOF. This has been exhibited many times in paddle wheel MOFs where different carboxylates and pillaring dipyridines or diamines have been used to create many series of isoreticular MOFs. If one considers this strategy for chiral

BINOL ligands, the easiest compound to use as a co-ligand would be achiral, inexpensive and readily available. For BINOL based ligands with carboxylate primary functional groups, the complementary co-ligand to use would be a dipyridine or such like, and conversely if the BINOL ligand had pyridine functional groups the complementary co-ligand would be a dicarboxylate.

3.2 Results and discussion

3.2.1 Simple dicarboxylic acid BINOL ligands

The initial synthetic approach was to synthesise small molecular weight BINOL dicarboxylic acid derivates where the carboxylic acid groups were at the terminal ends of the binaphthyl chiral axis either in the 4- and 4'-positions or the 5- and 5'-positions. These compounds would be isostructural to many of the linear dicarboxylates found as MOF ligands previously discussed. Tanaka and coworkers have synthesised a range of polycarboxylic acid BINOL compounds starting from the individual naphtholcarboxylic acids. The synthesis of **9** starts from the readily available 6-hydroxy-1-naphthoic acid (**10**) which can facilely be converted into the methyl ester (**11**) in multigram quantities by acid-catalysed esterification in methanol.[11] Oxidative homocoupling of the ester protected product gives a racemic mixture of the biaryl compound, **12** in good yield.[5] Base-catalysed hydrolysis of **12** followed by acidic workup gives the corresponding dicarboxylic acid, *rac*-**9**.[5] The *R* enantiomer of the racemate of **9** can then be separated by complexation with the chiral compound cinchonidine. Colourless crystals of a 1:2 complex of *R*-**9** and cinchonidine precipitate from a methanol solution left unperturbed for 24 h. Free *R*-**9** was obtained by decomplexation using dilute HCl in 7 % overall yield for the four steps (**Figure 3.1**).[12]

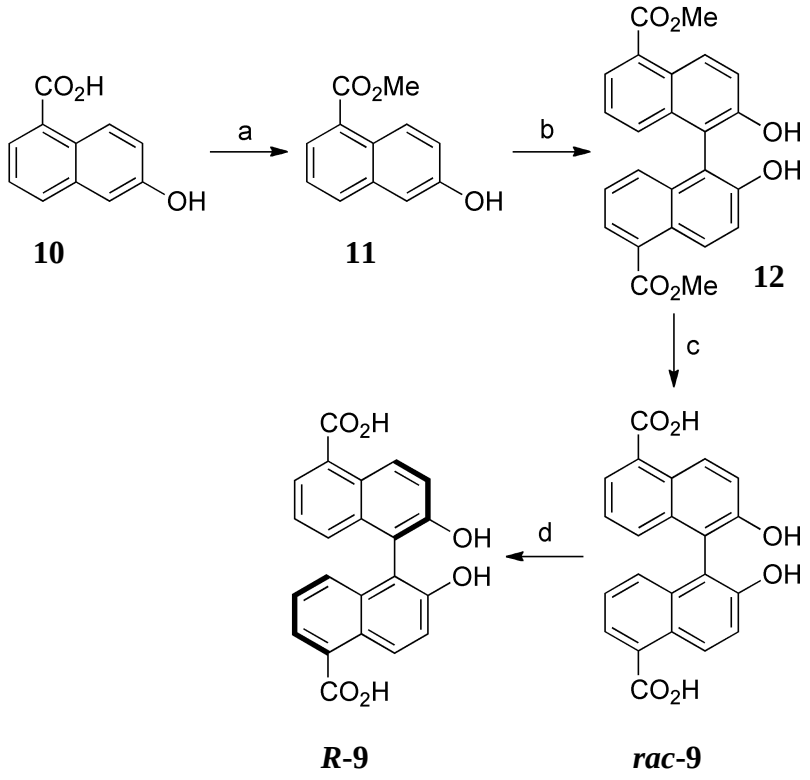

Figure 3.1: Reagents and conditions: a) $MeSO_3H$, MeOH, reflux, 99 %; b) $FeCl_3.6H_2O$, H_2O, 70 °C, 50 %; c) 10 % aq. NaOH, reflux, 99 %; d) cinchonidine, MeOH, 15 %.

The 4,4'-dicarboxylic acid (**13**) was synthesised *via* a different method by functional group interconversion of a 4,4'-dibromo binaphthalene (**14**) to the 4,4'-dinitrile species (**15**) using the Rosenmund-von Braun reaction followed by oxidation of the nitrile groups to carboxylic acids. The key intermediate in the synthesis, and the synthesis of many of the other ligands described later in this **Chapter**, is the known *rac*-4,4'-dibromo-2,2'-binaphthol (**14**).[13, 14] Compound **14** can be readily synthesised in multigram amounts by oxidative homocoupling of 4-bromo-2-naphthol, **16** The synthesis route starts by bromination of 1-naphthylamine (**17**) in acetic acid to give 2,4-dibromo-1-naphthylamine, **18**.[15] Diazotisation of **18** to the intermediate 4-bromonaphth[1,2-d][1,2,3]oxadiazole (**19**) in acetic acid by reduction with $NaBH_4$ in ethanol yields 4-bromo-2-naphthol, **20**. [15]Oxidative homocoupling of the single naphthol unit is again employed to give the corresponding biaryl species, in this instance, by using a copper (I) catalyst, CuCl(OH-TMEDA) (**Figure 3.2**).[14]

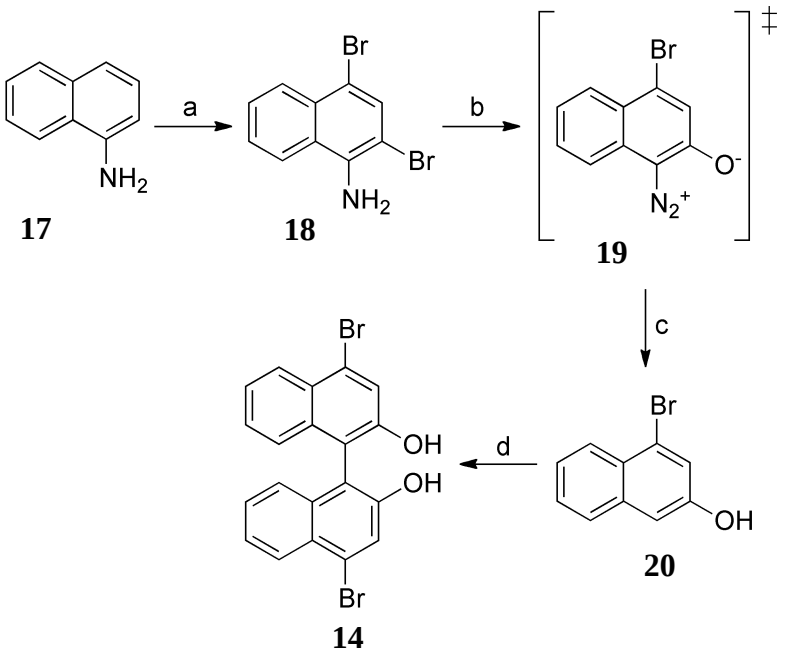

Figure 3.2: Reagent and conditions: a) Br_2, AcOH, 60 °C, 64 %; b) $NaNO_2$, AcOH; c) $NaBH_4$, EtOH, 0 °C, then conc. HCl, 26 %; d) CuCl(HO-TMEDA), DCM, 28 %.

As an aside, the separation of the enantiomers from the racemic mixture of **14** is achieved by reaction of the diol with a chiral sulfonyl chloride to give the corresponding bis-sulfonate, **21**.[14] The enantiomers of which have different polarities and can be separated slowly using silica gel chromatography eluting with toluene/ethyl acetate. Hydrolysis of the sulfonyl esters with aqueous NaOH in methanol regenerates the enantiopure diols (**Figure 3.3**). This procedure was performed and the characterisation for *R*-**14** agreed with the literature, however for ease and speed, the racemate was used in the synthesis described in this **Chapter**, unless otherwise stated.

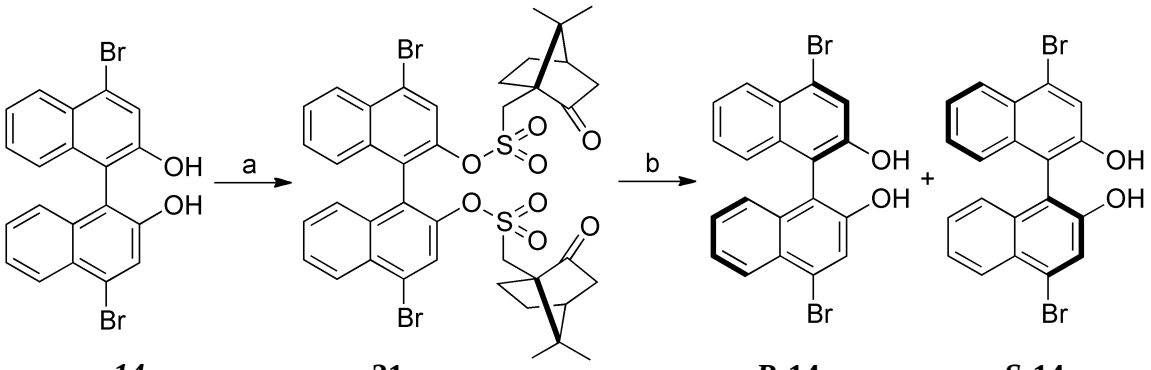

rac-14 **21** ***R*-14** ***S*-14**

Figure 3.3: Reagents and conditions: a) (1*S*)-camphor-10-sulfonyl chloride, NEt_3, DCM, 0 °C, 63 %; b) chromatographic separation, then 1.2 M aq. NaOH, MeOH, 60 °C, 89 %.

Cyanation of compound **14** was performed by refluxing an excess of cuprous cyanide in DMF to give the corresponding 4,4'-dinitrile binaphthalene, **8**.[12] Hydrolysis of the nitrile groups using aqueous NaOH and acidic workup gave the final 4,4'-dicarboxylic acid (**13**) in good yield (**Figure 3.4**).[12]

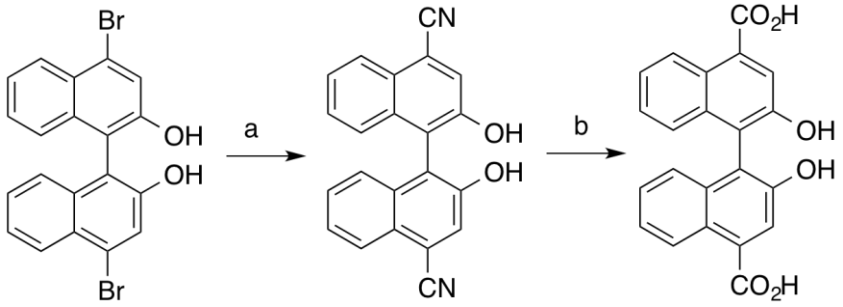

14 **15** **13**

Figure 3.4: Reagents and conditions: a) CuCN, DMF, reflux; b) 6 M aq. NaOH, reflux, then conc. HCl, 42 % overall yield.

The 6,6'dicarboxylic acid (**22**) was synthesised [5] *via* a similar methodology to the 5,5'-dicarboxylic acid. Oxidative homocoupling of methyl 6-hydroxy-2-naphthoate (**23**) gives a racemic mixture of the biaryl compound, **24** in good yield.[5] Base-catalysed hydrolysis of **24** followed by acidic workup gives the corresponding dicarboxylic acid, *rac*-**22**.[5] The *R* enantiomer of the racemate of **22** can then be separated by complexation with the chiral compound cinchonidine. Colourless crystals of a 1:2 complex of *R*-**22** and cinchonidine

precipitate from a methanol solution left unperturbed for 24 h. Free *R*-**22** was obtained by decomplexation using dilute HCl (**Figure 3.5**).[12]

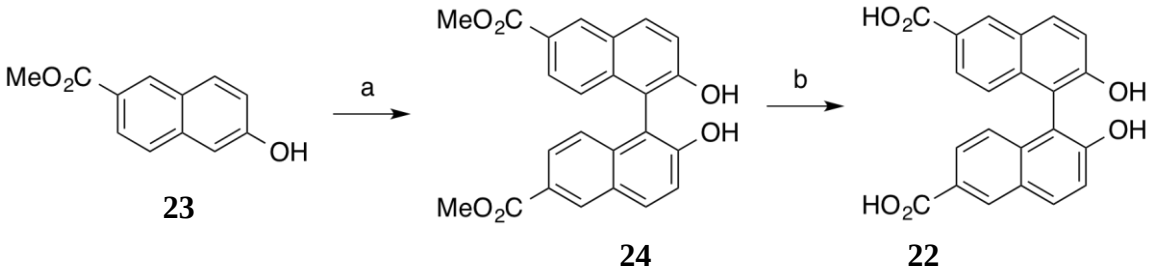

23 **24** **22**

Figure 3.5: Reagents and conditions: a) $FeCl_3.6H_2O$, H_2O, 70 °C, 46 %; b) 10 % aq. NaOH, reflux, 96 %.

3.3 Larger dicarboxylic acid and tetracarboxylic acid BINOL ligands

The selective bromination of BINOL can give the 6,6'-dibromo product; the 4,4',6,6'-tetrabromo product or the 4,4'-dibromo BINOL can be obtained as discussed previously. These brominated compounds are excellent precursors for Suzuki-Miyaura cross-coupling reactions with functionalised aryl-boronates. The resulting compounds would have a spacer unit between the BINOL core and the primary functional group for MOF synthesis.

3.3.1 General retrosynthesis of polycarboxylic acid BINOL ligands.

The polycarboxylic acids discussed in this section are all accessed *via* a similar route. When considering the synthesis of the final product, ideally deprotection of the carboxylic acids and diols should occur under the same conditions. Alkyl esters can easily be deprotected by acid or base hydrolysis in alcohol and alkyl ethers can be cleaved using BBr_3, which also cleaves esters. The carboxylic acid and diol protected intermediate can be obtained by Suzuki-Miyaura cross coupling[16] of the diol protected, brominated BINOL species with an aryl boronate where the carboxylic acid group is protected as an ester. Finally the starting protected diol can be obtained by many methods, but to match the final deprotection step, it would be convenient to use ester-protected diols (**Figure 3.6**).

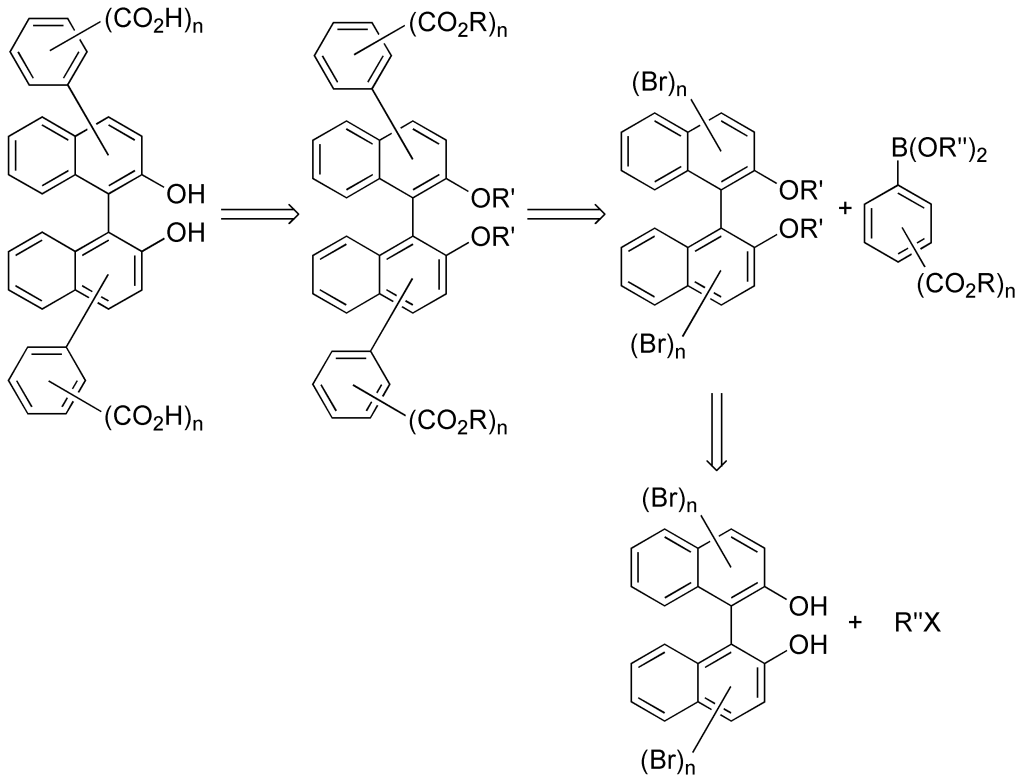

Figure 3.6: Retrosynthesis of polycarboxylic acid BINOL ligands.

3.3.2 Synthesis of 4,4'-(2,2'-dihydroxy-1,1'-binaphthalene-4,4'diyl)dibenzoic acid, 25

The initial route to synthesise **25** was to perform a cross coupling reaction with the free diol (**14**) with 4-methoxycarbonylphenylboronic acid. Refluxing with $Pd(PPh_3)_4$ and CsF in DME gave the expected product (**26**), however purification by column chromatography was achievable, but time consuming. After purification, **26** was converted to **25** by ester hydrolysis by refluxing in a 6M NaOH/EtOH mixture overnight (**Figure 3.7**). The structure of **25** was confirmed by ^{1}H and ^{13}C NMR. The purification of **26** was hampered because the compound is very polar and took time to separate on a column. It is also well known that these types of binaphthyl compounds are notoriously difficult to separate by column chromatography.[14] It was decided that protecting the diols of **14** first before performing the cross coupling reaction would enable faster purification (as the compound would be less polar) and may also increase the yield of the cross coupling reaction.[14]

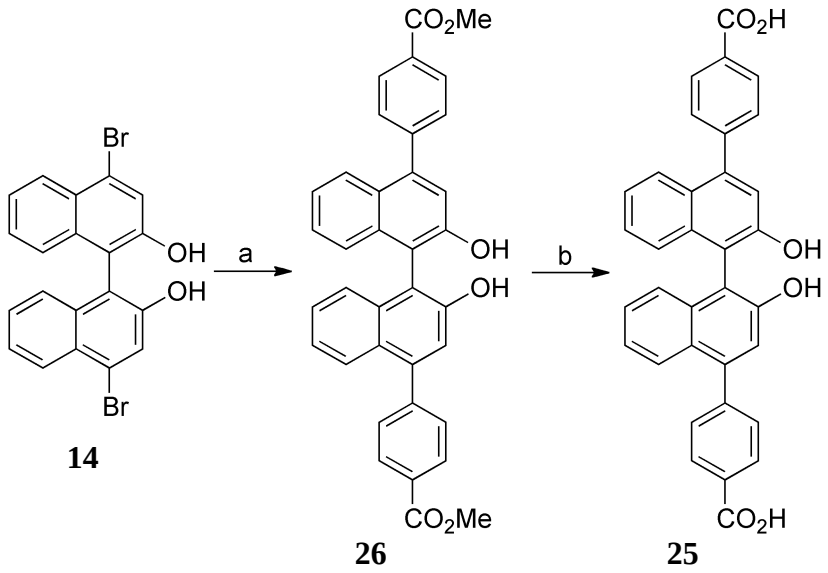

14 **26** **25**

Figure 3.7: Reagents and conditions: a) 4-(methoxycarbonyl)phenylboronic acid, 20 mol% $Pd(PPh_3)_4$, CsF, DME, reflux, 55 %; b) 6 M aq. NaOH, THF, EtOH, 80 °C, 76 %.

Reaction of compound **14** with Ac_2O and pyridine in DCM yields the bisacetyl ester compound (**27**) in good yield. This diol protected compound can then undergo a C-C cross coupling reaction with 4-methoxycarbonylphenylboronic acid refluxing in toluene using the Pd^{II} catalyst $Pd(dppf)_2Cl_2$ and aqueous Na_2CO_3 base to give **28**. The reaction mixture is vigorously degassed with nitrogen prior to the solid catalyst being added to the reaction flask. The mixture is immediately brought to reflux temperature and kept under a nitrogen atmosphere. This Suzuki-Miyaura reaction and the others in this **Chapter** are all sensitive to oxygen and thus this degassing procedure and continued nitrogen atmosphere is necessary for the reaction to proceed. After purification, **28** was converted to **25** by ester hydrolysis by refluxing in a 2M NaOH/THF/EtOH mixture overnight (**Figure 3.8**).

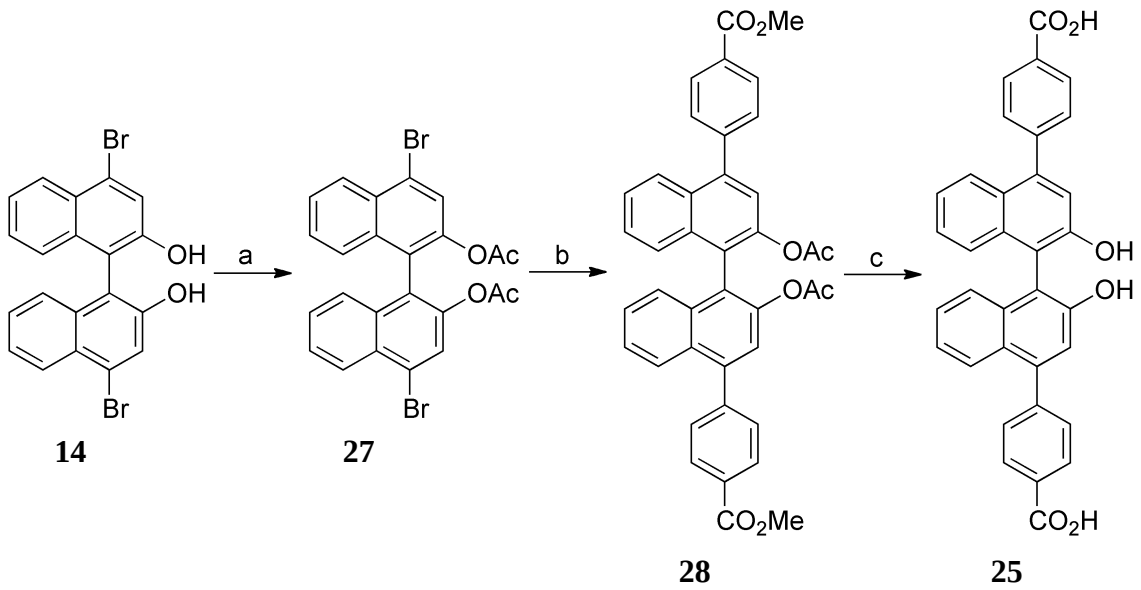

14 **27** **28** **25**

Figure 3.8: Reagents and conditions: a) Ac_2O, pyridine, DCM, 56 %; b) 4-(methoxycarbonyl)phenylboronic acid, 10 mol% $Pd(dppf)_2Cl_2$, 2 M aq. Na_2CO_3, PhMe, reflux, 55 %; c) 6 M aq. NaOH, THF, EtOH, 80 °C, 76 %.

This reaction was optimized by examination of the palladium catalyst, base, solvent and aryl boronate starting from using the same conditions employed by Lin *et al.*[17] in the synthesis of many of their BINOL based MOF ligands. Lin almost ubiquitously uses the system of $Pd(PPh_3)_4$ and CsF in 1,2-dimethoxyethane (DME) with the polybromo-BINOL derivate and an aryl boronic acid in a sealed reaction vessel. This system was found to produce many by-products including, homocoupled BINOL-BINOL species and homocoupled aryl-aryl species among others.

Table 3.1 Suzuki-Miyaura cross-coupling reactions of bismethoxy BINOL with aryl boronates (reagents and conditions: N_2 sparge, reflux, 48 h).

Entry	Catalyst	Coupling reagent	Base	Solvent	Reaction vessel	Yield
1	$Pd(PPh_3)_4$ 20 mol%	4-carboxyphenylboronic acid 2.5 eq	CsF 2.5 eq	DME	Bomb	0 %
2	$Pd(PPh_3)_4$ 20 mol%	4-carboxyphenylboronic acid 2.5 eq	CsF 2.5 eq	DME	Bomb	15 %

3	$Pd(PPh_3)_4$ 10 mol%	4-carboxyphenylboronic acid 3 eq	Cs_2CO_3 3.5 eq	1,4-dioxane	RBF	14 %
4	$Pd(PPh_3)_4$ 20 mol%	4-methoxycarbonylphenylboronic acid pinacol ester 3 eq	CsF 6 eq	DME	RBF	23 %
5	$Pd(dppf)_2Cl_2$ 5 mol%	4-carboxyphenylboronic acid 3 eq	Na_2CO_3 3 eq	toluene	RMF	55 %

The reaction conditions listed in Entry 5 of **Table 3.1** was found to give the highest yield of **28**, after purification. The lower loaded of $Pd(dppf)_2Cl_2$ coupled with aqueous Na_2CO_3 and toluene was found to be a particularly reactive system in the preparation of these large BINOL ligands.

3.3.3 Synthesis of 5,5'-(2,2'-dihydroxy-1,1'-binaphthalene-4,4'diyl), 29

The tetraacid, **29**, was the next synthetic target. Starting from the same dibromo precursor (**27**) as in the synthesis of compound **25**, and replacing the 4-methyl ester phenyl boronic acid with 3,5-bis methoxycarbonyl phenyl boronic acid pinacol ester, Suzuki cross-coupling yields the tetra methyl ester product, **30**. Facile base-catalysed hydrolysis of all 6 of the ester groups yields the final product, **29**, in good yield (**Figure 3.9**).

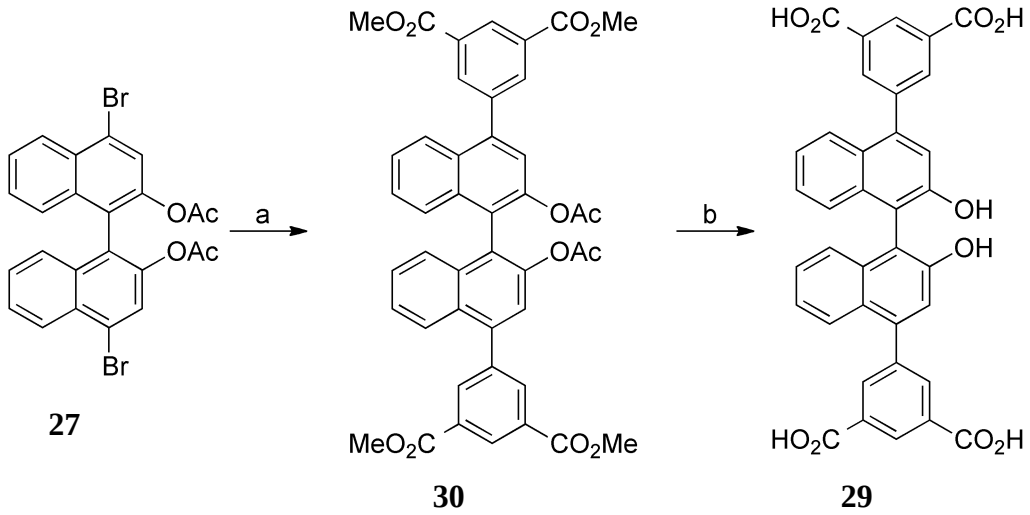

27 **30** **29**

Figure 3.9: Reagents and conditions: a) 3,5-bis(methoxycarbonyl)phenylboronic acid pinacol ester, 5 mol% $Pd(PPh_3)_4$, CsF, DME, 100 °C, 26 %; b) 2 M aq. NaOH, THF, EtOH, 80 °C, 70 %.

3.3.4 (*R*)-5,5'-(2,2'-dihydroxy-1,1'-binaphthyl-6,6'-diyl)diisophthalic acid, 31

BINOL can also selectively be brominated at the 6 and 6' positions generating a suitable precursor to Suzuki cross coupling reactions, that can lead the isostructural 6,6'- versions of the compounds discussed in earlier sections. However, the 4-methoxyphenyl carbonyl and the 4-pyridinyl (relevant later in this **Chapter**) have previously been synthesised and used in the synthesis of some 1D and 2D coordination networks that would not be suitable for this propose of this work.[18] Thus, the only unaccessed analogous compound is the diisophthalic compound, **31**. Controlled bromination of (*R*)-BINOL at the 6 and 6'-positions is readily achieved by adding a dilute bromine/DCM solution into a cold (-78 °C) DCM solution of (*R*)-BINOL.[19] Quenching the reaction after 4 h with $Na_2S_2O_3$ prevents further, unwanted polybromination. Subsequent ethylation of both hydroxyls using ethyl bromide and base, proceeds in good yield (**Figure 3.10**).[19]

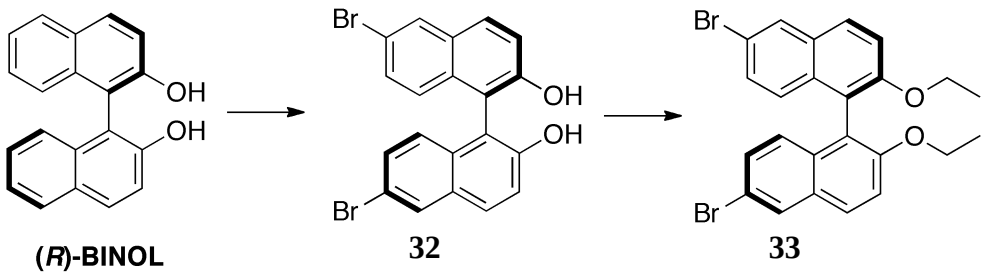

Figure 3.10: Reagents and conditions: a) Br_2, DCM, -78 °C→RT, 99%; b) K_2CO_3, NaI, EtBr, acetone, reflux, 75 %.

Suzuki coupling of **33** with 3,5-bis(methoxycarbonyl)phenylboronic acid pinacol ester with a Pd^0 or Pd^{II} catalyst yields **34**. However, deprotection of both the esters and the ether groups using BBr_3 under several different conditions does not yield the final product **31** cleanly. It was found that the ether cleavage often went to completion, leaving a mixture of compounds depending on the number of esters that were also cleaved. In an attempt to drive full ester cleavage, after reaction with BBr_3 and subsequent workup, the crude mixture of compounds with refluxed in an aqueous NaOH/EtOH/THF solution. This resulted in the desired product, but in an overall low yield (**Figure 3.11**)

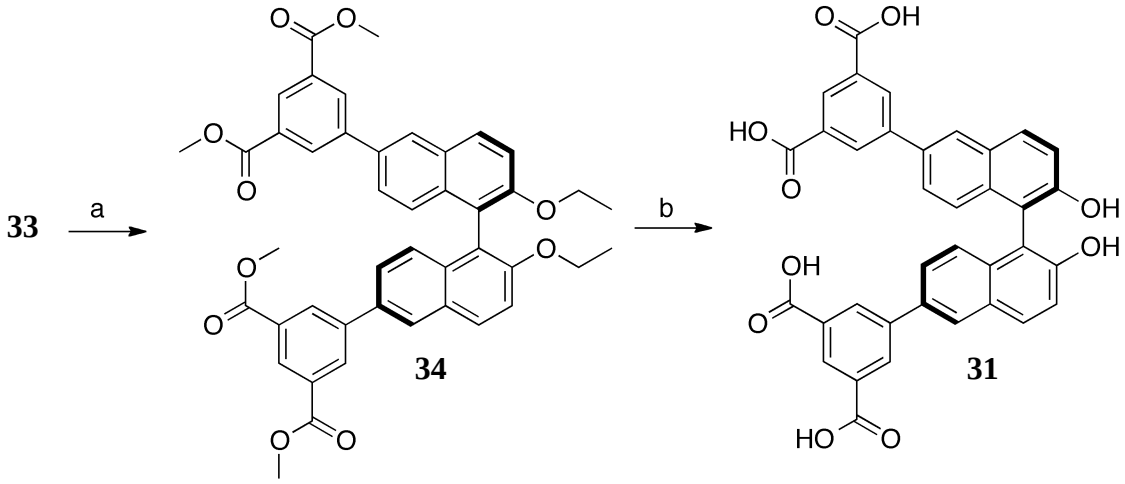

Figure 3.11: Reagents and conditions: a) 3,5-bis(methoxycarbonyl)phenylboronic acid pinacol ester, $Pd(PPh_3)_4$or $Pd(dppe)_2Cl_2$, base, reflux; b) BBr_3, DCM then aq. 6 M NaOH, EtOH/THF.

To overcome this low yielding route, a similar approach to that that described in Section 33.3 was employed. Starting from (*R*)-BINOL, acetylation of both hydroxyls is facilely archived by reaction with pyridine acetic anhydride in DCM to give **35**[20 21] (**Figure 3.12**).

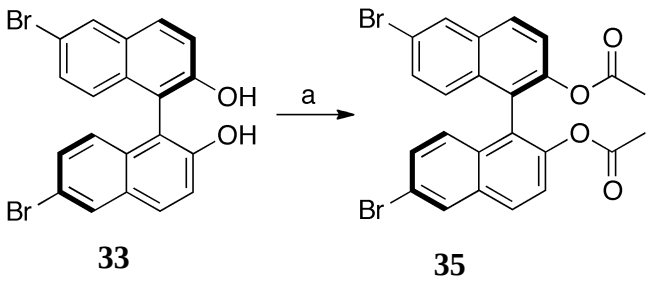

33 **35**

Figure 3.12: Reagents and conditions: a) pyridine, Ac_2O, DCM, RT, 40 %.

The Suzuki cross coupling conditions employed in the optimised synthesis of **28** (**Table 3.1**, Entry 5) was used to synthesise **36**. The same conditions work well to give a 59 % yield after purification by silica gel chromatography. Base catalysed hydrolysis of all 6 esters leads to the final product **31** after acidic workup (**Figure 3.13**).

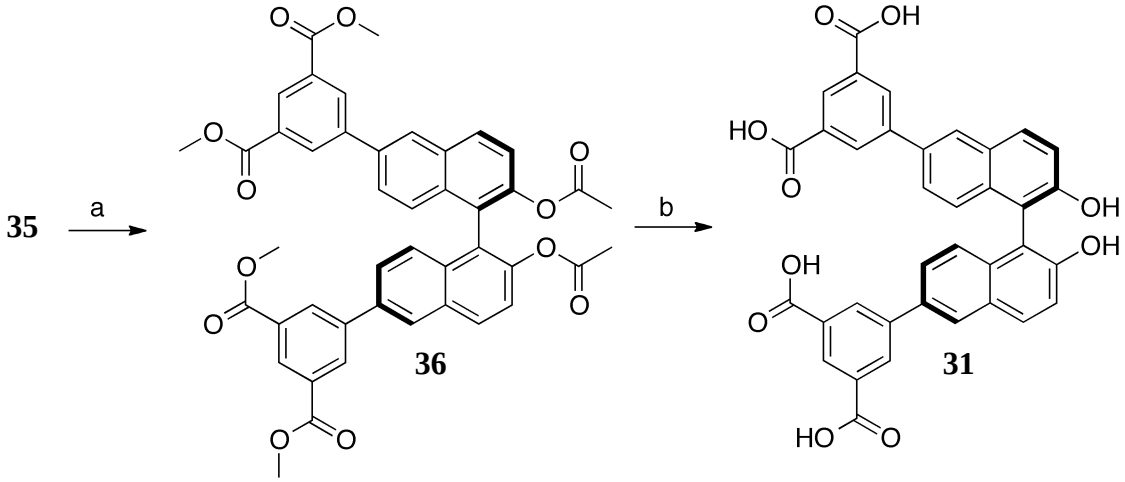

Figure 3.13: Reagents and conditions: a) 3,5-bis(methoxycarbonyl)phenylboronic acid pinacol ester, 5 mol% $Pd(dppf)_2Cl_2$, 2M aq. Na_2CO_3, PhMe, reflux, 59 %; b) 6M aq. NaOH, EtOH/THF, 80 °C, 37 %.

3.3.5 Synthesis of 4,4'-di(pyridine-4-yl)-1,1'-binaphthalene-2,2'-diol, 37

This part of the project started as alternative to the polycarboxylic acids synthesis. It was thought that the target compound (**37**) could be readily synthesised in 3 steps starting from compound **14**. Firstly, protecting the diols of compound **14** with methyloxy groups gives **38**[14] followed by Stille coupling of **38** with 4-(tributylstannyl)pyridine to give **39**. Deprotection of

the methoxy groups with an ether-cleaving reagent, such as BBr_3, should give **37** (**Figure 3.14**).

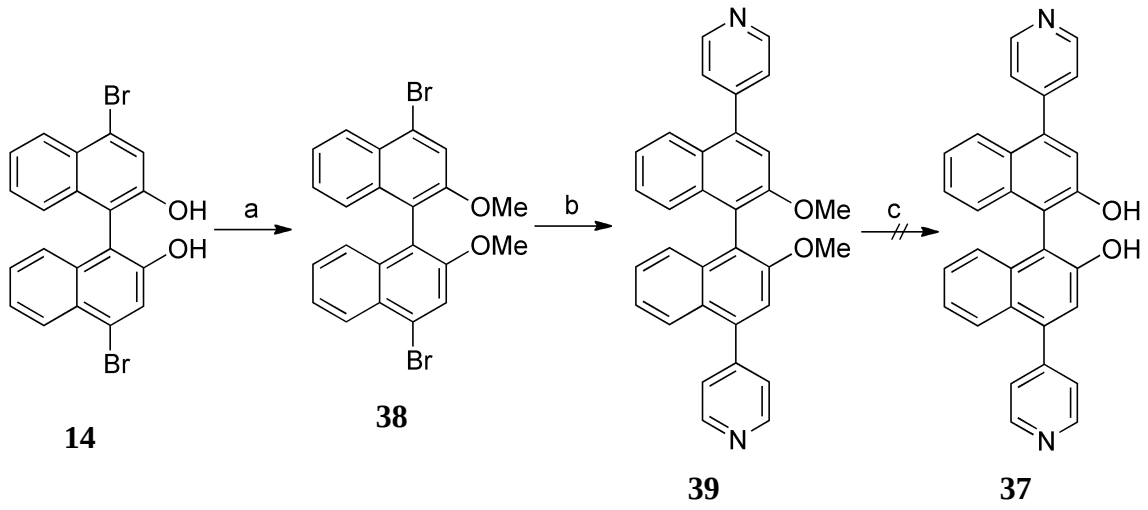

14 **38** **39** **37**

Figure 3.14: Reagents and conditions: a) MeI, Cs_2CO_3, acetone, 84 %; b) 4-(tributylstannyl)pyridine, $Pd(dppf)_2Cl_2$, PhMe, reflux, 69 %; c) BBr_3, DCM.

Stille coupling with 4-(trimethylstannyl)pyridine does lead to **39**, however a cleaner, similar yielding synthesis *via* Suzuki cross coupling of **38** with 4-pyridineboronic acid was quickly adopted as a cheaper synthesis. Brief optimisation of the reaction found that using Cs_2CO_3 in a toluene/water solvent system gave the highest yield of 64 % (**Table 3.2**).

Table 3.2 Cross-coupling reactions in the synthesis of **39** (reagents and conditions: 10 mol% cat., N_2 sparge, reflux, 48 h).

Entry	Pd catalyst	Coupling reagent	Base	Solvent	Yield
1	$Pd(dppf)_2Cl_2$	boronate	Cs_2CO_3	PhMe/water, 1:1	64 %
2	$Pd(dppf)_2Cl_2$	boronate	Cs_2CO_3	1,4-dioxane/water, 1:1	31 %
3	$Pd(PPh_3)_2Cl_2$	stannyl	LiCl	PhMe	30 %

The coupling reactions all give **39** in reasonable to good yield, however deprotection of the hydroxyls does not proceed so smoothly (**Table 3.3**). Employing BBr_3 in excess does yield the free diol, however this reaction does not proceed cleanly. The crude TLC plate contains

many spots; altering the column conditions to a very polar mixture of NEt_3/MeOH stills gives an impure mixture, with the free diol being the major component. Attempts to recrystallise the desired product from this more pure, but still crude mixture failed.

Table 3.3 Deprotection methods of **39** (reagents and conditions: N_2 sparge, overnight, stirring).

Entry	Deprotection reagent	Dry solvent	Temperature	Yield
1	15 eq. BBr_3[a]	DCM	0 °C → RT	5%
2	15 eq. BBr_3[a]	DCM	-78 °C → RT	9%
3	TBAF	THF	0 °C → RT	0 %

[a] 1 M in hexanes;

In order to increase the yield of the final free diol product, alternative hydroxyl protecting groups were sought to protect the pre-cross coupling compound that would employ deprotection conditions that give the free diol cleanly. To that end, benzyl ether groups, which are known to be readily cleaved by hydrogen to give toluene and the hydroxyl were employed. Addition of benzyl bromide to an acetone solution of compound **7** and KOH followed by refluxing for 3 hours yields the crude bisbenzyloxy compound **40** in good yield. A Molander cross-coupling reaction between compound **40** and potassium pyridine-4-trifluoroborate using the palladium catalyst $Pd(dppf)_2Cl_2$ then yielded the desired dipyridine species (**41**).[22] To speed up the purification, an excess of compound **40** was used, instead of an excess of borate. Then, using an ISOLUTE® Flash SCX-2 column (Biotage®), any unreacted **40** can be washed away, leaving just the bipyridinyl containing product on the column that can be removed by eluting with 1 M methanoic ammonia solution (**Figure 3.15**).

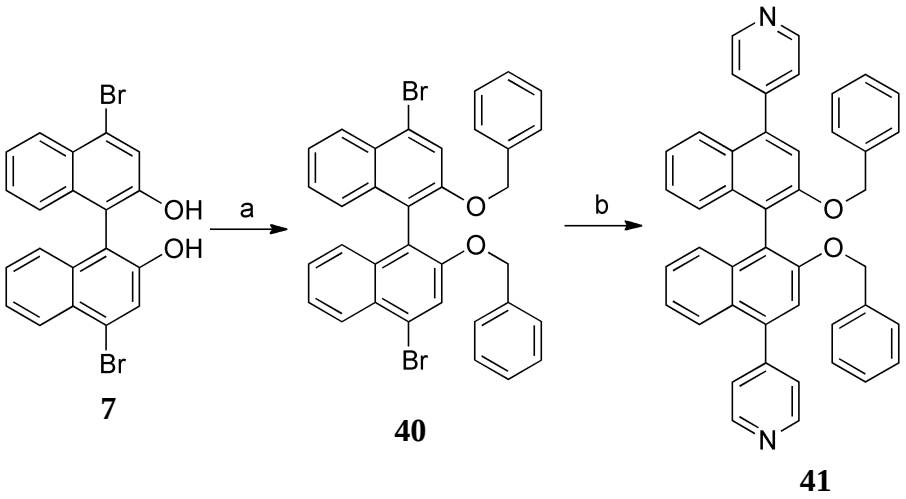

7 **40** **41**

Figure 3.15: Reagents and conditions: a) BnBr, KOH, acetone, reflux, 79 %; b) potassium pyridine-4-trifluoroborate, 10 mol% $Pd(dppf)_2Cl_2$, 2 M aq. Na_2CO_3, PhMe, reflux, 72 %.

Typical deprotection conditions of hydrogen gas were then used to attempt to deprotect the diols. The atmosphere in a flask containing a solution of **41** in ethanol was replaced with hydrogen. The solution was stirred for 24 hours and then the solvent removed. Unfortunately, no diol could be detected by ^{1}H NMR spectroscopy. A number of other conditions were tested using hydrogen, including vigorous bubbling of the gas through a solution of **41** to no avail (**Figure 3.16** and **Table 3.4**). Benzyl ethers are known to be unstable in extreme conditions of pH and temperature, thus compound **41** was refluxed in concentrated HCl solution for 2 hours where upon deprotection of the diols did occur, albeit in very low yield.

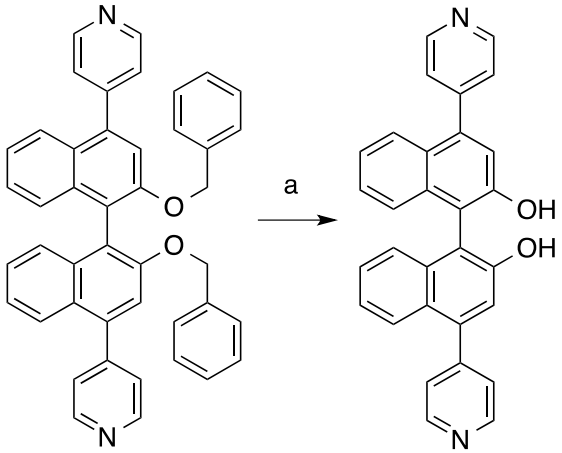

41 **37**

Figure 3.16: Reagents and conditions: a) 2 M aq. HCl, 80 °, 2h, 5%.

Table 3.4 Deprotection methods of **41** (reagents and conditions:).

Entry	Deprotection reagent(s)	Solvent	Temperature	Yield
1	H_2, Pd/C	EtOH	RT	0 %
2	H_2, Pd/C	MeOH	RT	0 %
3	H_2, Pd/C	MeOH	reflux	0 %
4	HCl	-	reflux	5 %
5	H_2, Pd/C, $Pd(OAc)_2$	MeOH	RT	0 %

3.4 Alternative methods of MOF-BINOL incorporation

The dimensions of the core BINOL molecule itself limit the number of possible MOFs, which contain a reactive functional group for PSM and also have apertures large enough for the BINOL molecule to diffuse through. Therefore, when designing a compound with a reactive functional group the compound must be kept as small and simple as possible. There are a variety of different reactions used in the PSM of MOFs some of which have already been discussed. One of the common is acid-amine coupling generally when the amino group is in the MOF and the acid or anhydride is the PSM reagent. A search of the literature for mono-substituted BINOL derivatives yielded many halo-substituted BINOLs at the 6-position. Using some of the chemistry already described in this **Chapter**, it was proposed that the cyanation of the diol protected, 6-bromo species followed by hydrolysis of the nitrile group and deprotection of the diols would give the target molecule, 2,2'-dihydroxy-1,1'-binaphthalene-6-carboxylic acid, **42**. Prior to beginning the synthesis, the molecule was drawn in Cambridge Software's Chem3D Pro and a MM2 energy minimized calculation was performed on the molecule. This gives the conformation shown in **Figure 3.17**.

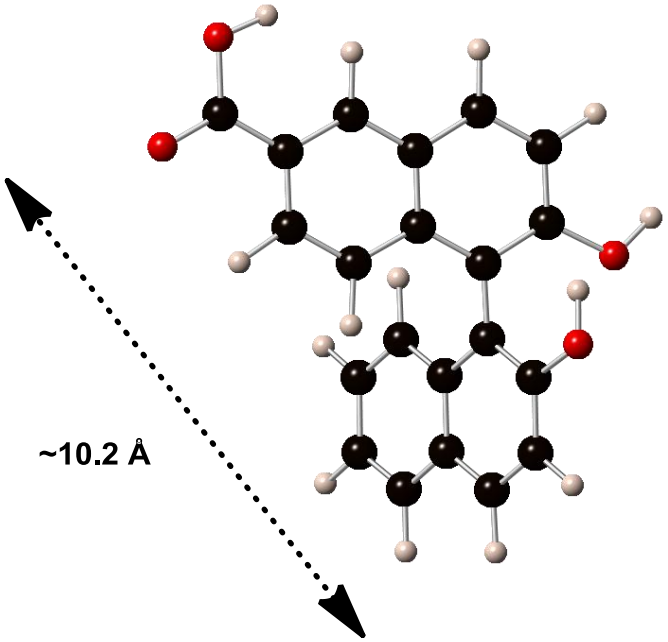

Figure 3.19: Molecular model of 2,2'-dihydroxy-1,1'-binaphthalene-6-carboxylic acid (**42**). Dihedral angle ~60 °.

The molecule is no larger than approximately 10 Å at its longest point. This fits well with several known MOFs, including the easily synthesisable UMCM-1-NH_2[23] which has apertures that are the same as its isostructural, unfunctionalised MOF, UMCM-1. UMCM-1 has two different channels within its structure, with the smallest opening being 14 Å.[24] Thus, it appears that the monocarboxylic acid, **42**, would be a suitable molecule for PSM of UMCM-1-NH_2.

Compound **42** can be prepared in three steps from the enantiomerically pure (*R*)-BINOL (**Figure 3.20**).[25] The 6- and 6'-positions of BINOL are equally activated toward electrophilic addition, however, esterification of one the 2-positions with a bulky pivaloyl group changes the electronics on the binaphthalene system to active the 6-position on the opposite ring to that of the esterification. Controlled monoesterification of (*R*)-BINOL by slow addition of pivaloyl chloride at 0 °C using freshly distilled NEt_3 as a base yields the 2'-pivaloyloxy ester (**43**) in good yield. Electrophilic addition of bromine to monoester proceeded as expected on the now activated 6-position to give (*R*)-6-bromo-2-hydroxy-2'-pivaloyloxy-1,1'-binaphthyl (**44**) in very good yield.

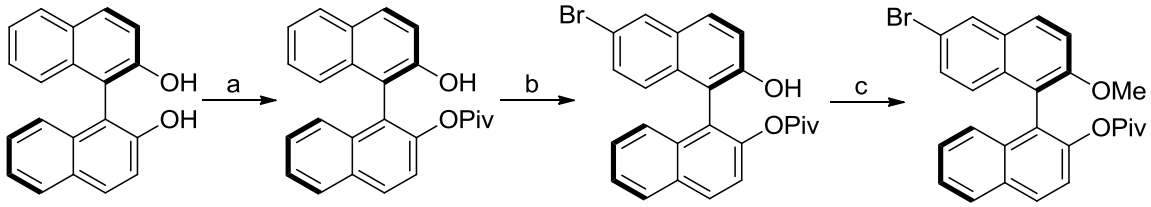

R-BINOL **43** **44** **45**

Figure 3.20: Reagents and conditions: a) PivCl, NEt_3, MeCN, 90 %; b) Br_2, MeCN, 0 °C, 99 %; c) MeI, K_2CO_3, DCM, reflux, 90 %.

Compound **44** should readily undergo cyanation by refluxing in high boiling point, aprotic solvents, to the corresponding mononitrile. However, after several attempts using different solvents and cyanide sources, the reaction yields were low and purification proved difficult (**Table 3.5**).

Table 3.5: Cyanation of **44** by various methods (reagents and conditions: N_2 sparge, reflux, 48 h).

Entry	Cyanide source	Solvent	Yield
1	CuCN	DMF	7 %
2	CuCN	NMP	4 %
3	$K_3[Fe(CN)_6]$, Pd/C	NMP	5 %
4	$Zn(CN)_2$, $Pd(dppf)_2Cl_2$	NMP	0 %

To overcome this, the remaining free hydroxyl was methylated by refluxing in DCM with methyl iodide to give **45** (**Figure 3.21**).[25] This compound readily undergoes cyanation with CuCN in DMF to give **46** in 83 % after 72 hours at reflux. After extensive washing with water to remove excess CuCN and DMF, the crude product can be easily purified by silica gel chromatography. The carboxylic acid can be prepared by hydrolysis of the nitrile group and at the same time the pivaloyl ester is also cleaved under the hydrolysis conditions to give **47** in good yield. Finally, the remaining methyl protected alcohol is demethylated by cleavage of the ether using BBr_3 in DCM to give the target compound **42** in an acceptable 34 % overall yield from (*R*)-BINOL (**Figure 3.21**).

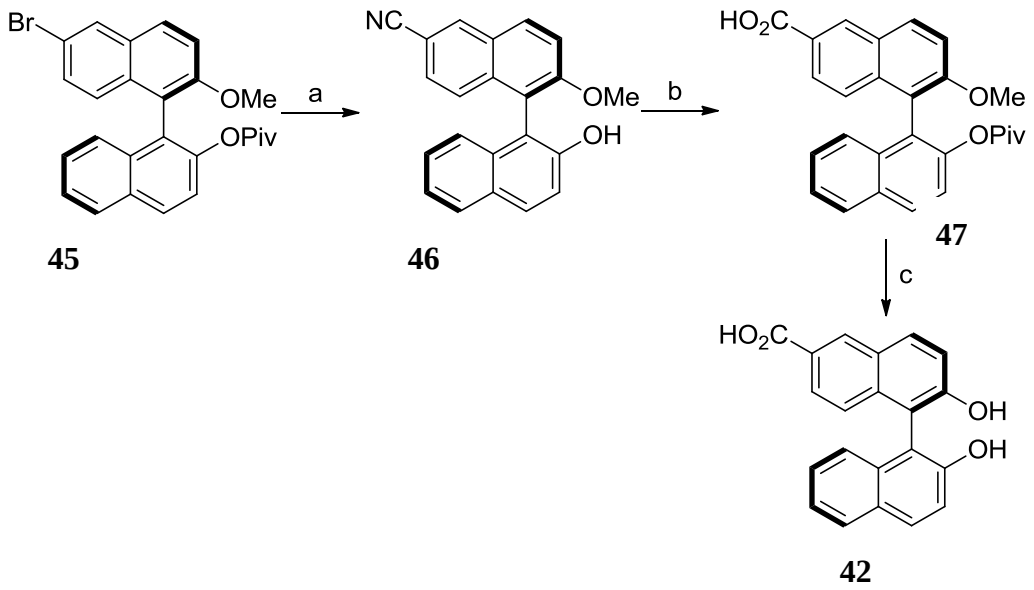

45 **46** **47** **42**

Figure 3.21: Reagents and conditions: a) CuCN, DMF, reflux, 83 %; b) 6 M aq. NaOH, EtOH, 80 °C, 80 %; c) 1 M BBr_3 in hexanes, DCM, 64 %; 42 % overall yield.

A sample of UMCM-1-NH_2 was synthesised according to literature procedures and solvent exchanged with $CHCl_3$ ready for further use. To perform the PSM, $CHCl_3$ was decanted from a sample of UMCM-1-NH_2 and a solution of $CHCl_3$ of compound **42** was poured into the vial with the MOF. The solution was swirled gently and then the vial was capped and left to stand for three days unperturbed. After which time, the MOF was washed with fresh $CHCl_3$ twice a day for three days, then the MOF was dried with heating (60 °C) under high vacuum. The dried material was sonicated in a DMSO-d_6 solution containing 2 drops of concentrated HCl. This solution was then placed in an NMR tube and ^{1}H NMR measured to ascertain the degree of the amine-acid coupling. If coupling had occurred, some of the 2-aminoterephthalate should appear in the spectrum as part of the resulting amide produced from the reaction. Unfortunately, no amide could be detected in the ^{1}H NMR spectrum and only the starting carboxylic acids were present. The procedure was repeated, this time with heating at 40 °C for 24 h. Again, no amide was found in the ^{1}H NMR spectrum. Attention was then turned to using some common amine-acid coupling reagents and these were trialed following the same procedure described above (**Table 3.6**).

Table 3.6 Attempted coupling of compound **1** with UMCM-1-NH_2.

Entry	Coupling reagent	Solvent	Temperature (°C)	Yield of amide*
1	-	$CHCl_3$	rt	0 %
2	-	$CHCl_3$	40	0 %
3	-	DCM	rt	0 %
4	-	DCM	30	0 %
5	HBTU[a]	$CHCl_3$	rt	#
6	HBTU[a]	$CHCl_3$	40	#

* as determined by NMR; [a] HBTU = *O*-(Benzotriazol-1-yl)-*N*,*N*,*N'*,*N'*,-tetramethyluronium hexafluorophosphate; b # MOF collapsed.

All the coupling reagents resulted in some degree of collapse of the MOF leading to no recoverable solid material in most cases. This unforeseen consequence effectively halted this investigation because it was reasonable to assume that similar MOFs would also degrade when the coupling reagents were employed and a suitable high stable MOF with large enough pores could not be identified in the literature.

3.5 Conclusions

This **Chapter** has the described the synthesis of seven BINOL-cored ligands and their derivatives as the starting materials in the synthesis of novel MOFs in **Chapter 4**. They include the known dicarboxylic acids **9** (**Ligand A**), **13** (**Ligand B**) and **22** (**Ligand C**) as well as the previously unknown **25** (**Ligand D**); the two tetraacids **29** (**Ligand E**) and **31** (**Ligand F**); and the dipyridinyl compound **37** (**Ligand G**).

The previously unknown monocarboxylic acid **47** was also trialed in the PSM of the MOF UMCM-1-NH_2, without success.

3.6 References

1. J. S. Seo, D. Whang, H. Lee, S. I. Jun, J. Oh, Y. J. Jeon and K. Kim, *Nature*, 2000, **404**, 982.

2. L. Q. Ma, C. Abney and W. B. Lin, *Chem. Soc. Rev.*, 2009, **38**, 1248.
3. C. Wolf, *Dynamic stereochemistry of chiral compounds : principles and applications*, RSC Publishing, Cambridge, UK, 2008.
4. S. H. Cho, B. Q. Ma, S. T. Nguyen, J. T. Hupp and T. E. Albrecht-Schmitt, *Chem. Commun.*, 2006, 2563.
5. K. Tanaka, H. Takano and Z. Urbanczyk-Lipkowska, *J. Inclusion Phenom. Macrocyclic Chem.*, 2006, **56**, 281.
6. K. Tanaka, S. Oda and M. Shiro, *Chem. Commun.*, 2008, 820.
7. L. Ma, J. M. Falkowski, C. Abney and W. Lin, *Nat. Chem.*, 2010, **2**, 838.
8. S. H. Gou and Z. M. A. Judeh, *Tetrahedron Lett.*, 2009, **50**, 281.
9. K. Pathak, A. P. Bhatt, S. H. R. Abdi, R. I. Kureshy, N. H. Khan, I. Ahmad and R. V. Jasra, *Tetrahedron-Asymmetr.*, 2006, **17**, 1506.
10. X. Lin, I. Telepeni, A. J. Blake, A. Dailly, C. M. Brown, J. M. Simmons, M. Zoppi, G. S. Walker, K. M. Thomas, T. J. Mays, P. Hubberstey, N. R. Champness and M. Schroder, *J. Am . Chem. Soc.*, 2009, **131**, 2159.
11. A. Akwabi-Ameyaw, J. Y. Bass, R. D. Caldwell, J. A. Caravella, L. Chen, K. L. Creech, D. N. Deaton, S. A. Jones, I. Kaldor, Y. Liu, K. P. Madauss, H. B. Marr, R. B. McFadyen, A. B. Miller, F. N. Iii, D. J. Parks, P. K. Spearing, D. Todd, S. P. Williams and G. B. Wisely, *Bioorg. Med. Chem. Lett.*, 2008, **18**, 4339.
12. K. Tanaka, S. Oda, S. Nishihote, D. Hirayama and Z. Urbanczyk-Lipkowska, *Tetrahedron-Asymmetr.*, 2009, **20**, 2612.
13. M. K. Ng, H. F. Chow, T. L. Chan and T. C. W. Mak, *Tetrahedron Lett.*, 1996, **37**, 2979.
14. H. F. Chow and M. K. Ng, *Tetrahedron-Asymmetr.*, 1996, **7**, 2251.
15. M. S. Newman, V. Sankaran and D. R. Olson, *J. Am. Chem. Soc.*, 1976, **98**, 3237.
16. N. Miyaura, K. Yamada and A. Suzuki, *Tetrahedron Lett.*, 1979, **20**, 3437.
17. L. Q. Ma, D. J. Mihalcik and W. B. Lin, *J. Am. Chem. Soc.*, 2009, **131**, 4610.
18. S. J. Lee, J. S. Kim and W. B. Lin, *Inorg. Chem.*, 2004, **43**, 6579.
19. C. Valente, E. Choi, M. E. Belowich, C. J. Doonan, Q. W. Li, T. B. Gasa, Y. Y. Botros, O. M. Yaghi and J. F. Stoddart, *Chem. Commun.*, 2010, **46**, 4911.
20. H. L. Ngo, A. G. Hu and W. B. Lin, *J. Mol. Catal. A-Chem.*, 2004, **215**, 177.

21. Q. S. Hu, D. Vitharana, X. F. Zheng, C. Wu, C. M. S. Kwan and L. Pu, *J. Org. Chem.*, 1996, **61**, 8370.
22. G. A. Molander and N. Ellis, *Acc. Chem. Res.*, 2007, **40**, 275.
23. K. K. Tanabe and S. M. Cohen, *Angew. Chem. Int. Ed.*, 2009, **48**, 7424.
24. K. Koh, A. G. Wong-Foy and A. J. Matzger, *Angew. Chem. Int. Ed.*, 2008, **47**, 677.
25. H. Hocke and Y. Uozumi, *Tetrahedron*, 2003, **59**, 619.
26. S. Bordiga, J. G. Vitillo, G. Ricchiardi, L. Regli, D. Cocina, A. Zecchina, B. Arstad, M. Bjorgen, J. Hafizovic and K. P. Lillerud, *J. Phys. Chem. B*, 2005, **109**, 18237.
27. W. L. F. Armarego and D. D. Perrin, *Purification of laboratory chemicals*, Butterworth Heinemann, Oxford, 1997.

4 Synthetic investigations towards reticular homochiral metal-organic frameworks

In this **Chapter**, the ligands synthesised in **Chapter 3** will be used to investigate synthesis towards novel MOFs. In each section there is a discussion of the structure and function of the parent MOF that is trying to be replicated, as well as a discussion of the synthesis conditions and outcome of each experiment.

A large number of reactions were carried out with each ligand and different metal salts and solvent systems. Therefore, in order to simplify the syntheses, the reaction conditions are plotted in the form of ternary phase diagrams, typically with the three axis of the plot being mole % of ligand, mole % of metal salt and mole % of (total) solvent(s). These are usually plotted for sets of ligands that are structurally similar, where the topology of the target MOF was envisioned to be the same, regardless of the ligand used. Full tables for each reaction can be found in Appendix 1. Full details of the crystallographic parameters and structure refinement for the single crystal x-ray structures described in this **Chapter** can be found in Appendix 2.

4.1 Homochiral MOFs from chiral ligands

As described in **Chapter 1**, the use of homochiral MOFs to create uniform active catalysts stems from their ability to produce uniform active catalytic sites with identical environments around them throughout the MOF. There are a few example of asymmetric catalysis with chiral MOFs in recent years.[1-7] Several of these examples are based on the chiral ligand approach discussed in Chapter 1, where chiral ligands based on 1,1'-bi-2-naphthol (BINOL)

are employed.[4, 6, 8-11] These BINOL ligands have several advantages over other possible chiral ligand candidates:

- the intrinsic rigidity of the BINOL core satisfies one of the major properties of a MOF ligand
- the bi-naphthene units in the BINOL structure can be selectively functionalised at different positions (e.g. 3,3'-, 4,4'-, 5,5'- and 6,6'-positons as well as combinations, e.g. 4,4',6,6'-positions)
- these functionalisations can lead to tuning:
    - the length of the BINOL ligand
    - the bulkiness of the BINOL ligand
    - the terminal (primary) functional group of the ligand
- the primary catalytic site is therefore well defined
- the secondary (diol) functional group is orthogonal to the primary functional groups and would likely decorate the pores of the resulting MOF[10]

The group of Lin *et al.* have pioneered this approach[9, 10, 12] and have reported mesoporous MOFs with the framework formula $[LCu_2(solvent)_2]$ (where L is a chiral tetracarboxylate ligand based on BINOL), that have the same topology, but with differing channel and pore dimensions.[10] The synthesis of these MOFs are very similar and an exemplary example of isoreticular synthesis. The frameworks are then treated with $Ti(O^iPr)_4$, which reacts with the chiral diol of the ligand to form Lewis acid (BINOLate)$Ti(O^iPr)_2$ compounds within the MOF structure. These materials exhibit asymmetric catalytic activity in the diethylzinc and alkynylzinc addition to aromatic aldehydes.

For the preparation of these complexes, reticular MOF chemistry appears to be ideal to obtain novel MOFs with known topologies and excellent properties, directly from metal ions and organic precursors (ligands). However, as will be outlined in this **Chapter**, adding functionality to the potential MOF ligands has implications for the success of the synthesis of the target MOF and the resulting topology.

4.2 Towards novel MOFs with the Zn_4O secondary building unit

There is a constantly growing reticular series of cubic MOFs based on Zn_4O SBUs with linear ditopic, dicarboxylic acids starting from the most simple structure and synthesis, which is that of MOF-5. Using MOF-5 as a worked example, the three components of the synthesis are the metal salt ($Zn(NO_3)_2$), the ligand (BDC) and the solvent (DMF or DEF). Displaying the molar ratios of these in a typical synthesis shows, as expected, the solvent is the dominating species.[13] Normalising the molar ratio of the three components by dividing the number of moles of each component by the total moles of all three components gives the molar fractions of each component (**Table 4.1**).

Table 4.1: Synthetic components of the MOF-5 synthesis[13]

	$Zn(NO_3)_2$	**BDC**	**DEF**
example mmol	0.15	0.05	4.2
Molar ratio	3	1	84
Normalised	3.4%	1.1%	95.5%

These can then be plotted as a single data point on a three-axis plot (**Figure 4.1**) in the form of a ternary phase diagram. These diagrams are often used for plotting metal alloys and ceramics and help to define the phase space explored in three-component systems. Employing these diagrams to plot the relative molar amounts of metal salt, ligand and solvent gives a map of the reactant combinations in a particular synthesis or series of similar synthesis targeting the same MOF.

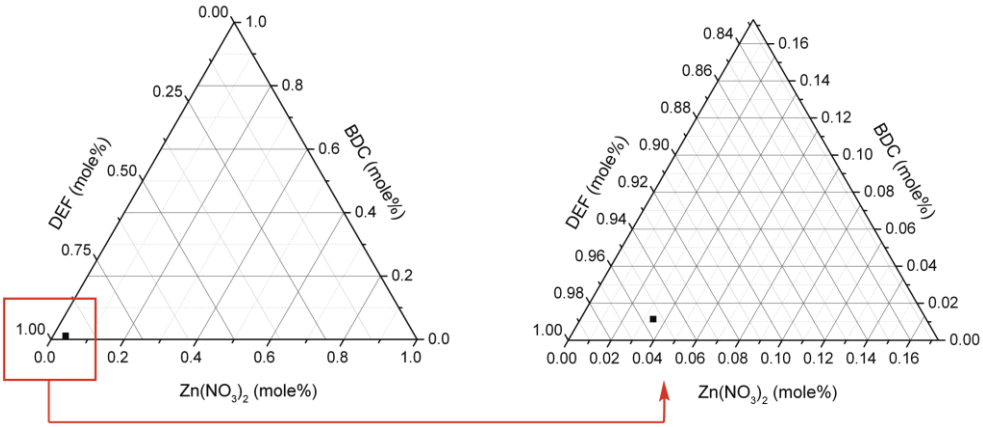

Figure 4.1: Ternary phase diagram showing the reaction compositions in the solvothermal synthesis of MOF-5.[13]

Throughout this **Chapter**, ternary phase diagrams will be used, where possible, to show the reaction combinations used in a particular MOF synthesis. When a synthesis becomes more complex by the addition of a second solvent or ligand for example, Tables will be used. All of the ligands used in this **Chapter** can be found in the pullout at the front of this thesis and the reaction combinations shown in this **Chapter** can be found collated in Appendix 1.

MOF synthesis will be broken down first by attempted MOF synthesis using only one ligand (the ligands discussed in **Chapter 3)**. In this section, Zn_4O containing MOFs will be discussed with **Ligands A**, **B** and **D** and then Cu_2 MOFs will be discussed using Ligands **C**, **E** and **F**. The next sections will discuss attempted MOF synthesis using one of the Ligands discussed in Chapter 2 and an achiral ligand. This section will be divided between mixed diacids and Zn_4O containing MOFs and then a section of pillared MOFs, divided by Zn_2 or Cu_2 paddle wheel SBUs.

4.2.1 Synthetic conditions of $Zn_4(O)$ MOFs

There is constantly growing reticular series of cubic MOFs based on Zn_4O SBUs with linear ditopic, dicarboxylic acids starting from the most simple structure and synthesis, which is that of MOF-5. Examining the synthesis conditions of MOFs structurally related to MOF-5 gives a

wide assortment of synthetic protocols. The example MOFs all contain the Zn_4O SBU and a linear ditopic dicarboxylic acid ligand structurally related to BDC, and are formulated as $[Zn_4(O)(L)_3]$ (where L = ligand) (with some solvent(s) within the formulae also). The ligands in these MOFs are shown in **Figure 4.2**.

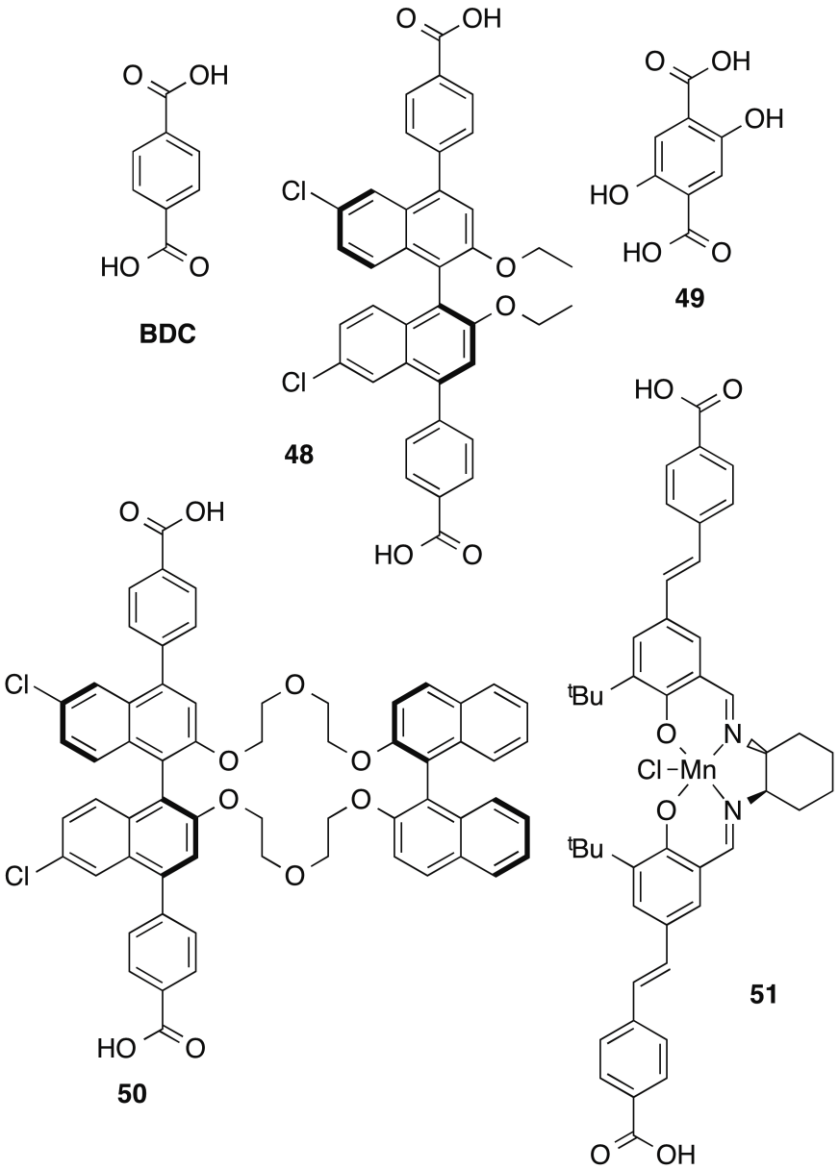

Figure 4.2: Ligands used in the synthesis of MOFs isostructural to MOF-5, all with the core structural formulae $[Zn_4(O)(L)_3]$ (BDC,[13, 14] **48**,[15] **49**,[14] **50**,[16] **51**[17]).

The synthesis conditions are summarised in **Table 4.2**.

Table 4.2: Synthesis reactants and conditions of several $Zn_4(O)$ containing MOFs.

Reactants (mmol)				**Molar ratios of reactants**	**Reaction temperature (°C)**	**Reaction time (h)**
$Zn(NO_3)_2.6H_2O$	BDC	DEF		3:1:84	100	20
0.15	0.05	4.2				
$Zn(NO_3)_2.6H_2O$	**48**[15]	DMF	MeOH	1:1:650:494	130 + 1 drop 2,6-lutidine	144
0.01	0.01	6.5	4.94			
$Zn(OAc)_2.2H_2O$	**49**[14]	DMF		2.6:1:432	RT	18
3.12	1.2	518.8				
$Zn(NO_3)_2.6H_2O$	**50**[16]	DMF		3.43:1:6617	80	48
0.0672	0.0196	129.7				
$Zn(NO_3)_2.6H_2O$	**51**[17]	DBF	EtOH	2.83:1:1833:1425	80	96
0.034	0.012	22	17.1			

These reaction conditions are plotted below in the form of ternary phase diagrams in **Figure 4.3**.

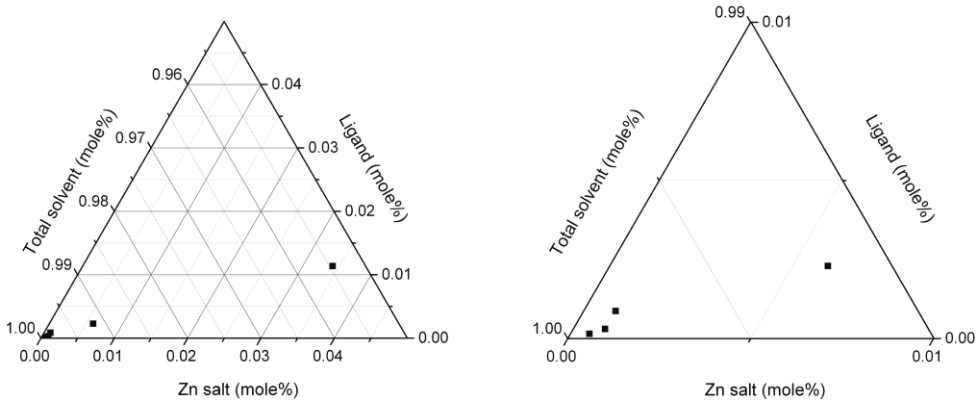

Figure 4.3: Ternary phase diagram showing the reaction compositions in the solvothermal synthesis of some typical $Zn_4(O)$ containing MOFs

It can be seen from the ternary phase diagram that these synthesise all occur at very high solvent concentrations compared to the ligand and Zn salt. Thus the solvent molar excess far outstrips the percentage proportions of the two components, even at saturation concentrations for the solid reactants. The ratio of Zn salt and ligand is close to 1:1 in most cases as this matches the 4:3 stoichiometry in the resulting MOF.

4.2.2 Attempted synthesis of novel MOF-5 analogues

As discussed it is well known that reacting a ditopic dicarboxylic acid with a rigid aromatic core with a source of Zn^{2+} in dialkylamides under solvothermal conditions leads to the formation of MOFs isoreticular to MOF-5. **Ligands A**, **B** and **D** are structurally similar to the dicarboyxlates that have been reported to form such frameworks and therefore are suitable to be used in the construction of novel MOFs of this type.

Initial work focused on using the easily accessible ligands **A** and **B**. As described in **Chapter 2**, the ligand can be obtained in bulk as the racemate, or both enanitomers can be resolved.[18, 19] For expedience the racemate was used in attempted MOF syntheses, unless otherwise stated. The ligands have previously been used in the construction of the chiral MOF, $[Cu_2(ligand)_2(H_2O)_2]$ (where ligand = **Ligand A** or **Ligand B**, by Tanaka *et al*. [18, 19] The MOF is synthesised by treatment of **Ligand A** or **B** with $Cu(NO_3)_2$ in aqueous MeOH by slow diffusion of *N*,*N*-dimethylaniline at room temperature for several days.[18] The structure contains Cu_2 paddle wheel SBUs linked by the ligand to form a 2D dinuclear square grid coordination network. The 2D grids interact to form layers along the *b* axis. Because the MOF is not truly a 3D network (i.e. it contains 2D layers stuck together but through non-covalent bonding), rather than resynthesise it, ligand **A** or **B** was used alone or with a co-ligand to try to produce novel MOFs.

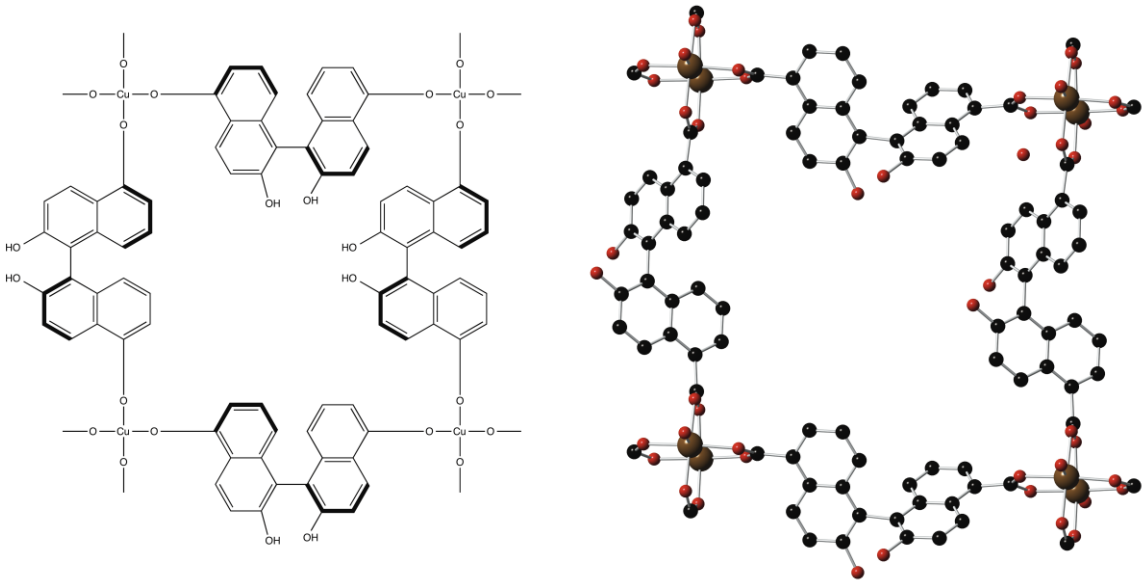

Figure 4.4: Structure of $[Cu_2(\textbf{Ligand A})_2(H_2O)_2]$ (H_2O and other solvent molecules removed for clarity; carbon [black]; copper [brown]; oxygen [red]) (the MOF with **Ligand B** is identical).

The novel **Ligand D** has been synthesised as discussed in **Chapter 3**.

4.2.3 Attempted MOF synthesis

The reaction conditions are plotted below for solvothermal reaction of zinc nitrate and DMF or DEF with either **Ligand A**, **B** or **D**. The synthetic protocols used closely match those of the example given in section 4.2.1.

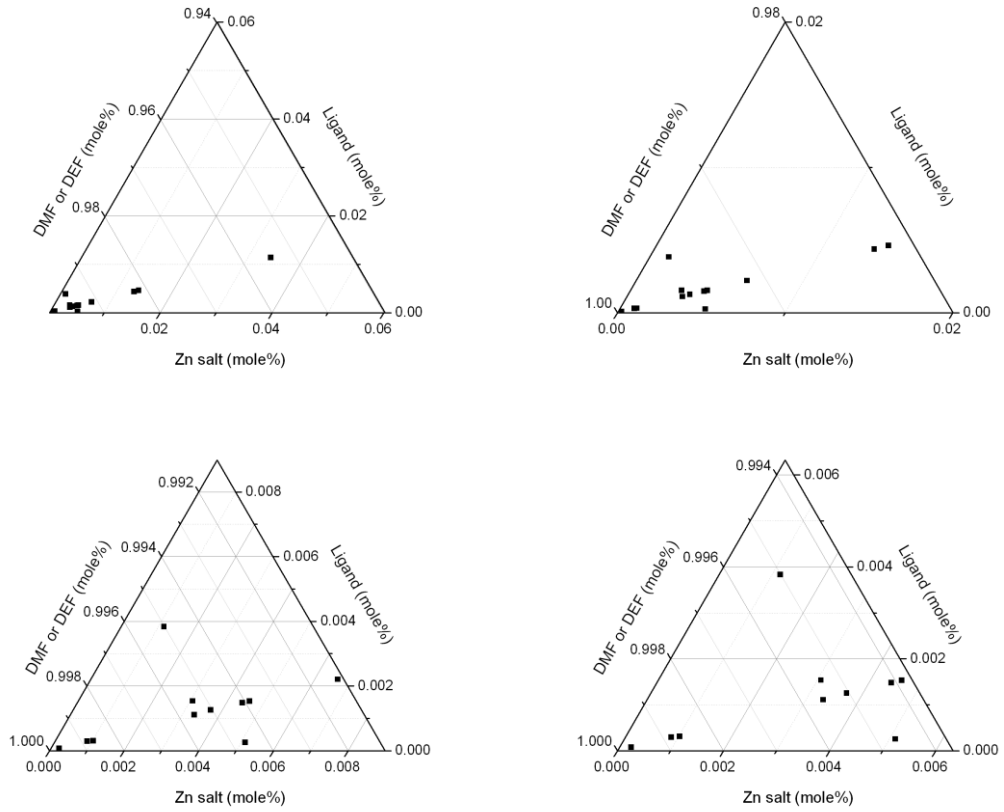

Figure 4.5: Ternary phase diagrams showing the attempted solvothermal MOF synthesis using **Ligands A**, **B** and **D** in either DMF or DEF. Diagrams zoom in from top left to lower right.

Unfortunately, none of the synthetic conditions summarised in **Figure 4.5** led to the formation of single crystalline materials. Even when over saturating the solution with zinc nitrate (by heating), no formation of crystalline material was observed.

Some of the example MOF syntheses use a mixture of solvents with DMF (or DEF) being the major solvent. Often methanol or ethanol is added as the additional solvent. In addition, tertiary amines such as dimethylaniline[15] or 2,6-lutidine[20] can also be added as very minor components to the synthesis. These presumably deprotonate the polycarboxylate ligand, which can either 1) further solubilise the ligand and/or 2) initiate the solvothermal reaction.

The addition of water, methanol and ethanol in varying ratios into this system did not result in crystalline materials. Nor did adding dimethylaniline or 2,6-lutidine. The attempted synthesis using these modifications are summarised in **Figure 4.6**.

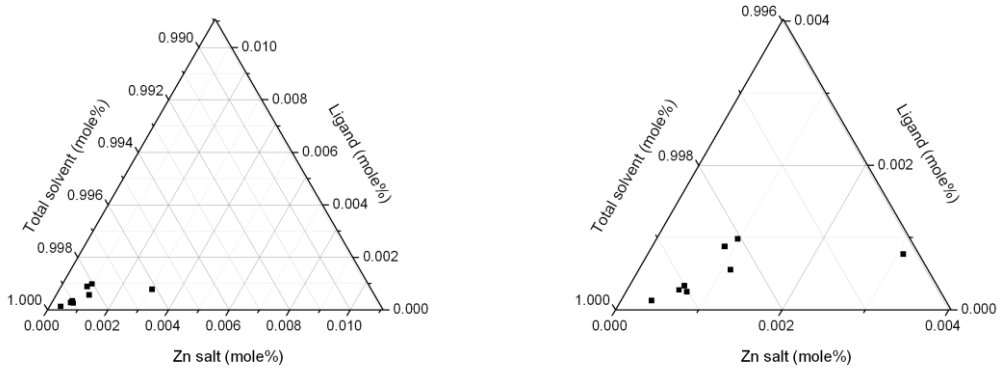

Figure 4.6: Ternary phase diagrams showing the attempted solvothermal MOF synthesis using **Ligands A**, **B** and **D** in either DMF or DEF with additional solvents. The diagram on the right shows a closer view of the diagram on the left.

It must be noted that some of the synthesis conditions did lead to a precipitate that was poorly crystalline. The apparent difficulty in producing novel MOF-5 analogues with BINOL based dicarboxylic acid ligands maybe attributed to:

- Coordination of the BINOL diols to metal salt precursors, thereby inhibiting SBU formation
- The length of the ligands along their chiral axis leading to highly interpenetrated networks that are formed of crystalline moieties unable to grow further

4.2.4 Modulated MOF synthesis

During this work, three reports of controlling the synthesis of well-known MOFs using a competing ligand emerged.[21-23] The competing ligands in the reports are compounds similar in structure to the ligand used to produce the MOF, but only having one coordination site (or one less coordinate site than the MOF ligand). The competing mono-coordinating ligand is termed a modulator. The modulator competes with the MOF ligand for coordination to the metal ion

or cluster during synthesis. These competing interaction slows nucleation and crystal growth and can be used to directly influence the size and shape of the MOF crystals. For example, Kitagawa *et al*. describe the modulated synthesis of $[Cu_2(NDC)_2(DABCO)]$ using acetic acid, a monocarboxylic acid. In the conventional synthesis of $[Cu_2(NDC)_2(DABCO)]$, nucleation and crystal growth occur to form the bulk crystal. The authors are able to show that by varying the concentration of modulator, anisotropic crystal growth can occur to form nanocubes, nanorods or nanosheets over the formation of bulk crystal.

In a later paper in 2010, Kitagawa shows size-controlled formation of $[Cu_3(BTC)_2]$ (HKUST-1) by varying the concentration of dodecanoic acid added to the synthesis mixture.[22] Kitagawa altered the original synthesis of HKUST-1, which is reported as the reaction of copper nitrate and BTC in water/ethanol mixtures or DMF,[24, 25] to using copper acetate as the metal source and butanol. At low concentrations of modulator, the crystallinity of the resulting MOF is poor. This is somewhat attributed to the faster reaction when using copper acetate, as this already contains the copper paddle-wheel unit present in the SBU of the MOF. Increasing the ratio of modulator to BTC to 10:1 shows a dramatic influence on the morphology of the resulting MOF crystals. Another important factor identified was the concentration of all the reagents in the synthesis. This can be clearly observed in the field-emission scanning electron microscopy (SEM) images in **Figure 4.7**.

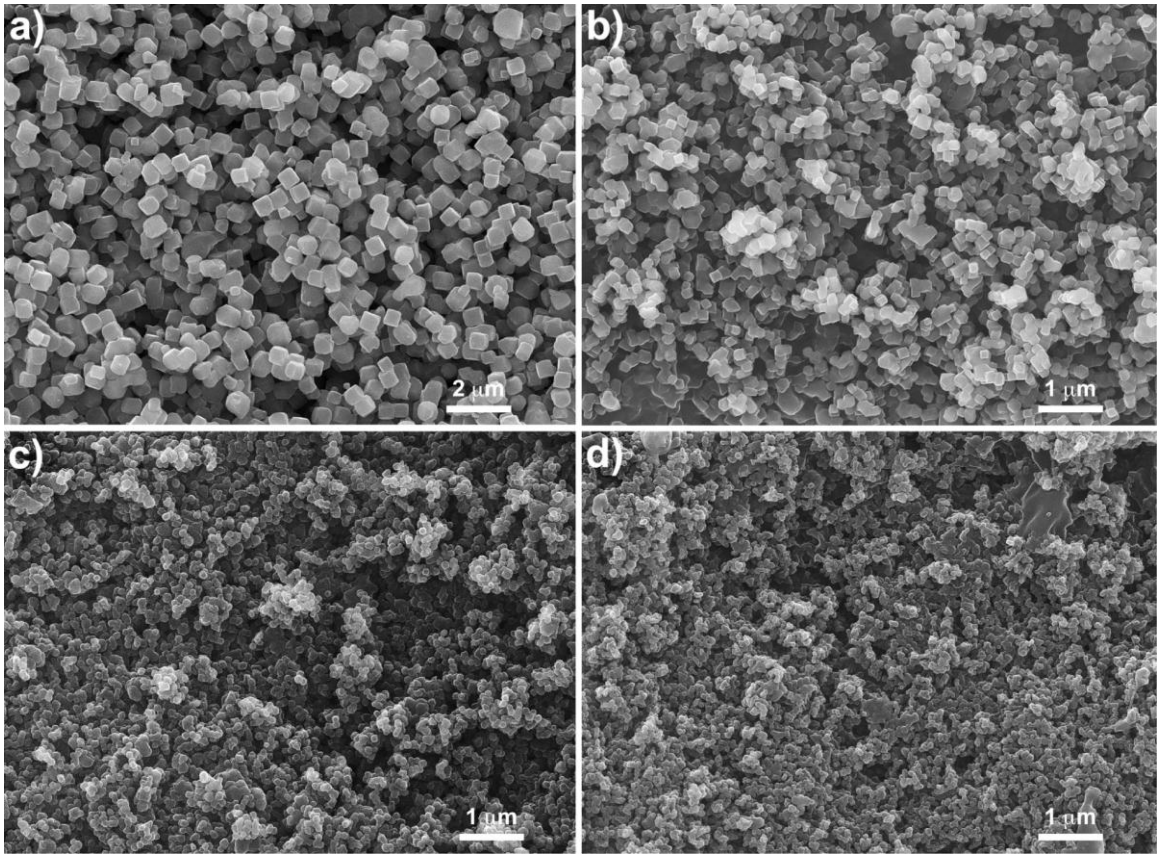

Figure 4.7: SEM images of HKUST-1 samples obtained with butanol solvent, dodecanoic acid modulator, and various concentrations (c) of starting material: (a) c = 0.063 M; (b) c = 0.032 M; (c) c = 0.016 M; and(d) c = 0.011 M. The ratio between dodecanoic acid and benzene-1,3,5-tricarboxylic acid was kept constant (r = 50: dodecanoic acid/butanol). Reproduced from S. Kitagawa *et al. Chem. Mater.*, 2010, 22, 4531.[22]

As well as in these copper MOFs, modulators have been used in the synthesis of the reticular UiO series of zirconium based MOFs.[23, 26] In the investigation by Behrens[23], benzoic acid and acetic acid were used as modulators in the synthesis of Zr–BDC (UiO-66), Zr–BDC–NH_2 (UiO-66–NH_2), Zr–BPDC (UiO-67), and Zr– TPDC–NH_2 (UiO-68–NH_2). The reported synthesis of these UiO MOFs is itself difficult to reproduce, often leading to poorly crystalline materials. By using benzoic acid as a modulator, Behrens found that addition of up to 3 equivalents of modulator to $ZrCl_4$ (the metal source) resulted in more crystalline, smaller crystals of the MOF than the original reported synthesis by Cava. This was evidenced by broadening of the reflections in the PXRD and DLS measurements (**Figure 4.8**).

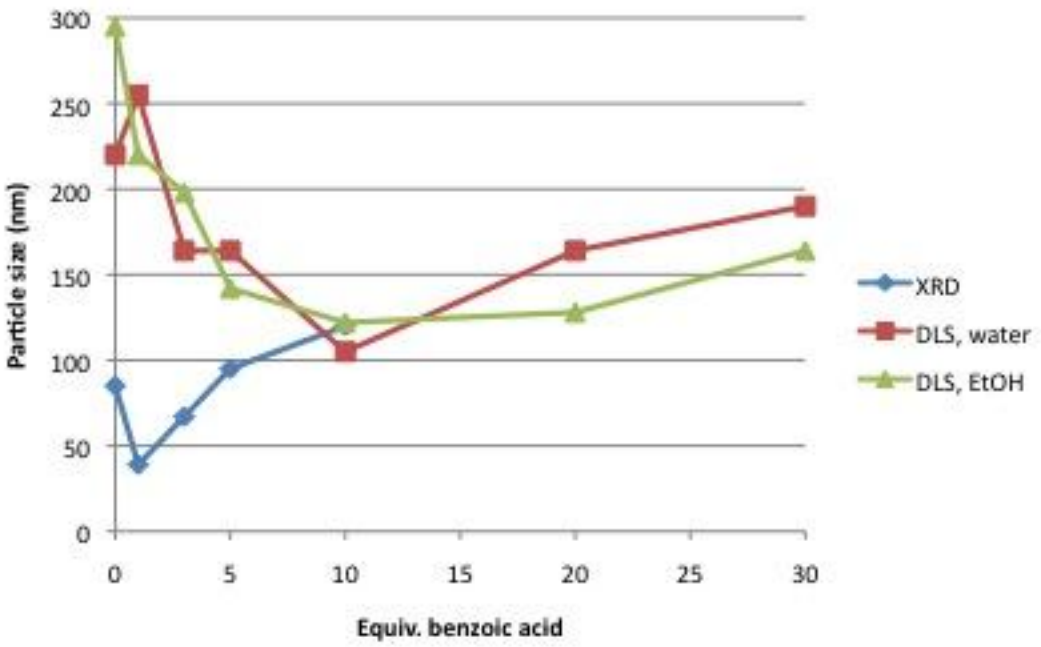

Figure 4.8: Size determination of Zr-BDC MOFs from benzoic acid modulated syntheses (crystallite sizes calculated from PXRD using Scherrer's equation; 20 and 30 equiv. out of scope for determination by Scherrer's equation).

Increasing the equivalents of modulator results in larger crystals, and the morphology also changes. Low equivalents of modulator in the synthesis, results in intergrown, small crystals. Higher equivalents of modulator resulted in larger octahedral shaped nanocrystals.

4.2.5 Evaluation of modulators for Zn_4O SBU containing MOF syntheses

While the examples of modulated MOF syntheses above show great potential in the control of crystal growth and morphology, there are no reported examples of this method for the MOF-5 isoreticular series of MOFs that are structural targets for this piece of work. Inspired by this, it was speculated that addition of modulator in the synthesis mixtures of those discussed in section 4.2.3 might promote MOF crystal growth. If indeed the functionality of the BINOL-based **Ligands A**, **B** and **D** was inhibiting the formation of SBUs, then modulated synthesis may overcome this.

4.2.6 Modulated MOF-5 synthesis

As a starting point for this work, benzoic acid was tested as a modulator for MOF-5. Several different equivalents of benzoic acid were directly added to the synthesis mixtures before the solutions were sealed in a scintillation vial and reacted solvothermally. The MOF-5 synthesis reported by Fang *et al.*[27] was used in these experiments and the synthesis conditions are collated in **Table 4.3**.

Table 4.3 Modulated MOF-5 synthesis (all reactions carried out at 100 °C).

Modulator Equiv.	**Reactants (mmol)**				**Molar ratios of reactants**	**Reaction time (h)**
1	$Zn(NO_3)_2.6H_2O$ 0.9	H_2BDC 0.3	Benzoic acid 0.3	DMF 778	3:1:1:2593	48
2	$Zn(NO_3)_2.6H_2O$ 0.9	H_2BDC 0.3	Benzoic acid 0.6	DMF 778	3:1:2:2593	48
3	$Zn(NO_3)_2.6H_2O$ 0.9	H_2BDC 0.3	Benzoic acid 0.9	DMF 778	3:1:3:2593	48
5	$Zn(NO_3)_2.6H_2O$ 0.9	H_2BDC 0.3	Benzoic acid 1.5	DMF 778	3:1:5:2593	72
10	$Zn(NO_3)_2.6H_2O$ 0.9	H_2BDC 0.3	Benzoic acid 3	DMF 778	3:1:10:2593	168
30	$Zn(NO_3)_2.6H_2O$ 0.9	H_2BDC 0.3	Benzoic acid 9	DMF 778	3:1:30:2593	168

Reactions containing 1 to 3 equivalents of benzoic acid all produced quantitative yields of crystalline material. Compared to the unmodulated synthesis of MOF-5 (not reported), in which crystals can be observed after approximately 5 hours, crystals were visible after 12 hours for 1 equivalent of modulator and after 24 hours for 2 and 3 equivalents. Reactions with 5 and 10 equivalents of modulator took several days to produce a small number of crystals, while the reaction containing 30 equivalents, showed no visible crystalline material after 1 week. Reactions containing 1 to 3 equivalents of modulator produced a suitable amount of material to characterise by PXRD. After removing the vials from the oven, the solutions were cooled; the crystals filtered and then dried by heating under vacuum. The PXRD of each sample was then measured (**Figure 4.9**).

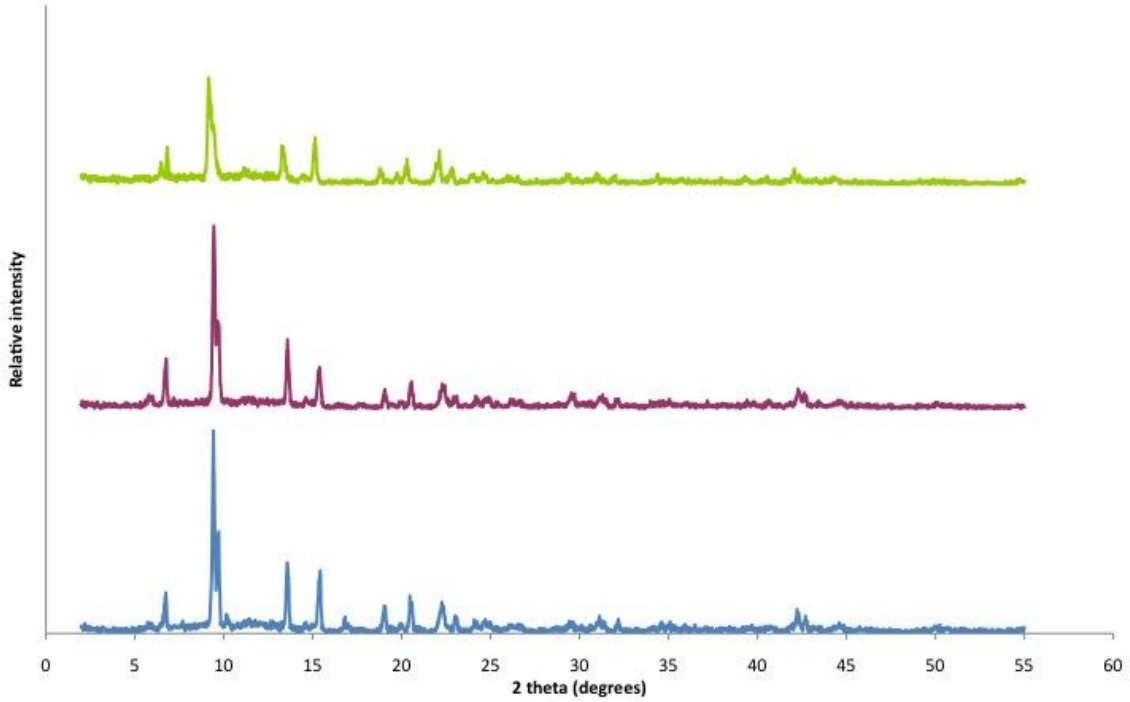

Figure 4.9: PXRD patterns of MOF-5 synthesised by addition of 1 equivalent (blue plot), 2 equivalents (dark pink plot) and 3 equivalents (green plot) of benzoic acid.

The diffractograms match well with those reported for decomposed, interpeneratrated MOF-5 samples by Fang *et al.*[27] and Yan *et al.*[28] As expected, the patterns do not match the predicted PXRD pattern from MOF-5 single crystal data. This is because MOF-5 is well known as being extremely moisture sensitive. The materials were also ground for 2 minutes before their PXRD patterns were measured which is likely to have facilitated their decomposition into the non-porous phase ZnBDC.xH_2O.[28] In this phase, some of the zinc-carbonyl bonds are hydrolysed by water as shown in **Figure 4.10**.

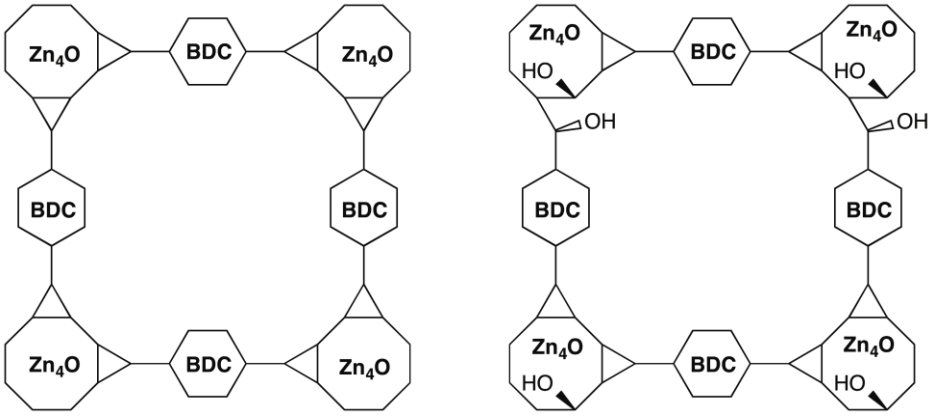

Figure 4.10: Model of MOF-5 (left) and ZnBDC.xH_2O (right) viewed along <100> and <010> axes.

The PXRD patterns confirm that MOF-5 was produced with the presence of benzoic acid in the synthesis mixtures and that the observed crystallisation times varied with increasing equivalents of benzoic acid. The delay in crystallisation due to competition of benzoic acid with BDC to Zn_4O units would fit with the models of modulator competition proposed for other MOF systems. [21-23, 29]

4.2.7 Phthalic acid as a modulator for MOF-5 synthesis

Phthalic acid (1,2-benzenedicarboxylic acid [1,2-BDC]) was also tested as a modulator for MOF-5. There are no examples of 1,2-BDC modulators, and it was speculated that the 1,2-connectivity of the compound would not be favourable for catenation of Zn_4O units; hence it could modulate the synthesis of MOF-5.

Using a typical proceedure,[27] 1 equivalent of 1,2-BDC was added to a to the typical MOF-5 synthesis mixture described previously. After heating at 100 ºC for 48 hours, two visibility different crystal shapes had formed. One appeared to be cubic, similar in shape to those of MOF-5 and the other rod-shaped, which was determined to be a new MOF-like material.

4.3 Synthesis and characterisation of $[Zn_4(O)(1,2\text{-}BDC)_3]_n$[30]

BDC was not included in the synthesis mixture; 1,2-BDC and zinc nitrate were dissolved in DEF in the same molar ratios as discussed above in a scintillation vial. The vial was heated at 100 °C for 48 h to produce a quantitative amount of thin, rod-shaped crystals. Single crystal x-ray analysis revealed that the crystals were a MOF-like coordination polymer formulated as $[Zn_4(O)(1,2\text{-}BDC)_3]\cdot 3DEF$. The repeat unit is shown in **Figure 4.11** and the single crystal x-ray diffraction data and the final crystallographic parameters are shown in **Table 4.4**.

Table 4.4 Crystal data and structure refinement information for $[Zn_4(O)(1,2\text{-}BDC)_3]\cdot 3DEF$.

Empirical formula	$C_{39}H_{45}N_3O_{16}Zn_4$
Formula weight	1073.26
Crystal system	Monoclinic
Space group	$P2_1/c$
a	18.3857(9) Å
b	16.2180(6) Å
c	14.4062(7) Å
β	90.011(3)°
Z	4
Reflections	32050
Independent reflections	7462 [R_{int} = 0.01104]
Final R indices [$F^2 > 2\sigma(F^2)$]	
R1	0.0713
w*R2*	0.1260

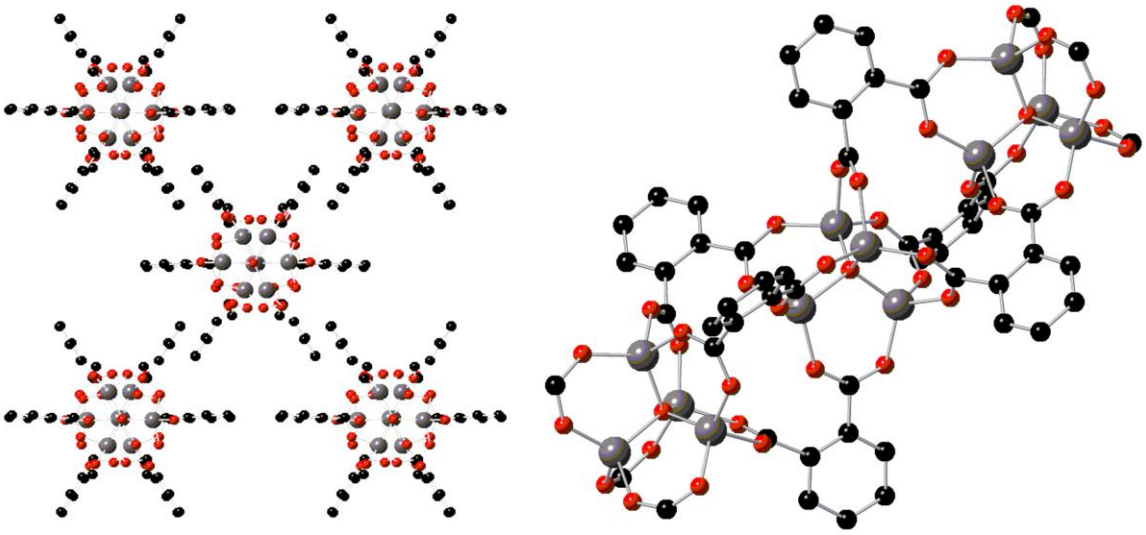

Figure 4.11: Two views of the crystal structure of $[Zn_4(O)(1,2\text{-BDC})_3]_n$ (DEF molecules omitted for clarity). Left: view of the rod packing along the *c* axis; right: side-on view of three Zn_4O units (carbon [black]; oxygen [red]; zinc [grey]).

The structure shows that the Zn_4O units are catentated by three 1,2-BDC units to from infinite 1D rods. Each pseudo-octahedral Zn_4O unit forms a triangular face from coordination to 1,2-BDC. The coordination polymer crystallises in the $P2_1/c$ space group with 3 DEF molecules per unit cell. The Zn_4O units stack face-to-face along the *c* axis, 7.208 Å apart. Three of the O_2CR groups point down forming one face and the other three groups point up forming the other face. Some bond lengths and angles of interest are summarised in **Table 4.5**.

Table 4.5 Some bond lengths of interest relating to the crystal structure of $[Zn_4(O)(1,2BDC)_3]\cdot 3DEF$ and related materials.

Material	**Bond lengths (Å)**	
$[Zn_4(O)(1,2\text{-BDC})_3]\cdot 3DEF$	μ_4O-Zn (average)	1.928
MOF-5	μ_4O-Zn (average)	1.922
$[Zn_4(O)(1,2\text{-BDC})_3]\cdot 3DEF$	μ_4O- μ_4O	7.208
MOF-5	μ_4O- μ_4O	12.916

As can be seen for **Figure 4.12**, the comparison of the experimental (as-synthesised and solvent exchanged materials) and simulated PXRD patterns shows that the product is one, pure phase with the simulated and experimental patterns matching well. The peaks of the simulated

pattern are shifted 0.4º to the left of the experimental results and the single peak in the simulated spectra at 2 theta = 7.26 becomes two peaks in the experimental results. The material has been found to be moisture sensitive. The openness of the SBU may account for this. When removed from solvent, the single crystals quickly desolvate. Thus thermogravmetric analysis proved meaningless. However, if handled briefly in air, the material is stable to solvent exchange and can be readily solvent exchanged into $CHCl_3$. The solvent exchanged PXRD shows good correlation to the as-synthesised pattern, showing the stability.

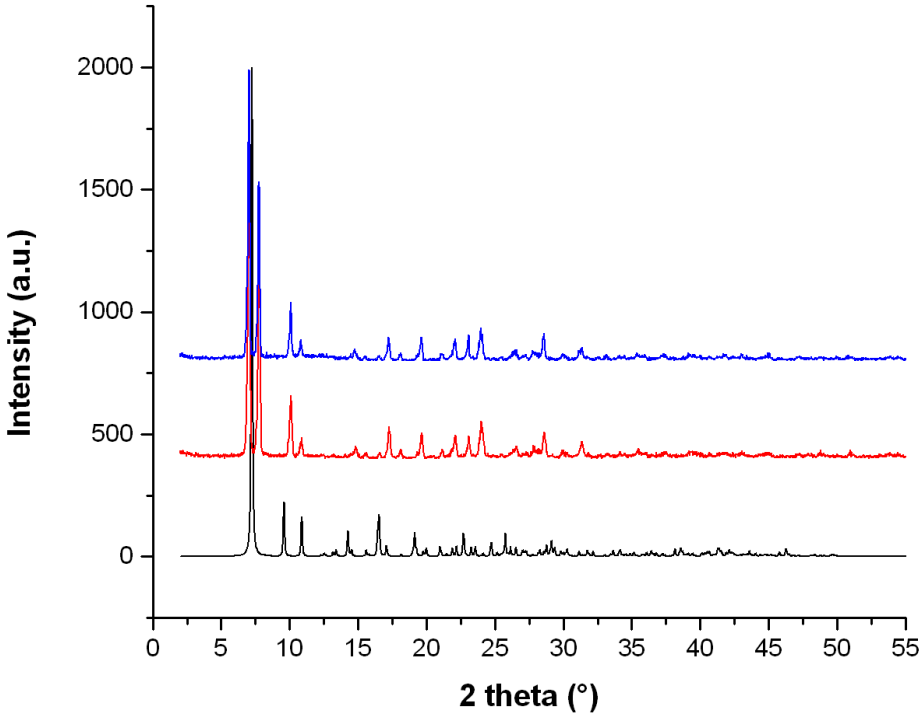

Figure 4.12: A comparison of solvent exchanged (blue line), as-synthesised (red line) and simulated PXRD patterns for $[Zn_4(O)(1,2\text{-BDC})_3]$. The simulated pattern is based upon the single crystal x-ray diffraction data.

The infrared spectrum of the dried material shows characteristic absorptions for an O-H stretch (w, 3384 cm^{-1}), aromatic C-H stretch (m, 3064 cm^{-1}), alkyl C-H stretches (w, 2954 and 2839 cm^{-1}), carboxylate C=O stretch (s, 1715 cm^{-1}) and aromatic C-C stretch (s, 1591 cm^{-1}) (**Chapter 6**). The weak O-H stretch suggests the presence of moisture in the sample or free

hydroxyls on the surface of the crystals. The presence of a small amount of DMF is shown by the alkyl C-H doublet.

4.4 Towards novel MOFs with the Cu_2 paddle-wheel secondary building unit

Perhaps an equally growing reticular series of MOFs to the Zn_4O series, are the Cu_2 paddle wheel MOFs, which contain tetracarboxylates. This work has been lead by Champness and Schroder *et al*., where as well as tetracarboxylates and Cu, a multitude of polytetracarboxylates and metal ions have been used in the construction of novel MOFs.[20, 31-35] These syntheses seem robust, requiring solvothermal reaction of copper nitrate and the polycarboxylate in a DMF/water solution, usually with the addition of a small amount of dilute aqueous HCl. Examining the di- and tetracarboxylic acids reported as ligands in these MOFs, structurally similar to BINOL based ligands, yields a handful of ligands with a biphenyl unit, as shown in **Figure 4.13**.

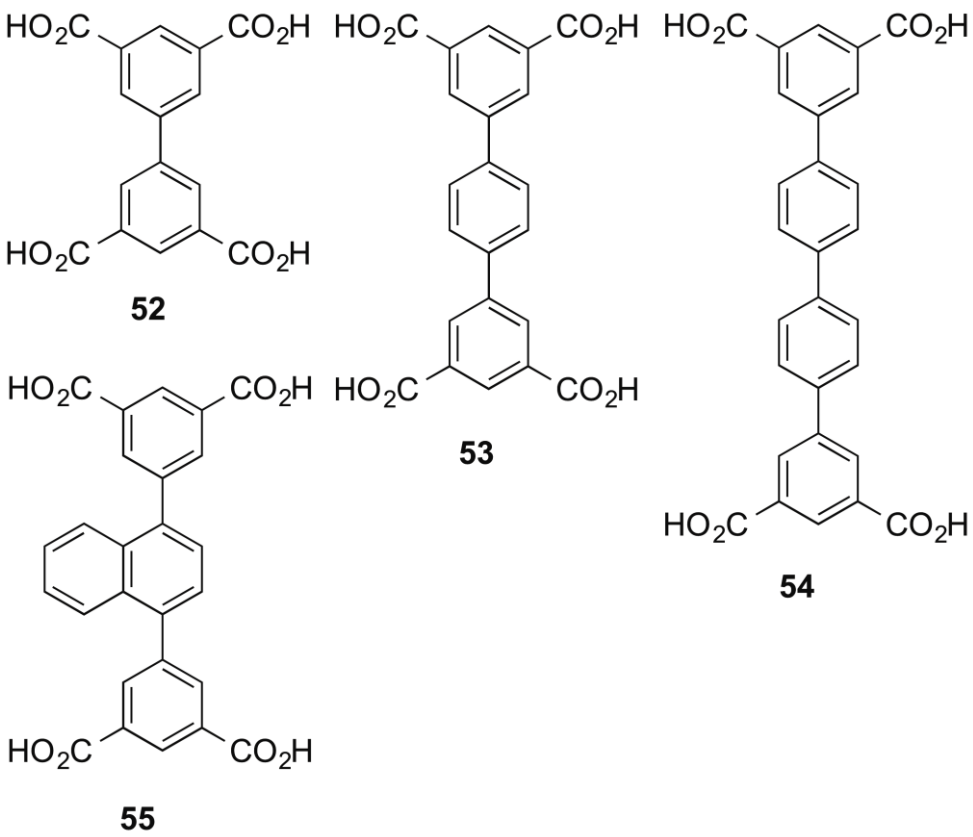

Figure 4.13: Selected ligands used in the reticular synthesis of a series of Cu_2 paddle wheel containing MOFs, all with the core structural formulae $[Cu_2(L)(H_2O)_2]$.[31]

The solvothermal reaction conditions for a selected number of these MOFs are shown in **Table 4.6** and plotted in **Figure 4.13**.

Table 4.6 Synthesis reactants and conditions of several Cu_2 paddle wheel containing MOFs. (all reactions include the addition of 1 drop of concentrated HCl.[31]

Reactants (mmol)					**Molar ratios of reactants**	**Reaction temperature (°C)**	**Reaction time (h)**
$Cu(NO_3)_2.4H_2O$	**52**	DMF	H_2O		2:1:605.2	85	24
1.0	0.5	302.6	647.4				
$Cu(NO_3)_2.4H_2O$	**53**	DMF	H_2O	1,4-dioxane	1:1:650:494	85	48
					3.5:1:1054:2		
0.43	0.123	129.7	277.5	58.62	256:477		
$Cu(NO_3)_2.4H_2O$	**54**	DMF	H_2O	1,4-dioxane	2.6:1:432	85	24
0.43	0.125	129.7	277.5	58.62	3.4:1:1038:2		

				220:469		
$Cu(NO_3)_2.4H_2O$	**55**	DMF	H_2O	3.43:1:6617	85	24
				3.84:1:1038:		
0.192	0.05	51.88	111.0	2220	85	25

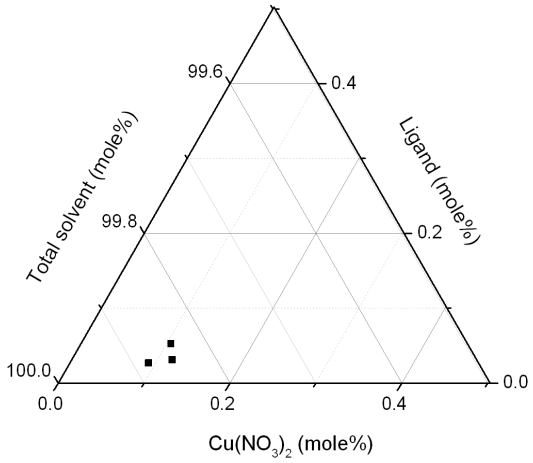

Figure 4.13: Ternary phase diagram showing the reaction compositions in the solvothermal synthesis of some typical Cu_2 paddle wheel-containing MOFs.[31]

4.4.1 Attempted MOF synthesis

Ligands C, **E** and **F** are isostructural to the di- and tetracarboxylates that have been reported to form these Cu_2 paddlewheel frameworks and therefore are suitable to be used in the construction of novel MOFs of this type. The synthesis of **Ligand C**,[18] **E** and **F** have been discussed in **Chapter 2**.

The reaction conditions are plotted below for solvothermal reaction of copper nitrate and **Ligand C, E** (**Figure 4.14**) or **Ligand F** (**Figure 4.15**). The synthetic protocols used closely match those of the example given in section 4.4.

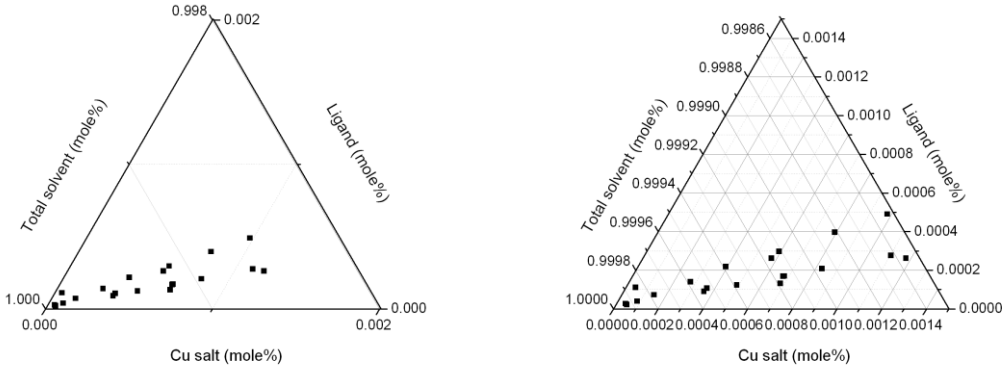

Figure 4.14: Ternary phase diagrams showing the attempted solvothermal MOF synthesis using Ligands C and E. The right diagram shows a closer view of the diagram on the left.

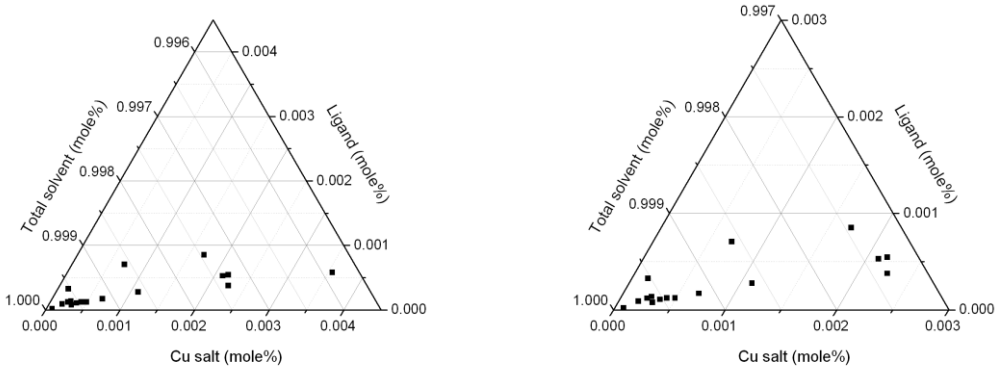

Figure 4.15: Ternary phase diagrams showing the attempted solvothermal MOF synthesis using Ligand F. The right diagram shows a closer view of the diagram on the left.

Several reactions resulted in a poorly crystalline precipitate, with some producing highly sensitive single crystals. The macroscopic structure of these crystals would often deteriorate rapidly upon desolvation, visibly cracking whilst being handled under a light microscope. Therefore, unfortunately none of the synthetic conditions summarised in **Figures 4.14** and **4.15** led to the formation of single crystalline materials that could be analysed by single crystal x-ray diffraction.

4.5 Homochiral MOFs from a mixture of achiral and chiral ligands

In this section, the attempted synthesis of pillared MOFs will be discussed. Examples of these MOFs have been discussed in **Chapter 1**. As has been shown, these materials have the potential to allow real tunability of MOF structures. The achiral ligand is often easier to modify compared to the chiral ligands that are commonly employed. By using the same chiral ligand, and differing the achiral ligand, the structural dimensions of the target MOF can be readily altered (**Figure 4.16**). There were two pillared MOF targets, those based on a Zn_2 paddle wheel SBU and those based on a Cu_2 paddle wheel. Both target MOFs are highly structurally similar, although there synthesis conditions are different.

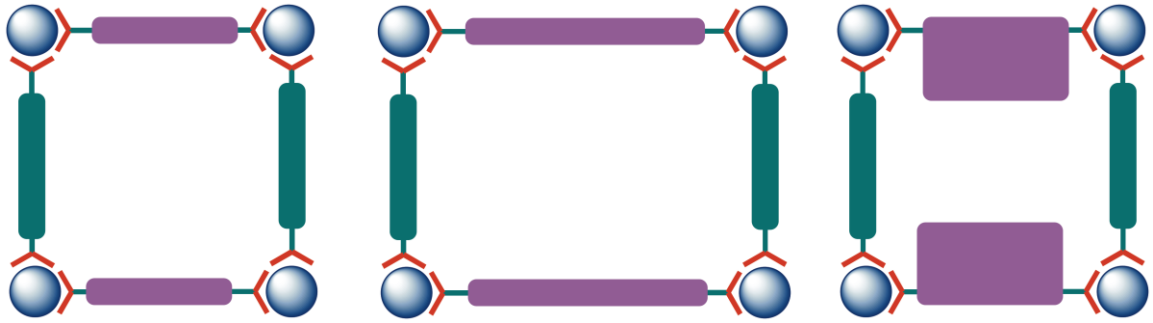

Figure 4.16: Schematic of the tunability of pillared MOFs showing how changing the achiral ligand can increase the dimensions of the MOF (centre image) or change the internal structure of the pore or channel (right image).

4.5.1 Attempted synthesis of novel pillared MOFs using chiral dicarboxylates

There have been a many examples of zinc and copper pillared MOFs reported over the last 10 years.[36-42] The majority of the synthesis conditions use DMF and BPY with dicarboxylates, where in the resulting MOF there are twice as many carboxylate ligands as pillaring ligands. This is reflected in the molar ratios of starting materials, with generally, a 2:2:1 ratio of metal salt:dicarboxylate:pillaring ligand. As discussed, **Ligand A** and **B** are structurally similar to BDC, which is a common ligand used in the synthesis of pillared MOFs. In these MOFs, the pillaring ligand is usually BPY.

The reaction conditions are plotted below for solvothermal reaction of zinc nitrate and either **Ligands A** or **B** in DMF. The synthetic protocols used closely match those of the examples referenced above.[36-42]

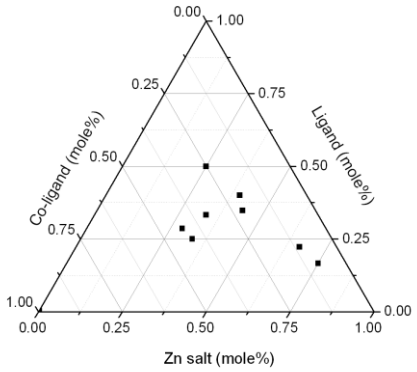

Figure 4.17: Ternary phase diagrams showing the attempted solvothermal MOF synthesis using **Ligand A** or **B** with a co-ligand to generate Zn_2 paddle wheel pillared MOFs.

The reaction conditions are plotted below for solvothermal reaction of copper nitrate and either **Ligands A** or **B** in DMF, or DEF or DMSO. The synthetic protocols used closely match those of the examples referenced above.[36-42]

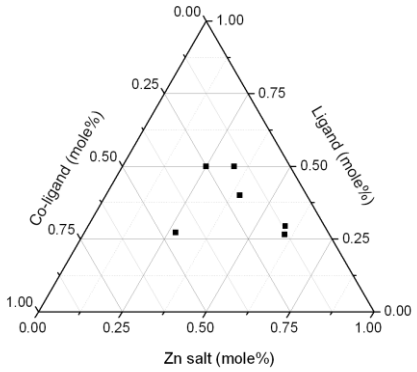

Figure 4.18: Ternary phase diagrams showing the attempted solvothermal MOF synthesis using **Ligand A** or **B** with a co-ligand to generate Cu_2 paddle wheel pillared MOFs.

Unfortunately, none of the synthetic conditions summarised in **Figures 4.17** and **4.18** led to the formation of single crystalline materials. Even when over saturating the solution with zinc nitrate (by heating), no formation of crystalline material was observed.

4.5.2 Attempted synthesis of novel pillared MOFs using chiral dipyridinyls

Switching this methodology and using a chiral bidentate ligand and an achiral dicarboxylate was also investigated using **Ligand G**. **Ligand G** is structurally similar to BPY which is almost ubiquitously used in the synthesis of pillared MOFs.[38] The reaction conditions are plotted below for solvothermal reaction of zinc nitrate and **Ligands G** in DMF with BDC (**Figure 4.19**).

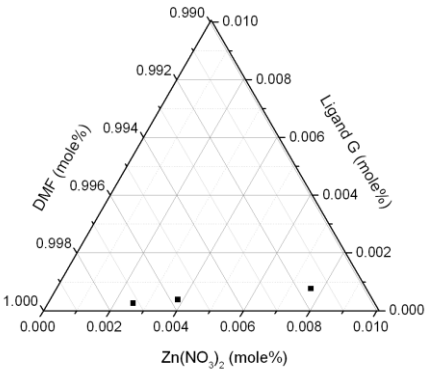

Figure 4.19: Ternary phase diagram showing the attempted solvothermal MOF synthesis using **Ligands G** in DMF reacting with zinc nitrate and BDC (BDC was kept at 0.02 mmol for all reactions).

Again, no crystalline product was observed from these reactions. Nor was any MOF-5 produced. This suggests that **Ligand G** ligand is inhibiting the formation of MOF-5 even though the synthesis conditions are very similar to those that would be employed to generate the well-known MOF.

With the lack of success using **Ligand G** to create pillared MOFs, the dibenzyl ether protected precursor to **Ligand G** was tested as an appropriate MOF ligand. By using a compound with protected diols, it was envisioned the desired pillar MOF could be formed; this could then establish synthesis conditions for the structurally similar MOF using **Ligand G**.

4.5.3 Synthesis and characterisation of [Zn(Ligand H)(BDC)]

Solvothermal reaction of the precursor, **Ligand H**, BDC and $Zn(NO_3)_2$ in DMF yields a quantitative amount of block colourless crystals. Single crystal x-ray diffraction analysis revealed that the material was not the expected Zn_2 pillared MOF, but a triply interpenetrated 3D framework that crystallises in the space group *C*2/*c*.

The molecular formula is [Zn(**Ligand H**)(BDC)] and the SBU/repeat unit is shown below in **Figure 4.20**. Instead on forming a Zn_2 paddle wheel SBU, the Zn^{2+} ion forms the SBU, and has a slightly distorted tetrahedral geometry. The Zn^{2+} ion coordinates to two pyridinyl groups from two **Ligand H** molecules and one oxygen from the carbonyl group of two BDC molecules.

Table 4.7: Crystal data and structure refinement information for [Zn(**Ligand H**)(BDC)] (Full details of the refinement can be found in the cif in the Appendix 2)

Empirical formula	$C_{52}H_{36}N_2O_6Zn$
Formula weight	850.20
Crystal system	Monoclinic
Space group	*C*2/*c*
a	20.06(3) Å
b	29.81(4) Å
c	13.610(18) Å
β	107.410(11)°
Z	8
Reflections	27129
Independent reflections	6825 [R_{int} = 0.1141]
Final *R* indices [$F^2 > 2\sigma(F^2)$]	
R1	0.1351

w*R2*	0.3646

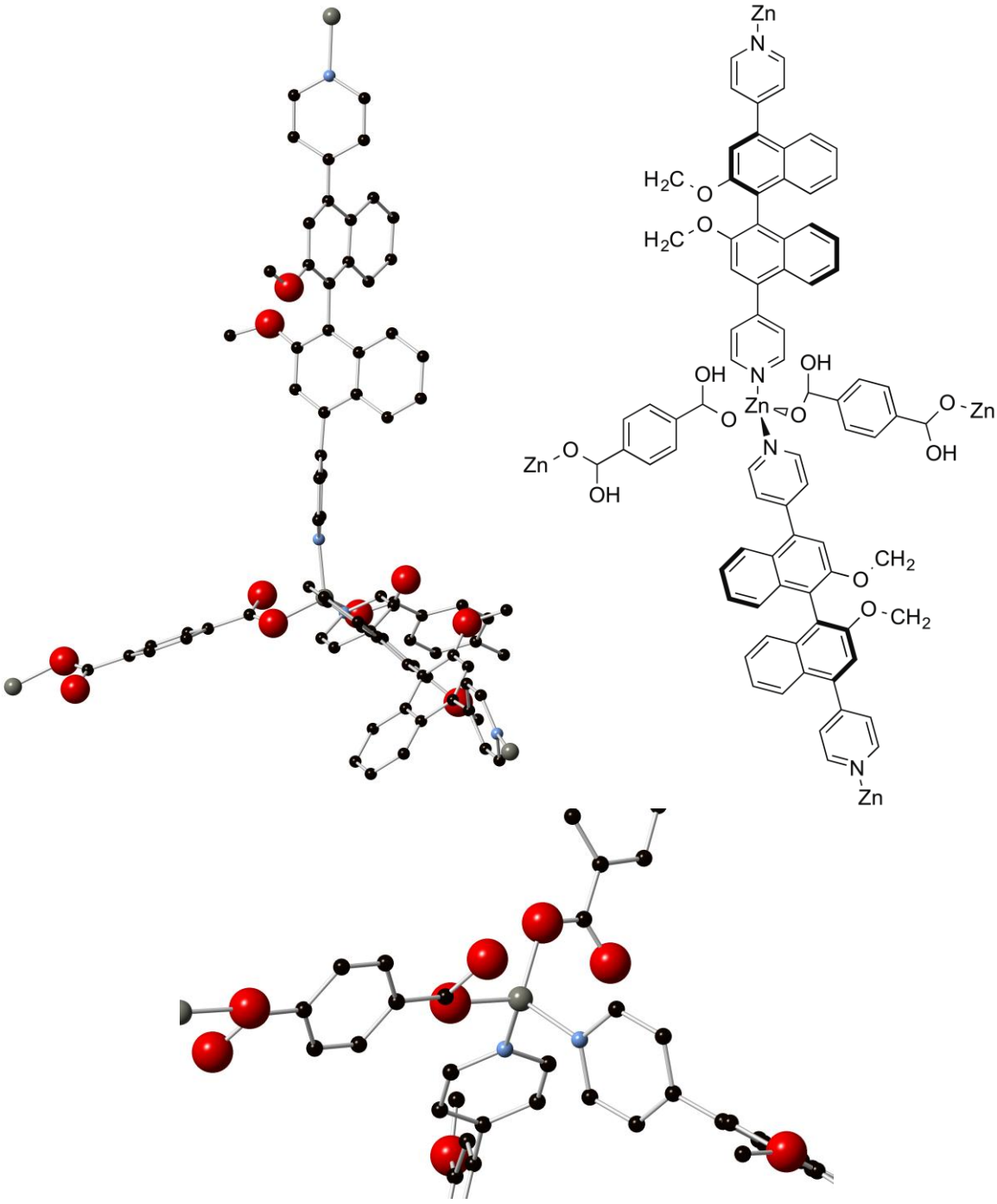

Figure 4.20: Section of [Zn(**Ligand H**)(BDC)] x-ray single crystal structure and zoomed in view of Zn^{2+} SBU (lower image) (highly disordered benzyl groups omitted) (carbon [black]; oxygen [red]; nitrogen [light blue]; zinc [grey]).

The BDC form a 2D, zigzag structure, bonding to the Zn^{2+} ions through alternating carboxylate oxygens. The dipyridinyl ligand also forms a zigzag 2D structure perpendicular to the BDC structure. These form a complicated 3D framework. The large size of the ligands allows triple interpenetration of the framework. As has been previously discussed, the introduction of longer ligands (dicarboxylates and/or bidentate pillar) often leads to the formation of multiple interpenetrated frameworks.[43] The interpenetration has occurred as a result of the larger voids (9.801 x 15.024 A) created by the BDC-Zn-Ligand H combination. The voids shown in **Figure 4.21** (viewed along the *c*-axis) are not as open as they appear because the benzene rings in the benzyl groups protecting the diols in the BINOL unit are highly disordered in the solid-state single crystal structure, and so have been omitted from the image. Interpenetrating net viewed along the *a*-axis

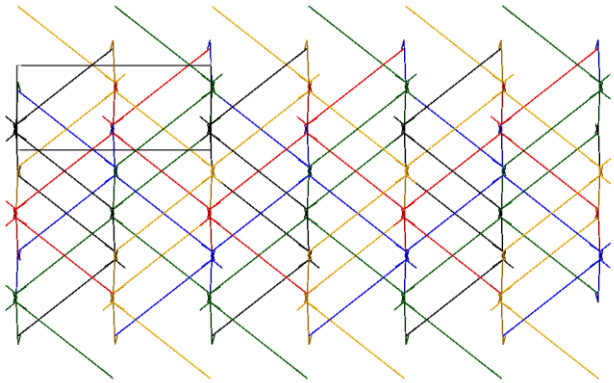

Interpenetrating net viewed along the *a*-axis

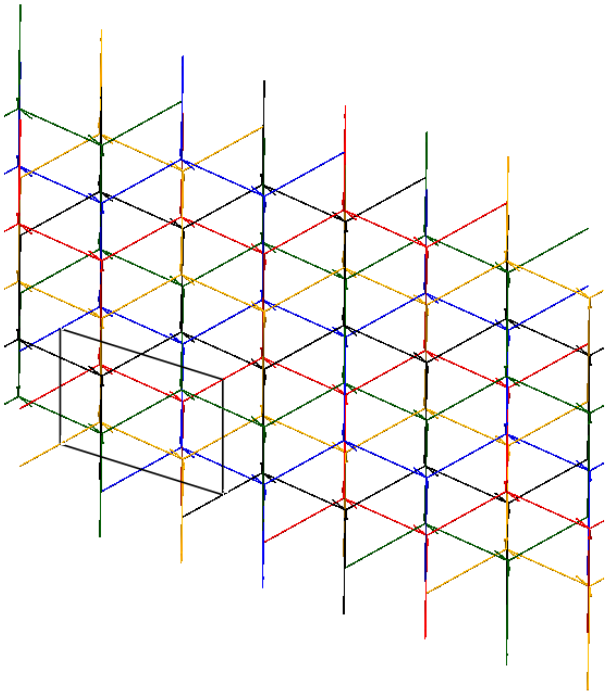

Interpenetrating net viewed along the *b*-axis

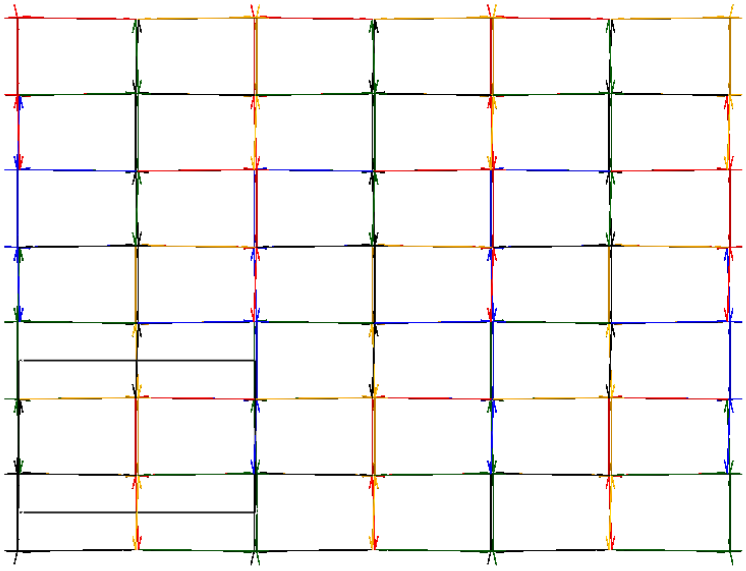

Interpenetrating net viewed along the *c*-axis

Figure 4.21: Interpenetrating views of [Zn(**Ligand H**)(BDC)] x-ray single crystal structure showing the 4 interpenetrated frameworks (each framework is a different colour; unit cell shown as grey box).

Although this structure was interesting, it was not the target Zn_2 pillared MOF. However, this is the first example in this thesis of a ligand with protected diols that has led to a homochiral MOF. The structurally similar unprotected diol ligand has not led to a MOF. The chemistry of the protected and unprotected diol ligands has been shown to be vastly different in the formation of single crystalline MOFs: in one case solvothermal reaction occurs producing a MOF and in the other, no solvothermal reaction occurs.

4.6 Other novel MOF-like materials

As has been well discussed in this **Chapter**, the BDC ligand has been well deployed in the synthesis of MOFs. Not so well employed in SBUs is cadmium. Cd^{2+} has similar binding modes to Zn^{2+}. **Ligand A** was tested with solvothermal reaction with $Cd(NO_3)_2$ in a number of different solvents (see Appendix 1) with no precipitate in all reactions. Reacting equimolar amounts of BDC and **Ligand A** with $Cd(NO_3)_2$ in MeOH did produce a quantitative amount of semi-crystalline precipitate. Adding water to the mixture and repeating the synthesis produced single crystal products a colourless lath shaped crystals. It was found a MeOH-water ratio of 4:1 gave a quantitative amount of single crystal product. The syntheses are summarised in **Figure 4.22**.

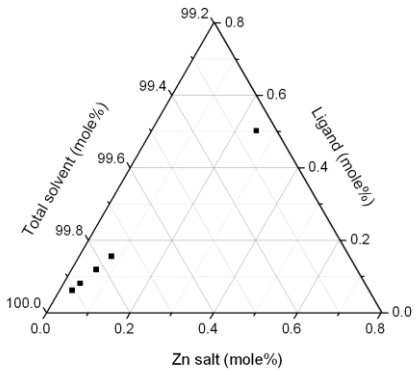

Figure 4.22: Ternary phase diagrams showing the attempted solvothermal MOF synthesis using equimolar mole% **Ligand A** and BDC in MeOH/H_2O (1:0 MeOH/H_2O → 6:1 MeOH/H_2O, v/v).

4.6.1 Synthesis of [Cd(BDC)(H_2O)$_3$]

The reaction of BDC, **Ligand A** and $Cd(NO_3)_2$ in a MeOH-water (4:1 v/v) solution at 80 ºC for 10 h produced a quantitative amount of block colourless crystals. Single crystal x-ray diffraction analysis revealed that the material is a coordination polymer of Cd-BDC repeat units crystallising to the space group *P*–1 and formulated as [Cd(BDC)(H_2O)$_3$].2.25H_2O. **Ligand A** is apparently ignored under these solvothermal conditions, with the linear coordination polymer being the preferred product (**Figure 4.23**).

Table 4.8: Crystal data and structure refinement information for [Cd(BDC)(H_2O)$_3$].2.25H_2O

Empirical formula	$C_8H_{14.50}CdO_{9.25}$
Formula weight	371.10
Crystal system	Triclinic
Space group	*P*-1
a	9.6820(12) Å
b	10.0226(14) Å
c	14.2989(17) Å
α	91.455(10)°
β	106.980(8)°
χ	109.358(5)°
Z	4
Reflections	8702
Independent reflections	4015 [R_{int} = 0.0526]
Final *R* indices [$F^2 > 2\sigma(F^2)$]	
R1	0.0684
w*R2*	0.1353

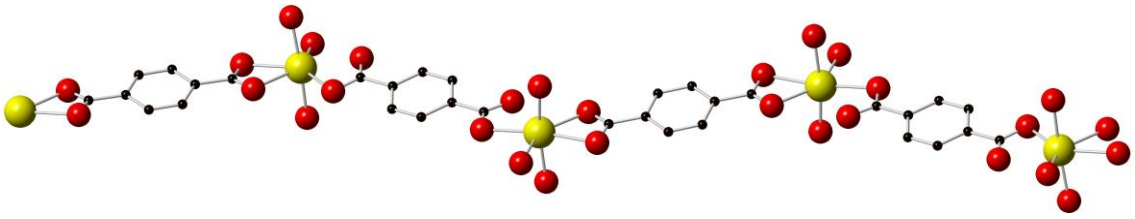

Figure 4.23: View of the crystal structure of $[Cd(BDC)(H_2O)_3].2.25H_2O$ (water solvent molecules omitted for clarity) (carbon [black]; oxygen [red]; cadmium [yellow]).

Each Cd centre has the same coordination environment, coordinating to three water molecules and four carboxylic oxygens. The Cd has a distorted pentagonal bipyramidal coordination geometry, with coordination number = 7, as shown by the bond lengths and angles shown in **Table 4.9**. The carboxylic oxygens and oxygen from one water molecule form the pentagonal plane around the Cd centre. This is almost planar as shown be combining the O-Cd-O bond angles, which equal 360.163°. As would be expected, one of the carboxylic acid oxygens from each BDC molecule has a shorter bond length to the Cd than the other oxygen on the acid.

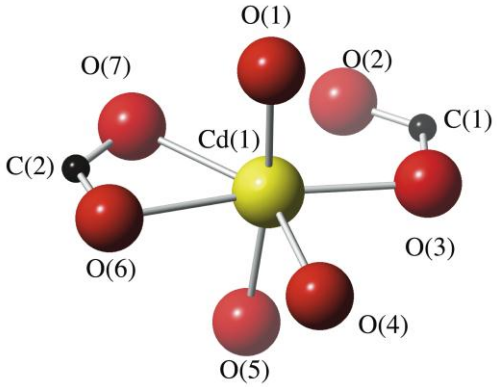

Table 4.9 Selected bond lengths and angles for Cd centre of $[Cd(BDC)(H_2O)_3].2.25H_2O$.

Bond lengths (Å)			
Cd(1)-O(1)	2.300	Cd(1)-O(7)	2.335
Cd(1)-O(2)	2.462	C(1)-O(2)	1.262
Cd(1)-O(3)	2.313	C(1)-O(3)	1.263
Cd(1)-O(4)	2.346	C(2)-O(6)	1.282
Cd(1)-O(5)	2.280	C(2)-O(7)	1.260
Cd(1)-O(6)	2.444		
Angles (°)			

O(1)-Cd(1)-O(2)	94.823	O(5)-Cd(1)-O(4)	85.803
O(1)-Cd(1)-O(3)	93.674	O(5)-Cd(1)-O(6)	86.567
O(1)-Cd(1)-O(4)	90.272	O(5)-Cd(1)-O(7)	89.678
O(1)-Cd(1)-O(5)	170.526	O(2)-Cd(1)-O(3)	54.323
O(1)-Cd(1)-O(6)	84.639	O(3)-Cd(1)-O(4)	81.458
O(1)-Cd(1)-O(7)	88.067	O(4)-Cd(1)-O(6)	87.346
O(5)-Cd(1)-O(2)	94.005	O(6)-Cd(1)-O(7)	54.400
O(5)-Cd(1)-O(3)	94.263	O(7)-Cd(1)-O(2)	82.536

4.7 Conclusion

The attempted preparation of many MOFs has been discussed via systematic investigations with some known and novel chiral polycarboxylate and polypyridinyl potential MOF ligands. All the ligands are structurally similar to ligands that have been reported to be used in the construction of MOFs. Unfortunately a large number of the syntheses reported did not yield any crystalline material. It has been speculated the free diols of the BINOL based ligands reported has a dramatic effect on the likelihood of formation of target MOFs. This has been shown be the case in the synthesis of [Zn(**Ligand H**)(BDC)], where the protected diol ligand is incorporated into a MOF, where the unprotected diol ligand is not under similar synthesis conditions.

Although the coordination polymers and MOFs described in this **Chapter** do not show any particularly novel properties, the design and synthesis of these MOFs may support the development of new materials with potentially important product applications in the future.

The coordination polymer $[Zn_4(O)(1,2\text{-}BDC)_3]$ completes the set of coordination polymers synthesised upon solvent–thermal reaction of zinc nitrate and simple benzene-dicarboxylates. Interestingly, the only way that the Zn_4O secondary building units can connect when benzene-1,2-dicarboxlyate is employed is to form a rod-like coordination polymer rather than a 2-D or 3-D structure. By using a ligand where the coordinating functional groups are constrained within close proximity to one another, a new material has been obtained. This system is yet

another example of the rigidity of the solvothermal synthesis employed to produce many other MOF-like structures.

4.8 References

1. L. Q. Ma, C. Abney and W. B. Lin, *Chem. Soc. Rev.*, 2009, **38**, 1248.
2. J. S. Seo, D. Whang, H. Lee, S. I. Jun, J. Oh, Y. J. Jeon and K. Kim, *Nature*, 2000, **404**, 982.
3. O. R. Evans, H. L. Ngo and W. B. Lin, *J. Am. Chem. Soc*, 2001, **123**, 10395.
4. C. D. Wu, A. Hu, L. Zhang and W. B. Lin, *J. Am. Chem. Soc.*, 2005, **127**, 8940.
5. S. H. Cho, B. Q. Ma, S. T. Nguyen, J. T. Hupp and T. E. Albrecht-Schmitt, *Chem. Commun.*, 2006, 2563.
6. C. D. Wu and W. B. Lin, *Angew. Chem. Int. Ed.*, 2007, **46**, 1075.
7. M. Banerjee, S. Das, M. Yoon, H. J. Choi, M. H. Hyun, S. M. Park, G. Seo and K. Kim, *J. Am. Chem. Soc.*, 2009, **131**, 7524.
8. L. Q. Ma and W. B. Lin, *J. Am. Chem. Soc.*, 2008, **130**, 13834.
9. L. Q. Ma, D. J. Mihalcik and W. B. Lin, *J. Am. Chem. Soc.*, 2009, **131**, 4610.
10. L. Ma, J. M. Falkowski, C. Abney and W. Lin, *Nat. Chem.*, 2010, **2**, 838.
11. K. Tanaka, H. Takano and Z. Urbanczyk-Lipkowska, *J. Inclusion Phenom.Macrocyclic Chem.*, 2006, **56**, 281.
12. L. Q. Ma, C. D. Wu, M. M. Wanderley and W. B. Lin, *Angew. Chem. Int. Ed.*, 2010, **49**, 8244.
13. M. Sabo, A. Henschel, H. Froede, E. Klemm and S. Kaskel, *J. Mater. Chem.*, 2007, **17**, 3827.
14. O. M. Yaghi, *Tetrahedron Lett.*, 2008, **64**, 8553.
15. B. Kesanli, Y. Cui, M. R. Smith, E. W. Bittner, B. C. Bockrath and W. B. Lin, *Angew. Chem. Int. Ed.*, 2005, **44**, 72.
16. C. Valente, E. Choi, M. E. Belowich, C. J. Doonan, Q. W. Li, T. B. Gasa, Y. Y. Botros, O. M. Yaghi and J. F. Stoddart, *Chem. Commun.*, 2010, **46**, 4911.
17. F. J. Song, C. Wang and W. B. Lin, *Chem. Commun.*, 2011, **47**, 8256.
18. K. Tanaka, S. Oda and M. Shiro, *Chem. Commun.*, 2008, 820.

19. K. Tanaka, K. Otani, T. Murase, S. Nishihote and Z. Urbanczyk-Lipkowska, *B. Chem. Soc. Jpn.*, 2012, **85**, 709.
20. X. Lin, A. J. Blake, C. Wilson, X. Z. Sun, N. R. Champness, M. W. George, P. Hubberstey, R. Mokaya and M. Schroder, *J. Am . Chem. Soc.*, 2006, **128**, 10745.
21. T. Tsuruoka, S. Furukawa, Y. Takashima, K. Yoshida, S. Isoda and S. Kitagawa, *Angew. Chem. Int. Ed.*, 2009, **48**, 4739.
22. S. Diring, S. Furukawa, Y. Takashima, T. Tsuruoka and S. Kitagawa, *Chem. Mater.*, 2010, **22**, 4531.
23. P. Behrens, A. Schaate, P. Roy, A. Godt, J. Lippke, F. Waltz and M. Wiebcke, *Chem-Eur. J.*, 2011, **17**, 6643.
24. S. S. Y. Chui, S. M. F. Lo, J. P. H. Charmant, A. G. Orpen and I. D. Williams, *Science*, 1999, **283**, 1148.
25. P. Krawiec, M. Kramer, M. Sabo, R. Kunschke, H. Frode and S. Kaskel, *Adv. Eng. Mater.*, 2006, **8**, 293.
26. J. H. Cavka, S. Jakobsen, U. Olsbye, N. Guillou, C. Lamberti, S. Bordiga and K. P. Lillerud, *J. Am . Chem. Soc.*, 2008, **130**, 13850.
27. B. Chen, X. Wang, Q. Zhang, X. Xi, J. Cai, H. Qi, S. Shi, J. Wang, D. Yuan and M. Fang, *J.Mater. Chem.*, 2010, **20**, 3758.
28. L. M. Huang, H. T. Wang, J. X. Chen, Z. B. Wang, J. Y. Sun, D. Y. Zhao and Y. S. Yan, *Microporous Mesoporous Mater.*, 2003, **58**, 105.
29. Y. Sakata, S. Furukawa, C. Kim and S. Kitagawa, *Chem. Lett.*, 2012, **41**, 1436.
30. S. M. Keltie, P. A. Gale, M. E. Light and M. Tromp, *J. Coord. Chem.*, 2013, **66**, 3058.
31. X. Lin, I. Telepeni, A. J. Blake, A. Dailly, C. M. Brown, J. M. Simmons, M. Zoppi, G. S. Walker, K. M. Thomas, T. J. Mays, P. Hubberstey, N. R. Champness and M. Schroder, *J. Am . Chem. Soc.*, 2009, **131**, 2159.
32. X. Lin, J. H. Jia, X. B. Zhao, K. M. Thomas, A. J. Blake, G. S. Walker, N. R. Champness, P. Hubberstey and M. Schroder, *Angew. Chem. Int. Ed.*, 2006, **45**, 7358.
33. Y. Yan, I. Telepeni, S. H. Yang, X. Lin, W. Kockelmann, A. Dailly, A. J. Blake, W. Lewis, G. S. Walker, D. R. Allan, S. A. Barnett, N. R. Champness and M. Schroder, *J. Am. Chem. Soc.*, 2010, **132**, 4092.

34. Y. X. Hu, H. B. Ma, B. Zheng, W. W. Zhang, S. C. Xiang, L. Zhai, L. F. Wang, B. L. Chen, X. M. Ren and J. F. Bai, *Inorg. Chem.*, 2012, **51**, 7066.
35. Y. B. He, S. C. Xiang, Z. J. Zhang, S. S. Xiong, C. D. Wu, W. Zhou, T. Yildirim, R. Krishna and B. L. Chen, *J. Mater. Chem. A*, 2013, **1**, 2543.
36. D. N. Dybtsev, H. Chun and K. Kim, *Angew. Chem. Int. Ed.*, 2004, **43**, 5033.
37. B. Q. Ma, K. L. Mulfort and J. T. Hupp, *Inorg. Chem.*, 2005, **44**, 4912.
38. H. Chun, D. N. Dybtsev, H. Kim and K. Kim, *Chem. Eur. J.*, 2005, **11**, 3521.
39. B. L. Chen, C. D. Liang, J. Yang, D. S. Contreras, Y. L. Clancy, E. B. Lobkovsky, O. M. Yaghi and S. Dai, *Angew. Chem. Int. Ed.*, 2006, **45**, 1390.
40. L. Sbircea, N. D. Sharma, W. Clegg, R. W. Harrington, P. N. Horton, M. B. Hursthouse, D. C. Apperley, D. R. Boyd and S. L. James, *Chem. Commun.*, 2008, 5538.
41. T. Yamada and H. Kitagawa, *J. Am . Chem. Soc.*, 2009, **131**, 6312.
42. K. L. Mulfort, O. K. Farha, C. L. Stern, A. A. Sarjeant and J. T. Hupp, *J. Am. Chem. Soc.*, 2009, **131**, 3866.
43. S. Horike, D. Tanaka, K. Nakagawa and S. Kitagawa, *Chem. Commun*, 2007, 3395.

5 Insights into the self-assembly of metal-organic frameworks

5.1 Introduction

The crystal growth of porous materials is crucial in controlling properties such as morphology, size, intergrowth, habit and composition, which ultimately affect their function. The self-assembly of these material plays an important part in the crystal growth. However, even for the extensively studied zeolites, the synthesis and crystal growth mechanism is still not well understood. Zeolites can be considered as the closest topologically related family of porous material to MOFs. Therefore, the theory of nucleation and growth of zeolites is comparable to that of MOFs.[1]

A select list of concepts regarding MOF synthesis that can be taken from the theory of nucleation and growth of zeolites follows:

- **Nucleation**

  The formation of a crystallisation phase from solution starts with a nucleation event. Nucleation is defined as the series of atomic or molecular processes by which the atoms or molecules of a reactant phase rearrange into a cluster of the product phase large enough to grow only irreversibly to a macroscopically larger size.[2] The cluster is defined as nucleus or critical nuclei.

- **Supersaturation**

  Supersaturation is the driving force needed for the nucleation and growth of a crystal. It is the difference in chemical potential between a molecule in solution and that in the bulk of the crystal phase.[2]

- **Nucleation rate**

  The rate of nucleation is the number of nuclei formed per unit time per unit volume. The rate of nucleation is practically zero unit a critical value of supersaturation is achieved.[2]

- **Induction time**

  Induction time is defined as the amount of time elapsed between the achievement of a supersaturated solution and the observation of crystals.[2]

- **Crystal growth**

  Crystal growth is the series of process by which an atom or molecule is incorporated into the surface of a crystal, causing an increase in size. These process can be separated into four steps: transport of atoms / molecules through solution → attachment of atoms / molecules to the surface → movement of atoms / molecule on the surface → attachment of atoms / molecules to edges and kinks.[2]

A typical crystallisation curve for zeolite synthesis is shown in **Figure 5.1**. Nucleation takes place only at the start of the synthesis after some induction time. There is an exponential increase in the rate of nucleation, then a decrease to zero. Crystal growth starts to occur after a certain number of nuclei have been formed. It increases rapidly reaching a steady state and then as the reactants are consumed, it decreases to zero. The theoretical supersaturation is also shown. The nucleation and growth are initiated by the increase in supersaturation. As the supersaturation flats out, the growth reaches a steady state, then as the reactants are consumed it decreases to zero.

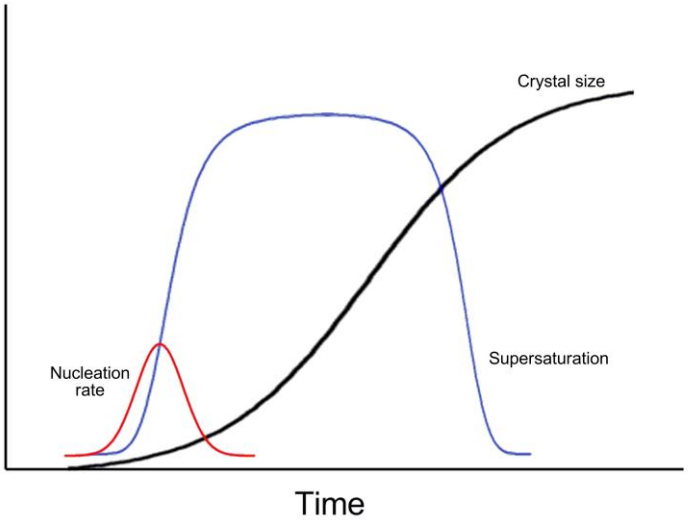

Figure 5.1 Schematic representation of zeolite synthesis.

The mechanism of nucleation and crystal growth in MOFs has been little studied.[1] Unlike with zeolites, there is no real understanding of the molecular processes involved in the self-assembly of MOFs. Answering this question may facilitate in the properties by design approach that is much sort after in porous materials. The main hindrance in understanding is the direct observation of molecular processes occurring during the MOF self-assembly process. Several groups have reported some insights into a handful of systems.

5.1.1 Examples of direct observation into the self-assembly of MOFs

Millange and co-workers have studied the *in situ* solvothermal crystallisation of HKUST-1 ($[Cu_3(BTC)_2 \cdot solvent]$) and MIL-53 ($[Fe^{III}(OH)(BDC) \cdot H_2O]$) using EDXRD (energy-dispersive XRD).[3] They monitored the crystallisation of HKUST-1 at five different temperatures over 30 minutes. Analysis of the crystallisation *vs.* temperature curves using the Avrami-Erofe'ev model suggested that crystallisation is controlled by nucleation events rather than diffusion of reactive species to the sites of nucleation or crystal growth: the continued formation of nuclei (nucleation events) over the synthesis dominants crystallisation. This has also been shown by a light scattering experiment reported by Zacher *et al.*[4] Interestingly, the solvothermal crystallisation of MIL-53 showed an intermediate phase formed that eventually became the expected product phase. Zacher and co-workers were able to trap this intermediate phase as a highly crystalline solid that is related to MOF-235 ($[Fe_3O(BDC)_3(DMF)_3][FeCl_4] \cdot (DMF)_3$).[5] The SBUs of this phase are

different to those in MIL-53. Therefore, they suggested that the first phase dissolves in solution, releasing reactive moieties that can then crystallise as the MIL-53 product.

The direct observation of a SBU in solution throughout a MOF synthesis has been reported by Férey *et al.*[6] during the synthesis of MIL-89 ($[Fe_3O(O_2C(CH_2)_4CO_2)_3(MeOH)_3{\cdot}Cl{\cdot}(MeOH)_3]$), an Fe^{III} oxycarboxylate.[7] MIL-89 is synthesised from trimeric $Fe(OAc)_3$ and the ligand *trans,trans*-muconic acid. The trimeric Fe^{III} acetate cluster exchanges the acetates for the dicarboxylates to form the MIL-89 structure. Férey used EXAFS at the Fe K-edge to show the presence of the Fe^{III} trimeric cluster in solution throughout the reaction. A pattern of interatomic correlations including an $Fe^{III} – Fe^{III}$ distance of 3.2 – 3.4 Å were characteristic of the trimeric cluster. While the observation of the SBU during the synthesis was the first discovery of its kind, the importance to crystallisation remains unknown.

Henderson *et al*. have used ESI-MS to elucidate the solution species present during the synthesis of the MOF $[Mg_2(Hcam)_3{\cdot}3H_2O]{\cdot}NO_3{\cdot}MeCN$.[8] The MOF is formed from reaction of $Mg(NO_3)_2$ and (+)-camphoric in acetonitrile. These are ideal conditions to follow the synthesis using ESI-MS as the technique is non-destructive to the species present in solution. The SBU of the MOF comprises of triply carboxylate-bridged Mg^{II} centres (a 3-fold paddle-wheel) within a Mg_3 trimeric aggregate. There are a variety of species found to be in solution such as the ions $[Mg(H_2cam)(Hcam)]^+$ and $[Mg(H_2cam)_2(Hcam)]^+$, but most interesting is the signal at 645 *m/z* which corresponds to the $[Mg_2(Hcam)_3]^+$ 3-fold paddle wheel. Analysis of this signal by increasing the cone voltage and by precursor MS–MS showed that it does not have a heavier parent ion and is a particularly stable ion. It is reasonable to suggest that the SBU is present in solution during crystallisation and that the self-assembly process relies on the cluster being soluble.

The difficulties of synthesising novel MOFs with ligands containing more complex functionalities have been highlighted in **Chapter 4**. The studies mentioned above constitute a good summary of the level of insight into the self-assembly mechanism of MOFs. The synthesis of new MOFs is still somewhat serendipitous, with high throughput screening of reagents and reaction conditions required to discover new materials with increasing complexity. An increased understanding of the self-assembly and crystal growth mechanisms would give insight into the 'black box' syntheses that are often reported.

Many reports of a reticular series of MOFs have vastly different synthesis conditions and synthetic protocols even though the reticular series of MOF reported have the same underlying topography. The efforts of researchers to screen synthesis conditions and narrow these down to produce the target materials could be attenuated with more understanding of the MOF synthesis processes.

In this **Chapter**, a novel method of studying the MOF ligands during the MOF synthesis has been developed and tested on a series of prototypical zinc containing MOFs.

5.2 NMR studies

5.2.1 Introduction

The interest in the self-assembly of HKUST-1 has been driven by the mild synthesises conditions which allow for easy *in situ* investigation. However, the more classical zinc containing MOFs have not been well studied. Prototypical MOF-5 and its family of isoreticular MOFs (discussed in **Chapters 1** and **4**) are synthesised in very similar solvothermal conditions and generally produce materials of a single phase, as high quality single crystals. Also, the isoreticular series of zinc paddle wheel MOFs are synthesised in similar conditions (solvent and temperature) and have some common properties when compared to other MOFs.

These MOFs are typically produced during solvothermal synthesis from a scintillation vial or autoclave. Using these vessels would any reaction monitoring difficult because of the specialised equipment needed to do it in combination with spectroscopy. In this study, a high pressure NMR tube (**Figure 5.2**) was used as a solvothermal reaction vessel. The solvothermal reactions were carried out in deuterated solvents, enabling the ^{1}H NMR resonances arising from the protons of the organic ligand(s) to be observed during the synthesis.

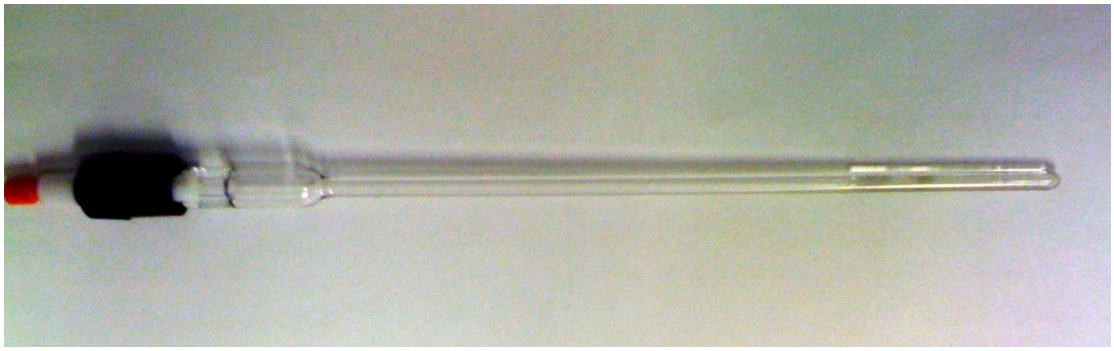

Figure 5.2: Photograph of the high-pressure NMR tube (Wilmad® NMR tube) used for experiments in this Chapter.

5.2.2 Methodology

Each MOF synthesis was scaled down from the literature report to a 0.2 ml solvent volume. A typical procedure is as follows:

- the starting materials were dissolved in DMF-d_7 and the solution was transferred to a high pressure NMR tube
- a ^{1}H NMR spectrum was recorded
- the tube was suspended in a hot oil bath to start the experiment by initiating the solvothermal reaction
- the tube was removed periodically and a ^{1}H NMR spectrum recorded. The tube was then placed back in the oil bath and the process repeated.

The high-pressure tube was chosen to serve as a suitable solvothermal reaction vessel to mimic the conditions of a scintillation vial. During crystallisation the organic component(s) bond to the inorganic moieties and form insoluble complexes (nanocrystallites). Thus, the concentration of dissolved organic ligands in solution will decrease as larger crystallites form and become insoluble. This decrease can be measured as a reduction in the proton integral of a resonance in the NMR spectrum. When the tube is removed from the hot oil bath, the solution in the tube rapidly cools to room temperature, thereby effectively quenching the solvothermal reaction. Then, when the tube is heated again, the reaction continues. Measuring a ^{1}H NMR spectrum periodically gives a time-resolved picture of the crystallisation process. A calibration between different concentrations of terephthalic acid in DMF the corresponding integral value was performed (Appendix 3). A good correlation was found and this was used to calibrate each NMR study.

Although the MOFs used in the studies outlined in this **Chapter** are well known and well studied, a number of assumptions are made:

- the MOF synthesis is reproducible, even when scaled down
- the high pressure NMR tube is a suitable solvothermal reaction vessel
- removing the tube from the heat source, effectively stops the solvothermal reaction
- the solvothermal reaction can be restarted upon placing the tube back in the heat source

5.3 MOF-5 study

Initially, the modified (using DMF instead of DEF as solvent) synthesis of MOF-5 at 100 °C reported by Kaskel *et al.* was trialled.[9] In this synthesis, the zinc-terephthalate molar ratio is 3:1. MOF-5 was chosen as the first system to investigate because it is often considered the simplest MOF synthesis and most reproducible. The concentration of reagents also worked well to give high quality ^{1}H NMR spectra. The reaction was setup using the general method described above. A ^{1}H NMR was measured at time zero and then hourly until hour nine. The tube was then left heating overnight and a final ^{1}H NMR was measured at hour 26. A stack plot of the ^{1}H NMR spectra is shown in **Figure 5.3**. This resulted in single crystalline material being produced in the NMR tube. By visual inspection the crystal had the same morphology of those on MOF-5.

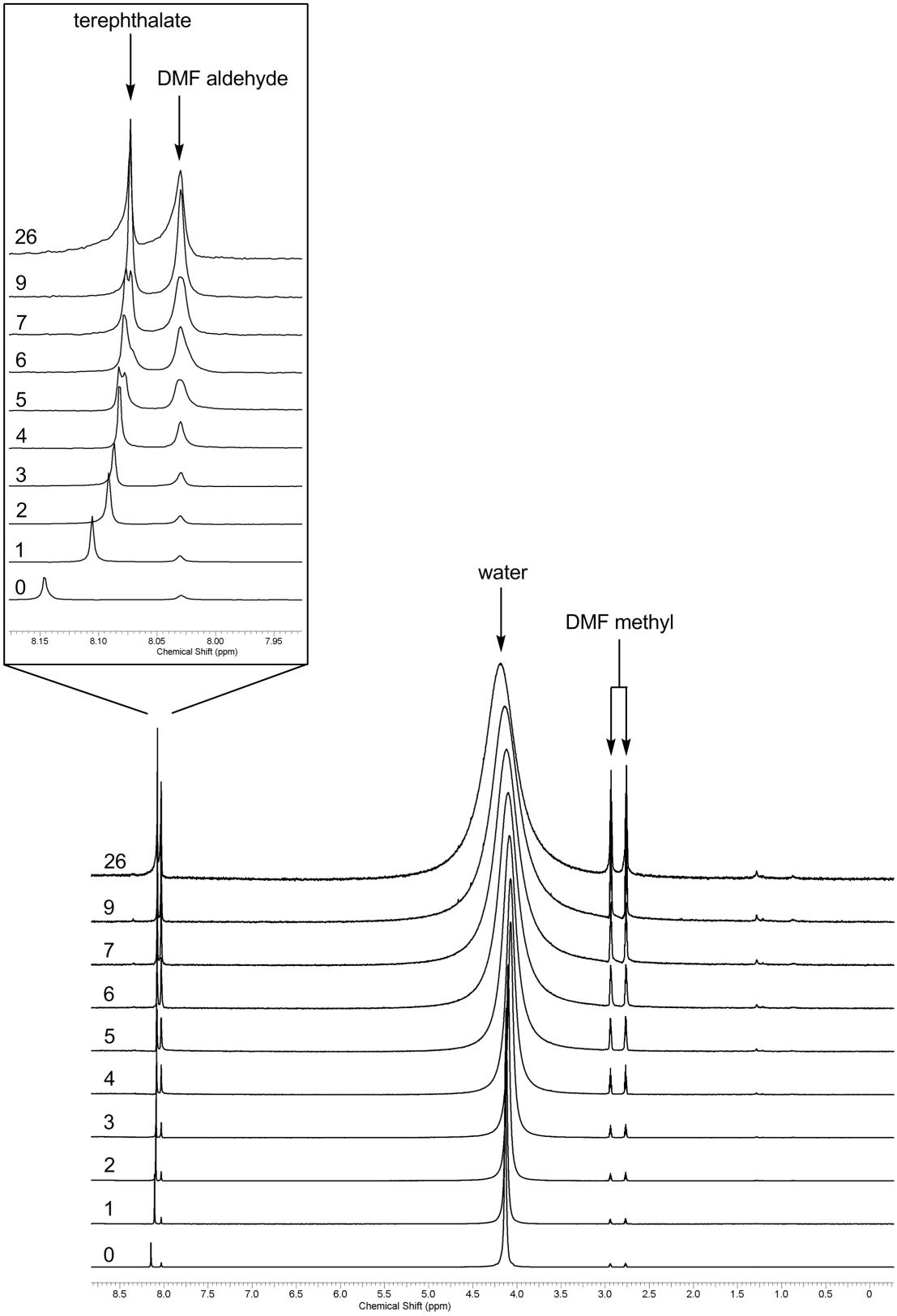

Figure 5.3 Stack plot of ^{1}H NMR spectra measured during the synthesis of MOF-5 [main]; expansion of terephthalate resonance [inset] from hour 0 to hour 26.

From the stack plot, the integral of the terephthalate protons *vs*. time can be plotted (**Figure 5.4**). The plot clearly shows that the integral remains unchanged until between hours 2 and 3, where upon it starts to exponentially decay until hour 4.

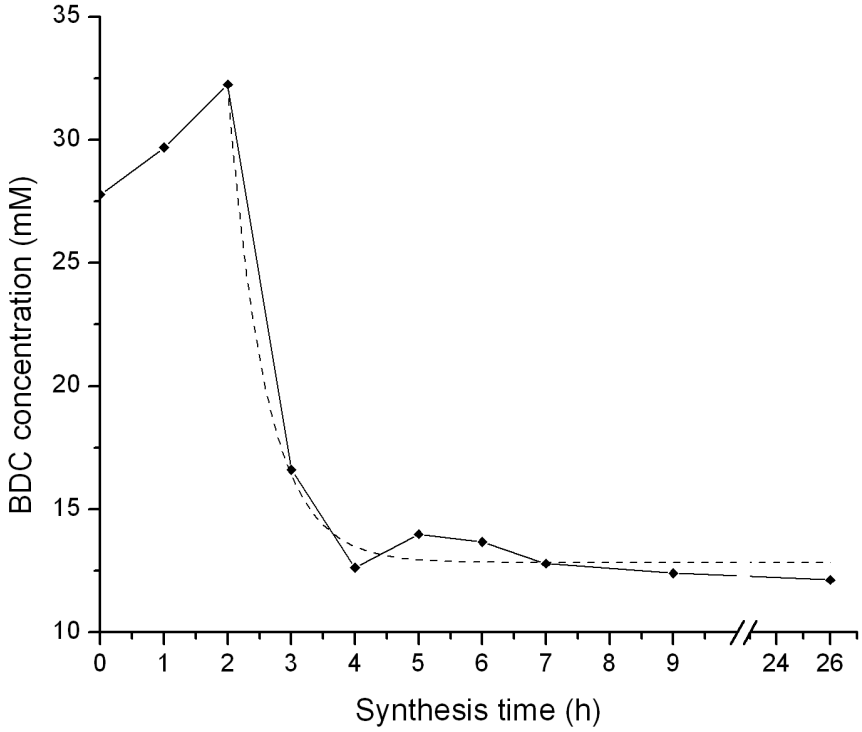

Figure 5.4: Plot of the terephthalic acid concentration *vs.* time during the MOF-5 synthesis.

The stack plot shows that the terephthalate singlet resonance from the four chemically equivalent protons shifts from 8.14 to 8.07 ppm from hour 0 to hour 26 (**Figure 5.5**). This shielding effect is presumably caused by electron density transfer from the electropositive Zn^{II} d^{10} metal centres upon coordination to the carboxylates.

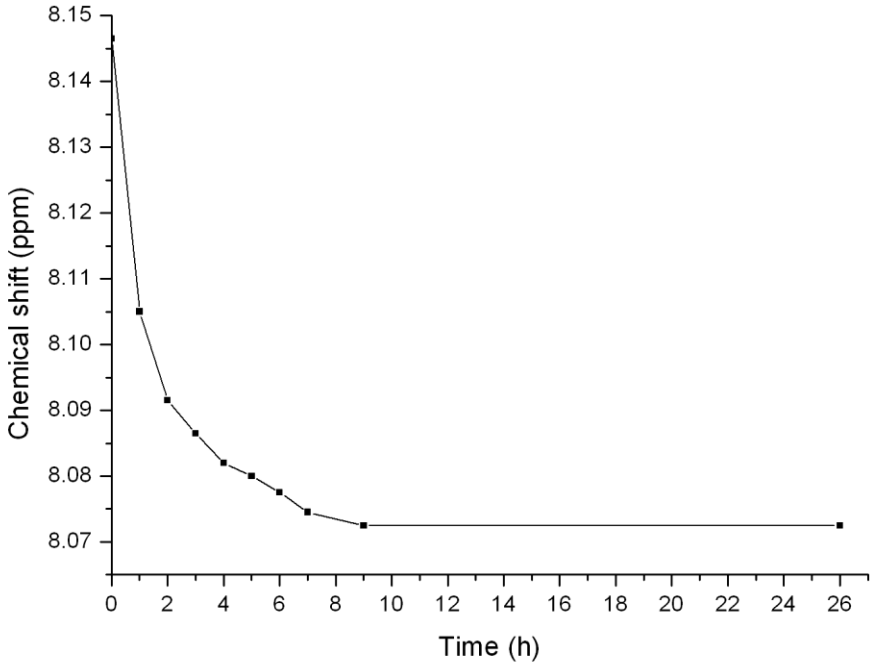

Figure 5.5: Plot of the chemical shift of the terephthalate proton resonance *vs.* time.

The multiplicity of the resonance changes from a singlet to a broader singlet almost immediately and then an apparent doublet at hour 5. At hour 9, it reserves back to an (broad) singlet. These observations suggest that the terephthalate binds to the zinc in solution almost intermediately as expected. Most likely, the DMF picks up the proton of the carboxylate group because it is in excess, the carboxylate then coordinates to the Zn^{II} displacing a nitrate group. The nitrate group can then pick up the proton from the protonated DMF. The remaining solvated zinc-BDC complexes must then undergo some rearrangement to form the Zn_4O cluster found in MOF-5. As the cluster is formed, the terephthalate can bind *via* one carboxylate group. This would then explain the apparent splitting of the aromatic proton resonance at from hour 5. The terephthalate-Zn_4O complexes become nanocrystallites and therefore nuclei and start crystallisation. When this happens they become insoluble and hence the decrease in the terephthalate integral starting from hour 2.

As an aside, the solvothermal reaction of zinc nitrate and BDC at lower ratios was also investigated.

5.3.1 Solvothermal reaction of zinc nitrate and BDC at Zn/BDC stoichiometry of 2:1 and 1:1

The exact same synthesis conditions were used in this experiment with the exception that the starting zinc nitrate-BDC ratio was decreased to 2:1. The stack plot of the ^{1}H NMR can be found in Appendix 3, a plot of terephthalate concentration *vs*. time is shown in **Figure 5.6**.

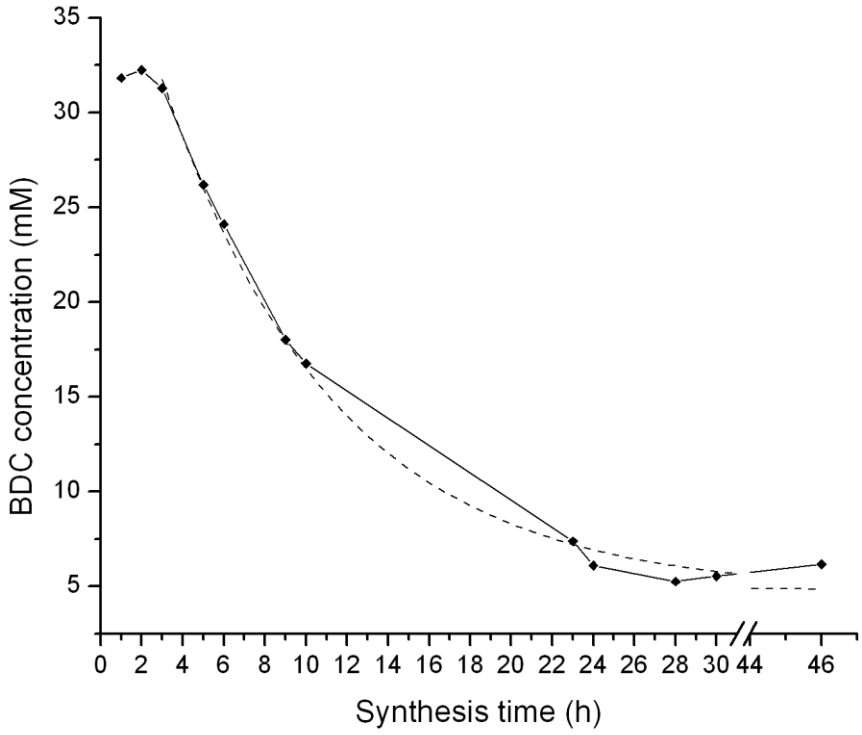

Figure 5.6: Terephthalic acid concentration *vs.* time for MOF-5 synthesis when Zn/BDC = 2:1 [solid line]; exponential decay fit [dashed line].

The plot shows a similar decay to that of MOF-5, with the BDC concentration over approximately the same time scale. There also appears to mixture same delay of 2 h at the start of the synthesis, with respect to the change in concentration of BDC. The synthesis also resulted in crystalline material within the NMR tube.

The solvothermal reaction of a 1:1 mixture of zinc nitrate and BDC using the same synthesis conditions was also performed. The stack plot of the ^{1}H NMR can be found in Appendix 3, a plot of terephthalate concentration *vs*. time is plotted in **Figure 5.7**.

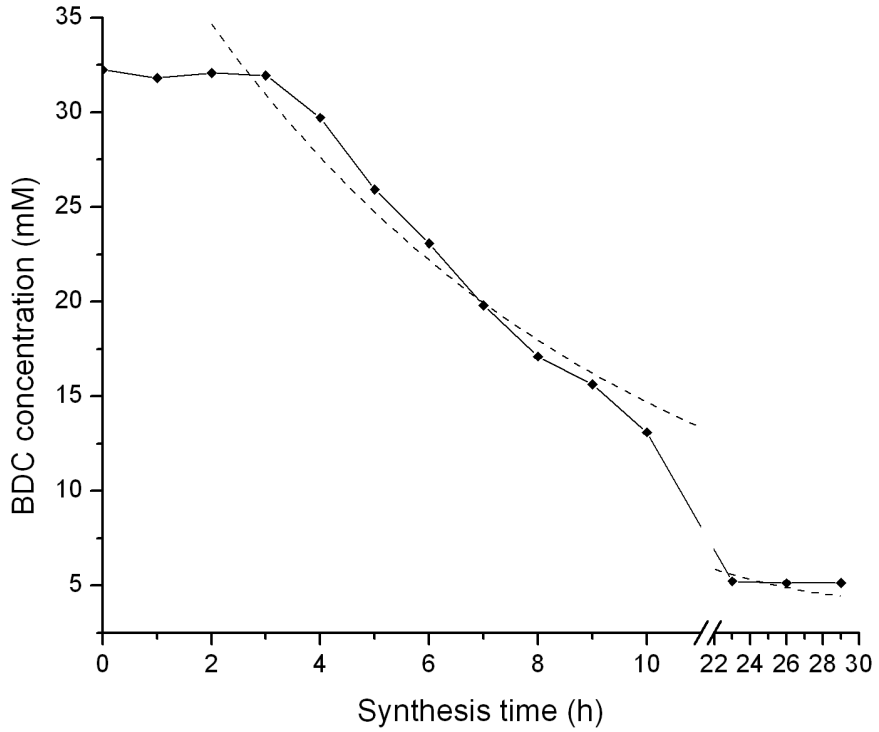

Figure 5.7: Terephthalic acid concentration *vs.* time for MOF-5 synthesis when Zn/BDC 1:1 [solid line]; exponential decay fit [dashed line].

A longer lag time is observed at the beginning of the synthesis. The BDC concentration does not fall until hour 3. The rate in the decrease of the BDC concentration is also less than the 3:1 and 2:1 syntheses.

To confirm what materials were being produced in the 2:1 and 1:1 syntheses (as these are not typical literature procedures), the same syntheses reported in the NMR studies were scaled-up to an oven-scale level. This would enable enough material to be produced for a powder X-ray pattern to be obtained. There are several differences between each pattern, which are shown in **Figure 5.8**.

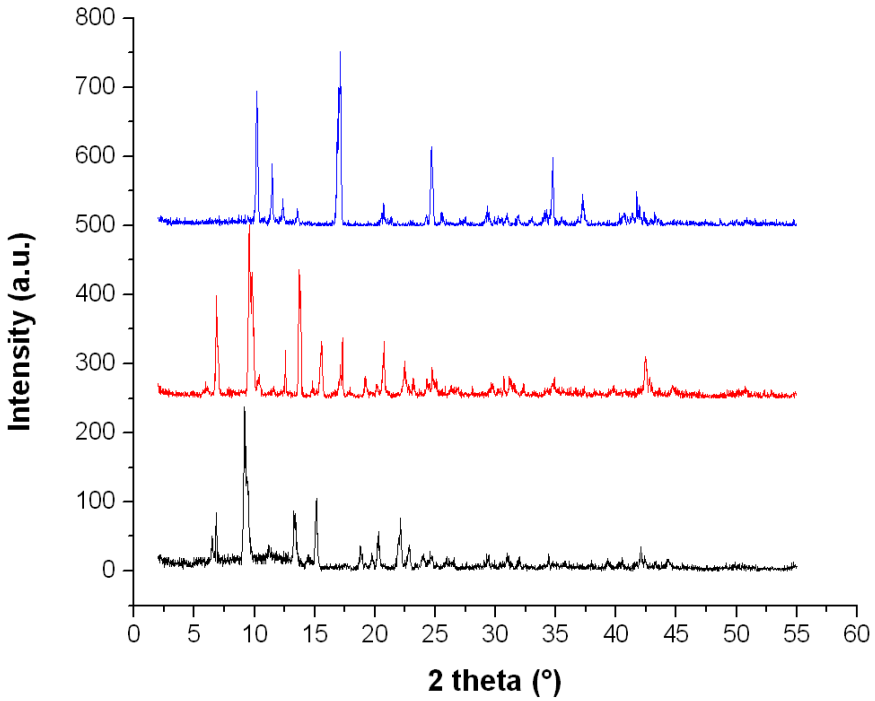

Figure 5.8: PXRD patterns of MOF-5 (black line) and the crystalline materials produced using a 2:1 zinc nitrate-BDC starting ratio (red line) and 1:1 zinc nitrate-BDC ratio (blue line).

The PXRD patterns obtained do not match the MOF-5 pattern. The 2:1 synthesis obtains a material with a similar PXRD pattern to MOF-5 with some subtle differences. The peaks that correspond to diffraction from MOF in the 2:1 sample are shifted 2 theta = 0.44º to the right. The pattern suggests that MOF-5 has been produced in the 2:1 synthesis. The PXRD pattern obtained from the 1:1 sample is very different to the other patterns obtained. The solvothermal reaction from a 1:1 mix of zinc nitrate and BDC is clearly a different material to MOF-5, the structure of which has not be identified.

5.3.2 Modulated MOF-5 synthesis study

As we known from **Chapter 4**, high quality crystals MOF-5 can be synthesised using 1 or 2 equivalents of benzoic acid modulator. The modulated synthesis of MOF-5 was studied using the NMR technique outlined in this **Chapter**. All the starting reagents were mixed together, before being heated in the NMR tube. The NMR tube synthesis resulted in a crystalline material being produced. A stack plots of the ^{1}H NMR spectra may be found in

Appendix 3. Plotted below are the proton integrals of the BDC and benzoic acid protons *vs.* time (**Figure 5.9** and **Figure 5.10**).

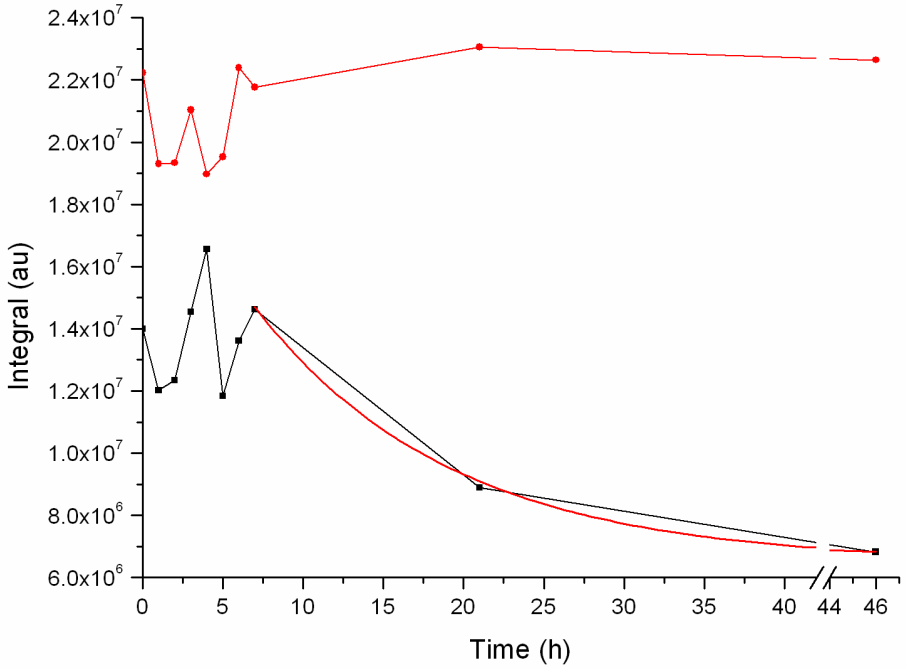

Figure 5.9: BDC (lower black line [fitted exponential decay curve is overlaid red line) and benzoic acid (upper red line) proton integrals *vs.* time for modulated MOF-5 synthesis with 1 equivalent of benzoic acid.

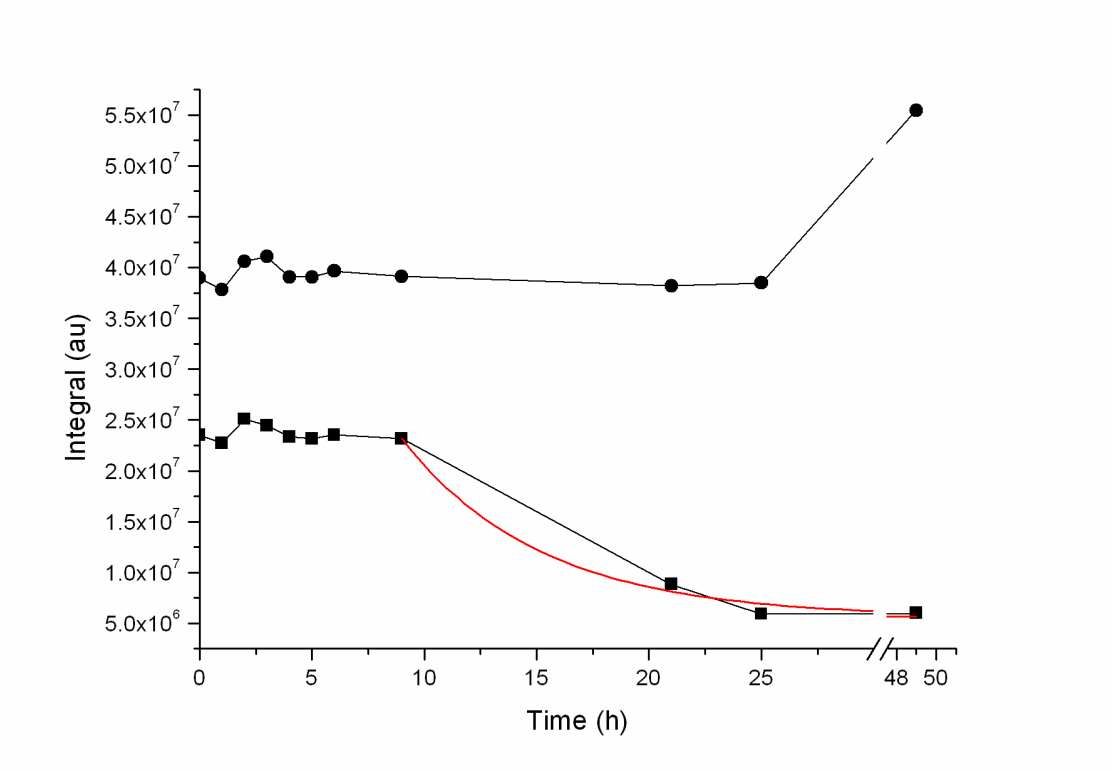

Figure 5.10: BDC (lower black line [fitted exponential decay curve is overlaid red line) and benzoic acid (upper black line) proton integrals *vs.* time for modulated MOF-5 synthesis with 2 equivalent of benzoic acid.

Both plots agree with visible observation made during the standard over solvothermal synthesis of modulated MOF-5: that the crystallisation is delayed for a number of hours. For 1 equivalent of benzoic acid this delay is approximately 6 hours and for 2 equivalents it is approximately 10 hours.

5.4 Other zinc SBU containing MOF studies

The following sections will describe NMR studies on Zn_4O containing MOFs with a number of different polycarboxylate ligands.

5.4.1 MOF-177 study

MOF-177 is a highly porous MOF constructed from the large BTB unit and the Zn_4O SBU. MOF-177 was synthesised according to literature proceedures.[10] The NMR tube synthesis resulted in a crystalline material being produced. A stack plot of the ^{1}H NMR spectra may

be found in Appendix 3. A plot of the BTB proton integral *vs*. time is plotted in **Figure 5.11**.

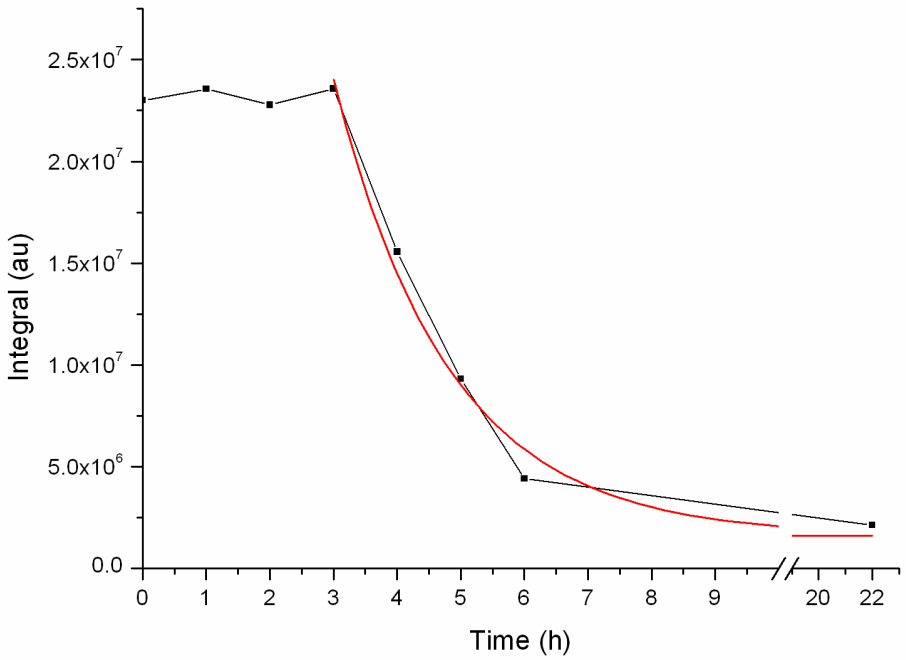

Figure 5.11: BTB proton integral *vs.* time for MOF-177 synthesis [black line]; exponential decay fit [red line].

The plots in **Figure 5.10** and **Figure 5.11** show that the MOF-177 has a similar profile to that of MOF-5. The lag time at the beginning of the synthesis is twice as long at 4 hour, before the proton resonance of the BTB ligand starts to decrease.

5.4.2 $[Zn_2(BDC)_2(DABCO)]$ MOF study

The next MOF studied was $[Zn_2(BDC)_2(DABCO)]$ reported by Kim *et al*. and discussed in **Chapter 1**.[11] This MOF comprises of two different ligands and a different SBU to that of MOF-5. It was hypothesised that perhaps the Zn^{II} and the terephthalate ligands would combine first, forming a 2D grid of Zn^{II} paddle wheel SBU linked by the terephthalate units. The DABCO could then bind to the apical sites of the Zn^{II}, thereby bringing the grids together to form a 3D structure. The MOF was synthesised according to Kim's reported procedure to produce clear needle crystals. A stack plot of selected ^1H NMR spectra is shown in **Figure 5.12** (a full stack plot may be found in Appendix 3).

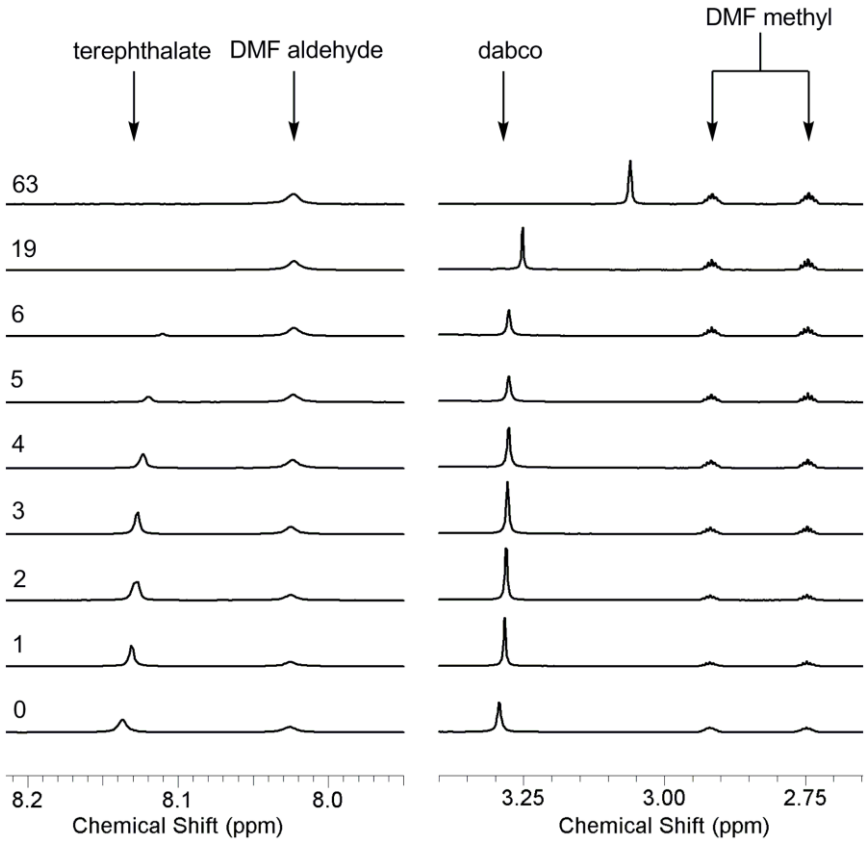

Figure 5.12: Stack plot of selected ^{1}H NMR spectra measured during the synthesis of $[Zn_2(BDC)_2(DABCO)]$ from hour 0 to hour 63 showing terephthalate and DABCO resonances.

From the stack plot, the integrals of the terephthalate protons and the DABCO protons *vs.* time can be plotted (**Figure 5.13**). The plot clearly shows that the integral remains unchanged until between hours 2 and 3, where upon in exponentially decays until hour 4.

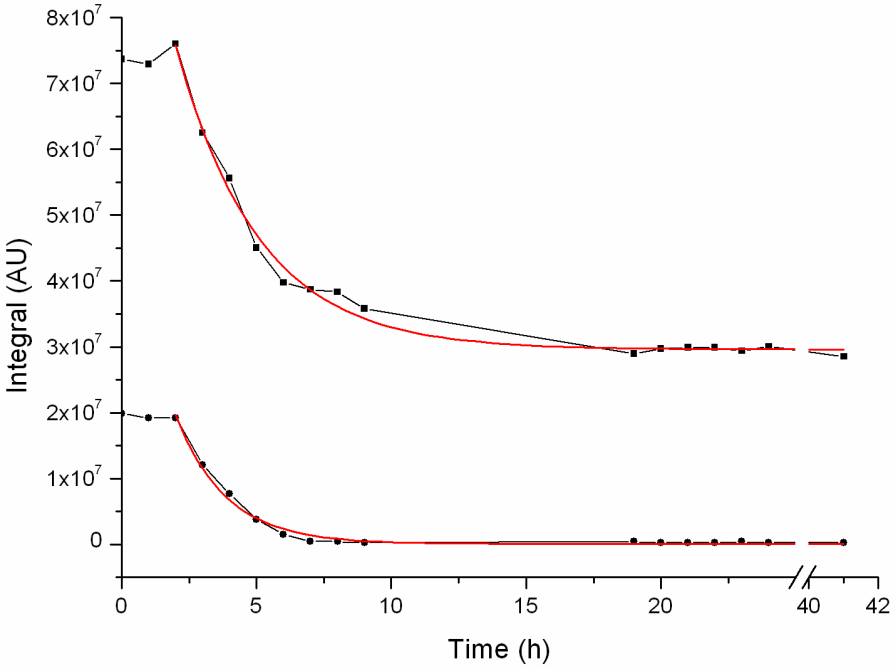

Figure 5.13: Terephthalic acid (lower line) and DABCO (upper line) proton integrals *vs.* time for $[Zn_2(BDC)_2(DABCO)]$ synthesis.

The plot in **Figure 5.13** shows an interesting result: the ^1H integral of the protons of BDC and DABCO begin to decrease at the same time during the synthesis. This appears to disprove the hypothesis made prior to the experiment. If indeed BDC and Zn(II) would have come together to form a 2D network prior to beginning connected together by the DABCO unit, then one would expect the BDC proton integral to start to decrease before the DABCO. It would be reasonable to assume that any large 2D layers of Zn-BDC would be insoluble and hence the BDC proton integral would decrease. As the integrals decrease at the same time, this would imply that MOF is being constructed of discrete BDC-Zn-DABCO units. The proton resonances move downfield over the course of the reaction. They do not split into discrete peaks. This would also suggest the protons on the BDC and DABCO units are all in similar environments as the reaction proceeds. i.e. some BDC are not free in solution, while some are coordinated to a SBU.

5.4.3 $[Zn_2(BDC)_2(BPY)]$ MOF study

To compare the pillared MOF above with a similar system, the pillared MOF [$Zn_2(BDC)_2(BPY)$] was also studied. This MOF, reported by Hupp *et al.*[12] is structurally similar too [$Zn_2(BDC)_2(DABCO)$], in that in comprises of 2D grids of Zn_2 paddle wheel SBUs linked by BDC ligands. BPY molecules then pillar these 2D grids. The NMR tube synthesis resulted in a crystalline material being produced. A stack plot of the ^1H NMR spectra may be found in Appendix 3. A plot of the BDC, and BPY proton integrals *vs.* time is plotted in **Figure 5.14**.

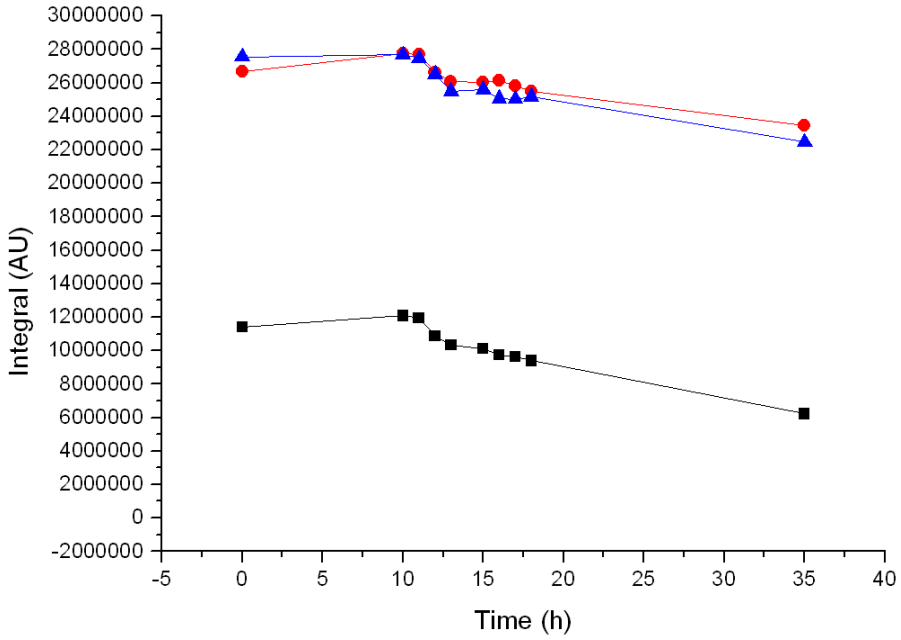

Figure 5.14: Terephthalic acid (lower line) and BPY (upper red and blue lines) proton integrals *vs.* time for [$Zn_2(BDC)_2(BPY)$] synthesis.

This synthesis occurs at a lower temperature than for the other pillared MOF. The reaction took almost 12 hours before any decrease in ligand integral was observed. The results present in **Figure 5.14** are therefore from a synthesis that was started at the end of the day, left overnight and monitored the following day. The plot clearly shows that both ligand proton integrals start to decrease and continue to gradually decrease at the same rate. This is comparable to the [$Zn_2(BDC)_2(DABCO)$] and suggests a trend in the self-assembly process of these Zn_2 paddle wheel pillared MOFs.

5.5 Conclusion

The solution NMR technique described and discussed in this **Chapter** appears to be a valid method of monitoring the solution behaviour of MOF ligands during solvothermal synthesis. A number of assumptions were made when initially thinking about this methodology. The MOFs studied by this technique, are well known in the literature and their synthesis has been shown to be reproducible in a number of different works[9, 13-20]. The selection of the NMR tube was also valid a solvothermal reaction vessel. Visible observation of the crystal formation was in line with the visible observations made for the synthesis of these MOFs *via* conventional methods. Removing the NMR tube from the heat source to record a ^{1}H NMR spectra was shown not to interfere with the self-assembly process. The proton integrals of the ligands do not fluctuate were the synthesis has started.

The series of Zn_4O containing MOF that were studied show similar behaviour. There is a lag time for the solvothermal reaction to start as shown by no change in the integral/concentration of the ligand. This would be expected as the zinc ions rearrange in to SBUs. It appears that once this rearrangement occurs, crystallisation occurs, and as it does the ligands are consumed into the growing crystallites. This is shown by the decrease in ligand integral resonance over time.

The pillared MOF that were studied show a similar lag time as for the Zn_4O examples, which may also be to do with the zinc ion rearrangement into SBUs. The study nicely shows that both the ligands are consumed at the same rate during the crystallisation process. Thus indicating the crystals are built as once continuing growing crystal, as supposed to layers of BDC-zinc paddle wheels forming first and then being connected by the pillaring ligands.

5.6 References

1. R. E. Morris, *ChemPhysChem*, 2009, **10**, 327.
2. P. Cubillas and M. W. Anderson, in *Zeolites and Catalysis*, Wiley-VCH Verlag GmbH & Co. KGaA, 2010, p. 1.

3. F. Millange, M. I. Medina, N. Guillou, G. Ferey, K. M. Golden and R. I. Walton, *Angew. Chem. Int. Ed.*, 2010, **49**, 763.
4. D. Zacher, J. N. Liu, K. Huber and R. A. Fischer, *Chem. Commun.*, 2009, 1031.
5. A. C. Sudik, A. P. Cote and O. M. Yaghi, *Inorg. Chem.*, 2005, **44**, 2998.
6. S. Surble, F. Millange, C. Serre, G. Ferey and R. I. Walton, *Chem. Commun.*, 2006, 1518.
7. C. Serre, F. Millange, S. Surble and G. Ferey, *Angew. Chem. Int. Ed.*, 2004, **43**, 6286.
8. J. A. Rood, W. C. Boggess, B. C. Noll and K. W. Henderson, *J. Am . Chem. Soc.*, 2007, **129**, 13675.
9. M. Sabo, A. Henschel, H. Froede, E. Klemm and S. Kaskel, *J. Mater. Chem.*, 2007, **17**, 3827.
10. H. K. Chae, D. Y. Siberio-Perez, J. Kim, Y. Go, M. Eddaoudi, A. J. Matzger, M. O'Keeffe and O. M. Yaghi, *Nature*, 2004, **427**, 523.
11. D. N. Dybtsev, H. Chun and K. Kim, *Angew. Chem. Int. Ed.*, 2004, **43**, 5033.
12. B. Q. Ma, K. L. Mulfort and J. T. Hupp, *Inorg. Chem.*, 2005, **44**, 4912.
13. S. Bordiga, J. G. Vitillo, G. Ricchiardi, L. Regli, D. Cocina, A. Zecchina, B. Arstad, M. Bjorgen, J. Hafizovic and K. P. Lillerud, *J. Phys. Chem. B*, 2005, **109**, 18237.
14. B. L. Huang, A. J. H. McGaughey and M. Kaviany, *Int. J. Heat. Mass Tran.*, 2007, **50**, 393.
15. D. J. Tranchemontagne, J. R. Hunt and O. M. Yaghi, *Tetrahedron*, 2008, **64**, 8553.
16. E. Biemmi, S. Christian, N. Stock and T. Bein, *Microporous and Mesoporous Mater.*, 2009, **117**, 111.
17. J. Lee, O. K. Farha, J. Roberts, K. A. Scheidt, S. T. Nguyen and J. T. Hupp, *Chem. Soc. Rev.*, 2009, **38**, 1450.
18. H. X. Deng, C. J. Doonan, H. Furukawa, R. B. Ferreira, J. Towne, C. B. Knobler, B. Wang and O. M. Yaghi, *Science*, 2010, **327**, 846.
19. Y. Sakata, S. Furukawa, C. Kim and S. Kitagawa, *Chem. Lett.*, 2012, **41**, 1436.
20. L. Sbircea, N. D. Sharma, W. Clegg, R. W. Harrington, P. N. Horton, M. B. Hursthouse, D. C. Apperley, D. R. Boyd and S. L. James, *Chem. Commun.*, 2008, 5538.

6 Future work

The successful synthesis of novel chiral MOF ligands was presented in this thesis. Their inclusion as ligands in novel MOFs was not achieved using the methodologies available at the time. It has become apparent through this work, and the wider literature in this area, that *de novo* approaches to producing new MOFs using new ligands with greater functionality is often problematic due to the formation of undesirable structures or side products during the MOF synthesis.[1]

Since the completion of this research, two interesting techniques/methods have been reported that could open the door to completing the objectives of this thesis by circumventing this *de novo* approach, which could then ultimately result in a MOF useful for asymmetric heterogeneous catalysis.

The group of Farha and Hupp have reported a method of ligand exchange within fully formed, crystalline MOFs.[2, 3] In this work several pillared MOFs constructed from a tetra-acid and pillaring dipyridinyl porphyrine struts are studied. Farha and Hupp show that in these known pillared MOFs, the pillaring ligand can be exchanged *via* solvent-assisted linker exchange (SALE). SALE involves completely replacing the pillaring ligand in a MOF crystal for that of a different pillaring ligand by heating the original MOF in a solution containing the new ligand as represented in (**Figure 6.1**).

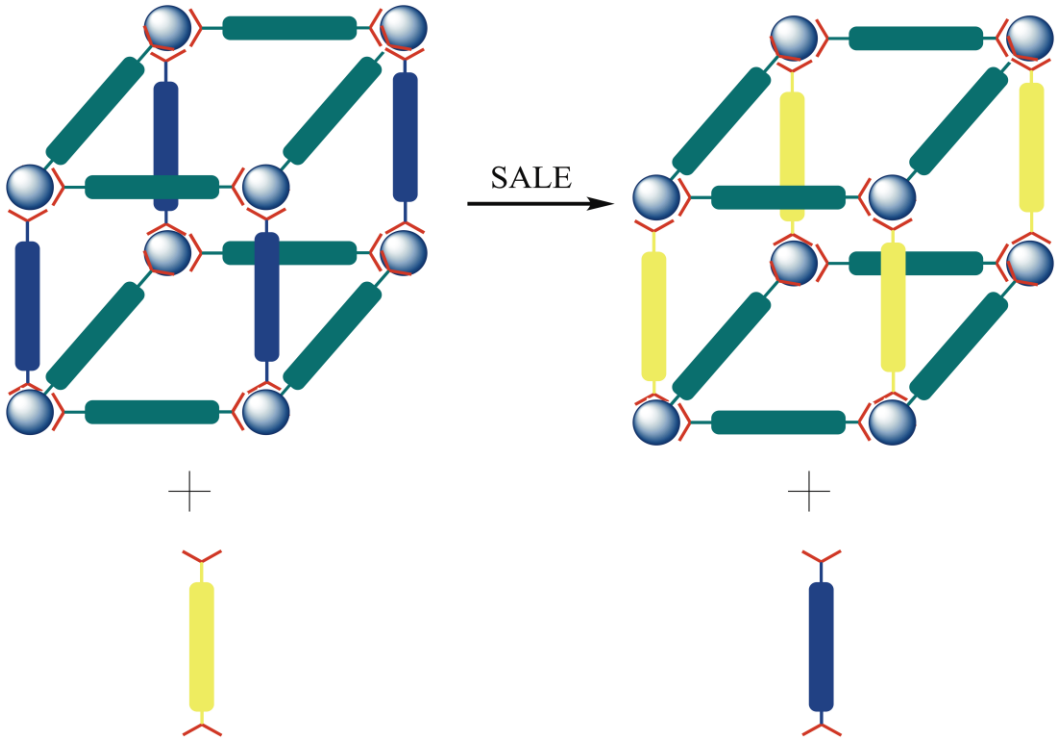

Figure 6.1: Representation of a pillar-based SALE reaction.

The single crystals of MOF are heated in a solvent solution that contain the new ligand/linker that they wish introduce into the MOF. After the SALE, the MOFs are repeatedly soaked and washed in fresh solvent to remove all ligands (whether from the MOF or the newly introduced ligands). To determine the extent of exchange, the MOF is digested using sonification in dilute acid and the sample analysed using inductively coupled plasma optical-emission spectroscopy and/or ^{1}H NMR spectroscopy.

As well as obtaining previously inaccessible MOFs, Farha and Hupp have also shown that SALE can be used to obtain previously unobtainable non-catenated versions of known MOFs.[3] Non-catenated systems are desirable because they contain larger apertures and pores, which would be highly appropriate for the catalysis targeted in this work.

Cohen *et al.* have shown that photochemistry can be used to reveal functionality within MOFs.[4] Their strategy is to form MOFs comprising of ligands with photo-labile protecting groups. These groups are then removed from the ligands by photoirradiation. This light driven process is an efficient and relatively gentle method to initiate chemical reactions in MOFs; the MOFs remain structurally intact after the process.[4] The first example of this was used to obtain MOFs with free hydroxyl groups, which are very rare in the literature.[5,

[6] Cohen reports that the MOFs UMCM-1-OBnNO_2 and UMCM-1-$(OBnNO_2)_2$ (where the BDC ligand in the MOF is the analogous 1,2-dihydoxyl-BDC in which the diols have been protected with *o*-nitrobenzyl groups), can be irradiated with 365 nm light for a period of 24-48 hours to remove the nitrobenzyl groups, revealing the diol functionality. This is confirmed by digestion ^{1}H NMR of the post-synthetically deprotected[7] MOF and by single X-ray crystallography.

These two reports show that there is great scope for future work, the bulk of which can be directly applied to the synthetic MOF targets in this work. It should be possible to prepare pillared MOFs using **Ligand G** as the pillaring ligand either by using SALE and the photochemical activation approach. The pillared MOFs reported by Kitagawa, Kim, Hupp, and many others[8-11] containing dipyridinyl pillaring ligands could readily be obtained. SALE using **Ligand G** with these MOFs should result in corresponding **Ligand G**-pillared MOF. This would be advantageous, as **Ligand G** could be used as is, without any further modifications.

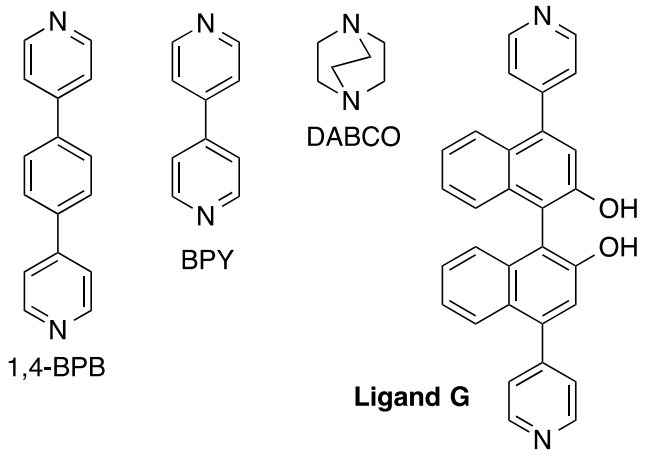

Figure 6.2: A selection of dipyridinyl ligands used in the synthesis of pillared MOFs and **Ligand G**.

SALE has not yet been shown to work with non-pillared MOFs and an investigation into the isoreticular series of Zn_4O containing MOFs could be performed. It would be interesting to observe ligand exchange in these MOFs the isoreticular series contains MOFs with some of the highest surface areas and porosities.[12]

The photochemical activation approach could be used on many of the diol ligands presented in this work. Protection of the diols with *o*-nitrobenzyl groups could be done

before the carbon-carbon coupling reactions in the synthetic protocols of **Ligands D – G**. The protecting should withstand the coupling reaction. For the polycarboxylate **Ligands D – F**, mild ester hydrolysis conditions will need to be employed in the final step to ensure that the protecting groups are not lost. An example synthesis for the nitrobenzyl capped analogue of **Ligand D** from 4,4'-dibromo-2,2'-binaphthol (**14**) is shown in **Figure 6.3** below.

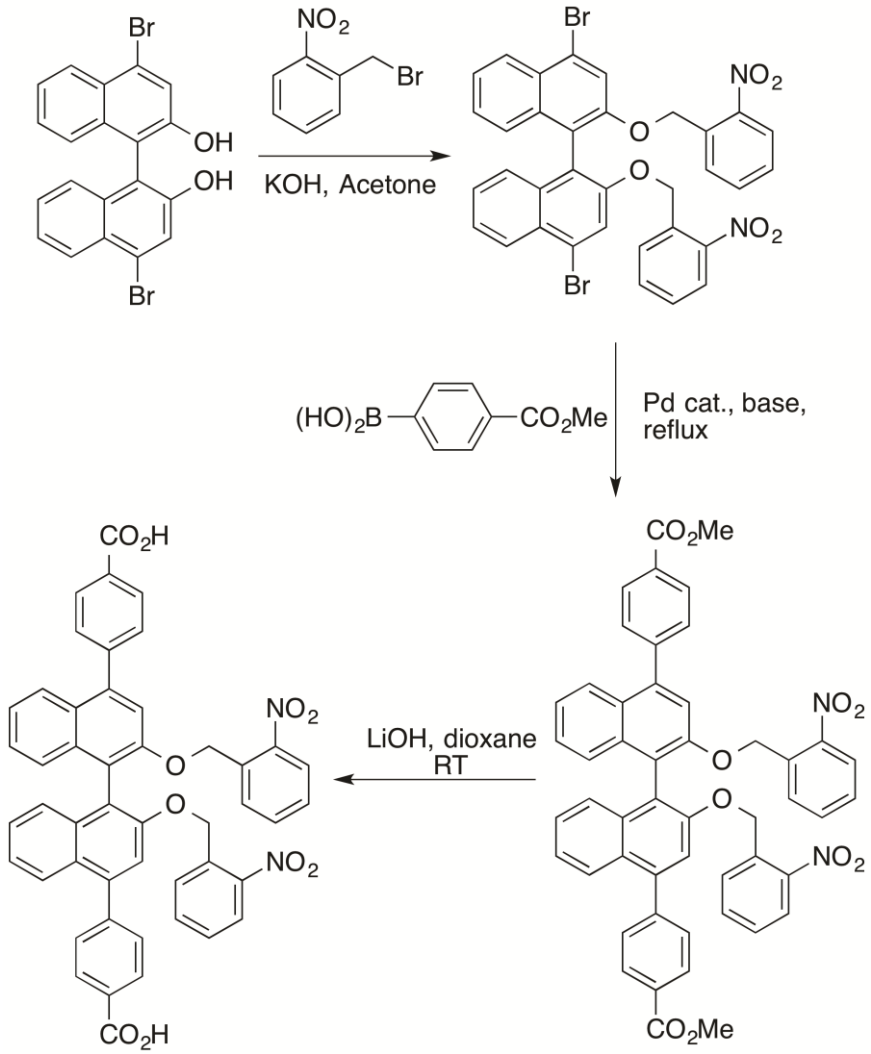

Figure 6.3: Proposed synthesis of an analogous compound to **Ligand D** with nitrobenzyl capped diols.

6.1 References

1. S. M. Cohen, *Chem. Rev.*, 2012, **112**, 970.
2. S. Takaishi, E. J. DeMarco, M. J. Pellin, O. K. Farha and J. T. Hupp, *Chem. Sci.*, 2013, **4**, 1509.

3. W. Bury, D. Fairen-Jimenez, M. B. Lalonde, R. Q. Snurr, O. K. Farha and J. T. Hupp, *Chem. Mater.*, 2013, **25**, 739.
4. K. K. Tanabe, C. A. Allen and S. M. Cohen, *Angew. Chem. Int. Ed.*, 2010, **49**, 9730.
5. D. Himsl, D. Wallacher and M. Hartmann, *Angew. Chem. Int. Ed.*, 2009, **48**, 4639.
6. T. Devic, P. Horcajada, C. Serre, F. Salles, G. Maurin, B. Moulin, D. Heurtaux, G. Clet, A. Vimont, J. M. Greneche, B. Le Ouay, F. Moreau, E. Magnier, Y. Filinchuk, J. Marrot, J. C. Lavalley, M. Daturi and G. Ferey, *J. Am. Chem. Soc.*, 2010, **132**, 1127.
7. S. M. Cohen, *Chem. Rev.*, 2012, **112**, 970.
8. V. Zelenak, Z. Vargova, M. Almasi, A. Zelenakova and J. Kuchar, *Microporous and Mesoporous Mater.*, 2010, **129**, 354.
9. H. Chun, D. N. Dybtsev, H. Kim and K. Kim, *Chem. Eur. J.*, 2005, **11**, 3521.
10. B. Q. Ma, K. L. Mulfort and J. T. Hupp, *Inorg. Chem.*, 2005, **44**, 4912.
11. T. K. Maji, K. Uemura, H. C. Chang, R. Matsuda and S. Kitagawa, *Angew. Chem. Int. Ed.*, 2004, **43**, 3269.
12. H. Furukawa, N. Ko, Y. B. Go, N. Aratani, S. B. Choi, E. Choi, A. O. Yazaydin, R. Q. Snurr, M. O'Keeffe, J. Kim and O. M. Yaghi, *Science*, 2010, **329**, 424.

7 Experimental

7.1 General remarks

^{1}H NMR (300 MHz) and ^{13}C[^{1}H] NMR (75 MHz) were determined on a Bruker AV300 spectrometer. Chemical shifts for ^{1}H NMR are reported in parts per million (ppm), calibrated to the solvent peak set. The following abbreviations are used for spin multiplicity: s = singlet, d = doublet, t = triplet, m = multiplet. Chemical shifts for ^{13}C[^{1}H] NMR are reported in ppm, relative to the central line of a septet at (= 39.52 ppm for DMSO-d_6. Infrared (IR) spectra were recorded on a Matterson Satellite (ATR). FTIR are reported in wavenumbers (cm-^{1}). HRMS(ES) spectra were recorded using a Bruker Apex III spectrometer and reported as m/z (relative intensity). All solvents and starting materials were purchased from commercial sources and used without further purification unless otherwise stated. Anhydrous DCM, MeOH and PhMe were obtained by drying with CaH_2, followed by distillation. Anhydrous THF was obtained by drying with sodium using benzophenone as an indicator, followed by distillation. Dry pyridine was distilled over KOH pellets. Column chromatography was performed using 60 silica of 230-400 mesh.

All reactions were carried at room temperature open to the atmosphere unless otherwise stated. Reactions requiring anhydrous conditions were performed in oven dried glassware. Triethylamine was purified by distillation over KOH pellets.

Solvothermal reactions were carried out using 25 ml volume scintillation vials (Chromacol) and were heated in a Memmert universal oven.

Unless preparations are supplied, all reagents were obtained from commercial sources, and used without further purification.

7.2 Synthesis of methyl 6-hydroxy-1-naphthoate, 10

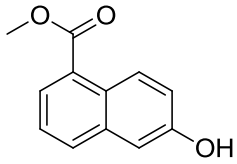

Methyl 6-hydroxy-1-naphthoate was synthesised according to literature procedures.[1] To a solution of 6-hydroxy-1-naphthoic acid (10.75 g, ~53 mmol) in MeOH (200 ml) was added $MeSO_3H$ (0.7 ml, 10.7 mmol). The mixture was heated to reflux overnight and then the solvent removed *in vacuo* to give a pure cream coloured solid. Yield 10.6 g (99%). NMR values agree with those previously reported.[1]

^{1}H NMR (+20°C, 300.13 MHz, DMSO-d_6): δ = 8.6 (m, 1H, ArH), 7.95 (d, J = 8.4 Hz, 1H, ArH), 7.88 (dd, J = 7.1, 1.3 Hz, 1H, ArH), 7.46 (dd, *J* = 8.1, 7.3 Hz, 1H, ArH), 7.22 (m, 2H, ArH), 3.91 (s, 3H, CO_2CH_3) ppm.
Mp: 112 – 114 °C.

7.3 Synthesis of dimethyl 2,2'-dihydroxy-1,1'-binaphthalene-5,5'-dicarboxylate, 11

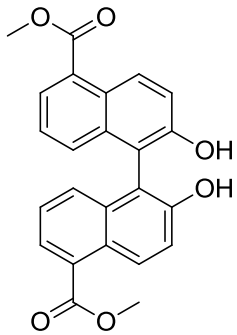

Dimethyl 2,2'-dihydroxy-1,1'-binaphthalene-5,5'-dicarboxylate was synthesised according to literature procedures.[2] Methyl 6-hydroxy-1-naphthoate (1.2 g, 5.93 mmol) and $FeCl_3.6H_2O$ (3.21 g, 11.9 mmol) were suspended in water (200 ml) and heated to 70 °C for 24 h. The crystalline precipitate was then filtered hot and the solid recrystallised from MeOH to give clear colourless needles. Yield 1.19 g (50 %). NMR values agreed with those previously reported.[2]

^{1}H NMR (+20°C, 300.13 MHz, $CDCl_3$): δ = 9.08 (d, *J* = 9.5 Hz, 2H, ArH), 8.05 (dd, *J* = 6.4, 2.0 Hz, 2H, ArH), 7.52 (d, *J* = 9.5 Hz, 2H, ArH), 7.33 (m, 4H, ArH), 5.07 (br. s, 2H, O*H*), 4.05 (s, 6H, CO_2CH_3) ppm.
Mp: 238 – 240 °C.

7.4 Synthesis of 2,2'-dihydroxy-1,1'-binaphthalene-5,5'-dicarboxylic acid, 9

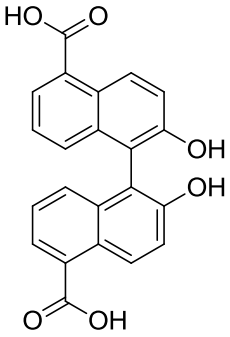

2,2'-dihydroxy-1,1'-binaphthalene-5,5'-dicarboxylic acid was synthesised according to literature procedures.[2] Dimethyl 2,2'-dihydroxy-1,1'-binaphthalene-5,5'-dicarboxylate (5 g, 13.4 mmol) was heated to reflux in aq. NaOH (10 %, 200 ml) solution overnight. After cooling to room temperature, the crude product was precipitated from solution by slow addition of concentrated H_2SO_4. The crude product was recrystallised from MeOH to give colourless needles. Yield 0.94 g (99%). NMR values agree with those previously reported.[2]

^{1}H NMR (+20°C, 300.13 MHz, DMSO-d_6): δ = 9.46 (s, 2H, O*H*), 8.79 (d, *J* = 9.1 Hz, 2H, ArH), 7.84 (d, *J* = 6.2 Hz, 2H, ArH), 7.43 (d, *J* = 9.1 Hz, 2H, ArH), 7.25 (m, 2H, ArH), 7.14 (m, 2H, ArH) ppm.
Mp: 315 - 318 °C.

7.5 Enantiomeric separation of (*R*)-2,2'-dihydroxy-1,1'-binaphthalene-5,5'-dicarboxylic acid:

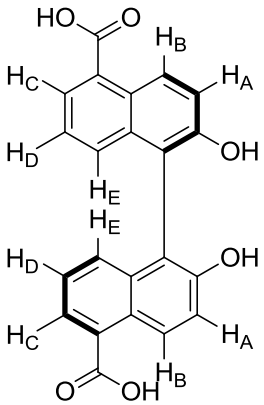

(*R*)-2,2'-dihydroxy-1,1'-binaphthalene-5,5'-dicarboxylic acid was separated from it's racemate according to literature procedures.[3] *rac*-2,2'-dihydroxy-1,1'-binaphthalene-5,5'-dicarboxylic acid (5 g, 13.4 mmol) and cinchonidine (7.86 g, 26.8 mmol) were dissolved in MeOH (750 ml) and left to stand for 24 h. After which time, colourless crystals of a 1:2 complex of (*R*)-2,2'-dihydroxy-1,1'-binaphthalene-5,5'-dicarboxylic acid and cinchonidine had formed (Mp: 201 – 202 °C). The crystals were recrystallised in MeOH to improve their purity and then acidified using dilute HCl and the mixture was extracted with EtOAc (400 ml). The organic was washed with brine (2 x 50 ml) and dried over $MgSO_4$. Evaporation of the solvent gave a pale yellow solid. Yield 0.37 g (15%). NMR values agree with those previously reported.

^{1}H NMR (+20°C, 400.13 MHz, CD_3CN): δ = 8.96 (d, *J* = 9.5 Hz, 2H, ArH), 7.99 (dd, *J* = 7.0, 1.5 Hz, 2H, H_D), 7.43 (d, *J* = 9.5 Hz, 2H, ArH), 7.28 (m, 2H, H_C), 7.23 (m, 2H, H_E) ppm.
Mp: 315 – 317 °C.

7.7 NMR shift reagent experiment to test the optical purity of (*R*)-2,2'-dihydroxy-1,1'-binaphthalene-5,5'-dicarboxylic acid:

(*R*)-2,2'-dihydroxy-1,1'-binaphthalene-5,5'-dicarboxylic acid (10 mg) was dissolved in CD_3CN (0.6 ml) and a ^{1}H NMR spectrum was measured. 10% w/w of europium tris[3-(heptafluoropropylhydroxymethylene)-(+)-camphorate] was then added to the NMR tube and another ^{1}H NMR spectrum was measured.

^{1}H NMR (+20°C, 400.13 MHz, CD_3CN): δ = 9.11 (br. s, 2H, ArH), 8.04 (br. s, 2H, H_D), 7.46 (br. s, 2H, ArH), 7.28 (br. s, 2H, H_C), 6.87 (br. s, 2H, H_E) ppm. *The largest chemical shift change occurs at the position closest to the Lewis Basic hydroxyl groups (H_E, 0.46 ppm) as expected.*

7.8 Synthesis of 2,4-Dibromonaphthalen-1-amine, 14

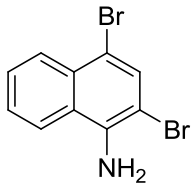

2,4-Dibromonaphthalen-1-amine was synthesised according to literature procedures.[4] A solution of 1-naphthylamine (10 g, 69.8 mmol) in AcOH (150 ml) was added to a cooled (~10 °C) solution of bromine (8 ml, 156 mmol) in AcOH (200 ml). The mixture was heated at 60 °C for 15 minutes and then filtered whilst hot and rinsed with fresh AcOH. The product was recrystallised from the minimum amount of hot EtOH to give large pale-purple crystals. Yield 13.4 g (64%). NMR values agree with those previously reported.[4]

^{1}H NMR (+20 °C, 400.13 MHz, DMSO-d_6): δ = 8.29 (d, *J* = 8.5 Hz, 1H, ArH), 8.0 (d, *J* = 8.5 Hz, 1H, ArH), 7.79 (s, 1H, ArH), 7.65 (m, 1H, ArH), 7.55 (m, 1H, ArH), 6.13 (s, 2H, -NH_2) ppm.
Mp: 115 – 117 °C.

7.9 Synthesis of 4-Bromo-2-naphthol, 20

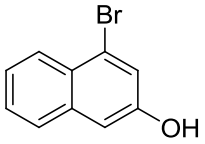

4-Bromo-2-naphthol (**17**) was synthesised by modified literature procedures[4] via the 4-bromo-1-diazonionaphthalen-2-olate intermediate (**19**). Solid $NaNO_2$ (3.51 g, 51 mmol) was added to a cooled (~10 °C) AcOH solution (350 ml) of 2,4-dibromoaniline (13.4 g, 44.2 mmol) and stirred for 15 minutes. The product was precipitated from 4 litres of water to yield a yellow solid. The solid (3.78 g, 15.2 mmol, uncharacterised) was dissolved in EtOH (30 ml) and cooled (~0 °C). Solid $NaBH_4$ (0.86 g, 22 mmol) was added slowly over 1 minute. The solution was stirred overnight and quenched with dilute aq. HCl and extracted into toluene. Yield 0.89 g (26%). NMR values agree with those previously reported.[4]

^{1}H NMR (+20°C, 400.13 MHz, DMSO-d_6): δ = 10.1 (br. s, 1H, -O*H*), 7.96 (d, *J* = 8.5 Hz, 1H, ArH), 7.76 (d, *J* = 8 Hz, 1H, ArH), 7.44 (m, 3H, ArH), 7.2 (d, *J* = 2 Hz, 1H, ArH) ppm.
Mp: 121 – 122 °C.

7.10 Synthesis of 4,4'-dibromo-2,2'-binaphthol, 14

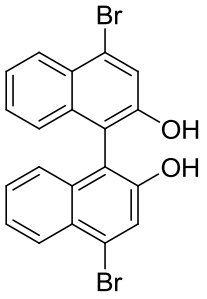

4,4'-dibromo-2,2'-binaphthol was synthesised according to literature procedures.[5] A mixture of 4-bromo-2-naphthol (0.89 g, 4 mmol) and CuCl(HO-TMEDA) catalyst (10 mol%, 186 mg, 0.4 mmol) in dry DCM (25 ml) was stirred at room temperature for 4 h. The dark brown mixture was diluted with DCM (50 ml), washed with saturated NH_4Cl solution (2 x 30 ml) and dried over $MgSO_4$. Solvent removal yielded a crude dark brown solid. Yield 500 mg (28%). NMR values agree with those previously reported.[5]

^{1}H NMR (+20°C, 300 MHz, $CDCl_3$): d = 8.3 (d, *J* = 8.4 Hz, 2H, ArH), 7.76 (s, 2H, ArH), 7.5 (m, 2H, ArH), 7.37 (m, 2H, ArH), 7.15 (d, *J* = 8.4 Hz, 2H, ArH), 5.07 (br. s, 2H, O*H*) ppm.
Mp: 213 – 214 °C.

7.11 Synthesis of (*R*)-Bicyclo[2.2.1]heptane-1-methanesulfonic acid, 7,7-dimethyl-2-oxo-, 4,4'-dibromo[1,1'-binaphthalene]-2,2'-diyl ester, 21

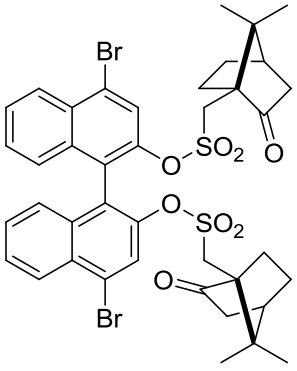

(*R*)-Bicyclo[2.2.1]heptane-1-methanesulfonic acid, 7,7-dimethyl-2-oxo-, 4,4'-dibromo[1,1'-binaphthalene]-2,2'-diyl ester was synthesised according to literature procedures.[5] To a cooled (0 °C) solution of *rac*-4,4'-dibromo-2,2'-binaphthol (1.15 g, 2.6 mmol) in dry DCM (20 ml) under a nitrogen atmosphere was added (1*S*)-camphor-10-sulfonyl chloride (2 g, 7.8 mmol). Dry NEt_3 (1.6 ml, 11.2 mmol) was then added. The

mixture was stirred cold for 2 h before being poured into water (50 ml). The aqueous phase was extracted with DCM, washed with brine and dried with $MgSO_4$. Solvent removal yielded a racemic mixture of diastereomers as a yellow solid. Separation of the diastereomers was achieved by silica gel chromatography (PhMe/EtOAc, 100:2, v/v). Yield of (*R*) 737 mg (63 %). NMR values agree with those previously reported.[5]

^{1}H NMR (+20°C, 300 MHz, $CDCl_3$): δ = 8.37 (m, 2H, ArH), 8.15 (s, 2H, ArH), 7.64 (m, 2H, ArH), 7.45 (m, 2H, ArH), 7.29 (m, 2H, ArH), 3.39 (d, *J* = 15.1 Hz, 2H), 2.51 (d, *J* = 14.9 Hz, 2H), 2.25 (m, 2H), 1.92 (m, 8H), 1.39 (m, 4H), 0.78 (s, 6H), 0.58 (s, 6H) ppm.
Mp: 190 – 191 °C.

7.12 Synthesis of (*R*)-4,4'-dibromo-2,2'-binaphthol, 14

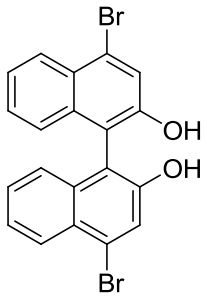

(*R*)-4,4'-dibromo-2,2'-binaphthol was synthesised according to literature procedures.[5] 1.2 M aq. NaOH (10 ml) was added to a stirred solution of diastrereomerically pure (*R*)-bicyclo[2.2.1]heptane-1-methanesulfonic acid, 7,7-dimethyl-2-oxo-, 4,4'-dibromo[1,1'-binaphthalene]-2,2'-diyl ester (400 mg, 0.46 mmol) in MeOH (20 ml). The resulting mixture was heated at 60 °C for 20 h. The solution was then cooled to 0 °C, and then acidified with dilute HCl solution. Excess MeOH was removed *in vacuo*, the residue was taken up into DCM (50 ml), washed with dilute HCl solution, brine and finally dried over $MgSO_4$. Solvent removal yielded a pure pale yellow solid. Yield 180 mg (89 %). NMR values agree with those previously reported.[5]

^{1}H NMR (+20°C, 300 MHz, $CDCl_3$): δ = 8.31 (d, *J* = 8.7 Hz, 2H, ArH), 7.76 (s, 2H, ArH), 7.5 (m, 2H, ArH), 7.37 (t, *J* = 7.5 Hz, 2H, ArH), 7.15 (d, *J* = 8.3 Hz, 2H, ArH), 5.0 (s, 2H, O*H*) ppm.
Mp: 214 – 215 °C.

7.13 Synthesis of 2,2'-dihydroxy-1,1'-binaphthalene-4,4'-dicarboxylic acid, 13

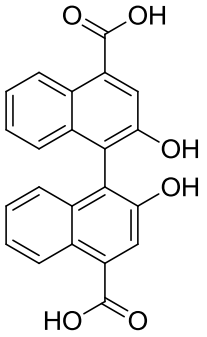

2,2'-dihydroxy-1,1'-binaphthalene-4,4'-dicarboxylic acid was synthesised according to literature procedures *via* the 2,2'-dihydroxy-1,1'-binaphthalene-4,4'-dicarbonitrile intermediate.[6] A mixture of 4,4'-dibromo-1,1'-binaphthalene-2,2'-diol (350 mg, 0.79 mmol) and CuCN (4 eq., 283 mg, 3.16 mmol) in DMF (8 ml) were heated to reflux for 3 days. The solution was diluted with EtOAc (100 ml) and washed several times with water (5 x 50 ml). The solvent was removed *in vacuo* to give a crude brown solid (uncharacterised). The solid was then refluxed in aq. NaOH (6 M, 10 ml) overnight. After cooling to room temperature, the reaction was neutralised with concentrated HCl. The precipitate was filtered and purified using silica gel chromatography (EtOAc, 100%) to give the pure diacid as a crystalline orange/brown solid. Yield 156 mg (42 %). NMR values agree with those previously reported.[6]

^{1}H NMR (+20°C, 300.13 MHz, DMSO-d_6): δ = 13.19 (br. s, 2H, CO_2H), 9.67 (s, 2H, O_H), 8.81 (d, *J* = 8.7 Hz, 2H, ArH), 7.97 (s, 2H, ArH), 7.37 (t, *J* = 7.5 Hz, 2H, ArH), 7.25 (t, *J* = 7.5 Hz, 2H, ArH), 6.99 (d, *J* = 8.7 Hz, 2H, ArH) ppm.
Mp: 323 – 326 °C.

7.14 Synthesis of dimethyl 2,2'-dihydroxy-1,1'-binaphthalene-6,6'dicarboxylate, 24

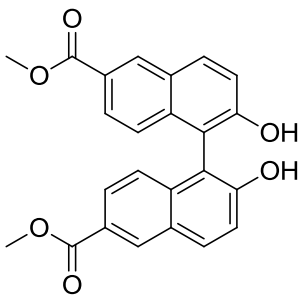

Dimethyl 2,2'-dihydroxy-1,1'-binaphthalene-6,6'dicarboxylate was synthesised according to literature procedures.[2] Methyl 6-hydroxy-2-naphthoate (1 g, 4.95 mmol) and

$FeCl_3.6H_2O$ (2.4 g, 9.9 mmol) were suspended in water (150 ml) and heated to 70 °C for 24 h. The crystalline precipitate was then filtered hot and the solid recrystallised from MeOH to give clear colourless needles. Yield 916 mg (46 %). NMR values agreed with those previously reported.[2]

^{1}H NMR (+20°C, 300.13 MHz, $CDCl_3$): δ = 8.67 (s, 2H, ArH), 8.12 (d, *J* = 8.7 Hz, 2H, ArH), 7.9 (d, *J* = 9 Hz, 2H, ArH), 7.47 (d, *J* = 9 Hz, 2H, ArH), 7.14 (d, *J* = 9 Hz, 2H, ArH), 3.96 (s, 6H, CO_2CH_3) ppm.
Mp: 319 – 322 °C.

7.15 Synthesis of 2,2'-dihydroxy-1,1'-binaphthalene-6,6'-dicarboxylic acid, 22

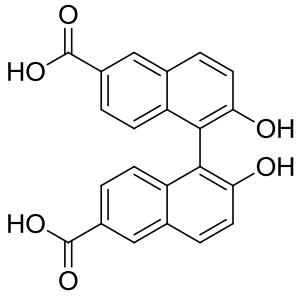

2,2'-dihydroxy-1,1'-binaphthalene-6,6'-dicarboxylic acid was synthesised according to literature procedures.[2] Dimethyl 2,2'-dihydroxy-1,1'-binaphthalene-6,6'dicarboxylate (900 mg, 2.24 mmol) was heated to reflux in aq. NaOH (10 %, 30 ml) solution for 2 h. After cooling to room temperature, the crude product was precipitated from solution by slow addition of concentrated HCl. The crude product was recrystallised from MeOH to give colourless needles. Yield 804 mg (96%). NMR values agree with those previously reported.[2]

^{1}H NMR (+20°C, 400.13 MHz, DMSO-d_6): δ = 12.75 (br. s, 2H, CO_2H), 9.71 (br. s, 2H, O*H*), 8.56 (d, *J* = 1.5 Hz, 2H, ArH), 8.07 (d, *J* = 9.1 Hz, 2H, ArH), 8.8 (dd, *J* = 8.8, 1.8 Hz, 2H, ArH), 7.41 (d, *J* = 9.1 Hz, 2H, ArH), 6.99 (d, *J* = 8.6 Hz, 2H, ArH) ppm.
^{13}C NMR (+20°C, 100.61 MHz, DMSO-d_6): δ = 167.62 (*C*O_2H), 155.31 (*C*OH), 136.32 (C), 130.93 (CH), 130.64 (CH), 127.1 (C), 125.44 (CH), 124.57 (C), 124.38 (CH), 119.35 (CH), 115.13 (C) ppm.
Mp: 324 – 325 °C.

7.16 Synthesis of 4,4'-dibromo-1,1'-binaphthalene-2,2'-diyl diacetate, 27

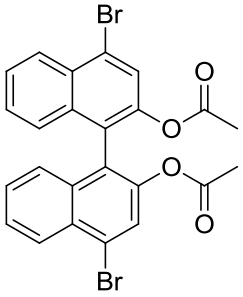

To a solution of 4,4'-dibromo-2,2'-binaphthol (1 g, 2.25 mmol) in dry DCM (25 ml) was added dry pyridine (5 eq., 0.9 ml, 11.25 mmol). The mixture was allowed to stir for 5 minutes before Ac_2O (5 eq., 1.1 ml, 11.25 mmol) was added. The solution was left to stir overnight. The mixture was diluted with DCM (100 ml), washed with water (3 x 20 ml) and dried over $MgSO_4$. The volatiles were then removed *in vacuo* and the crude residue purified by silica gel chromatography (hexane/EtOAc, 4:1, v/v) to yield a pure light brown solid. Yield 670 mg (56%).

^{1}H NMR (+20°C, 300.13 MHz, $CDCl_3$): δ = 8.34 (d, *J* = 8.3, 2H, ArH), 7.79 (s, 2H, ArH), 7.59 (ddd, *J* = 8.5, 7.0, 1.1 Hz, 2H, ArH), 7.35 (ddd, *J* = 8.4, 7.1, 1.1 Hz, 2H, ArH), 7.18 (d, *J* = 8.3 Hz, 2H, ArH), 1.9 (s, 6H, OC(O)CH_3) ppm.

^{1}H NMR (+20°C, 400.13 MHz, DMSO-d_6): δ = 8.27 (d, *J* = 8.1 Hz, 2H, ArH), 8.06 (s, 2H, ArH), 7.69 (td, *J* = 7.7, 1.3 Hz, 2H, ArH), 7.44 (td, *J* = 7.7, 1.3 Hz, 2H, ArH), 7.01 (d, *J* = 8.1 Hz, 2H, ArH), 1.86 (s, 6H, OC(O)CH_3) ppm.

^{13}C NMR (+20°C, 100.61 MHz, $CDCl_3$): δ = 168.96 (CO*C*(O)CH_3), 146.13 (*C*OC(O)CH_3), 133.65 (C), 130.19 (C), 127.67 (CH), 127.36 (CH), 127.19 (CH), 126.51 (CH), 126.03 (CH), 123.61 (C), 122.90 (CH), 20.5 (COC(O)*C*H_3) ppm.

IR: ν_{max} (film)/cm^{-1} = 3070 (aromatic C-H str.), 2960 (alkane C-H str.), 1750 (ester C-O str.), 1010 (ester C-O str.).

HRMS (ESI): m/z = 548.9289 ($[M+Na]^+$, requires 548.9313 $C_{24}H_{16}Br_2O_4Na$).

Mp: 184 – 186 °C.

7.17 Synthesis of dimethyl 4,4'-(2,2'-diacetoxy-1,1'-binaphthalene-4,4'-diyl)dibenzoate, 28

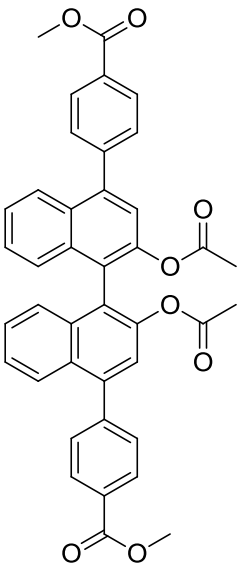

To a solution of 4,4'-dibromo-1,1'-binaphthalene-2,2'-diyl diacetate, (316 mg, 0.6 mmol) and 4-(methoxycarbonyl)phenylboronic acid (324 mg, 1.8 mmol) in toluene (10 ml) was added aq. Na_2CO_3 (2 M, 0.5 ml, 1.8 mmol). The solution was degassed with nitrogen for 20 minutes, then solid $Pd(dppf)_2Cl_2$ (10 mol%, 44 mg, 0.06 mmol) was added and the mixture immediately heated to reflux for 3 days. After cooling to room temperature, the solvent was removed *in vacuo* and the residue was taken up in DCM (150 ml), washed with water (3 x 30 ml) and dried over $MgSO_4$. Evaporation of the solvent yielded a crude brown solid. Purification by silica gel chromatography (hexane/EtOAc, 6:1, v/v) gave a pure off-white solid. Yield 211 mg (55 %).

^{1}H NMR (+20°C, 400.13 MHz, DMSO-d_6): δ = 8.19 (d, J = 8.1 Hz, 4H, ArH), 7.84 (d, J = 8.1 Hz, 4H, ArH), 7.8 (d, J = 7.6 Hz, 2H, ArH), 7.57 (s, 2H, ArH), 7.31 (m, 4H, ArH), 7.08 (m, 2H, ArH), 3.94 (s, 6H, CO_2CH_3), 3.79 (s, 6H, $OC(CO)CH_3$) ppm.

^{13}C NMR (+20°C, 100.13 MHz, DMSO-d_6): δ = 166.15 ($CO(O)CH_3$), 154.94 (CO_2CH_3), 144.85 ($COC(O)CH_3$), 139.93 (C), 133.85 (C), 130.48 (CH), 129.37 (CH), 128.8 (C), 126.65 (CH), 126.21 (C), 125.37 (CH), 125.09 (CH), 124.06 (CH), 118.59 (C), 115.19 (CH), 56.28 ($COC(O)CH_3$), 52.30 (CO_2CH_3) ppm.

IR (film): ν_{max}/cm^{-1} = 2910 (aromatic C-H str.), 1740 (ester C=O str.), 1605 (aromatic C-C str.), 1255 (ester C-O str.), 1050 (ether C-O str.).

HRMS (ESI): m/z = 661.1137 ($[M+Na]^+$, requires 661.1838 $C_{40}H_{30}O_8Na$).

Mp: 233 – 234 °C.

7.18 Synthesis of 4,4'-(2,2'-dihydroxy-1,1'-binaphthyl-4,4'-diyl)dibenzoic acid, 25

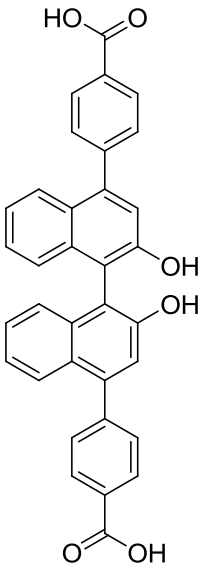

To a solution of dimethyl 4,4'-(2,2'-diacetoxy-1,1'-binaphthalene-4,4'-diyl)dibenzoate (100 mg, 0.16 mmol) in THF (5 ml) and EtOH (5 ml) was added aq. NaOH (2 M, 5 ml). The solution was heated at 80 °C for 24 h, and then allowed to cool to room temperature. After pouring into an ice/water/HCl mixture, the organic products were extracted with EtOAc (3 x 10 ml). The organic layer was washed with water and dried with $MgSO_4$. Solvent removal yielded a pale yellow solid. Yield 63 mg (76 %).

^{1}H NMR (+20°C, 400.13 MHz, DMSO-d_6): δ = 13.04 (br. s, 2H, CO_2H), 9.48 (br. s, 2H, O*H*), 8.15 (d, *J* = 8.5 Hz, 4H, ArH), 7.72 (m, 6H, ArH), 7.26 (m, 6H, ArH), 7.13 (m, 2H, ArH) ppm.

^{13}C NMR (+20°C, 300.13 MHz, DMSO-d_6): δ = 167.17 (CO_2H), 152.43 (*C*OH), 144.54, 139.41, 134.58, 129.98, 129.83, 129.53, 126.14, 125.72, 125.26, 125.04, 122.95, 119.32, 115.66 ppm.

IR (film): ν_{max}/cm^{-1} = 3470 (alcohol O-H str.), 3040 (carboxylic acid O-H str.), 2990 (aromatic C-H str.), 1680 (carboxylic acid C=O str.), 1540 (aromatic C-C str.), 1180 (C-O str.).

HRMS (ESI): m/z = 529.9891 ($[M]^+$, requires 530.1792 $C_{34}H_{26}O_6$).

Mp: 271 – 273 °C.

7.19 Synthesis of tetramethyl 5,5'-(2,2'-diacetoxy-[1,1'-binaphthalene]-4,4'-diyl)diisophthalate, 30

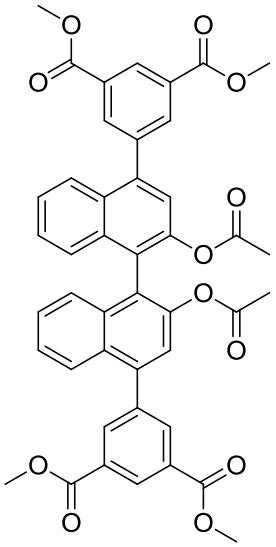

A solution of 4,4'-dibromo-1,1'-binaphthalene-2,2'-diyl diacetate (105 mg, 0.2 mmol) and 3,5-bis(methoxycarbonyl)phenylboronic acid pinacol ester (197 mg, 0.6 mmol) in toluene (3 ml) was added aq. Na_2CO_3 (2 M, 0.3 ml, 0.6 mmol). The solution was degassed with nitrogen for 20 minutes, then solid $Pd(dppf)_2Cl_2$ (5 mol%, 3 mg, 0.01 mmol) was added and the mixture immediately heated to reflux for 3 days. After cooling to room temperature, the solvent was removed *in vacuo* and the residue was taken up in DCM (100 ml), washed with water (3 x 30 ml) and dried over $MgSO_4$. Evaporation of the solvent yielded a crude brown residue. Purification by silica gel chromatography (DCM/EtOAc, 99:1, v/v) gave a pale yellow solid. Yield 39 mg (26 %).

^{1}H NMR (+20°C, 300.13 MHz, DMSO-d_6): δ = 8.7 (s, 2H, ArH), 8.37 (d, *J* = 1.7 Hz, 4H, ArH), 8.24 (d, *J* = 7.7 Hz, 2H, ArH), 7.83 (d, *J* = 1.5 Hz, 2H, ArH), 7.54 (m, 2H, ArH), ArH), 7.25 (m, 2H, ArH), 7.13 (d, *J* = 2.5 Hz, 2H, ArH), 3.96 (s, 12H, CO_2CH_3), 1.62 (s, 6H, OCH_3) ppm.

^{13}C NMR (+20°C, 75.48 MHz, $CDCl_3$): δ = 166.03 (CO_2CH_3), 164.34 (CO), 148.33 (C), 139.76 (C), 137.87 (C), 135.21 (C), 131.76 (C), 131.55 (C), 129.11 (CH), 128.1 (CH), 127.01 (CH), 126.55 (CH), 125.34 (CH), 1125.12 (CH), 121.63 (CH), 52.31 (CO_2CH_3), 22.14 (OCH_3) ppm.

IR (film): ν_{max}/cm^{-1} = 2930 (aromatic C-H str.), 1725 (ester C=O str.), 1615 (aromatic C-C str.), 1240 (ester C-O str.), 1055 (ether C-O str.).

HRMS (ESI): m/z = 754.2043 ($[M]^+$, requires 754.2050 $C_{34}H_{26}O_6$).

Mp: 282 – 286 °C.

7.20 Synthesis of 5,5'-2,2'-dihydroxy-1,1'-binaphthyl-4,4'-diyl)diisophthalic acid, 29

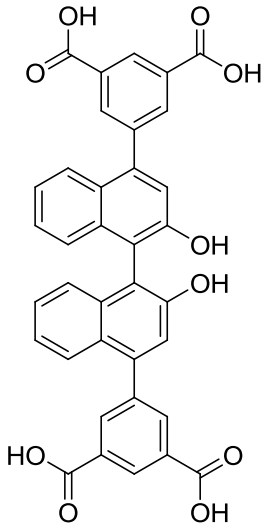

To a cold (0 °C) solution of tetramethyl 5,5'-(2,2'-dimethoxy-1,1'-binaphthyl-4,4'-diyl)diisophthalate (105 mg, 0.15 mmol) in dry DCM (10 ml) under a nitrogen atmosphere was added BBr_3 (1 M in hexanes, 2.25 ml, 2.25 mmol) drop wise. The solution was left to warm to room temperature overnight. The solution was then poured into an ice/water mixture and the organic products were extracted with EtOAc (3 x 30 ml). The organic layer was washed with water and dried with $MgSO_4$. Solvent removal yielded a pale yellow solid. The solid was then dissolved in EtOH/water (1:1 10 ml total), then 6 M aqueous NaOH (5 ml) was added. The solution was heated to 80 °C and stirred overnight. After cooling to room temperature, the solution was pour into an ice/water/HCl mixture and extracted with EtOAc (3 x 30 ml). The organic layer was washed with water and dried with $MgSO_4$. Solvent removal yielded a pure yellow solid. Yield 65 mg (70 %).

^{1}H NMR (+20°C, 300.13 MHz, DMSO-d_6): δ = 13.41 (br. s, 4H, CO_2H) 9.5 (s, 2H, O*H*), 8.61 (s, 2H), 8.32 (s, 4H), 7.68 (dd, *J* = 6.3, 3.3 Hz, 2H), 7.34 (s, 2H), 7.28 (dd, *J* = 6.6, 3.5 Hz, 2H), 7.16 (dd, *J* = 6.3, 3.3 Hz, 2H) ppm.

^{13}C NMR (+20°C, 300.13 MHz, DMSO-d_6): δ = 166.87 (*C*O_2H), 154.10 (*C*OH), 138.97, 138.74, 136.06, 132.21, 131.04, 128.32, 126.54, 126.32, 126.11, 125.45, 116.01, 111.46 ppm.

IR (film): ν_{max}/cm^{-1} = 2955 (aromatic C-H str.), 1710 (ester C=O str.), 1620 (aromatic C-C str.), 1270 (ester C-O str.), 1100 (ether C-O str.).

HRMS (ESI): m/z = 614.1208 ($[M]^+$, requires 614.1213 $C_{34}H_{26}O_6$).

Mp: 285 – 287 °C.

7.21 Synthesis of (*R*)-6,6'-Dibromo-1,1'-binaphthyl-2,2'-diol, 32

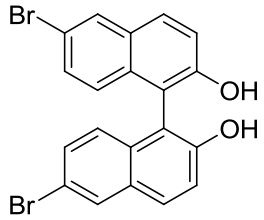

(*R*)-6,6'-Dibromo-1,1'-binaphthyl-2,2'-diol was synthesised according to literature procedures.[7] A solution of Br_2 (0.5 ml, 9.5 mmol) in DCM (20 ml) was added drop wise to a cold (-78 °C) stirred solution of (*R*)-1,1'-bi(2-naphthol) (1 g, 3.5 mmol) in DCM (20 ml). The resulting mixture was stirred for 2 h cold and then an additional 2 h at room temperature. The reaction was then quenched with aqueous $Na_2S_2O_3$, washed with brine and the organic layer dried with $MgSO_4$. Solvent removal gave a pure (*by ^1H NMR*) brown solid. Yield 1.54 g (99%). NMR values agree with those previously reported.[7]

^{1}H NMR (+20°C, 300.13 MHz, $CDCl_3$): δ = 8.06 (d, *J* = 2 Hz, 2H, ArH), 7.91 (d, *J* = 9.1 Hz, 2H, ArH), 7.39 (m, 4H, ArH), 6.97 (d, *J* = 9.1 Hz, 2H, ArH), 5.06 (br. s, 2H, O*H*) ppm.

Mp: 99 – 100 °C.

7.22 Synthesis of (*R*)-6,6'-Dibromo-2,2'-diethoxy-1,1'-ninaphthyl, 33

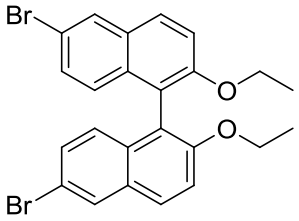

(*R*)-6,6'-Dibromo-2,2'-diethoxy-1,1'-ninaphthyl was synthesised according to literature procedures.[7] A solution of (*R*)-6,6'-dibromo-1,1'-binaphthyl-2,2'-diol (1.54 g, 3.5 mmol), K_2CO_3 (2.4 g, 17.2 mmol) and NaI (33 mg, 0.23 mmol) in acetone (20 ml) was heated to reflux. Then EtBr (1.9 ml, 25 mmol) was added drop wise through the top of the condenser. The mixture was refluxed overnight and then filtered whilst hot through a pad of Celite®. Solvent removal yielded a crude brown residue. This was dispersed in *n*-

pentane by sonification and filtered to give a fine white powder. Yield 1.32 g (75 %). NMR values agree with those previously reported.[7]

^{1}H NMR (+20°C, 300.13 MHz, $CDCl_3$): δ = 8.01 (d, *J* = 2.0 Hz, 2H, ArH), 7.85 (d, *J* = 9.1 Hz, 2H, ArH), 7.43 (d, *J* = 9.1 Hz 2H, ArH), 7.27 (dd, *J* = 8.6, 2 Hz, 2H, ArH), 6.96 (d, *J* = 8.6 Hz, 2H, ArH), 4.05 (m, 4H, O*C*$H_2$$CH_3$), 1.07 (t, *J* = 7.1 Hz, 6H, OCH_2*C*H_3) ppm.
Mp: 159 – 161 °C.

7.23 (*R*)-Tetramethyl-5,5'-(2,2'-diethoxy-1,1'-binaphthyl-6,6'-diyl)diisophthalate, 34

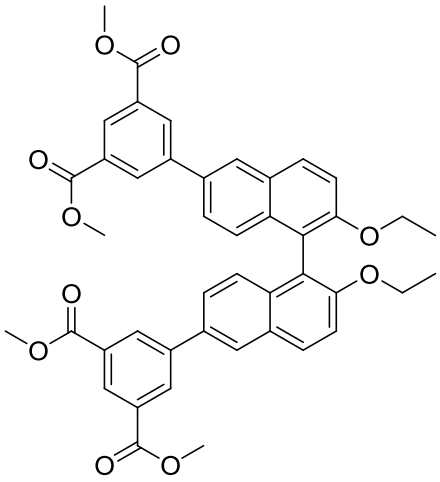

To (*R*)-6,6'-dibromo-2,2'-diethoxy-1,1'-binaphthyl (250 mg, 0.5 mmol) and 3,5-bis(methoxycarbonyl)phenylboronic acid pinacol ester (480 mg, 1.5 mmol) in toluene (5 ml) was added 2M aq. Na_2CO_3 (72 mg, 0.34 ml). The solution was degassed with nitrogen for 20 minutes. Solid $Pd(dppf)_2Cl_2$ (19 mg, 0.025 mmol) was then added and mixture was immediately heated to reflux for 3 days. After cooling to room temperature, the solvent was removed *in vacuo* and the residue was taken up in DCM (100 ml), washed with water (3 x 30 ml) and dried over $MgSO_4$. Evaporation of the solvent yielded a crude brown residue. Purification by silica gel chromatography (DCM/EtOAc, 98:2, v/v) gave a white solid. Yield 50 mg (14%).

^{1}H NMR (+20°C, 300.13 MHz, DMSO-d_6): δ = 8.51 (d, *J* = 1.5 Hz, 4H, ArH), 8.45 (d, *J* = 1.5 Hz, 2H ArH), 8.4 (d, *J* = 1.5 Hz, 2H ArH), 8.24 (d, *J* = 9.1 Hz, 2H ArH), 7.65 (m, 4H ArH), 7.09 (d, *J* = 9.1 Hz, 2H ArH), 4.13 (q, *J* = 6.9 Hz, 4H, O*CH*$_2$$CH_3$), 3.93 (s, 12H, CO_2*CH*$_3$), 1.05 (t, *J* = 6.8 Hz, 6H, OCH_2*CH*$_3$) ppm.

^{13}C NMR (+20°C, 75.48 MHz, DMSO-d_6): δ = 165.37 (-CO$_2$CH$_3$), 154.6, 141.39, 133.18, 132.67, 131.37, 131.05, 130.18, 128.9, 128.08, 126.39, 125.78, 125.05, 118.8, 116.11, 64.19 (-OCH$_2$CH$_3$), 52.62 (-CO$_2$$CH_3$), 14.79 (-OCH$_2$$CH_3$) ppm.

IR (film): ν_{max}/cm^{-1} = 2960 (alkane C-H str.), 1690 (ester C=O str.), 1600 (aromatic C-C str.), 1500 (aromatic C-C str.), 1420 (alkane C-H bend), 1260 (ether C-O str.).

HRMS (ESI): m/z = 727.2549 ([M+H]$^+$, requires 727.2543 $C_{44}H_{39}O_{10}$).

Mp: 194 – 196 °C.

7.24 Synthesis of (*R*)-6,6'-Dibromo-1,1'-binaphthyl-2,2'-diyl diacetate, 35

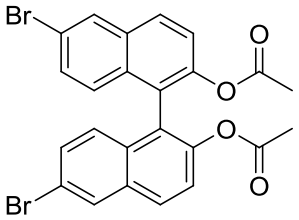

(R)-6,6'-Dibromo-1,1'-binaphthyl-2,2'-diyl diacetate was synthesised according to literature procedures.[8] To a solution of (*R*)-6,6'dibromo-1,1'-binaphthyl-2,2'-diol (500 mg, 0.89 mmol) in dry DCM (10 ml) was added freshly distilled pyridine (5 eq., 0.34 ml, 4.44 mmol) and acetic anhydride (5 eq., 0.43 ml, 4.44 mmol). The solution was stirred at room temperature for 24 h. The solvents were then removed *in vacuo* and the crude residue purified by silica gel chromatography (hexane/EtOAc, 7:2, v/v) to give a pure white solid. Yield 250 mg (40%). NMR values agree with those previously reported.[9]

^{1}H NMR (+20 °C, 400.13 MHz, CDCl$_3$): δ = 8.11 (d, *J* = 2.0 Hz, 2H, ArH), 7.92 (d, *J* = 9.1 Hz, 2H, ArH), 7.45 (d, *J* = 9.1 Hz, 2H, ArH), 7.37 (dd, *J* = 9.1, 2.0 Hz, 2H, ArH), 7.02 (d, *J* = 9.1 Hz, 2H, ArH), 1.89 (s, 6H, -OC(O)CH_3) ppm.

^{13}C NMR (+20°C, 100.61 MHz, CDCl$_3$): δ = 169.1 (COC(O)CH$_3$), 147.0 (COC(O)CH$_3$), 132.57 (C), 131.67 (C), 130.26 (CH), 130.07 (CH), 128.8 (CH), 127.71 (CH), 123.17 (C), 123.06 (CH), 120.05 (CBr), 20.48 (COC(O)CH$_3$) ppm.

Mp: 181 - 182 °C.

7.25 Synthesis of *(R)*-Tetramethyl 5,5'-(2,2'-diacetoxy-1,1'-binaphthyl-6,6'-diyl)diisophthalate, 36

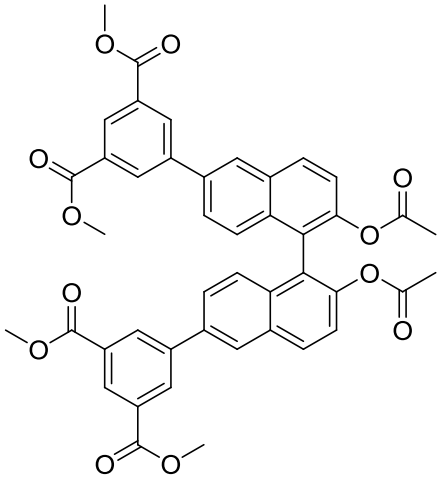

To a solution of (*R*)-6,6'-dibromo-1,1'-binaphthyl-2,2'-diyl diacetate (120 mg, 0.28 mmol) and 3,5-bis(methoxycarbonyl)phenylboronic acid pinacol ester (218 mg, 0.68 mmol) in toluene (3 ml) was added 2M aq. Na_2CO_3 (72 mg, 0.34 ml). The solution was degassed with nitrogen for 20 minutes. Solid $Pd(dppf)_2Cl_2$ (5 mol%, 8 mg, 0.0114 mmol) was then added and the mixture was immediately heated to reflux for 3 days. After cooling to room temperature, the solvent was removed *in vacuo* and the residue was taken up in DCM (100 ml), washed with water (3 x 30 ml) and dried over $MgSO_4$. Evaporation of the solvent yielded a crude brown residue. Purification by silica gel chromatography (DCM/EtOAc, 95:5, v/v) gave a white solid. Yield 125 mg (59 %).

^{1}H NMR (+20°C, 400.13 MHz, $CDCl_3$): δ = 8.68 (s, 2H), 8.57 (d, *J* = 1.1 Hz, 4H), 8.25 (d, *J* = 1.1 Hz, 2H), 8.13 (d, *J* = 9.0 Hz, 2H), 7.61 (dd, *J* = 9.0, 1.1 Hz 2H), 7.52 (d, *J* = 8.7 Hz, 2H), 7.33 (d, *J* = 8.7 Hz, 2H), 3.99 (s, 12H, CO_2CH_3), 1.93 (s, 6H, $OC(O)CH_3$) ppm.

^{13}C NMR (+20°C, 100.61 MHz, $CDCl_3$): δ = 169.3 ($OC(O)CH_3$), 166.16 (CO_2CH_3), 147.29 (C), 141.39 (C), 136.31 (C), 132.89 (C), 132.44 (CH), 131.74 (C), 131.29 (C), 130.07 (CH), 129.49 (CH), 127.09 (CH), 126.42 (CH), 126.01 (CH), 123.25 (C), 122.72 (CH), 52.47 (CO_2CH_3), 20.6 ($OC(O)CH_3$) ppm.

IR (film): ν_{max}/cm^{-1} = 3410 (alcohol O-H str.), 3070 (carboxylic acid O-H str.), 2980 (aromatic C-H str.), 1690 (carboxylic acid C=O str.), 1590 (aromatic C-C str.), 1210 (C-O str.).

HRMS (ESI): m/z = 330.1234 ($[M+H]^+$, requires 330.1235 $C_{21}H_{15}O_4$).

Mp: 221 – 224 °C

7.26 Synthesis of (*R*)-5,5'-(2,2'-dihydroxy-1,1'-binaphthyl-6,6'-diyl)diisophthalic acid, 31

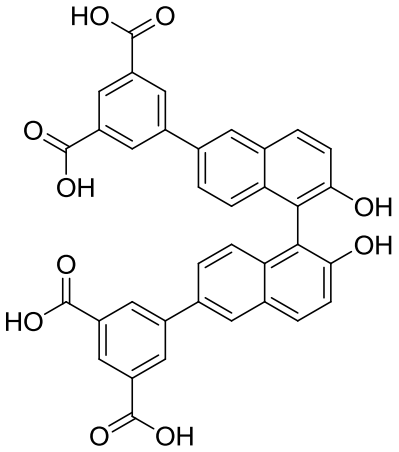

(*R*)-5,5'-(2,2'-diacetoxy-1,1'-binaphthyl-6,6'-diyl)diisophthalate (xmg, x mmol) was suspended in EtOH (5 ml), THF (2 ml) and 6M aqueous NaOH (1.5 ml), then heated at 80 °C overnight. After cooling to room temperature, the solution was pour into an ice/water/HCl mixture and extracted with EtOAc (3 x 10 ml). The organic layer was washed with water and dried with $MgSO_4$. The product was extracted with EtOAc and washed with water. The solvent was removed *in vacuo* to yield an off white solid. Yield 38 mg (37 %).

^{1}H NMR (+20°C, 300.13 MHz, DMSO-d_6): δ = 13.33 (br. s, 4H, CO_2H) 9.47 (s, 2H, O*H*) 8.47 (d, *J* = 1.1 Hz, 4H, ArH), 8.44 (s, 2H, ArH), 8.31 (d, *J* = 1.1 Hz, 2H, ArH), 8.07 (d, *J* = 9.0 Hz, 2H, ArH), 7.63 (dd, *J* = 9.0, 1.1 Hz, 2H, ArH), 7.4 (d, *J* = 8.7 Hz, 2H, ArH), 7.12 (d, *J* = 8.7 Hz, 2H, ArH) ppm.

^{13}C NMR (+20°C, 75.47 MHz, DMSO-d_6): δ = 166.6 (CO_2H), 153.78 (C), 141.23 (C), 133.82 (C), 133.09 (C), 132.15 (CH), 131.11 (C), 129.65 (C), 129.52 (C), 128.39 (CH), 126.17 (CH), 125.54 (CH), 124.81 (CH), 119.25 (C), 115.13 (CH), 122.87 (CH) ppm.

IR (film): ν_{max}/cm^{-1} = 3500 (alcohol O-H str.), 2990 (carboxylic acid O-H str.), 3010 (aromatic C-H str.), 1710 (carboxylic acid C=O str.), 1580 (aromatic C-C str.), 1510 (aromatic C-C str.).

HRMS (ESI): m/z = 615.1339 ($[M+H]^+$, requires 615.1291 $C_{36}H_{23}O_{10}$).

Mp: 267 – 268 °C.

7.27 Synthesis of 4,4'-Dibromo-2,2'-dimethoxy-1,1'-binaphthalene, 38

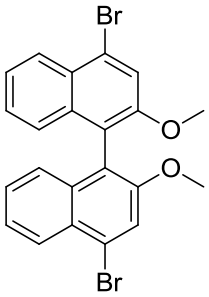

4,4'-Dibromo-2,2'-dimethoxy-1,1'-binaphthalene was synthesised according to literature procedures.[5] A mixture 4,4'-dibromo-2,2'-binaphthol (888 mg, 2 mmol), Cs_2CO_3 (2.7 mg, 8.5 mmol) and MeI (1.9 ml, 30.5 mmol) in acetone (30 ml) was stirred overnight. The mixture was filtered through a pad of celite and the filtrate concentrated to give a yellow solid. Yield 791 mg (84 %). NMR values agree with those previously reported.[5]

^{1}H NMR (+20°C, 400 MHz, $CDCl_3$): δ = 8.25 (d, *J* = 8.6 Hz, 2H, ArH), 7.77 (s, 2H, ArH), 7.43 (ddd, *J* = 8.3, 6.8, 1.0 Hz, 2H, ArH), 7.26 (*obscured by $CDCl_3$*, m, 2H, ArH), 7.1 (d, *J* = 8.6 Hz, 2H, ArH), 3.77 (s, 2H, OCH_3) ppm.
Mp: 209 – 210 °C.

7.28 Synthesis of 4,4'-(2,2'-dimethoxy-1,1'-binaphthalene-4,4'-diyl)dipyrdine, 39

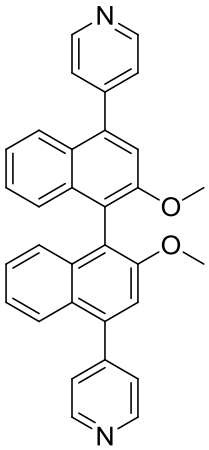

To a solution of 4,4'-dibromo-2,2'-dimethoxy-1,1'-binaphthyl (1.4 eq., 214 mg, 0.3 mmol) and potassium pyridine-4-trifluoroborate (2 eq., 79 mg, 0.43 mmol) in toluene (5 ml) was added aq. Na_2CO_3 (2 M, 0.43 ml, 0.86 mmol). The solution was degassed with nitrogen for 20 minutes. Solid $Pd(dppf)_2Cl_2$ (5 mol%, 11 mg, 0.015 mmol) was then added and the mixture was immediately heated to reflux for 3 days. After cooling to room temperature, the solvent was removed *in vacuo* and the residue was taken up in DCM (20 ml).

Purification by silica gel chromatography (Biotage® ISOLUTE® Flash SCX-2 eluting with DCM, then 1 M NH_3 in MeOH) gave a pale yellow solid. Yield 74 mg (69 %).

^{1}H NMR (+20°C, 300.13 MHz, DMSO-d_6): δ = 8.8 (d, *J* = 4.5 Hz, 4H, NC*H*), 7.82 (d, *J* = 7.9 Hz, 2H, ArH), 7.72 (d, *J* = 5.3, Hz, 4H, ArH), 7.6 (s, 2H, ArH), 7.34 (m, 4H, ArH), 7.08 (dd, J = 6.8, 1.9 Hz, 2H, ArH), 1.99 (s, 6H, OCH_3) ppm.
(No further characterisation performed, as compound not useful.)

7.29 Synthesis of 2,2'-bis(benzyloxy)-4,4'-dibromo-1,1'-binaphthalene, 40

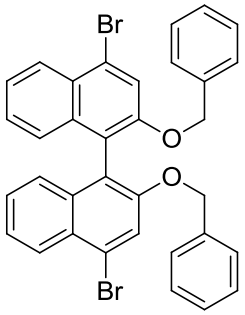

To a solution of 4,4'-dibromo-2,2'-binaphthol (570 mg, 1.28 mmol) in acetone (25 ml) was added KOH (720 mg, 12.8 mmol) and benzyl bromide (1.54 ml, 12.8 mmol). The mixture was refluxed for 3 h and the solvents then removed *in vacuo*. The crude residue was taken up in EtOAc (200 ml), the organic layer separated and washed with water (3 x 50 ml), then dried over $MgSO_4$. Purification by silica gel chromatography (EtOAc/water, 8:1, v/v) and subsequent recrystallisation from DCM/hexane (1:1, v/v) at -30 °C gave pure yellow crystals. Yield 631 mg (79 %).

^{1}H NMR (+20°C, 400.13 MHz, $CDCl_3$): δ = 8.27 (d, J = 8.6 Hz, 2H, ArH), 7.7 (s, 2H, ArH), 7.46 (ddd, *J* = 8.1, 7.07, 1.1 Hz, 2H, ArH), 7.28 (m, 2H, ArH), 7.16 (m, 8H, ArH), 7.1 (d, *J* = 7.1 Hz, 4H, ArH), 5.04 (s, 4H, OC$H_2C_6H_5$) ppm.
^{13}C NMR (+20°C, 100.13 MHz, $CDCl_3$): δ = 153.71 (*C*O$CH_2C_6H_5$), 136.7 (C), 134.62 (C), 128.25 (CH), 128.05 (C), 127.58 (CH), 127.25 (CH), 127.19 (CH), 126.71 (CH), 125.79 (CH), 125.21 (CH), 123.57 (C), 120.15 (CH), 120.12 (C), 71.43 (CO*C*$H_2C_6H_5$) ppm.
IR (film): ν_{max}/cm^{-1} = 3060 (aromatic C-H str.), 1580 (aromatic C-C str.), 1220 (ether C-O str.), 694 (C-Br str.).
HRMS (ESI): m/z = 645.0036 ($[M+Na]^+$, requires 645.0041 $C_{34}H_{24}Br_2O_2Na$).

Mp: 177 – 179 °C.

7.30 Synthesis of 4,4'-(2,2'-bis(benzyloxy)-1,1'-binaphthalene-4,4'-diyl)dipyridine, 41

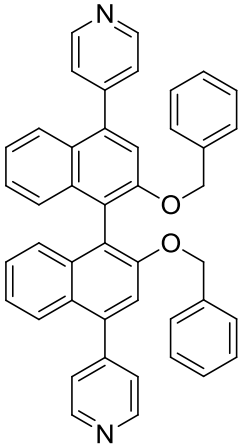

To 2,2'-bis(benzyloxy)-4,4'-dibromo-1,1'-binaphthalene (374 mg, 0.6 mmol) and potassium pyridine-4-trifluoroborate (185 mg, 1 mmol) in toluene (10 ml) was added aq. Na_2CO_3 (2 M, 0.5 ml, 1 mmol). The solution was degassed with nitrogen for 20 minutes. Solid $Pd(dppf)_2Cl_2$ (10 mol%, 44 mg, 0.06 mmol) was then added and the mixture was immediately heated to reflux for 3 days. After cooling to room temperature, the solvent was removed *in vacuo* and the residue was taken up in DCM (200 ml), washed with water (3 x 30 ml) and dried over $MgSO_4$. Evaporation of the solvent yielded a crude brown residue. Purification by silica gel chromatography (EtOAc, 100%) gave a white solid. Yield 258 mg (72 %).

^{1}H NMR (+20°C, 400.13 MHz, $CDCl_3$): δ = 8.8 (d, *J* = 5.7 Hz, 4H, ArH), 7.88 (d, *J* = 8.3 Hz, 2H, ArH), 7.52 (d, *J* = 5.7 Hz, 4H, ArH), 7.36 (m, 8H, ArH), 7.13 (m, 6H, ArH), 6.97 (d, *J* = 7.2 Hz, 4H), 5.1 (s, 4H, CO*C*$H_2C_6H_5$) ppm.

^{13}C NMR (+20°C, 100.13 MHz, $CDCl_3$): δ = 154.54 (*C*O$CH_2C_6H_5$), 134.49 (C), 127.8 (C), 127.23, 127.17, 126.94, 125.47, 124.93, 124.91, 123.79, 122.64 (C), 118.93, 118.45, 106.12, 56.97 ppm.

IR (film): ν_{max}/cm^{-1} = 3070 (aromatic C-H str.), 1590 (aromatic C-C str.), 1340 (aromatic C-N str.), 1020 (ether C-O str.).

HRMS (ESI): m/z = 621.2533 ($[M+H]^+$, requires 621.2542 $C_{44}H_{33}N_2O_2$).

Mp: 203 – 205 °C.

7.31 Synthesis of 4,4'-di(pyridin-4-yl)-[1,1'-binaphthalene]-2,2'-diol, 37

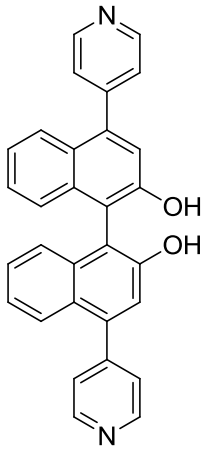

To solid 4,4'-(2,2'-bis(benzyloxy)-1,1'-binaphthalene-4,4'-diyl)dipyridine (50 mg, 0.009 mmol) was added an excess of 2 M aq. HCl (20 ml). The solution was stirred visously under rflux for 2h. The solution as colled in an ice bath, and 10 % aq. NaOH was added slowly until the solution was neutralised. The resulting white solid was filtered by vaccum filtration and dried in a desiccator. Yield 5%.

^{1}H NMR (+20°C, 400.13 MHz, $CDCl_3$): δ = 7.63 (m, 2H, ArH), 7.40 (m, 6H, ArH), 7.21 (s, 2H, ArH), 7.03 (m, 2H, ArH), 6.93 (m, 2H, ArH), 5.9 (br. s, 2H, OH) ppm.
^{13}C NMR (+20°C, 100.13 MHz, $CDCl_3$): δ = 154.20 , 151.05, 146.45, 139.54, 134.78, 131.22, 127.11, 126.34, 126.04, 125.75, 122.13, 115.02, 111.31 ppm.
IR (film): ν_{max}/cm^{-1} = 3050 (aromatic C-H str.), 1580 (aromatic C-C str.), 1360 (aromatic C-N str.), 1290 (ether C-O str.).
HRMS (ESI): m/z = 440.1517 ($[M+H]^+$, requires 440.1524 $C_{30}H_{20}N_2O_2$).
Mp: 203 – 205 °C.

7.32 Synthesis of (*R*)-2-Hydroxy-2'-pivaloyloxy-1,1'-binaphthyl, 43

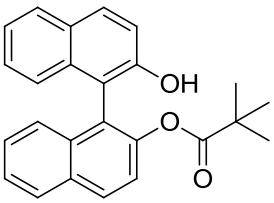

(*R*)-2-Hydroxy-2'-pivaloyloxy-1,1'-binaphthyl was synthesised according to literature procedures.[10] To a solution of (*R*)-2,2'-dihydroxy-1,1'-binaphthyl (3 g, 10.5 mmol) and NEt_3 (4.5 ml, 31.5 mmol) in MeCN (30 ml) was added pivaloyl chloride (1.01 eq., 1.32 mmol, 10.605 mmol) at 0 °C. The mixture was stirred for 1 hour at 0 °C, then for 4 hours

at room temperature. The solution was diluted with Et_2O (100 ml), washed with 1 M HCl (2 x 30 ml), saturated aq. $NaHCO_3$ (2 x 30 ml) and brine (2 x 30 ml). After drying over $MgSO_4$ the solvent was evaporated to give a crude residue. Purification by silica gel chromatography (hexane/EtOAc, 6:1 v/v) yielded a pure clear oil, which solidified on standing. Yield 3.5 g (90%). NMR values agree with those previously reported.[10]

^{1}H NMR (+20°C, 300.13 MHz, $CDCl_3$): δ = 8.08 (d, *J* = 9.1 Hz, 1H, ArH), 7.99 (d, *J* = 8.1 Hz, 1H, ArH), 7.89 (d, *J* = 9.1 Hz, 1H, ArH), 7.84 (d, *J* = 7.6 Hz, 1H, ArH), 7.52 (t, *J* = 6.44 Hz, 1H, ArH), 7.32 (m, 6H, ArH), 7.07 (d, *J* = 8.6 Hz, 1H, ArH), 5.16 (s, 1H, O*H*), 0.79 (s, 9H, OC(O)C(CH_3)$_3$) ppm.
Mp: 188 – 190 °C.

7.33 Synthesis of (*R*)-6-Bromo-2-hydroxy-2'-pivaloyloxy-1,1'-binaphthyl, 44

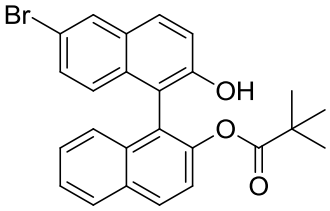

(*R*)-6-Bromo-2-hydroxy-2'-pivaloyloxy-1,1'-binaphthyl was synthesised according to literature procedures.[10] To a solution of (*R*)-2-hydroxy-2'-pivaloyloxy-1,1'-binaphthyl (1 g, 2.7 mmol) in MeCN (10 ml) at 0 °C was added Br_2 drop wise. The solution was then stirred at 0 °C for 2 hours before being quenched with aq. $Na_2S_2O_3$. The mixture was diluted with Et_2O (50 ml), washed with saturated aq. $NaHCO_3$, 1 M HCl and brine, and dried over $MgSO_4$. The solvent was removed to yield a pure clear viscous oil. Yield (1.2 g, 99%). NMR values agree with those previously reported.[10]

^{1}H NMR (+20°C, 300.13 MHz, $CDCl_3$): δ = 8.09 (d, *J* = 9.1 Hz, 1H, ArH), 7.99 (m, 2H, ArH), 7.8 (d, *J* = 9 Hz, 1H, ArH), 7.53 (t, *J* = 7.7 Hz, 1H, ArH), 7.34 (m, 5H, ArH), 6.94 (d, *J* = 9.0 Hz, 1H, ArH), 5.21 (s, 1H, O*H*), 0.82 (s, 9H, Ar-COC(O)C(CH_3)$_3$) ppm.
Mp: 142 – 143 °C.

7.34 Synthesis of (*R*)-6-Bromo-2-methoxy-2'-pivaloyloxy-1,1'-binaphthyl, 45

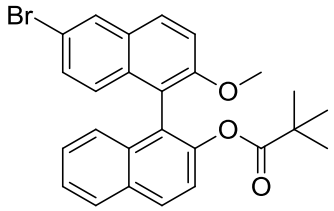

(*R*)-6-Bromo-2-methoxy-2'-pivaloyloxy-1,1'-binaphthyl was synthesised according to literature procedures.[10] To a mixture of (*R*)-6-bromo-2-hydroxy-2'-pivaloyloxy-1,1'-binaphthyl (900 mg, 2 mmol), methyl iodide (0.25 ml, 568 mg, 4 mmol) and K_2CO_3 (553 mg, 4 mmol) in acetone was refluxed overnight. The solvent was evaporated and the residue taken up into DCM/water. After DCM extraction (2 x 30 ml), the DCM layer was washed with water (20 ml) and dried over $MgSO_4$. The solvent was removed to yield a crude residue. Purification by silica gel chromatography (hexane/EtOAc, 2:1 v/v) yielded a pure white solid. Yield (834 mg, 90%). NMR values agree with those previously reported.[10]

^{1}H NMR (+20°C, 300.13 MHz, $CDCl_3$): δ = 7.99 (m, 2H, ArH), 7.95 (d, *J* = 8.3 Hz, 1H, ArH), 7.84 (d, *J* = 7.9 Hz, 1H, ArH), 7.43 (m, 1H, ArH), 7.4 (m, 1H, ArH), 7.31 (m, 3H, ArH), 7.23 (m, 1H, ArH), 7.14 (d, *J* = 8.7 Hz, 1H, ArH), 3.77 (s, 3H, OCH_3) 0.73 (s, 9H, COC(O)C(CH_3)$_3$) ppm.
Mp: 165 – 166 °C.

7.35 Synthesis of (*R*)-6'-cyano-2'-methoxy-1,1'-binaphthalen-2-yl pivalate, 46

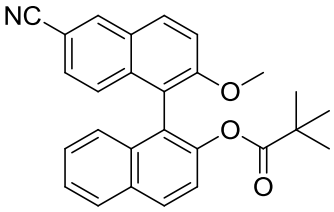

A solution of (*R*)-6'-bromo-2'-methoxy-1,1'-binaphthalen-2-yl pivalate (1 g, 2.16 mmol) in DMF (20 ml) was degassed with nitrogen for 30 minutes. Solid CuCN (5 eq., 967 mg, 10.8 mmol) was then added and mixture heated to reflux for 3 days. After cooling to room temperature, the solvent was removed *in vacuo* and the residue taken up into EtOAc (400 ml) and washed several times with water (10 x 100 ml) to remove excess DMF and CuCN. The organic layer was dried over $MgSO_4$ and the solvent removed to give a crude yellow

oil. Purification by silica gel chromatography (EtOAc/hexane, 1:4, v/v) gave a pure colourless oil. Yield 734 mg (83%).

^{1}H NMR (+20°C, 300.13 MHz, $CDCl_3$): δ = 8.24 (d, *J* = 1.5 Hz, 1H, ArH), 8.03 (m, 2H, ArH), 7.97 (d, *J* = 8.1 Hz, 1H, ArH), 7.53 (d, *J* = 9.1 Hz, 1H, ArH), 7.48 (m, 1H, ArH), 7.4 (d, *J* = 8.6 Hz, 1H, ArH), 7.33 (m, 2H, ArH), 7.2 (m, 2H, ArH), 3.82 (s, 3H, OC*H*$_3$), 0.75 (s, 9H, OC(O)C(C*H*$_3$)$_3$) ppm.

^{13}C NMR (+20°C, 100.61 MHz, $CDCl_3$): δ = 176.21 (Ar-CO*C*(O)C(CH$_3$)$_3$), 157.42 (Ar-*C*OCH$_3$), 147.03 (Ar-*C*OC(O)C(CH$_3$)$_3$), 135.34 (C), 134.07 (CH), 133.33 (C), 131.71 (C), 130.62 (CH), 129.53 (CH), 128.31 (CH), 127.48 (CH), 126.9 (CH), 126.69 (C), 126.65 (CH), 125.59 (CH), 125.47 (CH), 123.8 (C), 121.92 (CH), 119.51 (C), 118.32 (C), 114.75 (CH), 106.87 (C), 56.53 (Ar-CO*C*H$_3$), 38.58 (Ar-COC(O)*C*(CH$_3$)$_3$), 26.46 (Ar-COC(O)C(*C*H$_3$)$_3$) ppm.

IR (film): ν_{max}/cm^{-1} = 3070 (aromatic C-H str.), 2230 (nitrile C≡N str.), 1750 (ester C=O str.), 1590 (aromatic C-C str.), 1100 (ester/ether C-O str.).

HRMS (ESI): m/z = 432.1570 ($[M+Na]^+$, requires 432.1576 $C_{27}H_{23}NO_3Na$).

Mp: 178 – 180 °C.

7.36 Synthesis of (*R*)-2'-hydroxy-2-methoxy-1,1'-binaphthalene-6-carboxylic acid, 47

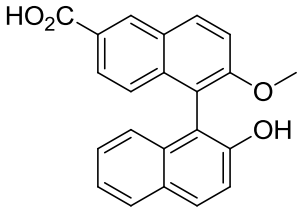

(*R*)-6'-cyano-2'-methoxy-1,1'-binaphthalen-2-yl pivalate (600 mg, 1.48 mmol) was dissolved in a mixture of aq. NaOH (6M, 50 ml) and EtOH (50 ml), then heated to 80 °C for 24 h. After cooling to room temperature, the mixture was poured into an ice/water/HCl solution and left to warm to room temperature. The organic product was extracted with EtOAc (3 x 150 ml). The organic layer was washed with water (2 x 50 ml) and dried over $MgSO_4$. Evaporation of the solvent yielded a pure white solid. Yield 410 mg (80%).

^{1}H NMR (+20°C, 400.13 MHz, $CDCl_3$): δ = 10.56 (br. s, 1H, CO_2H), 8.75 (s, 1H, O*H*), 8.21 (d, *J* = 9.1 Hz, 1H, ArH), 7.93 (d, *J* = 9.1 Hz, 1H, ArH), 7.88 (d, *J* = 8.6 Hz, 2H,

ArH), 7.57 (d, *J* = 9.1 Hz, 1H, ArH), 7.36 (d, *J* = 9.1 Hz, 1H, ArH), 7.32 (d, *J* = 7.1, 1H, ArH), 7.24 (m *obscured by $CDCl_3$*, 3H, ArH), 7.0 (d, *J* = 8.1 Hz, 1H, ArH), 3.86 (s, 3H, OCH_3) ppm.

^{13}C NMR (+20°C, 100.61 MHz, $CDCl_3$): δ = 162.13 (CO_2H), 158.13 (OCH_3), 153.08 (*C*OH), 151.9 (CH), 151.25 (C), 136.94 (C), 133.58 (C), 132.83 (CH), 132.46 (CH), 130.11 (CH), 129.72 (CH), 128.24 (CH), 126.81 (CH), 126.59 (C), 125.3 (C), 124.51 (CH), 123.38 (CH), 117.53 (C), 115.65 (C), 114.29 (CH), 56.9 (OCH_3) ppm.

IR (film): ν_{max}/cm^{-1} = 3070 (O-H str.), 2980 (aromatic C-H str.), 1750 (carboxylic acid C=O str.), 1590 (aromatic C-C str.), 1210 (ether C-O str.).

HRMS (ESI): m/z = 367.0941 ($[M+Na]^+$, requires 367.0946 $C_{22}H_{16}O_4Na$).

Mp: 210 – 212 °C.

7.37 Synthesis of (*R*)-2,2'-dihydroxy-1,1'-binaphthalene-6-carboxylic acid, 42

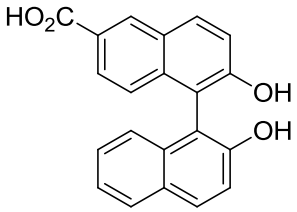

A solution of 2'-hydroxy-2-methoxy-1,1'-binaphthalene-6-carboxylic acid (100 mg, 0.29 ml) in DCM (10 ml) was degassed with nitrogen for 20 minutes and cooled to 0 °C. A solution of BBr_3 (1 M in hexanes, 2.25 ml, 2.25 mmol) was then added drop wise. The mixture was left to stir and warm to room temperature overnight. The solution was then poured into an ice/water mixture and extracted with DCM (3 x 40 ml) and dried over $MgSO_4$. Solvent removal gave a crude pale yellow solid. Purification by silica gel chromatography (EtOAc, 100% eluting up to EtOAc/MeOH 4:1, v/v) gave a pure off-white solid. Yield 61 mg (64 %).

^{1}H NMR (+20°C, 400.13 MHz, DMSO-d_6): δ = 12.53 (br. s, 1H, CO_2H), 9.61 (br. s, 1H, 6-O*H*), 9.26 (br. s, 1H, 6'-O*H*), 8.54 (s, 1H, ArH), 8.05 (d, *J* = 9.1 Hz, 1H, ArH), 7.86 (m, 2H, ArH), 7.67 (d, *J* = 8.6 Hz, 1H, ArH), 7.4 (d, *J* = 9.1 Hz, 1H, ArH), 7.32 (d, *J* = 8.6, 1H ArH), 7.21 (m, 2H, ArH), 7.0 (d, *J* = 9.1 Hz, 1H, ArH), 6.93 (d, *J* = 8.6 Hz, 1H, ArH) ppm.

^{13}C NMR (+20°C, 100.61 MHz, DMSO-d_6): δ = 167.63 (CO_2H), 155.27 (6-*C*OH), 153.01 (6'-*C*OH), 136.44 (C), 133.95 (C), 130.85 (CH), 130.37 (CH), 128.86 (CH), 128.1 (C),

127.9 (CH), 127.07 (C), 125.97 (CH), 125.25 (CH), 124.56(C), 124.45 (CH), 124.15 (CH), 122.31 (CH), 119.32 (CH), 118.53 (CH), 115.68(C), 114.81(C) ppm.

IR (film): ν_{max}/cm^{-1} = 3410 (alcohol O-H str.), 3070 (carboxylic acid O-H str.), 2980 (aromatic C-H str.), 1690 (carboxylic acid C=O str.), 1590 (aromatic C-C str.), 1210 (C-O str.).

HRMS (ESI): m/z = 353.0618 ($[M+Na]^+$, requires 353.0790 $C_{21}H_{14}O_4Na$).

Mp: 221 – 224 °C.

7.38 Synthesis of UMCM-1-NH_2 [$Zn_4O(BDC\text{-}NH_2)(BTB)_{4/3}$]

A mixture of $Zn(NO_3)_2.6H_2O$ (321.3 mg, 1.08 mmol), 2-aminoterethphalic acid (49 mg, 0.27 mmol) and 1,3,5-tris(4-carboxyphenyl)benzene (42.4 mg, 0.097 mmol) were dissolved in DMF (10 ml) and heated at 85 °C for 48 h as previously reported.[11] The MOF was then solvent-exchanged with chloroform over three days to yield approximately 50 mg of material.

7.39 Modulated benzoic acid synthesis of MOF-5

In a typical synthesis, $Zn(NO_3)_2.6H_2O$ (270 mg, 0.9 mmol), 1,2-benzenedicarboxylic acid (48 mg, 0.3 mmol) and benzoic acid (1 equivalent, 37 mg, 0.3 mmol) were dissolved in DMF (60 ml) by sonification for 20 minutes. The clear solution was then transferred equally to six 12 ml scintillation vials. The vials were sealed and heated to 100 °C for 48 h in an isothermal oven. After cooling to room temperature, the crystalline product was quickly filtered, washed with fresh DMF and transferred to a singled necked RBF. The flask was heated to 90 °C under vacuum for 2 hours. The sample was then ground for 2 minutes before a PXRD pattern was recorded.

7.40 Attempted modulated synthesis of MOF-5 using 1,2-benzenedicarboxylic acid [1,2-BDC])

In a 12 ml scintillation vial $Zn(NO_3)_2.6H_2O$ (45 mg, 0.15 mmol), 1,4-benzenedicarboxylic acid (8 mg, 0.05 mmol) and 1,2-benzenedicarboxylic acid (1 equiv., 8 mg, 0.05 mmol) were dissolved in DEF (10 ml) by sonification for 10 minutes. The vial was sealed and

heated to 100 °C for 48 h in an isothermal oven. After cooling to room temperature, crystals of the rod-shaped product were removed for X-ray crystallography.

7.41 Synthesis of $[Zn_4(O)(1,2\text{-}BDC)_3]$

In a 12 ml scintillation vial $Zn(NO_3)_2.6H_2O$ (45 mg, 0.15 mmol) and 1,2-benzenedicarboxylic acid (8 mg, 0.05 mmol) were dissolved in DMF (10 ml) by sonification for 20 minutes. The vial was then sealed and heated to 100 °C for 48 h in an isothermal oven. After cooling to room temperature, the crystalline product was quickly filtered and washed with fresh DMF. The solid was then stored in fresh DMF in a sealed vial until further use.

As-synthesised material:

After filtering and washing, the solid was placed in a vial and dried at 60 °C under high vacuum for 2 h.

Solvent exchanged material:

After filtering and washing, the solid was further washed with $CHCl_3$ and then placed in a sealed vial containing fresh $CHCl_3$. The solution was decanted once a day and refilled with fresh $CHCl_3$ for three days. The solution was then decanted for a final time and the solid was placed in a vial and dried at 60 °C under high vacuum for 2 h.

FTIR spectrum of evacuated sample of $[Zn_4O(1,2\text{-}BDC)_3]$.

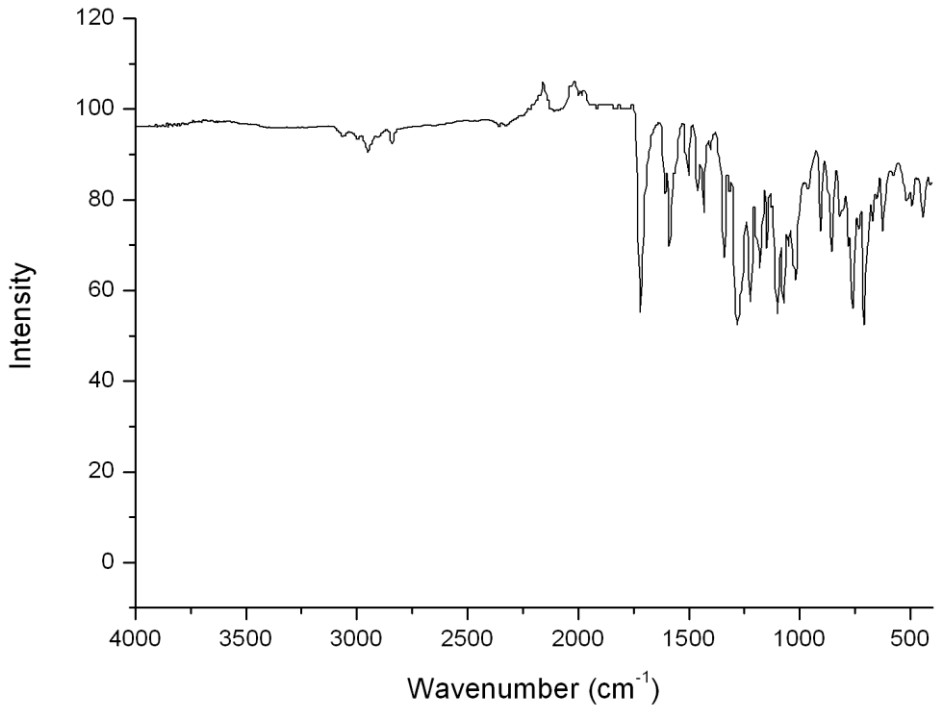

7.42 Synthesis of [Zn(Ligand H)(BDC)]

In a 12 ml scintillation vial $Zn(NO_3)_2.6H_2O$ (3 mg, 0.01 mmol), 1,2-benzenedicarboxylic acid (3.3 mg, 0.02 mmol) and 4,4'-(2,2'-bis(benzyloxy)-1,1'-binaphthalene-4,4'-diyl)dipyridine (**Ligand H**) (6.2 mg, 0.01 mmol) were dissolved in DMF (1 ml) by sonification for 20 minutes. The vial was then sealed and heated to 80 °C for 48 h in an isothermal oven. After cooling to room temperature, the crystalline product was rapidly removed from the mother lqiuor for single crystal x-ray analysis.

7.43 Synthesis of $[Cd(BDC)(H_2O)_3].2.25H_2O$

In a 12 ml scintillation vial $Cd(NO_3)_2.4H_2O$ (20 mg, 0.0625 mmol), Ligand A (47 mg, 0.0125 mmol) and 1,2-benzenedicarboxylic acid (21 mg, 0.125 mmol) were dissolved in MeOH/H2O (5 ml, 4:1 v/v) by sonification for 20 minutes. The vial was then sealed and heated to 80 °C for 10 h in an isothermal oven. A quantative amount of lath-shaped crystals formed in the vial.

7.44 References

1. A. Akwabi-Ameyaw, J. Y. Bass, R. D. Caldwell, J. A. Caravella, L. Chen, K. L. Creech, D. N. Deaton, S. A. Jones, I. Kaldor, Y. Liu, K. P. Madauss, H. B. Marr, R. B. McFadyen, A. B. Miller, F. N. Iii, D. J.Parks, P. K. Spearing, D. Todd, S. P. Williams and G. B. Wisely, *Bioorg. Med. Chem. Lett.*, 2008, **18**, 4339.
2. K. Tanaka, H. Takano and Z. Urbanczyk-Lipkowska, *J. Inclusion Phenom.Macrocyclic Chem.*, 2006, **56**, 281.
3. K. Tanaka, S. Oda and M. Shiro, *Chem. Commun.*, 2008, 820.
4. M. S. Newman, V. Sankaran and D. R. Olson, *J. Am. Chem. Soc.*, 1976, **98**, 3237.
5. H. F. Chow and M. K. Ng, *Tetrahedron-Asymmetr.*, 1996, **7**, 2251.
6. K. Tanaka, S. Oda, S. Nishihote, D. Hirayama and Z. Urbanczyk-Lipkowska, *Tetrahedron-Asymmetr.*, 2009, **20**, 2612.
7. C. Valente, E. Choi, M. E. Belowich, C. J. Doonan, Q. W. Li, T. B. Gasa, Y. Y. Botros, O. M. Yaghi and J. F. Stoddart, *Chem. Commun.*, 2010, **46**, 4911.
8. H. L. Ngo, A. G. Hu and W. B. Lin, *J. Mol. Catal. A-Chem.*, 2004, **215**, 177.
9. Q. S. Hu, D. Vitharana, X. F. Zheng, C. Wu, C. M. S. Kwan and L. Pu, *J. Org. Chem.*, 1996, **61**, 8370.
10. H. Hocke and Y. Uozumi, *Tetrahedron*, 2003, **59**, 619.
11. Z. Q. Wang, K. K. Tanabe and S. M. Cohen, *Inorg. Chem.*, 2009, **48**, 296.

A1 Attempted MOF synthesises from Chapter 4

The attempted and sucessful MOF or coordination polymer synthesises reported in ternary pase diagrams in **Chapter 4** are tabulated in full. The ternary phase diagram where the synthesis is reported in **Chapter 4** is listed next to the synthetic conditions. All reactant, solvent and additive amounts are listed in mmol.

A1.1 Chapter 3

Table A1.1 Attempted solvothermal MOF synthesis using Ligands A, B and D in either DMF or DEF and with DMF or DEF with additional solvents

Reported in Figure	Reactants														Reaction temperature	Reaction time
	Ligand	Metal salt	Solvent	Metal salt (mmol)	Ligand (mmol)	Solvent (mmol)	Solvent	Solvent 2 (mmol)	Solvent 3	Solvent 3 (mmol)	coligand	coligand (mmol)	Additive			
4.5	A	Zn(NO3)2	DEF	0.15	0.05	4.20									100	20
4.5	A	Zn(NO3)2	DEF	0.008	0.00267	35.90							PhNMe2, 2 drops		100	20
4.5	A	Zn(NO3)2	DMF	0.04	0.02	12.97							2M NaOH, 2 drops		85	72
4.5	A	Zn(NO3)2	DEF	0.03	0.01	4.49									80	48
4.5	A	Zn(NO3)2	DMF	0.2	0.01	38.91									90	24
4.5	A	Zn(NO3)2	DEF	0.06	0.02	4.49							H2O, 1 drop		100	72
4.5	A	Zn(NO3)2	DEF	0.024	0.008	1.70									100	48
4.5	B	Zn(NO3)2	DMF	0.03	0.01	6.49								60 for 24 h, 70 for 24 h, 80 for 24h	120	72
4.5	B	Zn(NO3)2	DMF	0.015	0.05	12.97									120	24
4.5	D	Zn(NO3)2	DEF	0.06	0.02	13.47									100	30
4.5	D	Zn(NO3)2	DMF	0.017	0.0057	19.50								65 for 24 h, 75 for 24 h, 85 for 24 h	80	72
4.5	D	Zn(NO3)2	DMF	0.033	0.01	32.40									80	48
4.5	D	Zn(NO3)2	DMF	0.05	0.017	13.47									80	48
4.5	D	Zn(NO3)2	DEF	0.03	0.01	8.98									100	48
4.6	A	Zn(NO3)2	EtOH	0.15	0.05	192.67	H2O	208.33			401.00		NaOH, 2eq., 0.1 mmol		180	48
4.6	A	Zn(NO3)2	DMF	0.06	0.02	25.94	H2O	55.56			81.50		2 drops of 2M NaOH		85	72
4.6	A	Zn(ClO4)2	DMF	0.01	0.01	6.49	MeOH	4.94			11.43		5 uL Me2NPh		80	48
4.6	B	Zn(ClO4)2	DMF	0.01	0.01	6.49	MeOH	4.94			11.43		5 uL Me2NPh		80	48
4.6	B	Zn(NO3)2	DMF	0.04	0.01	12.97					12.97		NEt3/DMF in outer vial		80	48
4.6	B	Zn(NO3)2	DMF	0.023	0.01	19.46	EtOH	17.13			36.59				80	72
4.6	D	Zn(ClO4)2	DMF	0.01	0.01	6.49	MeOH	4.9			11.39		1 drop Me2NPh		80	48
4.6	D	Zn(ClO4)2	DMF	0.01	0.01	6.49	MeOH	4.9			11.39		1 drop Me2NPh		80	48
4.6	D	ZnI2	DMF	0.01	0.005	6.49	EtOH	8.56			15.05		1 drop of 1 drop of conc. HCl in 1 ml H2O		80	72
4.6	D	ZnI2	DMF	0.01	0.005	3.89	EtOH	5.14			9.03		1 drop of 1 drop of conc. HCl in 1 ml H2O		100	48
4.6	D	ZnI2	DMF	0.01	0.01	6.49	EtOH	3.43	H2O	0.28	10.20		1 drop of MeNPh		50	48
4.6	D	Zn(ClO4)2	DMF	0.01	0.01	6.49	MeOH	4.94			11.43		1 drop of MeNPh		50	48

Table A1.2 Attempted solvothermal MOF synthesis using Ligands C, E and F with copper nitrate.

	Reactants														
Report in Figu	Ligand	Metal salt	Solvent	Metal salt (mm	Ligand (mmol	Solvent (mmo	Solvent 2	Solvent 2 (mm	Solvent 3	Solvent 3 (mm	coligand	coligand mmo	Additive	Reaction temp	Reaction time
4.14	C	Cu	DMF	0.022	0.01	12.97	DMSO	14.08	H2O	11.11	38.16			90	48
4.14	E	Cu	DEF	0.0036	0.00163	13.47	H2O	27.78			41.25		3 drops 3M HC	80	48
4.14	E	Cu	DMF	0.0039	0.00195	8.56	H2O	18.33			26.89		1 drop conc. H	80	40
4.14	E	Cu	DMF	0.02	0.005	12.97	H2O	27.78			40.75		1 drop of 1 dr	80	72
4.14	E	Cu	DMF	0.0065	0.0033	9.73	H2O	13.89			23.62		3 drops 3M HC	80	72
4.14	E	Cu	DMF	0.001	0.0026	6.49	H2O	13.89	dioxane	2.93	23.31		1 drop conc. H	80	72
4.14	E	Cu	DEF	0.009	0.004	71.81	H2O	111.11			182.92			60	48
4.14	E	Cu	DMF	0.02	0.005	5.19	DEF	1.8	H2O	11.11	18.1			80	48
4.14	E	Cu	DMF	0.02	0.005	5.19	DEF	1.8	H2O	11.11	18.1			60	168
4.14	E	Cu	DMF	0.02	0.005	2.59	H2O	5.56			8.15		1 uL trans(NH	60	48
4.14	E	Cu	DEF	0.0075	0.005	71.81	H2O	111.11			182.92			60	48
4.14	E	Cu	DEF	0.009	0.005	8.98	H2O	13.89			22.87			60	48
4.14	E	Cu	DMF	0.02	0.005	12.97	H2O	16.67			29.64		1 drop conc Hl	80	48
4.14	E	Cu	DMF	0.02	0.005	12.97	H2O	11.11			24.08		1 drop of trans	80	48
4.14	E	Cu	DEF	0.02	0.005	7.18	H2O	22.22			29.4			80	48
4.14	E	Cu	DMF	0.017	0.005	12.97	H2O	27.78	dioxane	5.86	46.61			85	24
4.14	E	Cu	DEF	0.01	0.005	4.49	MeOH	12.36			16.85		1 ml of MeNPH	65	24
4.14	E	Cu	DMF	0.04	0.02	12.97	H2O	27.78			40.75		1 drop of conc	80	48
4.14	E	Cu	DMSO	0.01	0.005	7.04	H2O	5.56			12.6		1 drop of pyrid	80	48
4.14	E	Cu	H2O	0.02	0.005	55.56					55.56		1 drop of 2,6-	100	48
4.14	E	Cu	MeOH	10	4.9	4.94	H2O	2.22			7.16		Me2NPH in ou	RT	164
4.14	E	Cu	DMF	0.045	0.01	12.97	DMSO	14.08	H2O	11.11	38.16			90	48
4.14	E	Cu	DMF	0.026	0.005	12.97	DMSO	14.08	H2O	11.11	38.16			50	48
4.15	F	Cu	DMF	0.02	0.005	12.97	H2O	27.78			40.75			80	48
4.15	F	Cu	DMF	0.02	0.005	5.19	DEF	1.8	H2O	11.11	18.1			80	48
4.15	F	Cu	DEF	0.02	0.005	7.18	H2O	22.22			29.4			80	48
4.15	F	Cu	DEF	0.02	0.005	8.98	H2O	55.56			64.54			80	48
4.15	F	Cu	DEF	0.02	0.005	80.79	H2O	166.67			247.46			80	48
4.15	F	Cu	DMF	0.017	0.005	12.97	H2O	27.78	dioxane	5.86	46.61			80	48
4.15	F	Cu	DMF	0.017	0.005	12.97	H2O	27.78			40.75		1 drop of 1 dr	60	48
4.15	F	Cu	MeOH	0.01	0.005	24.71	dioxane	11.73			36.44			80	24
4.15	F	Cu	H2O	0.01	0.005	55.56					55.56		1 drop of 2,6-	80	24
4.15	F	Cu	dioxane	0.01	0.005	5.86					5.86			80	48
4.15	F	Cu	DMF	0.02	0.005	3.89	H2O	5.56			9.45		1 drop of 3M H	80	48
4.15	F	Cu	DEF	0.02	0.005	3.59	H2O	5.56			9.15			80	48
4.15	F	Cu	DEF	0.01	0.005	13.47	H2O	27.78			41.25			80	96
4.15	F	Cu	DEF	0.0027	0.006	8.98	H2O	9.44			18.42			80	48
4.15	F	Cu	DMF	0.009	0.009	7.78	MeOH	4.94	Pyridine		12.72		0.035 ml pyrid	80	48
4.15	F	Cu	DMF	0.043	0.007	6.49	H2O	5.55			12.04		1 drop of 10%	80	48
4.15	F	Cu	DMSO	0.06	0.01	14.1	MeOH	12.36			26.46			80	48
4.15	F	Cu	dioxane	0.06	0.01	14.08	MeOH	12.36			26.44			80	48

Table A1.3 Attempted solvothermal MOF synthesis using Ligands A and B with zinc nitrate or copper nitrate to produce pillared MOFs

	Reactants																		
Reported in Figure	Ligand	Co-Ligand	Metal salt	Solvent	Metal salt (mmol)	Ligand (mmol)	Co-ligand (mmol)	Solvent (mmol)	Solvent 2	Solvent 2 (mmol)	Solvent 3	Solvent 3 (mmol)	Colligand	Colligand (mmol)	Additive	Reaction temperature	Reaction time
	4.17 A	DABCO	Zn	DMF	0.027	0.027	12.97031058	0.01								120	48
	4.17 A	BUC	Zn	DEF	0.225	0.05	0.025	4.20								100	20
	4.17 A	BPY	Zn	DMF	0.05	0.05	0.075	77.82	EtOH	8.57	H2O	27.78				60	48
	4.17 A	BPY	Zn	DEF	0.01	0.02	0.01	26.93	H2O	55.56					NaOH, 2eq., 0.1 mmol	90	72
	4.17 A	BPY	Zn	DMF	0.02	0.02	0.01	2.59	MeOH	4.94						120	48
	4.17 A	1,4-BPB	Zn	DMF	0.02	0.02	0.01	2.59	MeOH	4.94						120	48
	4.17 A	BPY	Zn	DMF	0.0125	0.01	0.00625	2.08								55	168
	4.17 A	1,4-BPB	Zn	DMF	0.0125	0.01	0.00625	2.08								55	168
	4.17 A	BPY	Zn	DMF	0.00267	0.00267	0.00134	19.46	EtOH	25.69						100	20
	4.17 A	BPY	Zn	DMF	0.00267	0.00267	0.00134	6.49	xylene	4.07						120	48
	4.17 A	BPY	Zn	DMF	0.0129	0.0129	0.00645	16.73								80	48
	4.17 A	BPY	Zn	DMF	0.00534	0.00534	0.00267	6.93								80	48
	4.17 A	1,4-BPB	Zn	DMF	0.00534	0.00534	0.00267	6.93								80	48
	4.17 A	BPY	Zn	DMF	0.04	0.03	0.05	12.97								85	72
	4.17 A	1,4-BPB	Zn	DMF	0.04	0.03	0.05	12.97								85	72
	4.17 A	BPY	Zn	DMF	0.01	0.01	0.005	6.49								80	48
	4.17 A	DPE	Zn	DMF	0.01	0.01	0.01	2.60								80	72
	4.17 B	BPY	Zn	DMF	0.01	0.01	0.005	12.97							1 drop conc. HCl	80	24
	4.17 B	BPY	Zn	DMF	0.01	0.01	0.005	12.97								80	24
	4.17 B	BPY	Zn	DMF	0.05	0.05	0.025	64.85	EtOH	8.56	H2O	27.78				60	24
	4.17 B	BPY	Zn	DMF	0.006	0.002	0.001	64.85	Dioxane	58.62						120	48
	4.17 B	BPY	Zn	DMF	0.006	0.002	0.001	64.85	Dioxane	58.62					1 drop of 1 drop of conc	120	72
	4.17 B	BPY	Zn	DMF	0.01	0.01	0.005	19.46								80	72
	4.18 A	BPY	Cu	DEF	0.113	0.05	0.025	4.2								100	20
	4.18 A	DABCO	Cu	DEF	0.113	0.05	0.025	4.2								100	20
	4.18 A	BPY	Cu	DEF	0.01	0.02	0.01	26.93	H2O	55.56					NaOH, 2eq., 0.1 mmol	90	72
	4.18 A	BPY	Cu	DEF	0.03	0.03	0.05	6.73	H2O	13.89					1 drop 3M aq. HCl	85	72
	4.18 A	BPY	Cu	DMSO	0.1	0.05	0.02	35.2								120	24
	4.18 B	BPY	Cu	DMSO	0.1	0.1	0.05	4.22								125	24
	4.18 B	BPY	Cu	H2O	0.02	0.03	0.01	55.56								80	72
	4.18 B	BPY	Cu	DMF	0.02	0.03	0.01	38.91	H2O	55.56						80	72

Table A1.4 Attempted solvothermal MOF synthesis using Ligand G with zinc nitrate and BDC to produce pillared MOFs

	Reactants													
Reported in Figure	Ligand	Metal salt	Solvent	Metal salt (mmol)	Ligand (mmol)	Solvent (mmol)	Solvent	Solvent 2 (mmol)	Solvent 3	Solvent 3 (mmol)	coligand	coligand (mmol)	Additive	Reaction temperature	Reaction time
	4.19 G	Zn(NO3)2	DMF	0.1	0.01	12.97	DMF				BDC	0.02		80	48
	4.19 G	Zn(NO3)2	DMF	0.1	0.01	25.94	DMF				BDC	0.02		80	48
	4.19 G	Zn(NO3)2	DMF	0.1	0.01	38.91	DMF				BDC	0.02		80	48
	4.19 G	Zn(NO3)2	DMF	1	0.01	12.97	DMF				BDC	0.02		80	48
	4.19 G	Zn(NO3)2	DMF	0.1	0.01	12.97	DMF				BDC	0.02		100	48
	4.19 G	Zn(NO3)2	DMF	0.1	0.01	12.97	DMF				BDC	0.02		60	48

Appendix 1 Attempted MOF synthesises from Chapter 4

A2 X-ray Crystal Structure Data

The EPSRC National Crystallography Service (Dr Mark E. Light) solved the crystal structures presented in **Chapter 3**. The refinement of the structures and the fractional coordinates are report for the sake of completeness and so that the structure may be regenerated from the text of this thesis if necessary.

A2.1 Chapter 3

A2.1.1 $[Zn_4(O)(1,2\text{-}BDC)_3]$

Table A2.1 Crystal data and structure refinement details.

Identification code	**2010SMK0012**
Empirical formula	$C_{39}H_{45}N_3O_{16}Zn_4$
Formula weight	1073.26
Temperature	120(2) K
Wavelength	0.71073 Å
Crystal system	Monoclinic
Space group	$P2_1/c$
Unit cell dimensions	a = 18.3857(9) Å
	b = 16.2180(6) Å β = 90.011(3)°
	c = 14.4062(7) Å
Volume	4295.6(3) Å^3
Z	4
Density (calculated)	1.660 Mg / m^3
Absorption coefficient	2.281 mm^{-1}
F(000)	2192
Crystal	Block; Colourless
Crystal size	0.20 × 0.10 × 0.10 mm^3
θ range for data collection	3.09 – 25.03°
Index ranges	$-21 \le h \le 21$, $-19 \le k \le 18$, $-17 \le l \le 15$
Reflections collected	32050
Independent reflections	7462 [R_{int} = 0.1104]
Completeness to θ = 25.03°	98.4 %
Absorption correction	Semi–empirical from equivalents
Max. and min. transmission	0.8040 and 0.6583
Refinement method	Full-matrix least-squares on F^2
Data / restraints / parameters	7462 / 344 / 560
Goodness-of-fit on F^2	1.074
Final R indices [$F^2 > 2\sigma(F^2)$]	$R1$ = 0.0713, $wR2$ = 0.1260
R indices (all data)	$R1$ = 0.1298, $wR2$ = 0.1515
Largest diff. peak and hole	0.986 and –0.726 e Å^{-3}

Diffractometer: *Nonius KappaCCD* area detector (ϕ scans and ω scans to fill *asymmetric unit*). **Cell determination:** DirAx (Duisenberg, A.J.M.(1992). J. Appl. Cryst. 25, 92-96.) **Data collection:** Collect (Collect: Data collection software, R. Hooft, Nonius B.V., 1998). **Data reduction and cell refinement**: *Denzo* (Z. Otwinowski & W. Minor, *Methods in Enzymology* (1997) Vol. **276**: *Macromolecular Crystallography*, part A, pp. 307–326; C. W. Carter, Jr. & R. M. Sweet, Eds., Academic Press). **Absorption correction**: Sheldrick, G. M. SADABS - Bruker Nonius area detector scaling and absorption correction - V2.10 S**tructure solution**: *SHELXS97* (G. M. Sheldrick, Acta Cryst. (1990) A**46** 467–473). S**tructure refinement**: *SHELXL97* (G. M. Sheldrick (1997), University of Göttingen, Germany). **Graphics:** Cameron - A Molecular Graphics Package. (D. M. Watkin, L. Pearce and C. K. Prout, Chemical Crystallography Laboratory, University of Oxford, 1993).

Special details: The structure was refined as a pseudo merohedral twin – monoclinic with beta 90.011 emulating orthorhombic. The twin law -1 0 0 0 -1 0 0 0 1 was applied with the twin fraction refining to ca. 47%
Various thermal parameter restraints were applied to chemically similar groups within the structure. The 3 diethylformamide molecules were restrained to have similar geometries.

Table A2.2. Atomic coordinates [× 10^4], equivalent isotropic displacement parameters [$Å^2$ × 10^3] and site occupancy factors. U_{eq} is defined as one third of the trace of the orthogonalized U^{ij} tensor.

Atom	*x*	*y*	*z*	U_{eq}	*S.o.f.*
Zn1	2560(1)	1277(1)	9099(1)	24(1)	1
Zn2	2521(1)	2451(1)	10818(1)	19(1)	1
Zn3	3399(1)	2948(1)	9014(2)	23(1)	1
Zn4	1649(1)	2907(1)	9030(2)	21(1)	1
O1	2545(6)	2419(3)	9475(4)	22(2)	1
O2	2559(7)	498(4)	10110(5)	30(2)	1
O3	2588(6)	1343(4)	11353(4)	24(2)	1
O4	3370(6)	1071(7)	8241(9)	27(3)	1
O5	3958(5)	2275(7)	8180(9)	26(3)	1
O6	1739(6)	1025(6)	8272(9)	23(3)	1
O7	1089(5)	2211(7)	8161(10)	23(3)	1
O8	3377(5)	3086(7)	11269(8)	24(3)	1
O9	3999(5)	3428(7)	10001(10)	30(3)	1
O10	3111(6)	3940(7)	8278(10)	27(3)	1
O11	1887(5)	3857(7)	8260(10)	21(3)	1
O12	1124(6)	3471(7)	9975(10)	37(3)	1
O13	1739(5)	3168(7)	11303(8)	25(3)	1
C1	2549(9)	636(5)	10968(7)	23(2)	1
C2	3836(9)	1515(12)	7953(14)	29(5)	1
C3	1199(8)	1497(11)	7998(13)	22(4)	1
C4	3906(7)	3404(9)	10848(16)	23(3)	1
C5	2494(9)	4189(5)	8057(6)	17(2)	1
C6	1227(8)	3485(8)	10860(16)	24(3)	1
C7	4481(7)	3824(10)	11398(12)	20(3)	1
C8	4433(8)	3891(11)	12378(14)	26(3)	1
C9	4984(9)	4317(12)	12863(14)	33(4)	1
C10	5549(9)	4681(11)	12433(14)	32(4)	1
C11	5581(9)	4630(12)	11478(14)	36(4)	1
C12	5049(8)	4229(9)	11002(16)	29(3)	1
C13	2489(11)	5006(5)	7546(6)	26(2)	1
C14	2416(8)	5693(6)	8121(7)	26(3)	1
C15	2416(9)	6487(6)	7723(8)	31(3)	1
C16	2491(11)	6569(6)	6772(7)	34(2)	1
C17	2510(11)	5879(5)	6217(6)	29(2)	1
C18	2520(9)	5103(5)	6601(6)	19(2)	1
C19	634(7)	3925(10)	11431(12)	20(3)	1
C20	45(8)	4290(9)	10914(16)	29(3)	1
C21	–495(9)	4709(10)	11411(14)	29(3)	1
C22	–473(9)	4720(11)	12370(16)	33(4)	1
C23	109(8)	4339(10)	12854(15)	29(4)	1
C24	638(9)	3934(11)	12407(14)	28(3)	1
O14	1226(6)	1655(7)	10260(9)	47(3)	1
N1	125(5)	1714(8)	11017(9)	44(3)	1
C25	841(7)	1623(10)	10985(13)	49(5)	1
C26	–249(8)	1645(10)	11892(12)	52(6)	1
C27	–744(9)	2366(11)	12107(13)	44(4)	1

C28	−301(8)	1831(10)	10166(10)	62(4)	1
C29	−829(10)	1116(12)	9992(16)	91(6)	1
O15	4068(7)	1404(8)	10193(10)	67(4)	1
N2	5060(7)	1437(9)	11147(10)	63(4)	1
C30	4354(7)	1489(11)	10981(11)	47(4)	1
C31	5339(8)	1544(10)	12071(11)	45(4)	1
C32	5856(10)	2271(11)	12181(19)	71(8)	1
C33	5606(9)	1178(12)	10454(12)	84(5)	1
C34	5793(11)	1886(13)	9811(15)	98(6)	1
O16	1782(9)	8138(10)	4906(9)	127(6)	1
N3	2146(7)	8970(11)	6100(11)	71(4)	1
C35	1635(9)	8582(12)	5606(13)	91(6)	1
C36	2904(7)	8867(9)	5857(16)	60(5)	1
C37	3259(12)	9706(11)	5733(14)	106(8)	1
C38	1994(9)	9454(11)	6926(11)	79(5)	1
C39	2315(8)	9126(8)	7830(9)	55(4)	1

Table A2.3. Bond lengths [Å] and angles [°].

Zn1–O2	1.927(7)	C7–C8	1.42(2)
Zn1–O1	1.930(6)	C8–C9	1.41(2)
Zn1–O4	1.965(11)	C8–C2^{i}	1.53(2)
Zn1–O6	1.966(12)	C9–C10	1.34(2)
Zn1–Zn3	3.122(2)	C10–C11	1.38(3)
Zn1–Zn2	3.1251(14)	C11–C12	1.36(2)
Zn1–Zn4	3.132(2)	C13–C18	1.371(12)
Zn2–O1	1.937(6)	C13–C14	1.396(13)
Zn2–O3	1.959(6)	C14–C15	1.409(14)
Zn2–O13	1.976(10)	C15–C16	1.383(14)
Zn2–O8	1.989(10)	C16–C17	1.377(13)
Zn2–Zn4	3.124(3)	C17–C18	1.375(12)
Zn3–O1	1.909(10)	C18–C1^{ii}	1.507(12)
Zn3–O5	1.920(11)	C19–C24	1.41(2)
Zn3–O9	1.962(13)	C19–C20	1.44(2)
Zn3–O10	1.997(12)	C20–C21	1.40(2)
Zn4–O12	1.903(12)	C21–C22	1.38(3)
Zn4–O1	1.938(10)	C22–C23	1.42(2)
Zn4–O11	1.948(12)	C23–C24	1.34(2)
Zn4–O7	1.974(12)	C24–C3^{i}	1.51(2)
O2–C1	1.256(11)	O14–C25	1.262(14)
O3–C1	1.276(11)	N1–C25	1.326(13)
O4–C2	1.19(2)	N1–C26	1.440(14)
O5–C2	1.29(2)	N1–C28	1.467(14)
O6–C3	1.31(2)	C26–C27	1.513(14)
O7–C3	1.20(2)	C28–C29	1.534(16)
O8–C4	1.26(2)	O15–C30	1.259(14)
O9–C4	1.23(3)	N2–C30	1.322(14)
O10–C5	1.247(19)	N2–C31	1.438(14)
O11–C5	1.273(19)	N2–C33	1.477(15)
O12–C6	1.29(3)	C31–C32	1.524(14)
O13–C6	1.25(2)	C33–C34	1.514(17)
C1–C18^{i}	1.507(12)	O16–C35	1.268(16)
C2–C8^{ii}	1.53(2)	N3–C35	1.336(15)
C3–C24^{ii}	1.51(2)	N3–C36	1.446(13)
C4–C7	1.49(2)	N3–C38	1.454(16)
C5–C13	1.515(11)	C36–C37	1.520(16)
C6–C19	1.54(2)	C38–C39	1.525(16)
C7–C12	1.36(2)		

O2–Zn1–O1	114.6(3)	O1–Zn1–Zn3	35.4(3)
O2–Zn1–O4	111.4(5)	O4–Zn1–Zn3	75.4(4)
O1–Zn1–O4	110.5(5)	O6–Zn1–Zn3	122.4(3)
O2–Zn1–O6	108.8(5)	O2–Zn1–Zn2	78.50(19)
O1–Zn1–O6	111.0(4)	O1–Zn1–Zn2	36.15(17)
O4–Zn1–O6	99.5(3)	O4–Zn1–Zn2	128.3(4)
O2–Zn1–Zn3	126.8(3)	O6–Zn1–Zn2	126.1(3)

Zn3–Zn1–Zn2	60.87(6)	Zn1–O1–Zn2	107.8(3)
O2–Zn1–Zn4	125.3(3)	Zn3–O1–Zn4	113.6(3)
O1–Zn1–Zn4	36.0(3)	Zn1–O1–Zn4	108.2(5)
O4–Zn1–Zn4	121.9(4)	Zn2–O1–Zn4	107.5(4)
O6–Zn1–Zn4	75.2(3)	C1–O2–Zn1	128.8(6)
Zn3–Zn1–Zn4	61.96(3)	C1–O3–Zn2	130.6(6)
Zn2–Zn1–Zn4	59.90(6)	C2–O4–Zn1	131.3(12)
O1–Zn2–O3	111.5(3)	C2–O5–Zn3	127.3(11)
O1–Zn2–O13	112.7(5)	C3–O6–Zn1	129.9(11)
O3–Zn2–O13	116.5(5)	C3–O7–Zn4	126.1(11)
O1–Zn2–O8	108.8(5)	C4–O8–Zn2	131.8(13)
O3–Zn2–O8	107.3(5)	C4–O9–Zn3	128.8(10)
O13–Zn2–O8	99.0(3)	C5–O10–Zn3	129.6(9)
O1–Zn2–Zn4	36.3(3)	C5–O11–Zn4	131.5(9)
O3–Zn2–Zn4	125.0(2)	C6–O12–Zn4	129.9(10)
O13–Zn2–Zn4	77.2(3)	C6–O13–Zn2	127.6(12)
O8–Zn2–Zn4	123.6(3)	O2–C1–O3	125.9(8)
O1–Zn2–Zn1	36.01(17)	O2–C1–C18^{i}	117.0(8)
O3–Zn2–Zn1	75.6(2)	O3–C1–C18^{i}	117.0(8)
O13–Zn2–Zn1	130.9(3)	O4–C2–O5	127.7(17)
O8–Zn2–Zn1	123.8(3)	O4–C2–C8^{ii}	116.4(16)
Zn4–Zn2–Zn1	60.16(5)	O5–C2–C8^{ii}	115.0(16)
O1–Zn3–O5	113.7(4)	O7–C3–O6	129.1(16)
O1–Zn3–O9	112.9(4)	O7–C3–C24^{ii}	116.3(15)
O5–Zn3–O9	112.2(5)	O6–C3–C24^{ii}	114.6(15)
O1–Zn3–O10	109.2(4)	O9–C4–O8	126.7(16)
O5–Zn3–O10	105.5(6)	O9–C4–C7	114.4(14)
O9–Zn3–O10	102.4(5)	O8–C4–C7	118.8(19)
O1–Zn3–Zn1	35.81(18)	O10–C5–O11	127.0(8)
O5–Zn3–Zn1	78.2(3)	O10–C5–C13	114.4(14)
O9–Zn3–Zn1	126.4(4)	O11–C5–C13	118.5(14)
O10–Zn3–Zn1	126.1(3)	O13–C6–O12	127.5(16)
O12–Zn4–O1	113.0(4)	O13–C6–C19	116.8(18)
O12–Zn4–O11	98.1(5)	O12–C6–C19	115.6(14)
O1–Zn4–O11	108.7(4)	C12–C7–C8	115.3(16)
O12–Zn4–O7	117.6(5)	C12–C7–C4	123.0(18)
O1–Zn4–O7	114.8(4)	C8–C7–C4	121.5(15)
O11–Zn4–O7	102.1(5)	C9–C8–C7	119.1(15)
O12–Zn4–Zn2	77.5(4)	C9–C8–C2^{i}	117.3(17)
O1–Zn4–Zn2	36.25(19)	C7–C8–C2^{i}	123.5(15)
O11–Zn4–Zn2	122.7(4)	C10–C9–C8	122.7(18)
O7–Zn4–Zn2	130.9(3)	C9–C10–C11	117.9(17)
O12–Zn4–Zn1	130.8(4)	C12–C11–C10	120.0(18)
O1–Zn4–Zn1	35.84(19)	C7–C12–C11	125(2)
O11–Zn4–Zn1	124.5(3)	C18–C13–C14	120.1(8)
O7–Zn4–Zn1	79.4(3)	C18–C13–C5	125.7(8)
Zn2–Zn4–Zn1	59.94(5)	C14–C13–C5	114.1(8)
Zn3–O1–Zn1	108.8(4)	C13–C14–C15	119.2(10)
Zn3–O1–Zn2	110.7(5)	C16–C15–C14	119.5(9)

C17–C16–C15	120.0(9)
C16–C17–C18	120.7(9)
C13–C18–C17	120.3(8)
C13–C18–C1^{ii}	120.7(8)
C17–C18–C1^{ii}	119.0(8)
C24–C19–C20	121.0(16)
C24–C19–C6	122.4(15)
C20–C19–C6	116.5(16)
C21–C20–C19	117.9(19)
C22–C21–C20	119.8(17)
C21–C22–C23	120.5(18)
C24–C23–C22	122(2)
C23–C24–C19	118.9(16)
C23–C24–C3^{i}	116.9(18)
C19–C24–C3^{i}	124.2(15)
C25–N1–C26	119.8(12)
C25–N1–C28	120.9(12)
C26–N1–C28	119.2(11)
O14–C25–N1	125.6(15)
N1–C26–C27	114.0(13)
N1–C28–C29	112.1(13)
C30–N2–C31	120.6(12)
C30–N2–C33	124.3(13)
C31–N2–C33	114.7(12)
O15–C30–N2	124.4(14)
N2–C31–C32	114.4(14)
N2–C33–C34	110.7(15)
C35–N3–C36	119.7(15)
C35–N3–C38	123.7(14)
C36–N3–C38	116.5(13)
O16–C35–N3	122.7(16)
N3–C36–C37	109.8(15)
N3–C38–C39	115.9(14)

Symmetry transformations used to generate equivalent atoms:
(i) x,−y+1/2,z+1/2 (ii) x,−y+1/2,z−1/2

Table A2.4. Anisotropic displacement parameters [$Å^2 \times 10^3$]. The anisotropic displacement factor exponent takes the form: $-2\pi^2[h^2a^{*2}U^{11} + \cdots + 2\ h\ k\ a^*\ b^*\ U^{12}]$.

Atom	U^{11}	U^{22}	U^{33}	U^{23}	U^{13}	U^{12}
Zn1	28(1)	23(1)	20(1)	−1(1)	1(1)	−1(1)
Zn2	19(1)	19(1)	18(1)	0(1)	0(1)	−2(1)
Zn3	22(1)	24(1)	22(1)	−1(1)	3(1)	1(1)
Zn4	23(1)	23(1)	18(1)	−1(1)	1(1)	1(1)
O1	30(4)	15(3)	21(3)	−3(2)	10(6)	5(5)
O2	37(5)	27(3)	25(4)	−4(3)	0(6)	12(5)
O3	26(5)	21(3)	25(3)	6(3)	−12(5)	3(5)
O4	27(6)	38(7)	17(7)	−2(6)	6(5)	3(5)
O5	33(5)	25(6)	18(7)	−12(6)	6(5)	0(4)
O6	24(6)	19(6)	27(8)	−4(5)	5(5)	2(4)
O7	13(5)	25(7)	31(8)	9(6)	5(5)	−4(4)
O8	23(4)	31(4)	18(5)	−1(3)	−6(3)	−3(3)
O9	21(5)	40(7)	29(8)	0(6)	−3(5)	−7(4)
O10	36(6)	25(6)	21(6)	9(5)	−1(5)	4(4)
O11	10(4)	24(4)	28(5)	3(4)	1(3)	−2(3)
O12	42(6)	48(8)	21(8)	7(6)	7(5)	24(5)
O13	18(5)	32(5)	25(6)	−8(4)	−2(4)	13(4)
C1	23(6)	25(5)	22(5)	−2(4)	8(10)	−10(7)
C2	28(8)	33(9)	25(9)	−2(7)	−7(7)	24(7)
C3	19(5)	25(6)	22(6)	7(4)	5(4)	−4(4)
C4	25(5)	24(5)	21(5)	0(4)	−5(4)	−3(4)
C5	15(4)	17(3)	19(3)	−5(3)	−5(4)	2(4)
C6	32(7)	11(6)	29(8)	−2(6)	3(8)	−8(5)
C7	14(6)	26(8)	20(6)	−10(6)	−5(5)	−4(5)
C8	27(7)	27(7)	23(6)	−2(6)	3(6)	−10(5)
C9	30(7)	50(10)	18(7)	−10(8)	−2(6)	−14(7)
C10	30(8)	37(10)	29(8)	−2(8)	−3(7)	−10(6)
C11	24(8)	46(10)	37(8)	6(8)	6(6)	−13(6)
C12	31(7)	24(7)	32(8)	11(7)	−4(6)	−4(5)
C13	29(5)	18(4)	32(5)	0(3)	−9(10)	−8(8)
C14	24(7)	24(4)	31(5)	−9(3)	6(7)	−11(6)
C15	28(7)	21(4)	45(5)	−4(4)	−3(8)	−14(7)
C16	38(6)	24(4)	40(5)	6(4)	−5(11)	−15(9)
C17	31(5)	28(4)	28(5)	0(3)	−4(10)	−10(8)
C18	12(3)	19(3)	25(3)	−2(3)	−1(4)	−2(4)
C19	9(6)	22(7)	28(7)	14(6)	−3(5)	1(5)
C20	36(7)	30(8)	19(7)	10(7)	0(6)	11(6)
C21	31(7)	10(7)	47(8)	3(7)	−8(6)	7(5)
C22	33(7)	22(8)	43(8)	2(8)	8(7)	13(6)
C23	33(8)	17(8)	39(9)	5(7)	0(6)	10(6)
C24	31(5)	27(5)	24(5)	6(4)	1(4)	10(4)
O14	45(7)	52(7)	46(7)	3(6)	−3(6)	15(5)
N1	29(7)	56(8)	48(9)	−13(7)	−2(7)	4(6)
C25	36(8)	34(9)	77(15)	−4(10)	15(10)	8(7)

C26	24(8)	44(10)	89(16)	−5(10)	−9(9)	−6(6)
C27	47(9)	46(10)	39(10)	−4(8)	4(8)	5(7)
C28	44(9)	95(12)	47(10)	−13(9)	−8(8)	17(8)
C29	85(7)	101(7)	86(8)	0(5)	−1(5)	−5(5)
O15	69(9)	78(9)	54(8)	−8(7)	−15(7)	−30(7)
N2	52(7)	74(10)	63(8)	−28(7)	−4(5)	−19(7)
C30	57(7)	52(10)	33(8)	−5(9)	9(7)	−21(8)
C31	32(8)	50(10)	54(8)	−10(8)	8(7)	0(7)
C32	48(10)	40(11)	120(20)	−15(11)	−42(12)	−3(8)
C33	68(10)	124(15)	61(10)	−10(9)	17(9)	−34(11)
C34	97(7)	101(7)	95(7)	4(5)	3(5)	−7(5)
O16	163(15)	168(15)	50(8)	16(8)	−13(9)	−95(12)
N3	43(6)	102(11)	67(9)	−1(7)	3(7)	−1(7)
C35	59(10)	135(17)	80(12)	18(9)	−16(10)	−42(11)
C36	39(6)	47(9)	93(14)	3(10)	10(9)	−2(7)
C37	162(18)	90(13)	67(13)	−32(11)	35(14)	−83(14)
C38	72(12)	93(14)	72(10)	4(8)	17(8)	6(9)
C39	52(13)	39(7)	74(8)	−8(7)	5(8)	1(7)

Table A2.5. Hydrogen coordinates [× 10^4] and isotropic displacement parameters [$Å^2$ × 10^3].

Atom	*x*	*y*	*z*	U_{eq}	*S.o.f.*
H9	4955	4349	13521	39	1
H10	5913	4963	12775	38	1
H11	5975	4875	11153	43	1
H12	5076	4232	10344	34	1
H14	2367	5626	8774	32	1
H15	2364	6961	8104	37	1
H16	2530	7102	6503	41	1
H17	2517	5940	5561	35	1
H20	25	4248	10257	34	1
H21	−876	4984	11090	35	1
H22	−850	4986	12708	39	1
H23	123	4372	13513	35	1
H25	1085	1524	11555	58	1
H26A	116	1596	12394	63	1
H26B	−542	1133	11889	63	1
H27A	−976	2279	12712	66	1
H27B	−1119	2409	11626	66	1
H27C	−458	2876	12123	66	1
H28A	35	1880	9631	74	1
H28B	−579	2351	10213	74	1
H29A	−1108	1223	9424	136	1
H29B	−1163	1065	10519	136	1
H29C	−554	602	9920	136	1
H30	4042	1597	11492	57	1
H31A	5596	1034	12257	55	1
H31B	4924	1620	12501	55	1
H32A	6025	2301	12826	106	1
H32B	5603	2783	12020	106	1
H32C	6275	2198	11768	106	1
H33A	5413	711	10086	101	1
H33B	6052	989	10776	101	1
H34A	6159	1704	9360	147	1
H34B	5987	2347	10174	147	1
H34C	5354	2064	9481	147	1
H35	1141	8642	5787	109	1
H36A	2944	8547	5274	72	1
H36B	3157	8557	6353	72	1
H37A	3774	9633	5577	159	1
H37B	3217	10021	6311	159	1
H37C	3014	10005	5230	159	1
H38A	1460	9494	7000	95	1
H38B	2181	10020	6826	95	1
H39A	2183	9495	8341	82	1
H39B	2845	9098	7776	82	1
H39C	2121	8574	7953	82	1

A2.1.2[Zn(XXX)(BDC)]

Table A2.6. Crystal data and structure refinement details.

Identification code	**2011sot0540** (SK570)
Empirical formula	$C_{52}H_{36}N_2O_6Zn$
Formula weight	850.20
Temperature	100 K
Wavelength	**0.68890 Å**
Crystal system	Monoclinic
Space group	*C*2/*c*
Unit cell dimensions	a = 20.06(3) Å
	b = 29.81(4) Å β = 107.410(11)°
	c = 13.610(18) Å
Volume	7766(19) Å^3
Z	8
Density (calculated)	1.454 Mg / m^3
Absorption coefficient	0.692 mm^{-1}
F(000)	3520
Crystal	Block; Colourless
Crystal size	0.05 × 0.02 × 0.01 mm^3
θ range for data collection	2.97 – 25.03°
Index ranges	$-19 \le h \le 23$, $-33 \le k \le 35$, $-16 \le l \le 15$
Reflections collected	27129
Independent reflections	6825 [R_{int} = 0.1141]
Completeness to θ = 25.03°	99.4 %
Absorption correction	Semi–empirical from equivalents
Max. and min. transmission	0.9931 and 0.9662
Refinement method	Full-matrix least-squares on F^2
Data / restraints / parameters	6825 / 1103 / 618
Goodness-of-fit on F^2	1.315
Final R indices [$F^2 > 2\sigma(F^2)$]	*R1* = 0.1351, *wR2* = 0.3646
R indices (all data)	*R1* = 0.1715, *wR2* = 0.3933
Largest diff. peak and hole	1.883 and –0.739 e Å^{-3}

Diffractometer: *Nonius KappaCCD* area detector (ϕ scans and ω scans to fill *asymmetric unit*). **Cell determination:** DirAx (Duisenberg, A.J.M.(1992). J. Appl. Cryst. 25, 92-96.) **Data collection:** Collect (Collect: Data collection software, R. Hooft, Nonius B.V., 1998). **Data reduction and cell refinement**: *Denzo* (Z. Otwinowski & W. Minor, *Methods in Enzymology* (1997) Vol. **276**: *Macromolecular Crystallography*, part A, pp. 307–326; C. W. Carter, Jr. & R. M. Sweet, Eds., Academic Press). **Absorption correction**: Sheldrick, G. M. SADABS - Bruker Nonius area detector scaling and absorption correction - V2.10 S**tructure solution**: *SHELXS97* (G. M. Sheldrick, Acta Cryst. (1990) A**46** 467–473). S**tructure refinement**: *SHELXL97* (G. M. Sheldrick (1997), University of Göttingen, Germany). **Graphics:** Cameron - A Molecular Graphics Package. (D. M. Watkin, L. Pearce and C. K. Prout, Chemical Crystallography Laboratory, University of Oxford, 1993).

Table A2.7. Atomic coordinates [× 10^4], equivalent isotropic displacement parameters [$Å^2$ × 10^3] and site occupancy factors. U_{eq} is defined as one third of the trace of the orthogonalized U^{ij} tensor.

Atom	*x*	*y*	*z*	U_{eq}	*S.o.f.*
Zn1	2555(1)	54(1)	2011(1)	68(1)	1
N1	2478(2)	−4440(1)	−6062(2)	68(1)	1
C1	1961(2)	−4114(1)	−6329(3)	108(3)	1
C2	1956(3)	−3767(1)	−5648(3)	121(3)	1
C3	2468(3)	−3747(1)	−4700(3)	78(2)	1
C4	2986(2)	−4074(1)	−4432(2)	109(2)	1
C5	2991(2)	−4420(1)	−5113(3)	102(2)	1
C13A	2456(3)	−2678(3)	−2801(7)	95(3)	0.582(5)
C12A	1976(3)	−3012(2)	−2860(6)	101(3)	0.582(5)
C11A	1488(4)	−2979(3)	−2322(7)	124(3)	0.582(5)
C10A	964(5)	−3300(4)	−2466(9)	143(4)	0.582(5)
C9A	927(5)	−3652(4)	−3148(10)	174(4)	0.582(5)
C8A	1415(5)	−3685(3)	−3686(9)	142(4)	0.582(5)
C7A	1940(4)	−3365(3)	−3542(7)	99(3)	0.582(5)
C6A	2457(4)	−3413(3)	−3993(7)	86(2)	0.582(5)
C15A	2929(5)	−3076(2)	−3912(8)	96(3)	0.582(5)
C14A	2939(4)	−2717(2)	−3267(8)	98(3)	0.582(5)
O1A	3409(3)	−2391(3)	−3137(7)	118(3)	0.582(5)
C16A	3889(4)	−2384(3)	−3651(8)	109(3)	0.582(5)
C17A	4298(4)	−2002(3)	−3333(8)	126(3)	0.582(5)
C22A	4730(6)	−1860(4)	−3901(9)	158(4)	0.582(5)
C21A	5142(6)	−1480(4)	−3600(13)	183(5)	0.582(5)
C20A	5122(7)	−1242(3)	−2730(13)	186(6)	0.582(5)
C19A	4689(8)	−1385(3)	−2162(10)	166(5)	0.582(5)
C18A	4277(6)	−1765(3)	−2464(8)	140(4)	0.582(5)
C13B	2435(2)	−2670(1)	−2717(3)	90(3)	0.418(5)
C14B	2992(3)	−2692(2)	−3099(4)	88(3)	0.418(5)
C11B	3515(3)	−2369(2)	−2852(5)	103(4)	0.418(5)
C16B	4074(3)	−2399(2)	−3253(6)	97(4)	0.418(5)
C9B	4111(3)	−2753(3)	−3901(6)	100(4)	0.418(5)
C8B	3587(3)	−3076(2)	−4148(5)	80(3)	0.418(5)
C15B	3028(3)	−3046(2)	−3747(4)	82(3)	0.418(5)
C6B	2509(3)	−3359(2)	−3997(3)	82(3)	0.418(5)
C7B	1966(4)	−3330(2)	−3593(5)	95(3)	0.418(5)
C12B	1939(2)	−2975(1)	−2950(3)	97(3)	0.418(5)
O1B	1406(3)	−2939(2)	−2557(4)	129(4)	0.418(5)
C10B	747(3)	−2988(3)	−3200(8)	166(5)	0.418(5)
C17B	518(4)	−3425(3)	−3152(10)	165(5)	0.418(5)
C18B	−3(8)	−3596(5)	−3987(13)	223(8)	0.418(5)
C19B	−243(10)	−4032(6)	−3960(20)	251(9)	0.418(5)
C20B	39(11)	−4297(4)	−3090(20)	273(10)	0.418(5)
C21B	560(12)	−4126(5)	−2257(18)	227(9)	0.418(5)
C22B	800(9)	−3690(5)	−2287(12)	195(7)	0.418(5)

C23	2463(3)	−2283(2)	−2049(4)	95(2)	1
C24	2071(2)	−1909(1)	−2426(3)	95(2)	1
C25	1621(3)	−1900(1)	−3426(3)	108(2)	1
C26	1218(3)	−1521(2)	−3786(3)	127(3)	1
C27	1265(3)	−1151(2)	−3146(4)	124(3)	1
C28	1716(3)	−1160(1)	−2147(4)	107(2)	1
C29	2119(3)	−1539(1)	−1787(3)	97(2)	1
C30	2551(4)	−1558(2)	−798(5)	91(2)	1
C31	2912(4)	−1943(2)	−438(5)	94(2)	1
C32	2878(4)	−2301(2)	−1091(5)	97(2)	1
O2	3220(3)	−2684(1)	−774(4)	110(2)	1
C33	3846(4)	−2692(2)	−18(6)	125(3)	1
C34	4147(3)	−3115(1)	−26(4)	122(3)	1
C35	4282(3)	−3385(2)	843(4)	124(3)	1
C36	4529(4)	−3820(2)	818(5)	131(3)	1
C37	4641(4)	−3983(2)	−76(6)	140(3)	1
C38	4506(4)	−3712(2)	−946(5)	138(3)	1
C39	4259(4)	−3278(2)	−921(4)	136(3)	1
C40	2604(2)	−1196(1)	−91(3)	91(2)	1
C41	2401(2)	−1247(1)	793(3)	102(2)	1
C42	2421(3)	−882(1)	1438(3)	99(2)	1
N2	2644(2)	−466(1)	1198(3)	74(1)	1
C43	2847(3)	−415(1)	314(3)	101(2)	1
C44	2827(3)	−779(1)	−331(3)	103(2)	1
O3	1152(2)	−12(1)	916(3)	74(1)	1
O4	1772(2)	11(1)	2522(3)	73(1)	1
C45	1204(4)	−8(2)	1862(5)	69(2)	1
C46	590(3)	−7(2)	2181(4)	63(1)	1
C47	626(3)	2(2)	3196(4)	67(2)	1
C48	57(4)	0(2)	3524(4)	69(2)	1
O5	3286(4)	−419(3)	3650(6)	170(3)	1
O6	3400(3)	176(2)	3035(5)	135(2)	1
C49	3693(4)	−53(3)	3494(7)	135(3)	1
C50	4366(4)	−26(2)	4262(5)	99(2)	1
C51	4898(4)	215(3)	4137(5)	121(3)	1
C52	4505(5)	−243(4)	5172(5)	131(3)	1

Table A2.8. Bond lengths [Å] and angles [°].

Zn1–O6	1.881(6)	C10B–C17B	1.389(9)
Zn1–O4	1.902(6)	C17B–C18B	1.3900
Zn1–N2	1.943(4)	C17B–C22B	1.3900
Zn1–N1^{i}	1.974(3)	C18B–C19B	1.3900
Zn1–C49	2.576(7)	C19B–C20B	1.3900
N1–C1	1.3900	C19B–C21B^{iii}	1.96(6)
N1–C5	1.3900	C20B–C21B	1.3900
N1–Zn1^{ii}	1.974(3)	C21B–C22B	1.3900
C1–C2	1.3900	C21B–C19B^{iii}	1.96(4)
C2–C3	1.3900	C23–C32	1.322(7)
C3–C4	1.3900	C23–C24	1.373(6)
C3–C6A	1.389(9)	C24–C25	1.3900
C3–C6B	1.489(7)	C24–C29	1.3900
C4–C5	1.3900	C25–C26	1.3900
C13A–C14A	1.313(8)	C26–C27	1.3900
C13A–C12A	1.370(7)	C27–C28	1.3900
C12A–C11A	1.3900	C28–C29	1.3900
C12A–C7A	1.3900	C29–C30	1.366(6)
C11A–C10A	1.3900	C30–C31	1.367(8)
C10A–C9A	1.3900	C30–C40	1.430(7)
C9A–C8A	1.3900	C31–C32	1.378(7)
C8A–C7A	1.3900	C32–O2	1.336(6)
C7A–C6A	1.364(8)	O2–C33	1.365(7)
C6A–C15A	1.362(9)	C33–C34	1.400(7)
C15A–C14A	1.379(8)	C34–C35	1.3900
C14A–O1A	1.329(8)	C34–C39	1.3900
O1A–C16A	1.350(9)	C35–C36	1.3900
C16A–C17A	1.393(8)	C36–C37	1.3900
C17A–C22A	1.3900	C37–C38	1.3900
C17A–C18A	1.3900	C38–C39	1.3900
C22A–C21A	1.3900	C40–C41	1.3900
C21A–C20A	1.3900	C40–C44	1.3900
C20A–C19A	1.3900	C41–C42	1.3900
C19A–C18A	1.3900	C42–N2	1.3900
C13B–C12B	1.314(6)	N2–C43	1.3900
C13B–C14B	1.368(7)	C43–C44	1.3900
C14B–C11B	1.3900	O3–C45	1.261(8)
C14B–C15B	1.3900	O4–C45	1.223(8)
C11B–C16B	1.3900	C45–C46	1.422(10)
C16B–C9B	1.3900	C46–C47	1.362(9)
C9B–C8B	1.3900	C46–C48^{iv}	1.365(9)
C8B–C15B	1.3900	C47–C48	1.343(10)
C15B–C6B	1.363(7)	C48–C46^{iv}	1.365(9)
C6B–C7B	1.363(9)	O5–C49	1.417(12)
C7B–C12B	1.384(8)	O6–C49	0.992(9)
C12B–O1B	1.335(7)	C49–C50	1.442(9)
O1B–C10B	1.358(8)	C50–C51	1.338(7)

C50–C52	1.350(7)	C52–C51^{v}	1.285(10)
C51–C52^{v}	1.285(10)		

O6–Zn1–O4	113.7(3)	C21A–C22A–C17A	120.0
O6–Zn1–N2	111.1(2)	C22A–C21A–C20A	120.0
O4–Zn1–N2	112.42(19)	C19A–C20A–C21A	120.0
O6–Zn1–N1^{i}	100.5(3)	C20A–C19A–C18A	120.0
O4–Zn1–N1^{i}	114.89(17)	C19A–C18A–C17A	120.0
N2–Zn1–N1^{i}	103.16(19)	C12B–C13B–C14B	121.4(4)
O6–Zn1–C49	18.5(3)	C13B–C14B–C11B	121.2(4)
O4–Zn1–C49	109.9(3)	C13B–C14B–C15B	118.8(4)
N2–Zn1–C49	97.8(3)	C11B–C14B–C15B	120.0
N1^{i}–Zn1–C49	117.1(2)	C16B–C11B–C14B	120.0
C1–N1–C5	120.0	C11B–C16B–C9B	120.0
C1–N1–Zn1^{ii}	119.21(17)	C8B–C9B–C16B	120.0
C5–N1–Zn1^{ii}	120.71(17)	C15B–C8B–C9B	120.0
N1–C1–C2	120.0	C6B–C15B–C8B	120.2(4)
C1–C2–C3	120.0	C6B–C15B–C14B	119.7(4)
C4–C3–C2	120.0	C8B–C15B–C14B	120.0
C4–C3–C6A	119.1(5)	C7B–C6B–C15B	120.0(6)
C2–C3–C6A	120.9(5)	C7B–C6B–C3	114.3(5)
C4–C3–C6B	118.9(3)	C15B–C6B–C3	125.7(6)
C2–C3–C6B	120.9(3)	C6B–C7B–C12B	119.3(6)
C6A–C3–C6B	6.6(5)	C13B–C12B–O1B	119.1(5)
C5–C4–C3	120.0	C13B–C12B–C7B	120.8(5)
C4–C5–N1	120.0	O1B–C12B–C7B	120.1(6)
C14A–C13A–C12A	121.0(7)	C12B–O1B–C10B	118.3(7)
C13A–C12A–C11A	120.7(5)	O1B–C10B–C17B	110.1(7)
C13A–C12A–C7A	119.0(5)	C10B–C17B–C18B	118.9(7)
C11A–C12A–C7A	120.0	C10B–C17B–C22B	121.1(7)
C12A–C11A–C10A	120.0	C18B–C17B–C22B	120.0
C11A–C10A–C9A	120.0	C19B–C18B–C17B	120.0
C8A–C9A–C10A	120.0	C18B–C19B–C20B	120.0
C9A–C8A–C7A	120.0	C18B–C19B–C21B^{iii}	111.2(7)
C6A–C7A–C8A	120.7(5)	C20B–C19B–C21B^{iii}	50.0(13)
C6A–C7A–C12A	119.1(5)	C21B–C20B–C19B	120.0
C8A–C7A–C12A	120.0	C22B–C21B–C20B	120.0
C15A–C6A–C7A	119.3(7)	C22B–C21B–C19B^{iii}	95.3(8)
C15A–C6A–C3	115.5(7)	C20B–C21B–C19B^{iii}	113(3)
C7A–C6A–C3	124.0(6)	C21B–C22B–C17B	120.0
C6A–C15A–C14A	120.1(8)	C32–C23–C24	121.5(5)
C13A–C14A–O1A	117.9(7)	C23–C24–C25	120.9(3)
C13A–C14A–C15A	120.3(7)	C23–C24–C29	119.1(3)
O1A–C14A–C15A	121.8(7)	C25–C24–C29	120.0
C14A–O1A–C16A	122.0(7)	C26–C25–C24	120.0
O1A–C16A–C17A	107.2(7)	C27–C26–C25	120.0
C22A–C17A–C18A	120.0	C26–C27–C28	120.0
C22A–C17A–C16A	119.0(7)	C27–C28–C29	120.0
C18A–C17A–C16A	121.0(7)	C30–C29–C28	120.8(3)

C30–C29–C24	119.2(3)	$C51^{v}$–C52–C50	122.2(8)
C28–C29–C24	120.0		
C31–C30–C29	120.0(5)		
C31–C30–C40	117.9(5)		
C29–C30–C40	121.9(5)		
C30–C31–C32	120.0(6)		
C23–C32–O2	117.7(5)		
C23–C32–C31	120.0(5)		
O2–C32–C31	122.2(5)		
C32–O2–C33	121.6(5)		
O2–C33–C34	108.0(5)		
C35–C34–C39	120.0		
C35–C34–C33	119.4(5)		
C39–C34–C33	120.4(5)		
C36–C35–C34	120.0		
C35–C36–C37	120.0		
C38–C37–C36	120.0		
C37–C38–C39	120.0		
C38–C39–C34	120.0		
C41–C40–C44	120.0		
C41–C40–C30	121.1(4)		
C44–C40–C30	118.8(4)		
C40–C41–C42	120.0		
C41–C42–N2	120.0		
C43–N2–C42	120.0		
C43–N2–Zn1	120.4(2)		
C42–N2–Zn1	119.1(2)		
N2–C43–C44	120.0		
C43–C44–C40	120.0		
C45–O4–Zn1	115.1(5)		
O4–C45–O3	121.6(7)		
O4–C45–C46	118.5(6)		
O3–C45–C46	119.8(5)		
$C47–C46–C48^{iv}$	117.5(6)		
C47–C46–C45	121.5(6)		
$C48^{iv}$–C46–C45	121.0(6)		
C48–C47–C46	123.1(5)		
$C47–C48–C46^{iv}$	119.4(6)		
C49–O6–Zn1	124.5(7)		
O6–C49–O5	111.4(8)		
O6–C49–C50	131.8(9)		
O5–C49–C50	113.2(7)		
O6–C49–Zn1	37.0(5)		
O5–C49–Zn1	78.3(4)		
C50–C49–Zn1	168.4(6)		
C51–C50–C52	114.8(7)		
C51–C50–C49	123.2(6)		
C52–C50–C49	121.9(7)		
$C52^{v}$–C51–C50	123.0(7)		

Symmetry transformations used to generate equivalent atoms:
(i) −x+1/2,y+1/2,−z−1/2 (ii) −x+1/2,y−1/2,−z−1/2
(iii) −x,y,−z−1/2 (iv) −x,y,−z+1/2 (v) −x+1,−y,−z+1

Table A2.9. Anisotropic displacement parameters [$Å^2 \times 10^3$]. The anisotropic displacement factor exponent takes the form: $-2\pi^2[h^2a^{*2}U^{11} + ... + 2\ h\ k\ a^*\ b^*\ U^{12}\ ]$.

Atom	U^{11}	U^{22}	U^{33}	U^{23}	U^{13}	U^{12}
Zn1	69(1)	68(1)	60(1)	1(1)	10(1)	2(1)
N1	67(3)	73(3)	61(3)	2(2)	13(2)	1(2)
C1	101(5)	92(5)	112(5)	−19(4)	0(4)	32(4)
C2	132(6)	107(5)	102(4)	−21(4)	2(4)	44(5)
C3	90(4)	69(3)	75(3)	−1(2)	23(3)	5(3)
C4	130(5)	99(4)	81(4)	−15(3)	8(4)	43(4)
C5	119(5)	105(5)	64(4)	−15(3)	1(4)	24(4)
C13A	115(5)	72(6)	105(6)	−9(5)	44(5)	4(4)
C12A	116(5)	89(6)	114(6)	−17(5)	57(4)	−4(5)
C11A	124(6)	132(8)	136(7)	−37(6)	71(5)	−15(5)
C10A	117(6)	181(9)	156(8)	−57(6)	77(6)	−47(6)
C9A	158(7)	207(9)	189(10)	−83(7)	99(6)	−74(8)
C8A	149(7)	146(9)	155(9)	−50(7)	81(6)	−49(6)
C7A	114(5)	90(6)	101(6)	−17(5)	42(5)	−6(5)
C6A	100(5)	70(5)	89(5)	−8(4)	30(4)	7(4)
C15A	111(6)	78(5)	107(7)	−17(4)	43(5)	−6(4)
C14A	111(5)	77(5)	118(7)	−24(5)	51(5)	−1(4)
O1A	142(5)	99(5)	129(6)	−45(4)	68(4)	−19(4)
C16A	115(6)	105(7)	111(7)	7(5)	42(5)	−8(5)
C17A	99(6)	108(7)	161(8)	14(5)	24(6)	4(5)
C22A	125(8)	134(9)	220(9)	46(7)	63(7)	3(7)
C21A	123(10)	170(11)	241(9)	48(9)	33(8)	−24(8)
C20A	131(10)	159(11)	238(11)	40(8)	8(8)	−21(9)
C19A	168(12)	97(8)	205(12)	9(8)	16(9)	−14(8)
C18A	116(9)	110(9)	179(9)	−12(7)	20(8)	−6(7)
C13B	119(5)	64(7)	97(8)	−13(6)	45(5)	−2(5)
C14B	115(5)	67(6)	92(7)	−17(5)	45(5)	−13(5)
C11B	113(6)	96(8)	96(8)	−28(7)	27(6)	−23(6)
C16B	116(7)	75(7)	100(9)	−14(6)	34(6)	−33(7)
C9B	103(7)	95(8)	105(9)	−28(6)	36(7)	−34(6)
C8B	75(6)	81(7)	78(7)	−27(6)	15(5)	−8(5)
C15B	105(5)	75(6)	74(7)	−11(5)	37(5)	−14(5)
C6B	95(6)	66(6)	90(7)	−8(5)	35(5)	−4(5)
C7B	112(6)	82(7)	102(8)	−19(5)	50(5)	−16(6)
C12B	117(5)	76(7)	112(8)	−18(6)	54(5)	−7(6)
O1B	128(5)	141(9)	139(8)	−49(7)	71(5)	−13(6)
C10B	120(6)	213(7)	180(12)	−61(8)	66(8)	−14(9)
C17B	101(9)	209(7)	195(10)	−79(7)	60(8)	−13(7)
C18B	186(16)	247(9)	220(12)	−121(9)	37(10)	−23(11)
C19B	203(18)	246(11)	258(12)	−118(10)	1(13)	−32(12)
C20B	221(18)	258(12)	293(16)	−87(9)	4(15)	−30(14)
C21B	190(18)	199(10)	262(15)	−67(10)	22(13)	−13(13)
C22B	166(13)	212(10)	215(11)	−55(9)	67(10)	−14(11)
C23	114(5)	67(3)	108(4)	−13(3)	39(3)	4(3)
C24	114(5)	75(4)	98(4)	−6(3)	35(3)	3(3)

C25	127(5)	93(4)	102(4)	−12(3)	33(4)	10(4)
C26	147(7)	101(5)	110(5)	−9(4)	4(5)	1(5)
C27	154(7)	83(4)	123(5)	−1(4)	25(5)	8(5)
C28	131(6)	86(4)	101(4)	−4(3)	32(4)	19(4)
C29	129(5)	71(3)	98(4)	−7(3)	42(3)	9(3)
C30	110(5)	73(3)	93(3)	−4(3)	36(3)	7(3)
C31	119(5)	63(3)	104(4)	−4(3)	38(4)	9(3)
C32	124(5)	74(4)	98(4)	−6(3)	38(4)	7(3)
O2	143(4)	60(2)	117(4)	−8(2)	23(3)	14(2)
C33	166(6)	73(4)	112(6)	−12(3)	5(5)	20(4)
C34	147(6)	88(4)	119(5)	−1(3)	19(5)	25(4)
C35	141(7)	88(4)	140(5)	5(4)	39(5)	8(4)
C36	149(7)	86(4)	160(5)	12(4)	50(6)	10(5)
C37	174(8)	83(5)	152(6)	−19(4)	29(6)	−1(5)
C38	156(8)	102(5)	138(5)	−15(4)	17(6)	19(5)
C39	164(8)	107(5)	121(5)	−14(4)	15(5)	25(5)
C40	120(5)	65(3)	96(4)	−2(3)	44(3)	10(3)
C41	142(6)	82(4)	92(4)	−6(3)	52(4)	−8(4)
C42	138(6)	72(4)	100(4)	−4(3)	53(4)	2(4)
N2	85(3)	64(3)	74(3)	−8(2)	28(2)	−3(2)
C43	121(5)	82(4)	116(5)	−19(3)	60(4)	−11(4)
C44	133(5)	68(3)	126(5)	−1(3)	66(4)	−6(4)
O3	74(3)	88(3)	56(2)	−7(2)	14(2)	−4(2)
O4	62(2)	88(3)	62(2)	1(2)	7(2)	4(2)
C45	71(3)	61(3)	66(3)	3(2)	5(2)	−3(2)
C46	71(3)	58(3)	54(3)	2(2)	7(2)	0(2)
C47	59(3)	77(3)	51(3)	6(2)	−5(2)	2(2)
C48	74(4)	77(4)	46(3)	5(2)	3(2)	−3(3)
O5	132(5)	191(6)	150(6)	25(5)	−16(4)	−5(4)
O6	130(4)	109(3)	120(4)	−37(3)	−31(3)	39(3)
C49	119(5)	115(6)	135(6)	−39(4)	−15(5)	32(4)
C50	98(4)	104(5)	79(4)	−11(3)	3(3)	23(3)
C51	174(6)	100(5)	62(4)	17(3)	−6(4)	−36(5)
C52	126(6)	192(8)	75(4)	−3(4)	30(4)	−51(6)

Table A2.10. Hydrogen coordinates [× 10^4] and isotropic displacement parameters [$Å^2$ × 10^3].

Atom	*x*	*y*	*z*	U_{eq}	*S.o.f.*
H1	1610	−4127	−6977	130	1
H2	1602	−3544	−5831	145	1
H4	3336	−4060	−3784	130	1
H5	3344	−4644	−4931	122	1
H11A	1513	−2738	−1856	148	0.582(5)
H10A	630	−3277	−2099	172	0.582(5)
H9A	569	−3871	−3246	209	0.582(5)
H8A	1391	−3926	−4151	170	0.582(5)
H15A	3251	−3087	−4300	116	0.582(5)
H16A	3656	−2374	−4403	130	0.582(5)
H16B	4184	−2657	−3492	130	0.582(5)
H22A	4744	−2022	−4496	189	0.582(5)
H21A	5438	−1382	−3988	220	0.582(5)
H20A	5403	−982	−2524	223	0.582(5)
H19A	4675	−1222	−1568	199	0.582(5)
H18A	3982	−1862	−2076	168	0.582(5)
H11B	3490	−2128	−2409	123	0.418(5)
H16C	4432	−2178	−3084	116	0.418(5)
H9B	4493	−2773	−4176	120	0.418(5)
H8B	3612	−3317	−4591	96	0.418(5)
H7B	1609	−3551	−3750	114	0.418(5)
H10B	739	−2918	−3914	200	0.418(5)
H10C	430	−2776	−3001	200	0.418(5)
H18B	−196	−3415	−4578	267	0.418(5)
H19B	−599	−4148	−4527	301	0.418(5)
H20B	−124	−4595	−3071	328	0.418(5)
H21B	753	−4307	−1666	273	0.418(5)
H22B	1156	−3573	−1717	234	0.418(5)
H25	1588	−2152	−3863	130	1
H26	910	−1515	−4469	152	1
H27	989	−892	−3392	148	1
H28	1748	−907	−1710	128	1
H31	3188	−1963	262	113	1
H33A	3775	−2635	660	150	1
H33B	4157	−2455	−146	150	1
H35	4206	−3274	1454	148	1
H36	4622	−4005	1412	157	1
H37	4810	−4280	−93	169	1
H38	4582	−3824	−1557	165	1
H39	4166	−3093	−1515	164	1
H41	2249	−1531	957	122	1
H42	2282	−917	2042	119	1
H43	3000	−130	150	121	1
H44	2966	−744	−935	124	1
H47	1073	9	3695	80	1

H48	106	4	4240	83	1
H51	4831	373	3509	145	1
H52	4150	–422	5305	157	1

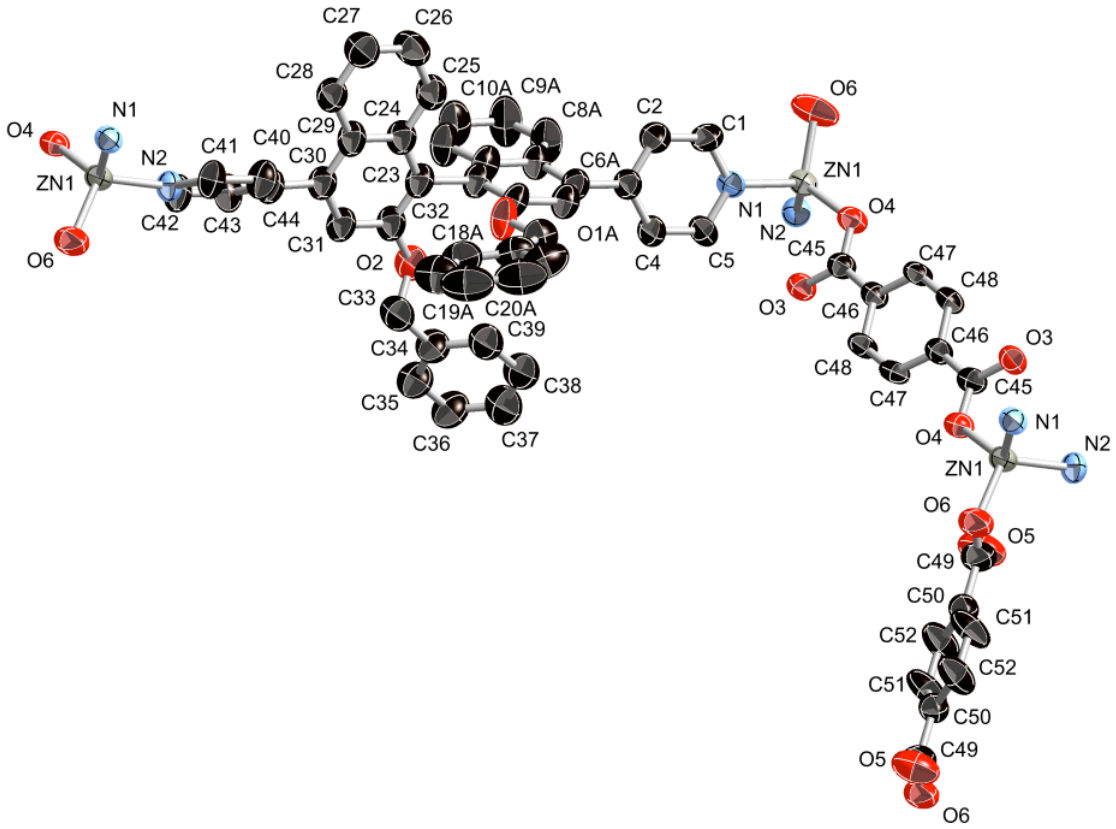

Part of the 3D structure showing asymmetric unit plus selected symmetry related atoms. Thermal ellipsoids drawn at the 30% probability level, hydrogens, disorder and selected labels omitted for clarity.

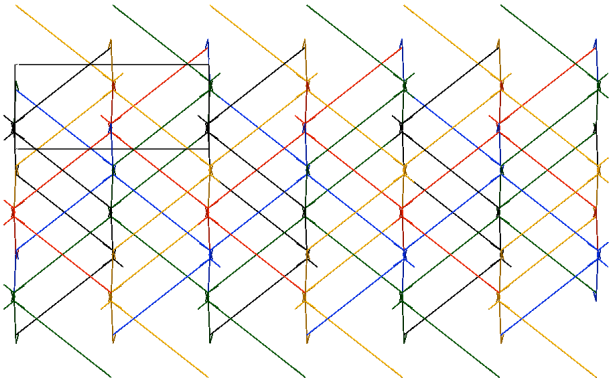

Interpenetrating net viewed along the a-axis

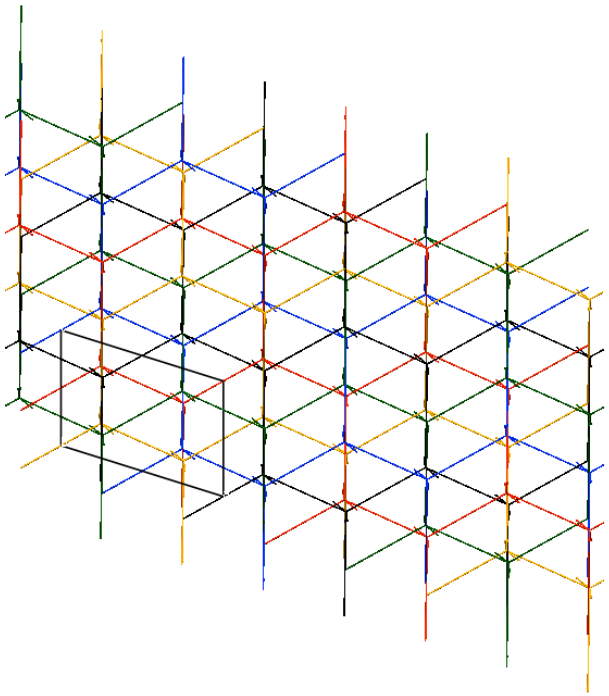

Interpenetrating net viewed along the b-axis

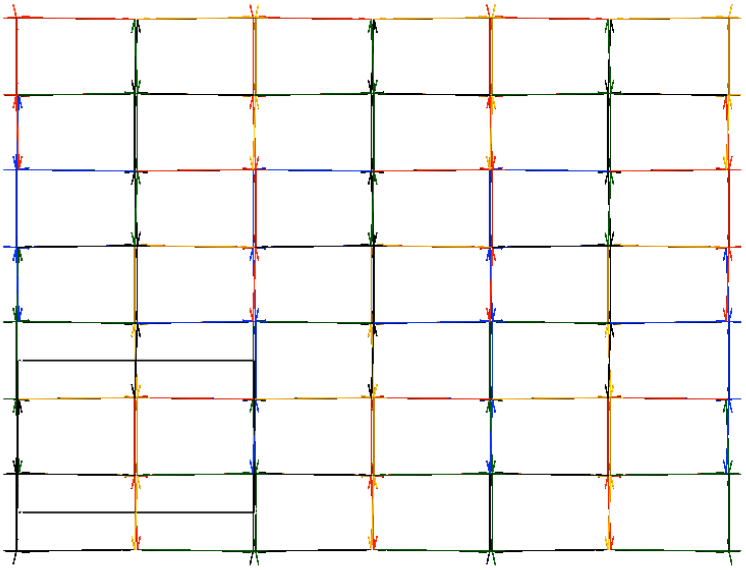

Interpenetrating net viewed along the c-axis

A2.1.3[Cd(BDC)(H_2O)$_3$].2.25H_2O

Table A2.11. Crystal data and structure refinement details.

Identification code	**2009sot0614 (SK065M)**	
Empirical formula	$C_8H_{14.50}CdO_{9.25}$	
	$C_8H_4O_4$. Cd(H_2O)3 . 2.25(H_2O)	
Formula weight	371.10	
Temperature	120(2) K	
Wavelength	0.71073 Å	
Crystal system	Triclinic	
Space group	*P*–1	
Unit cell dimensions	a = 9.6820(12) Å	α = 91.455(10)°
	b = 10.0226(14) Å	β = 106.980(8)°
	c = 14.2989(17) Å	γ = 109.358(5)°
Volume	1240.5(3) Å^3	
Z	4	
Absorption coefficient	1.800 mm^{-1}	
F(000)	738	
Crystal	Lath; Colourless	
Crystal size	0.3 × 0.04 × 0.01 mm^3	
θ range for data collection	3.01 – 25.03°	
Index ranges	$-11 \le h \le 11$, $-11 \le k \le 11$, $-16 \le l \le 15$	
Reflections collected	8702	
Independent reflections	4015 [R_{int} = 0.0526]	
Completeness to θ = 25.03°	91.5 %	
Absorption correction	Semi–empirical from equivalents	
Max. and min. transmission	0.9822 and 0.6043	
Refinement method	Full-matrix least-squares on F^2	
Data / restraints / parameters	4015 / 0 / 337	
Goodness-of-fit on F^2	1.095	
Final *R* indices [$F^2 > 2\sigma(F^2)$]	*R1* = 0.0684, *wR2* = 0.1353	
R indices (all data)	*R1* = 0.0941, *wR2* = 0.1488	
Largest diff. peak and hole	1.004 and –0.858 e Å^{-3}	

Diffractometer: *Nonius KappaCCD* area detector (ϕ scans and ω scans to fill *asymmetric unit*). **Cell determination:** DirAx (Duisenberg, A.J.M.(1992). J. Appl. Cryst. 25, 92–96.) **Data collection:** Collect (Collect: Data collection software, R. Hooft, Nonius B.V., 1998). **Data reduction and cell refinement**: *Denzo* (Z. Otwinowski & W. Minor, *Methods in Enzymology* (1997) Vol. **276**: *Macromolecular Crystallography*, part A, pp. 307–326; C. W. Carter, Jr. & R. M. Sweet, Eds., Academic Press). **Absorption correction**: Sheldrick, G. M. SADABS – Bruker Nonius area detector scaling and absorption correction – V2.10 S**tructure solution**: *SHELXS97* (G. M. Sheldrick, Acta Cryst. (1990) A**46** 467–473). S**tructure refinement**: *SHELXL97* (G. M. Sheldrick (1997), University of Göttingen, Germany). **Graphics:** Cameron – A Molecular Graphics Package. (D. M. Watkin, L. Pearce and C. K. Prout, Chemical Crystallography Laboratory, University of Oxford, 1993).

Special details: All hydrogen atoms were placed in idealised positions and refined using a riding model. Half way through the data collection the crystal suddenly curled up into a sickle shape. The inference is that the structure lost water and thus its structural integrity. The refinement was carried out using only the data from the early part of the collection; a 92% completeness results. It was not possible to locate the hydrogens.

Table A2.12. Atomic coordinates [× 10^4], equivalent isotropic displacement parameters [$Å^2$ × 10^3] and site occupancy factors. U_{eq} is defined as one third of the trace of the orthogonalized U^{ij} tensor.

Atom	*x*	*y*	*z*	U_{eq}	*S.o.f.*
Cd1	7471(1)	4171(1)	3348(1)	22(1)	1
Cd2	12149(1)	–4282(1)	1785(1)	25(1)	1
O1	7273(6)	6385(6)	3923(4)	29(2)	1
O2	9604(6)	6368(6)	4062(4)	26(2)	1
O3	7031(6)	1835(6)	2487(4)	28(2)	1
O4	9392(6)	3242(6)	3325(4)	27(2)	1
O5	9906(6)	–3545(6)	1591(4)	27(2)	1
O6	12249(6)	–2035(6)	2299(5)	34(2)	1
O7	10232(6)	–6479(6)	1037(4)	27(2)	1
O8	12593(6)	–6466(6)	1405(4)	26(1)	1
C1	11573(9)	10670(9)	5419(6)	26(2)	1
C2	10971(10)	9283(9)	5013(6)	26(2)	1
C3	9377(8)	8558(9)	4595(6)	22(2)	1
C4	8729(9)	7016(10)	4166(6)	26(2)	1
C5	8451(8)	2068(9)	2796(6)	21(2)	1
C6	9068(9)	934(9)	2591(6)	25(2)	1
C7	10635(9)	1164(9)	2972(6)	25(2)	1
C8	11207(9)	113(9)	2787(6)	26(2)	1
C9	10171(9)	–1196(9)	2221(6)	25(2)	1
C10	8627(9)	–1402(9)	1857(6)	26(2)	1
C11	8077(9)	–341(9)	2032(6)	25(2)	1
C12	10807(9)	–2322(9)	2032(6)	24(2)	1
C13	11139(9)	–7116(8)	992(6)	20(2)	1
C14	9008(9)	–9267(9)	–38(6)	22(2)	1
C15	10563(8)	–8607(9)	493(6)	19(2)	1
C16	11546(9)	–9355(9)	516(6)	25(2)	1
O1W	7539(6)	3420(7)	4861(4)	31(2)	1
O2W	4802(6)	3224(6)	3056(5)	32(2)	1
O3W	7219(6)	5005(7)	1890(4)	32(2)	1
O4W	14842(6)	–3144(7)	2376(5)	35(2)	1
O5W	12177(7)	–5058(7)	3287(5)	38(2)	1
O6W	12344(6)	–3750(7)	277(4)	29(2)	1
O7W	5600(6)	1430(7)	397(5)	35(2)	1
O8W	14548(6)	–6307(7)	337(4)	31(2)	1
O9W	15094(7)	–404(8)	3226(5)	46(2)	1
O10W	5315(13)	1020(14)	4996(10)	37(3)	0.50
O11W	5836(14)	6745(16)	5209(10)	41(3)	0.50
O11*Z*	5178(15)	6167(17)	4920(10)	41(3)	0.50

Table A2.13. Bond lengths [Å] and angles [°].

Cd1–O3W	2.244(6)	O7–C13	1.259(10)
Cd1–O1W	2.299(6)	O8–C13	1.281(9)
Cd1–O2W	2.340(5)	C1–C2	1.354(11)
Cd1–O4	2.347(6)	C1–C3^{i}	1.381(12)
Cd1–O2	2.407(5)	C2–C3	1.401(11)
Cd1–O1	2.434(6)	C3–C1^{i}	1.381(12)
Cd1–O3	2.462(6)	C3–C4	1.498(12)
Cd2–O6W	2.280(6)	C5–C6	1.506(12)
Cd2–O5W	2.299(7)	C6–C11	1.371(11)
Cd2–O6	2.313(6)	C6–C7	1.390(11)
Cd2–O7	2.334(5)	C7–C8	1.394(12)
Cd2–O4W	2.347(5)	C8–C9	1.408(11)
Cd2–O8	2.444(6)	C9–C10	1.373(11)
Cd2–O5	2.462(6)	C9–C12	1.506(12)
Cd2–C12	2.756(9)	C10–C11	1.384(12)
O1–C4	1.273(9)	C13–C15	1.488(11)
O2–C4	1.263(11)	C14–C16^{ii}	1.382(11)
O3–C5	1.252(9)	C14–C15	1.388(10)
O4–C5	1.276(9)	C15–C16	1.387(12)
O5–C12	1.262(9)	C16–C14^{ii}	1.382(11)
O6–C12	1.263(9)		

O3W–Cd1–O1W	173.8(2)	O5W–Cd2–O4W	90.3(2)
O3W–Cd1–O2W	93.2(2)	O6–Cd2–O4W	81.5(2)
O1W–Cd1–O2W	82.5(2)	O7–Cd2–O4W	141.7(2)
O3W–Cd1–O4	97.3(2)	O6W–Cd2–O8	86.6(2)
O1W–Cd1–O4	88.8(2)	O5W–Cd2–O8	84.7(2)
O2W–Cd1–O4	135.7(2)	O6–Cd2–O8	168.68(18)
O3W–Cd1–O2	87.5(2)	O7–Cd2–O8	54.40(19)
O1W–Cd1–O2	92.8(2)	O4W–Cd2–O8	87.3(2)
O2W–Cd1–O2	138.9(2)	O6W–Cd2–O5	94.0(2)
O4–Cd1–O2	84.63(19)	O5W–Cd2–O5	94.8(2)
O3W–Cd1–O1	85.1(2)	O6–Cd2–O5	54.31(18)
O1W–Cd1–O1	90.0(2)	O7–Cd2–O5	82.54(19)
O2W–Cd1–O1	84.7(2)	O4W–Cd2–O5	135.7(2)
O4–Cd1–O1	138.92(18)	O8–Cd2–O5	136.95(17)
O2–Cd1–O1	54.41(19)	O6W–Cd2–C12	95.4(2)
O3W–Cd1–O3	87.9(2)	O5W–Cd2–C12	94.0(3)
O1W–Cd1–O3	96.0(2)	O6–Cd2–C12	27.1(2)
O2W–Cd1–O3	83.4(2)	O7–Cd2–C12	109.7(2)
O4–Cd1–O3	54.31(18)	O4W–Cd2–C12	108.6(2)
O2–Cd1–O3	137.63(19)	O8–Cd2–C12	164.1(2)
O1–Cd1–O3	165.84(18)	O5–Cd2–C12	27.24(19)
O6W–Cd2–O5W	170.5(2)	C4–O1–Cd1	91.3(5)
O6W–Cd2–O6	94.3(2)	C4–O2–Cd1	92.7(5)
O5W–Cd2–O6	93.7(2)	C5–O3–Cd1	90.1(5)
O6W–Cd2–O7	89.7(2)	C5–O4–Cd1	94.8(5)
O5W–Cd2–O7	88.1(2)	C12–O5–Cd2	89.5(5)
O6–Cd2–O7	136.8(2)	C12–O6–Cd2	96.4(5)
O6W–Cd2–O4W	85.8(2)	C13–O7–Cd2	96.1(4)

C13–O8–Cd2	90.4(5)
C2–C1–C3^{i}	120.6(8)
C1–C2–C3	122.2(8)
C1^{i}–C3–C2	117.2(8)
C1^{i}–C3–C4	121.3(7)
C2–C3–C4	121.4(8)
O2–C4–O1	121.6(8)
O2–C4–C3	120.9(7)
O1–C4–C3	117.5(8)
O3–C5–O4	120.7(8)
O3–C5–C6	120.4(7)
O4–C5–C6	118.9(7)
C11–C6–C7	119.5(8)
C11–C6–C5	119.9(7)
C7–C6–C5	120.5(7)
C6–C7–C8	120.6(7)
C7–C8–C9	119.1(7)
C10–C9–C8	119.3(8)
C10–C9–C12	122.3(7)
C8–C9–C12	118.4(7)
C9–C10–C11	121.0(7)
C6–C11–C10	120.4(8)
O5–C12–O6	119.8(8)
O5–C12–C9	120.3(7)
O6–C12–C9	120.0(7)
O5–C12–Cd2	63.3(4)
O6–C12–Cd2	56.5(4)
C9–C12–Cd2	176.2(5)
O7–C13–O8	118.8(7)
O7–C13–C15	121.7(7)
O8–C13–C15	119.5(7)
C16^{ii}–C14–C15	120.6(8)
C16–C15–C14	118.4(7)
C16–C15–C13	121.9(7)
C14–C15–C13	119.7(8)
C14^{ii}–C16–C15	121.0(7)

Symmetry transformations used to generate equivalent atoms:
(i) −x+2,−y+2,−z+1 (ii) −x+2,−y−2,−z

Table A2.14. Anisotropic displacement parameters [$Å^2 \times 10^3$]. The anisotropic displacement
factor exponent takes the form: $-2\pi^2[h^2a^{*2}U^{11} + ... + 2\ h\ k\ a^*\ b^*\ U^{12}\ ]$.

Atom	U^{11}	U^{22}	U^{33}	U^{23}	U^{13}	U^{12}
Cd1	20(1)	19(1)	26(1)	−2(1)	2(1)	7(1)
Cd2	21(1)	18(1)	32(1)	−2(1)	6(1)	7(1)
O1	25(3)	25(3)	33(3)	−5(3)	7(2)	7(2)
O2	20(3)	25(3)	27(3)	−5(2)	−3(2)	11(2)
O3	25(3)	28(3)	38(3)	1(3)	7(2)	20(2)
O4	32(3)	26(3)	26(3)	2(2)	10(2)	14(2)
O5	23(3)	17(3)	38(3)	−4(2)	9(2)	6(2)
O6	24(3)	22(3)	56(4)	−7(3)	11(3)	12(2)
O7	21(3)	18(3)	37(3)	−6(3)	6(2)	4(2)
O8	20(3)	30(3)	26(3)	−2(2)	6(2)	9(2)
C1	29(4)	21(4)	25(5)	10(3)	5(3)	9(3)
C2	41(4)	19(4)	25(4)	3(3)	10(4)	18(3)
C3	20(4)	24(4)	18(4)	3(3)	6(3)	4(3)
C4	30(4)	34(5)	16(4)	5(4)	5(3)	16(4)
C5	21(4)	23(4)	22(4)	−4(3)	10(3)	8(3)
C6	27(4)	33(5)	24(4)	11(3)	16(3)	16(3)
C7	33(4)	22(4)	24(4)	1(3)	15(3)	9(3)
C8	24(4)	23(5)	29(5)	−4(4)	10(3)	6(3)
C9	26(4)	22(4)	33(5)	3(3)	14(3)	14(3)
C10	28(4)	13(4)	31(5)	−2(3)	10(4)	2(3)
C11	27(4)	27(5)	23(4)	9(3)	11(3)	9(3)
C12	24(4)	21(4)	27(5)	−2(3)	4(3)	11(3)
C13	25(4)	18(4)	13(4)	2(3)	5(3)	6(3)
C14	28(4)	20(4)	22(4)	3(3)	14(3)	9(3)
C15	22(4)	21(4)	11(4)	−1(3)	4(3)	4(3)
C16	22(4)	27(5)	23(4)	−6(4)	5(3)	8(3)
O1W	22(3)	43(4)	31(3)	12(3)	5(2)	18(2)
O2W	21(3)	31(3)	40(4)	2(3)	9(2)	5(2)
O3W	31(3)	33(4)	23(3)	5(3)	2(2)	5(3)
O4W	21(3)	31(4)	41(4)	2(3)	0(3)	4(3)
O5W	38(3)	41(4)	31(4)	2(3)	10(3)	8(3)
O6W	21(3)	40(4)	26(3)	0(3)	8(2)	11(2)
O7W	24(3)	34(4)	36(4)	−2(3)	−2(3)	7(3)
O8W	23(3)	34(3)	31(3)	5(3)	5(2)	7(3)
O9W	40(4)	50(4)	34(4)	−1(3)	2(3)	7(3)
O10W	39(6)	40(7)	43(7)	17(6)	23(5)	19(5)
O11W	34(5)	59(7)	25(6)	−9(5)	−2(4)	20(5)
O11*Z*	34(5)	59(7)	25(6)	−9(5)	−2(4)	20(5)

Table A2.15. Hydrogen coordinates [× 10^4] and isotropic displacement parameters [$Å^2$ × 10^3].

Atom	*x*	*y*	*z*	U_{eq}	*S.o.f.*
H1	12658	11116	5717	31	1
H2	11652	8785	5012	32	1
H7	11323	2045	3362	30	1
H8	12281	278	3040	31	1
H10	7924	−2287	1480	31	1
H11	7007	−497	1764	30	1
H14	8319	−8766	−73	26	1
H16	12617	−8912	865	30	1

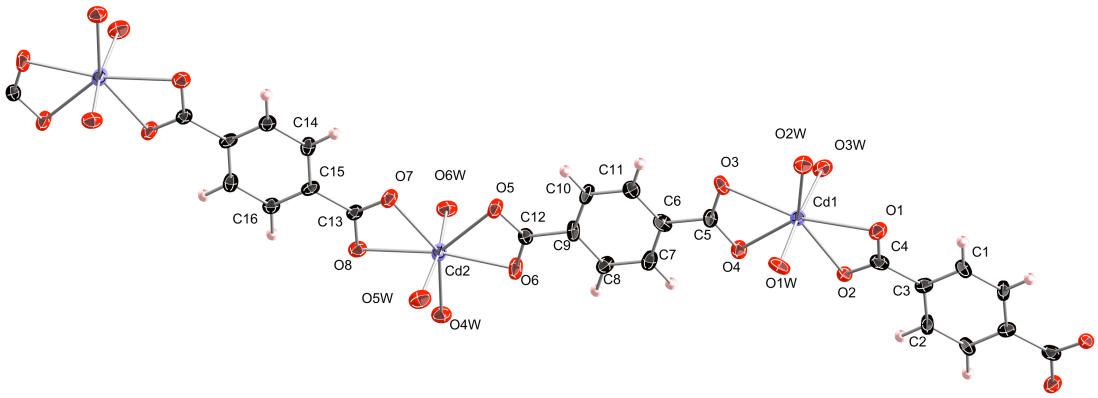

Thermal ellipsoids drawn at the 35% probability level. Lattice waters omitted for clarity, asymmetric unit labelled.

A3 NMR data from Chapter 5

Fitting of the ^{1}H NMR studies for kinetic modelling is shown in this Appendix. The calibration of BDC proton resonnaces is shown below: For the stack plots presented in **Figures A3.2 – A3.11**, the reaction time in hours is displayed to the left of each plot.

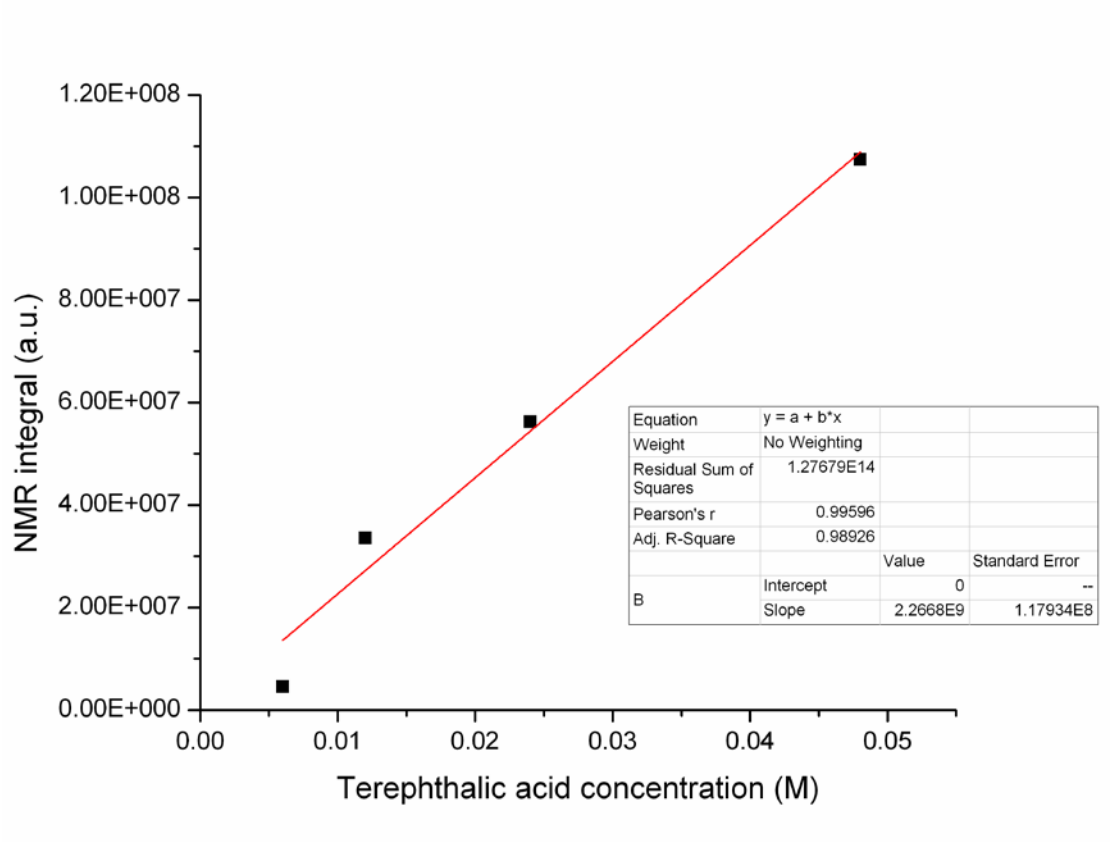

Figure A3.1: Terephthalic acid concentration–^{1}H NMR integral calibration plot.

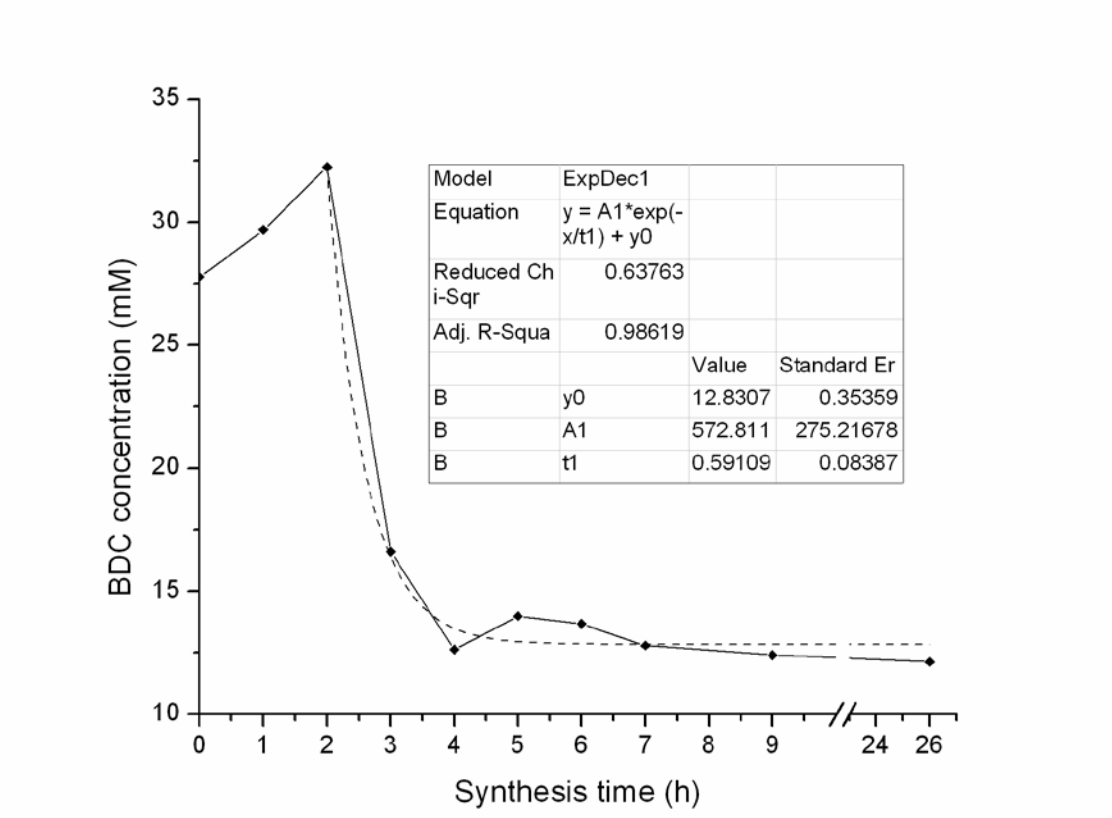

Figure A3.2: Terephthalic acid concentration *vs.* time for MOF-5 synthesis [solid line]; exponential decay fit [dashed line].

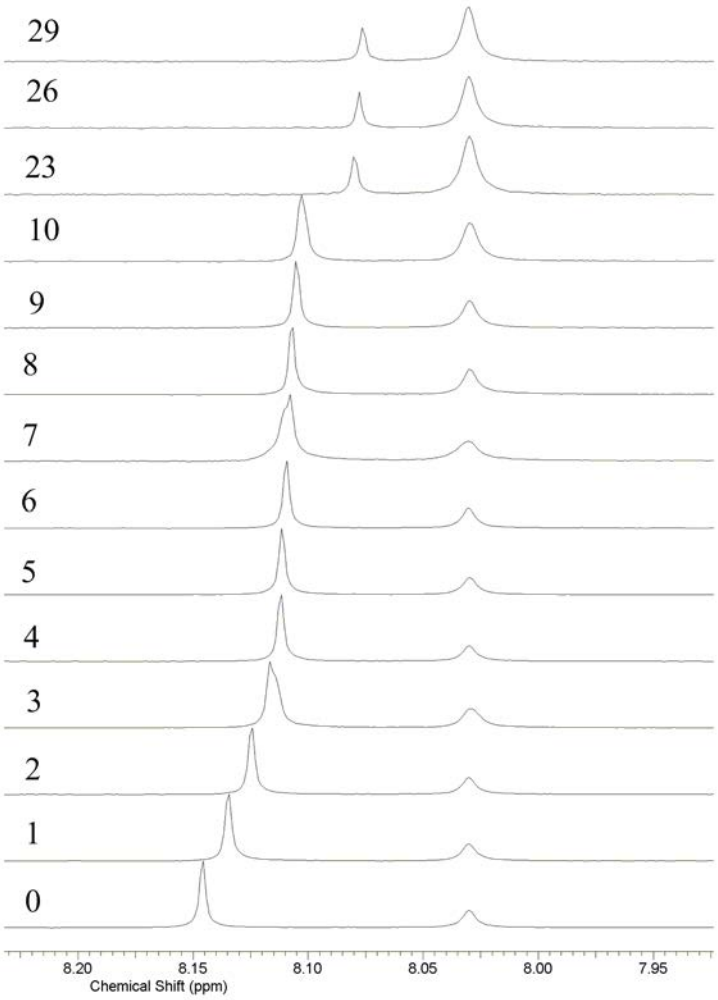

Figure A3.3: Stack plot of the ^{1}H NMR spectra measured during the MOF-5 synthesis when Zn/BDC = 1:1.

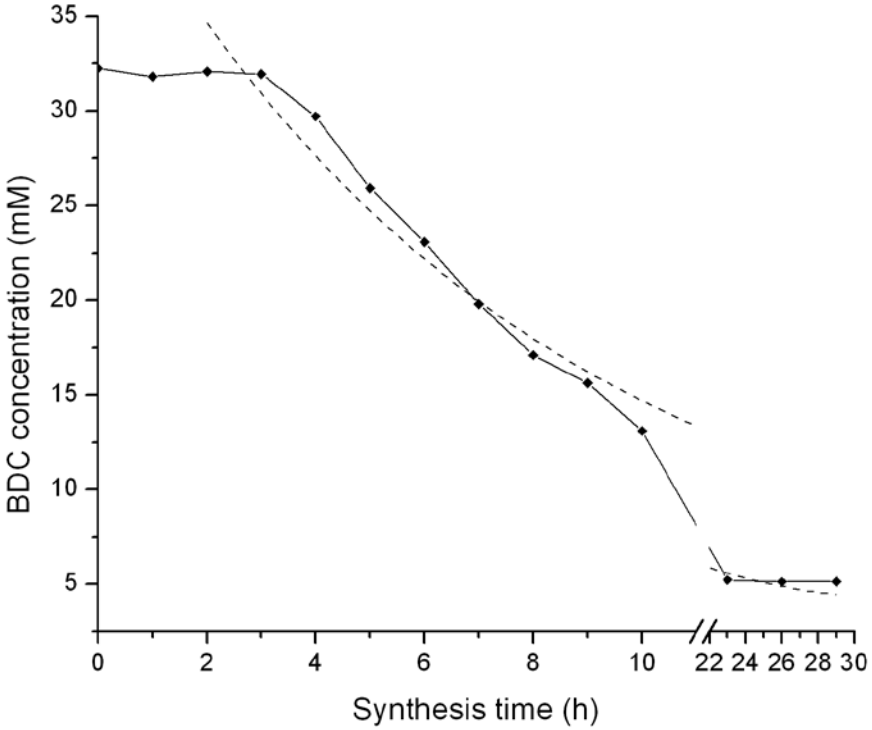

Figure A3.4: Terephthalic acid concentration *vs.* time for MOF-5 synthesis when Zn/BDC = 1:1 [solid line]; exponential decay fit [dashed line].

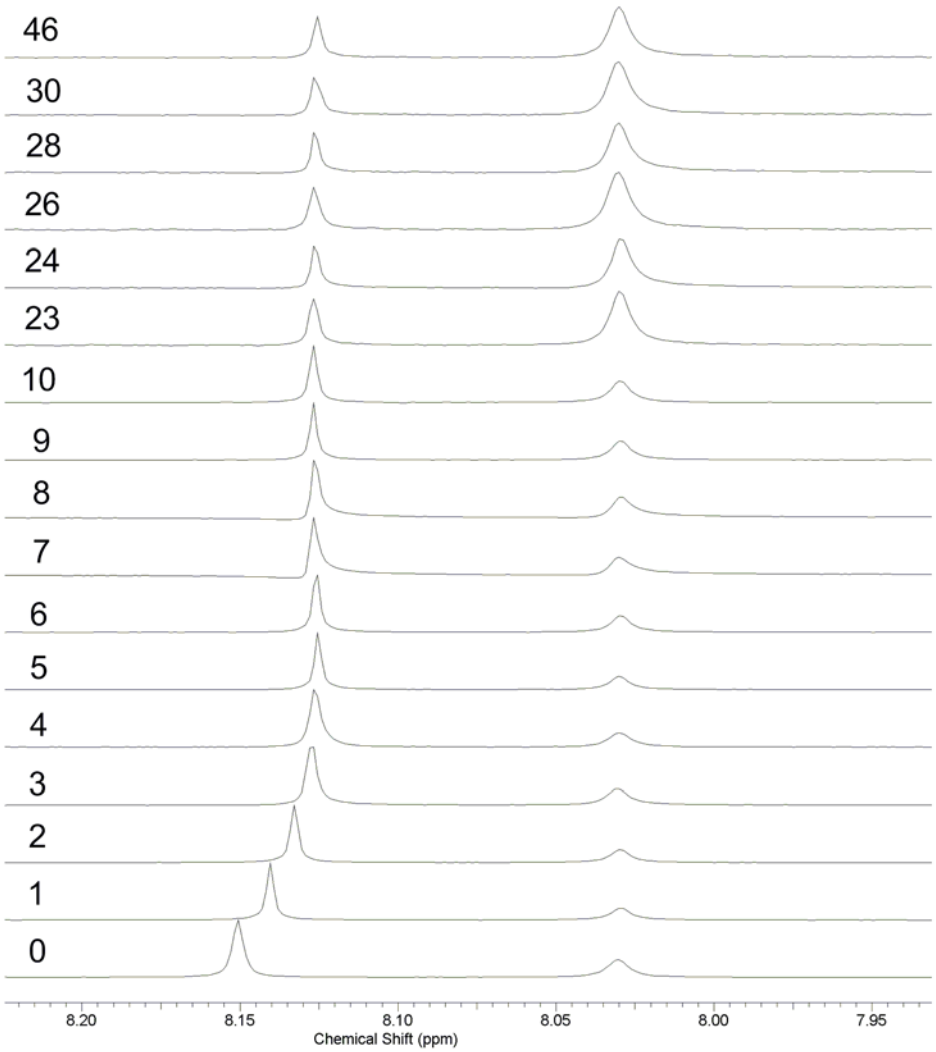

Figure A3.5: Stack plot of the ^{1}H NMR spectra measured during the MOF-5 synthesis when Zn/BDC = 2:1.

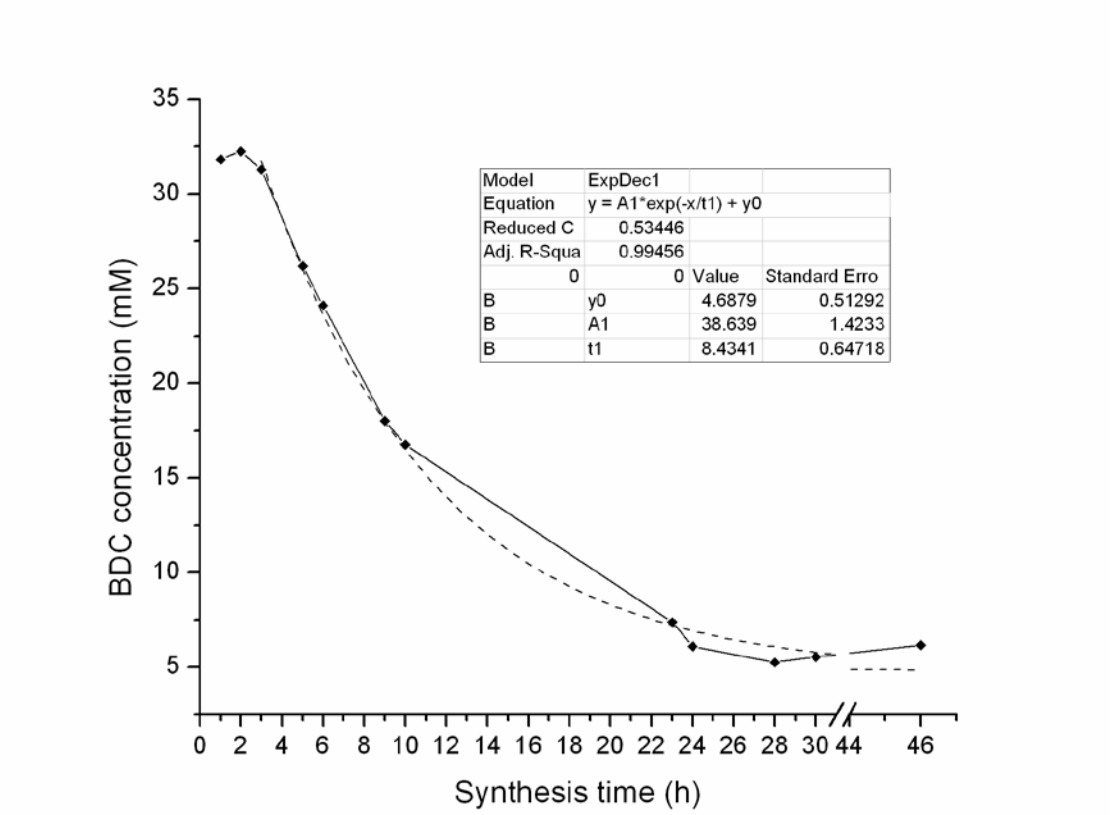

Figure A3.6: Terephthalic acid concentration *vs.* time for MOF-5 synthesis when Zn/BDC = 2:1 [solid line]; exponential decay fit [dashed line].

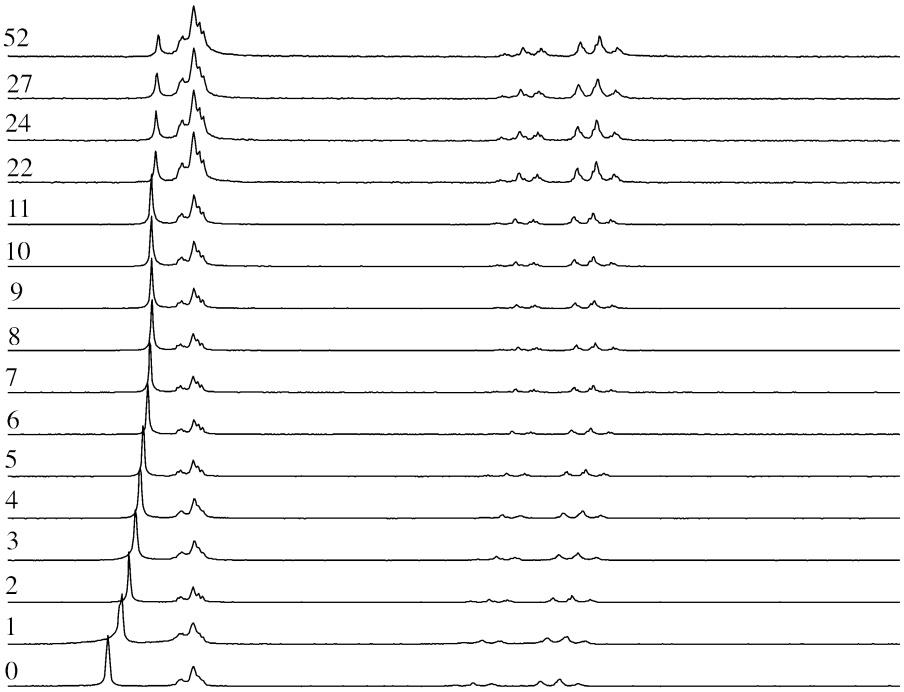

Figure A3.7: Stack plot of the ^{1}H NMR spectra measured during the modulated MOF-5 synthesis with 1 equvalent of benzoic acid.

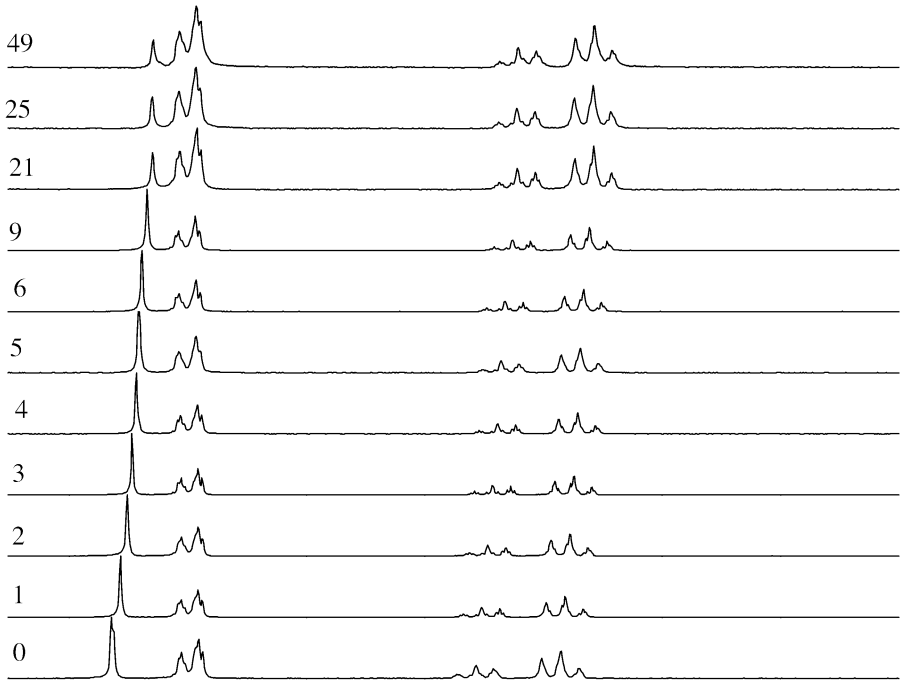

Figure A3.8: Stack plot of the ^{1}H NMR spectra measured during the modulated MOF-5 synthesis with 2 equvalents of benzoic acid.

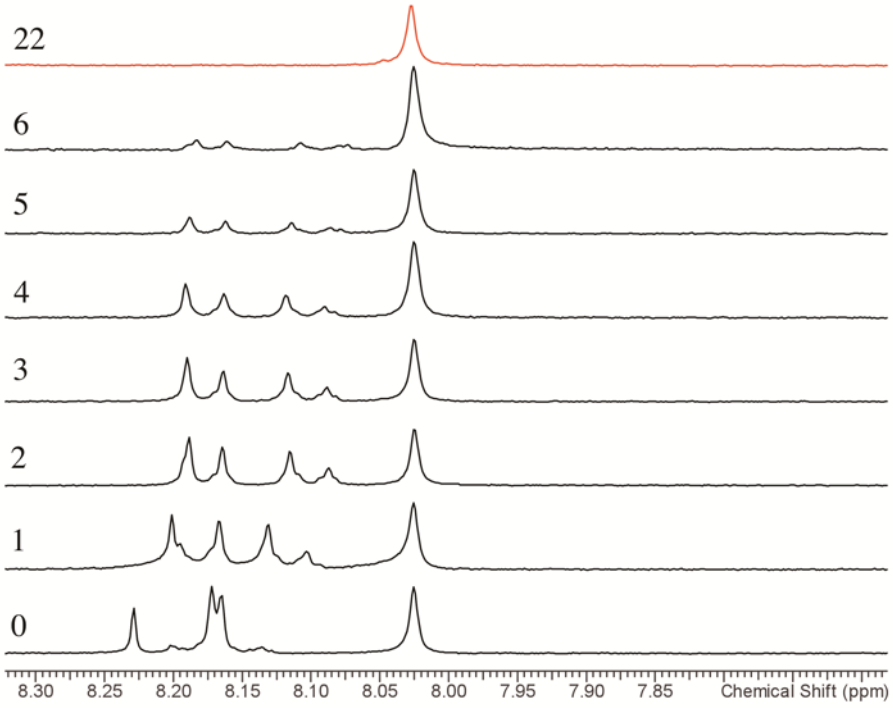

Figure A3.9: Stack plot of the ^{1}H NMR spectra measured during the MOF-177 synthesis.

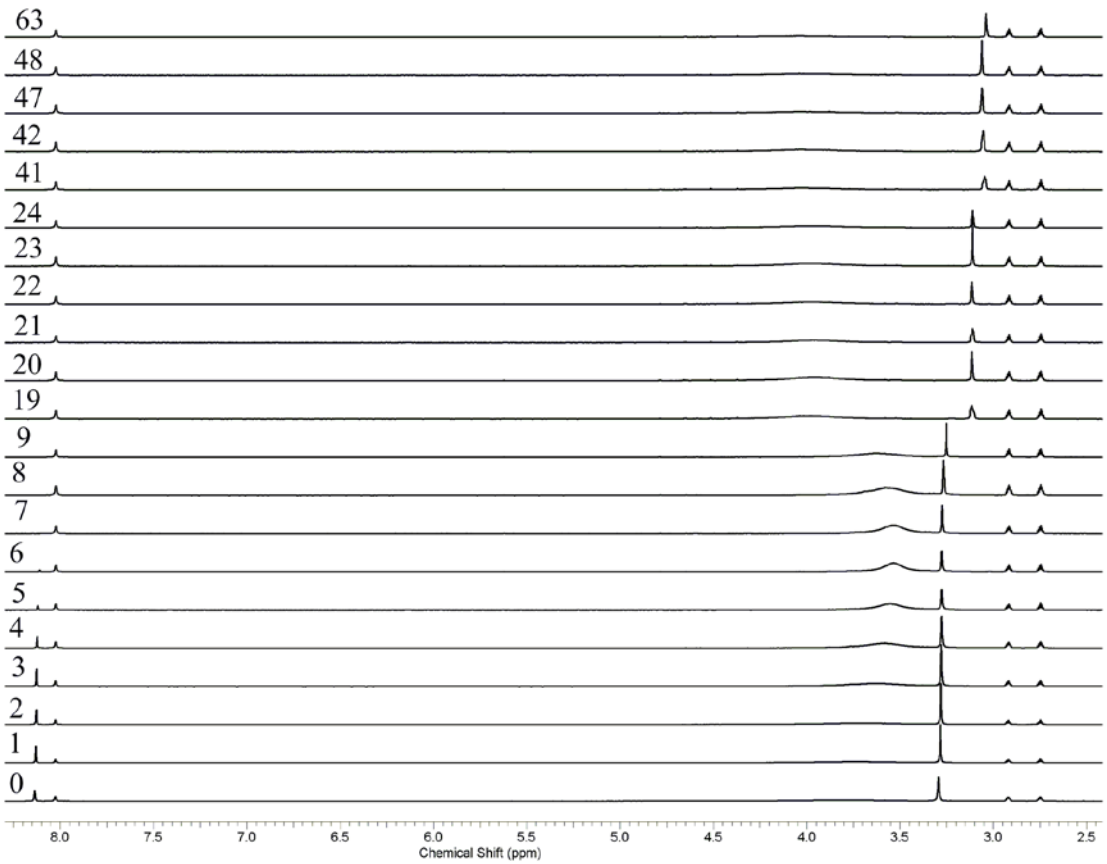

Figure A3.10: Stack plot of the ^{1}H NMR spectra measured during the synthesis of $[Zn_2(BDC)_2(DABCO)]$

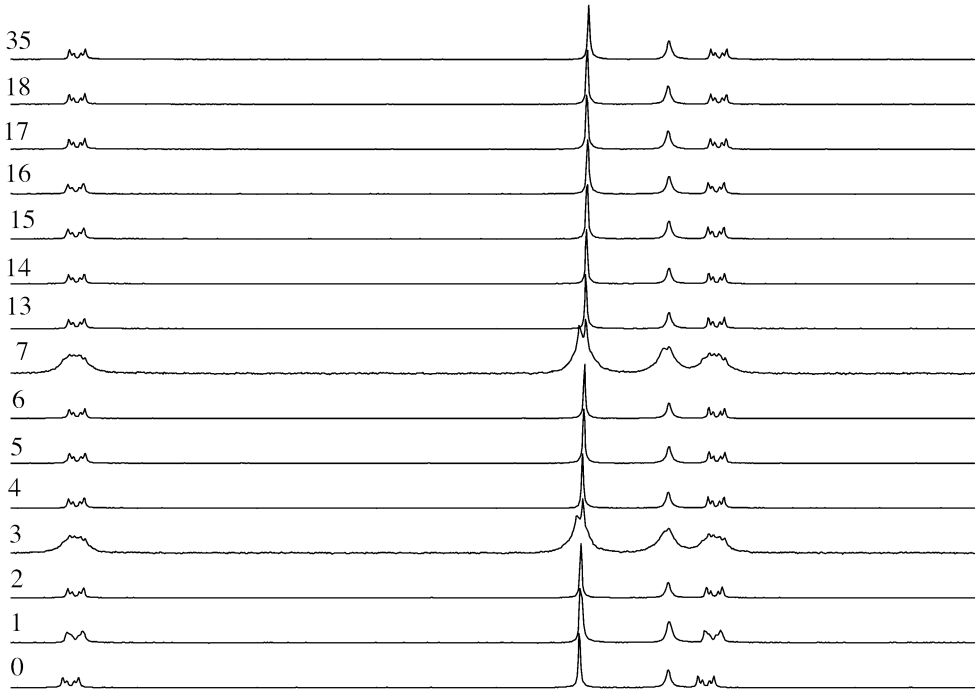

Figure A3.11: Stack plot of the ^{1}H NMR spectra measured during the synthesis of $[Zn_2(BDC)_2(BPY)]$